Technical Report ITL-93-3
September 1993

US Army Corps of Engineers
Waterways Experiment Station

Computer-Aided Structural Engineering (CASE) Project

Soil-Structure Interaction Study of Red River Lock and Dam No. 1 Subjected to Sediment Loading

by *Robert M. Ebeling, Reed L. Mosher, Kevin Abraham*
Information Technology Laboratory

John F. Peters
Geotechnical Laboratory

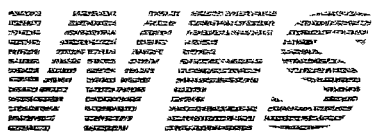

Prepared for U.S. Army Engineer District, Vicksburg

PRINTED ON RECYCLED PAPER

Computer-Aided Structural Engineering (CASE) Project

Technical Report ITL-93-3
September 1993

Soil-Structure Interaction Study of Red River Lock and Dam No. 1 Subjected to Sediment Loading

by Robert M. Ebeling, Reed L. Mosher, Kevin Abraham
Information Technology Laboratory

John F. Peters
Geotechnical Laboratory

U.S. Army Corps of Engineers
Waterways Experiment Station
3909 Halls Ferry Road
Vicksburg, MS 39180-6199

Final report

Prepared for U.S. Army Engineer District, Vicksburg
Vicksburg, MS 39180

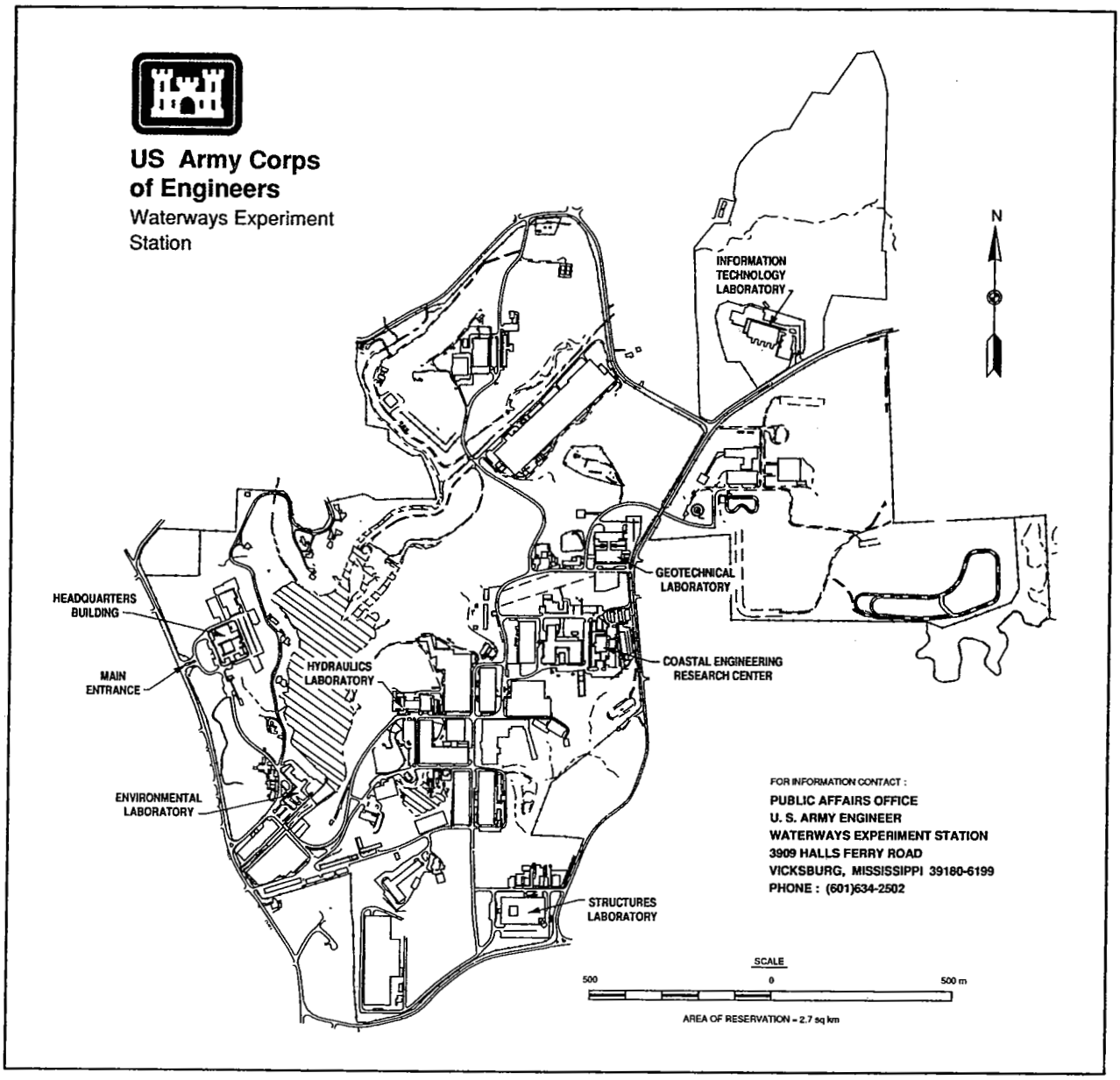

Waterways Experiment Station Cataloging-in-Publication Data

Soil-structure interaction study of Red River Lock and Dam No. 1 subjected to Sediment loading / by Robert Ebeling ... [et al.] ; prepared for U.S. Army Engineer District, Vicksburg.
283 p. : ill. ; 28 cm. — (Technical report ; ITL-93-3)
Includes bibliographical references.
1. Locks (Hydraulic engineering) — Red River (Tex.-La.) 2. Sediment transport. 3. River engineering — Red River (Tex.-La.) 4. Bed load. I. Ebeling, Robert M. II. United States. Army. Corps of Engineers. Vicksburg District. III. U.S. Army Engineer Waterways Experiment Station. IV. Computer-aided Structural Engineering Project. V. Series: Technical report (U.S. Army Engineer Waterways Experiment Station) ; ITL-93-3.
TA7 W34 no.ITL-93-3

Contents

List of Figures iv

List of Tables xv

Preface xvii

Conversion Factors, Non-SI to SI Units of Measurement xviii

1—Introduction, Project Description, Objectives, and Methods . . . 1

Introduction 1
Project Description 2
Study Objectives 17
Lock Monolith Analyzed 17
Analysis Description 18
Soil-to-Lock Interface Model 20
Organization of Documentation 25

2—Results of the Phase 1 Studies - Comparison to Field Instrumentation Measurements 26

Instrumentation at Lock Monolith No. 10 27
Dewatering and Excavation 31
Construction Stage A - Initial State of Stress Prior to Construction 33
Construction Stage B - Lower Water Table 35
Construction Stage C - Excavation 47
Lock Construction and Backfilling 69
Finite Element Model for Lock Construction 69
Comparison of Lock Construction Analysis to Instrumentation Measurements 73
Key Operational Load Cases 97
Summary 128

3—Results of the Phase 2 Studies - Reinforced Berm Analyses 133

Introduction 133
Descriptions of Cases Analyzed 134
Geometry of the Berm and Layout of the Reinforcement . . . 142
Initial Conditions Prior to Excavation 143
Excavation of Riverside Backfill to El 13.5 for Reinforced Berm 143
Construction of Reinforced Berm to El 45 147
Soil Reinforcement within the Berm 149
Results of Soil-Structure Interaction Analyses 152
Submergence of Berm - River and Pool in Lock at El 60.5 181
Siltation to El 55, Riverside - River and Pool in Lock at El 60.5 192
Lowering the Pool in Lock to El 40 and the River to El 4 208
Lowering the Pool in Lock to El 4 - River at El 4 223
Summary 237

4—Summary, Limitations, Conclusions, and Recommendations 245

Summary 245
Limitations 246
Conclusions 248
Recommendations 248
Geoinclusion between Reinforced Soil Berm and Lock Wall 251

References 255

Appendix A: Incremental Construction Procedure for Modeling Nonlinear Stress-Strain Behavior for Soils and Interface Elements A1

Nonlinear Soil Model A1
Soil-to-Lock Interface Model A2

List of Figures

Figure 1. Project site location 3

Figure 2. Vicinity map 4

Figure 3. Plan view of Red River Lock and Dam No. 1 5

Figure 4. Plan view of lock monolith numbers 6

Figure 5. Cross section through lock monolith no. L-10 7

Figure 6. Plan view of locations of borings made at site prior to construction 10

Figure 7. Geologic profiles C-C′, D-D′, and E-E′, looking upstream 11

Figure 8. Boring 12U, center line of lock, water contents, and Atterberg Limits, cross section E-E′ 12

Figure 9. Boring 13U, center line of lock, water contents, and Atterberg Limits, cross section D-D′ 13

Figure 10. Boring 14U, center line of lock, water contents, and Atterberg Limits, cross section C-C′ 14

Figure 11. Geologic profile D-D′ 15

Figure 12. Borings 1-61,1-93, and 13U, along geologic profile D-D′ 16

Figure 13. Hyperbolic representation of stress-strain curve for soil 21

Figure 14. Hyperbolic representation of interface shear stress-relative shear displacement curve 22

Figure 15. Layout of stress meters at lock monolith no. 10, station 4+12L 28

Figure 16. Layout of stress meters and piezometers at lock monolith no. 10, station 4+10L 29

Figure 17. Layout of piezometers at lock monolith no. 10, station 4+12L 30

Figure 18. Range in preconsolidation pressures from consolidation tests on clay samples 33

Figure 19. Initial finite element mesh - prior to excavation at section D-D′ 34

Figure 20. Material regions corresponding to initial finite element mesh - water table at el 40 36

Figure 21. Initial major principal effective stresses for select foundation elements 37

Figure 22. Five sections along which variation K_h* with depth is computed 38

Figure 23. Ratio of effective horizontal stresses to effective vertical stresses along section A-A′ 39

Figure 24. Ratio of effective horizontal stresses to effective vertical stresses along section B-B′ 40

Figure 25. Ratio of effective horizontal stresses to effective vertical stresses along section C-C′ 41

Figure 26. Ratio of effective horizontal stresses to effective vertical stresses along section D-D′ 42

Figure 27. Ratio of effective horizontal stresses to effective vertical stresses along section E-E′ 43

Figure 28. Material regions corresponding to initial finite element mesh - water table at el -35 44

Figure 29. Vertical displacements of select nodal points after lowering water table from 40 to -35 ft assuming complete dissipation of excess pore water pressure . . . 45

Figure 30. Major principal effective stresses for select foundation elements after lowering water table from 40 to -35 ft . . 46

Figure 31. Finite element mesh after excavation 48

Figure 32. Material regions corresponding to finite element mesh after excavation - water table at el -35 49

Figure 33. Vertical rebounds at select nodal points due to excavation assuming complete dissipation of excess pore water pressures 50

Figure 34. Major principal effective stresses for select foundation elements after excavation 51

Figure 35. Relationships between Mohr-Coulomb failure criteria and parameters used to describe stress paths 53

Figure 36. Locations of finite elements within foundation for which stress paths were computed 54

Figure 37. Stress paths for backswamp deposit element 761, below center line of lock at el -26.5 56

Figure 38. Stress paths for sand substratum element 764, below center line of lock at el -60 57

Figure 39. Stress paths for backswamp deposit element 725, below riverside stem at el -26.5 58

Figure 40. Stress paths for backswamp deposit element 803, below landside stem at el -26.5 59

Figure 41. Stress paths for backswamp deposit element 653, adjacent to corner of riverside culvert at el -20 60

Figure 42. Stress paths for backswamp deposit element 876, adjacent to corner of landside culvert at el -20 61

Figure 43. Stress paths for backswamp deposit element 595, 21 ft riverside of culvert at el -20 62

Figure 44. Stress paths for point bar sand element 949, 38 ft landside of culvert at el -20 63

Figure 45. Stress paths for sand substratum element 952, 38 ft landside of culvert at el -60 64

Figure 46. Stress paths for point bar silt element 357, 216 ft riverside of center line of lock at el 2 65

Figure 47. Stress paths for point bar silt element 360, 216 ft riverside of center line of lock at el -18 66

Figure 48. Stress paths for sand substratum element 356, 216 ft riverside of center line of lock at el -60 67

Figure 49. Outline of lock monolith no. 10 and backfill superimposed on finite element mesh of foundation . . . 70

Figure 50. Chronology of lock construction and backfilling of lock monolith no. 10 71

Figure 51. Finite element mesh after lock construction and backfilling 72

Figure 52. Material regions corresponding to finite element mesh after lock construction and backfilling - water table at el -35 74

Figure 53. View of finite element mesh modeling lock monolith no. 10 75

Figure 54. Material regions corresponding to finite element mesh modeling lock monolith no. 10 76

Figure 55. Comparison of changes in effective normal base pressures after placement of 5 ft of backfill 77

Figure 56. Vertical displacements of select nodal points due to construction of lock and placement of backfill 79

Figure 57. Major principal effective stresses for select foundation elements after construction of lock and placement of backfill 80

Figure 58. Normal pressures after lock construction and placement of backfill 81

Figure 59. Mobilized friction angles along exterior of lock after lock construction and placement of backfill 83

Figure 60. Horizontal earth pressure coefficients, K_h, after lock construction and placement of backfill 84

Figure 61. Vertical earth pressure coefficients, K_v, after lock construction and placement of backfill 86

Figure 62. Locations of finite elements within foundation and backfill for which stress paths were computed . . . 88

Figure 63. Stress paths for compacted sand backfill element 649, adjacent to riverside culvert at el -6 89

Figure 64. Stress paths for compacted sand backfill element 872, adjacent to landside culvert at el -6 90

Figure 65. Stress paths for compacted sand backfill element 591, 21 ft riverside of culvert at el -6 91

Figure 66. Stress paths for compacted sand backfill element 714, adjacent to riverside stem wall at el 13 92

Figure 67. Stress paths for compacted sand backfill element 819, adjacent to landside stem wall at el 13 93

Figure 68. Stress paths for compacted select clay backfill element 471, 80 ft riverside of stem wall at el 20 94

Figure 69. Stress paths for compacted select clay backfill element 475, 80 ft riverside of stem wall at el 3 95

Figure 70. Stress distributions across two sections within lock after lock construction and placement of backfill 96

Figure 71. Distribution of factored moments after lock construction and placement of backfill and design moment capacity 98

Figure 72. Total normal pressure - river at el 11, pool in lock at els 11 and 35 100

Figure 73. Effective normal pressure - river at el 11, pool in lock at els 11 and 35 102

Figure 74. Mobilized friction angle along exterior of lock - river at el 11, pool in lock at els 11 and 35 103

Figure 75. Horizontal earth pressure coefficient, K_h, - river at el 11, pool in lock at els 11 and 35 105

Figure 76. Vertical earth pressure coefficient, K_v, - river at el 11, pool in lock at els 11 and 35 107

Figure 77. Distribution of factored moments and design moment capacity - river at el 11, pool in lock at els 11 and 35 108

Figure 78. Total normal pressures - lower pool and pool in lock at el 40, phreatic surface at el 35 110

Figure 79. Effective normal pressures - lower pool and pool in lock at el 40, phreatic surface at el 35 112

Figure 80. Mobilized friction angles along exterior of lock - lower pool and pool in lock at el 40, phreatic surface at el 35 113

Figure 81. Horizontal earth pressure coefficient, K_h, - lower pool and pool in lock at el 40, phreatic surface at el 35 . . . 114

Figure 82. Vertical earth pressure coefficient, K_v, - lower pool and pool in lock at el 40, phreatic surface at el 35 . . . 116

Figure 83. Distribution of factored moments and design moment capacity - lower pool and pool in lock at el 40, phreatic surface at el 35 117

Figure 84. Silt deposition at lock monolith no. 10 on 4 April 1985 119

Figure 85. Total normal pressures after deposition of 7 ft of riverside silt against lock with river and pool in lock at el 45 120

Figure 86. Effective normal pressures after deposition of 7 ft of riverside silt against lock, river and pool in lock at el 45 122

Figure 87. Mobilized friction angle along exterior of lock after deposition of 7 ft of riverside silt against lock, river and pool in lock at el 45 123

Figure 88. Horizontal earth pressure coefficient, K_h, after deposition of 7 ft of riverside silt against lock, river and pool in lock at el 45 124

Figure 89. Vertical earth pressure coefficient, K_v, after deposition of 7 ft of riverside silt against lock, river and pool in lock at el 45 126

Figure 90. Distribution of factored moments and design moment capacity after deposition of 7 ft of riverside silt against lock, river and pool in lock at el 45 127

Figure 91. Distribution of factored moments, including CUFRAM results, after deposition of 7 ft of riverside silt against lock, river and pool in lock at el 45 129

Figure 92. Lock monolith no. 10 and material regions with lower pool and pool in lock at el 11 135

Figure 93. Riverside excavation for reinforced berm with lower pool and pool in lock at el 11 136

Figure 94. Riverside reinforced berm with lower pool and pool in lock at el 11 137

Figure 95. Riverside reinforced berm with lower pool and pool in lock at el 60 138

Figure 96. Reinforced berm with lower pool and pool in lock at el 60, deposition of riverside silt to el 55 139

Figure 97. Reinforced berm with lower pool at el 4, pool in lock at el 40, and riverside silt at el 55 140

Figure 98. Reinforced berm with lower pool and pool in lock at el 4, riverside silt at el 55 141

Figure 99. Enlargement of finite element mesh region encompassing lock structure after riverside excavation for reinforced berm 145

Figure 100. Material regions of finite element mesh region encompassing lock structure after riverside excavation for reinforced berm 146

Figure 101. Finite element mesh after construction of reinforced berm 148

Figure 102. Enlargement of finite element mesh region encompassing lock structure after construction of reinforced berm 150

Figure 103. Material regions of finite element mesh region encompassing lock structure after construction of reinforced berm 151

Figure 104. Relative displacements of lock, berm, and foundation after construction of reinforced berm 154

Figure 105. Four sections along which values of vertical effective stress are compared to range in preconsolidation pressure values within foundation 156

Figure 106. Values of effective vertical stress along section A-A′ 157

Figure 107. Values of effective vertical stress along section B-B′ 158

Figure 108. Values of effective vertical stress along section C-C′ 159

Figure 109. Values of effective vertical stress along section D-D′ 160

Figure 110. Total normal pressures after construction of reinforced berm, river and pool in lock at el 11 162

Figure 111. Effective normal pressures after construction of reinforced berm, river and pool in lock at el 11 . . . 163

Figure 112. Mobilized friction angle along exterior of lock after construction of reinforced berm, river and pool in lock at el 11 165

Figure 113. Ratio of effective vertical stress to effective overburden pressure after construction of reinforced berm, river and pool in lock at el 11 166

Figure 114. Horizontal earth pressure coefficient after construction of reinforced berm, river and pool in lock at el 11 167

Figure 115. Ratio of effective horizontal stress to effective vertical stress after construction of reinforced berm, river and pool in lock at el 11 169

Figure 116. Vertical earth pressure coefficient after construction of reinforced berm, river and pool in lock at el 11 170

Figure 117. Ratio of shear stress to effective vertical stress after construction of reinforced berm, river and pool in lock at el 11 171

Figure 118. Distribution of factored moments after construction of reinforced berm and design moment capacity - river and pool in lock at el 11 172

Figure 119. Distribution of factored moments, including CUFRAM results, after construction of reinforced berm - river and pool in lock at el 11 174

Figure 120. Locations of finite elements within reinforced berm for which stress paths were computed 175

Figure 121. Stress paths for reinforced berm sand element 715, adjacent to riverside stem at el 16.5 176

Figure 122. Stress paths for reinforced berm sand element 1152, adjacent to riverside stem at el 31 177

Figure 123. Stress paths for reinforced berm sand element 623, 77 ft riverside of lock center line at el 28 178

Figure 124. Stress paths for reinforced berm sand element 563, 101 ft riverside of lock center line at el 28 179

Figure 125. Stress paths for active and passive Rankine states of stress within backfill 180

Figure 126. Variations in mobilized shear strength within reinforced berm after construction of berm 182

Figure 127. Variations in reinforcement force within reinforced berm after construction of berm 183

Figure 128. Relative displacements of lock, berm, and foundation after submergence of reinforced berm 185

Figure 129. Total normal pressures after submergence of reinforced berm, river and pool in lock at el 60.5 187

Figure 130. Effective normal pressures after submergence of reinforced berm, river and pool in lock at el 60.5 . . . 188

Figure 131. Mobilized friction angles along exterior of lock after submergence of reinforced berm, river and pool in lock at el 60.5 189

Figure 132. Horizontal earth pressure coefficients after submergence of reinforced berm, river and pool in lock at el 60.5 . . 191

Figure 133. Vertical earth pressure coefficients after submergence of reinforced berm, river and pool in lock at el 60.5 . . 193

Figure 134. Distribution of factored moments after submergence of reinforced berm and design moment capacity - river and pool in lock at el 60.5 194

Figure 135. Variation in mobilized shear strength within reinforced berm after submergence of berm 195

Figure 136. Variation in reinforcement force within reinforced berm after submergence of berm 196

Figure 137. Relative displacements of lock, berm, and foundation after riverside siltation to el 55 198

Figure 138. Total normal pressures after riverside siltation to el 55, river and pool in lock at el 60.5 199

Figure 139. Effective normal pressures after riverside siltation to el 55, river and pool in lock at el 60.5 201

Figure 140. Mobilized friction angle along exterior of lock after siltation to el 55, river and pool in lock at el 60.5 . . . 202

Figure 141. Horizontal earth pressure coefficient after riverside siltation to el 55, river and pool in lock at el 60.5 . . . 203

Figure 142. Vertical earth pressure coefficient after riverside siltation to el 55, river and pool in lock at el 60.5 . . . 205

Figure 143. Distribution of factored moments after riverside siltation to el 55 and design moment capacity - river and pool in lock at el 60.5 206

Figure 144. Distribution of factored moments, including CUFRAM results, after riverside siltation to el 55 - river and pool in lock at el 60.5 207

Figure 145. Variation in mobilized shear strength within reinforced berm after riverside siltation to el 55 209

Figure 146. Variation in reinforcement force within reinforced berm after riverside siltation to el 55 210

Figure 147. Relative displacements of lock, berm, and foundation after lowering pool in lock to el 40 and river to el 4 . . 212

Figure 148. Total normal pressures after lowering pool in lock to el 40 and river to el 4 214

Figure 149. Effective normal pressures after lowering pool in lock to el 40 and river to el 4 215

Figure 150. Mobilized friction angle along exterior of lock after lowering pool in lock to el 40 and river to el 4 . . 217

Figure 151. Horizontal earth pressure coefficient after lowering pool in lock to el 40 and river to el 4 218

Figure 152. Vertical earth pressure coefficient after lowering pool in lock to el 40 and river to el 4 219

Figure 153. Distribution of factored moments and design moment capacity - pool in lock at el 40 and river at el 4 221

Figure 154. Distribution of factored moments, including CUFRAM results - pool in lock at el 40 and river at el 4 222

Figure 155. Variation in mobilized shear strength within reinforced berm after lowering pool in lock to el 40 and river to el 4 224

Figure 156. Variation in reinforcement forces within reinforced berm after lowering pool in lock to el 40 and river to el 4 . . 225

Figure 157. Relative displacements of lock, berm, and foundation after lowering pool in lock to el 4 - river at el 4 227

Figure 158. Total normal pressures after lowering pool in lock to el 4 - river at el 4 229

Figure 159. Effective normal pressures after lowering pool in lock to el 4 - river at el 4 230

Figure 160. Mobilized friction angles along exterior of lock after lowering pool in lock to el 4 - river at el 4 232

Figure 161. Horizontal earth pressure coefficients after lowering pool in lock to el 4 - river at el 4 233

Figure 162. Vertical earth pressure coefficients after lowering pool in lock to el 4 - river at el 4 235

Figure 163. Distribution of factored moments and design moment capacity - pool in lock at el 4 and river at el 4 236

Figure 164. Variation in mobilized shear strength within reinforced berm after lowering pool in lock to el 4 - river at el 4 . 238

Figure 165. Variation in reinforcement force within reinforced berm after lowering pool in lock to el 4 - river at el 4 . 239

Figure 166. Lateral earth pressure reduction by use of geoinclusion and lateral reinforcement 253

List of Tables

Table 1. Drained Hyperbolic Stress-Strain and Strength Parameters 23

Table 2. Interface Parameters 24

Table 3. Phase 1 Finite Element Analyses - Construction Stages 26

Table 4. Phase 1 Finite Element Analyses - Operational Load Cases 31

Table 5. Descriptions of Load Cases for Stress Path Point Numbers 55

Table 6. Average Values of Horizontal and Vertical Earth Pressure Coefficients after Construction of Lock and Placement of the Backfill 85

Table 7. Average Values of Horizontal and Vertical Earth Pressure Coefficients - River at El 11, Pool in Lock at El 11 104

Table 8. Average Values of Horizontal and Vertical Earth Pressure Coefficients - River at El 11, Pool in Lock at El 35 106

Table 9. Average Values of Horizontal and Vertical Earth Pressure Coefficients - Lower Pool and Pool in Lock at El 40, Phreatic Surface at El 35 115

Table 10. Average Values of Horizontal and Vertical Earth Pressure Coefficients after Deposition of 7 ft of Riverside Silt Against Lock, River and Pool in Lock at El 45 125

Table 11. Range of Average Values of Horizontal Earth Pressure Coefficients - Four Operational Load Cases 131

Table 12. Range of Average Values of Vertical Earth Pressure Coefficients - Four Operational Load Cases 131

Table 13. Seven Stages of Phase 2 Finite Element Analyses 134

Table 14. Material Parameters Assigned to Reinforcement Used within Berm 152

Table 15. Average Values of Horizontal and Vertical Earth Pressure Coefficients after Construction of Reinforced Berm 168

Table 16. Average Values of Horizontal and Vertical Earth Pressure Coefficients after Submergence of Reinforced Berm 192

Table 17. Average Values of Horizontal and Vertical Earth Pressure Coefficients after Riverside Siltation to El 55 204

Table 18. Average Values of Horizontal and Vertical Earth Pressure Coefficients after Lowering Pool in Lock to El 40 and River to El 4 220

Table 19. Average Values of Horizontal and Vertical Earth Pressure Coefficients after Lowering Pool in Lock to El 4 - River at El 4 234

Table 20. Range of Average Values of Horizontal Earth Pressure Coefficients - Phase 2 Finite Element Analyses 242

Table 21. Range of Average Values of Vertical Earth Pressure Coefficients - Phase 2 Finite Element Analyses 243

Preface

This report describes the soil-structure interaction analyses used to assess potential lock performance with the construction of a reinforced soil retaining wall adjacent to the riverside lock wall at Red River Lock and Dam No. 1. Funding for this study was provided by the U.S. Army Engineer District (USAED), Vicksburg, and the Computer-Aided Structural Engineering Project sponsored by Headquarters, U.S. Army Corps of Engineers (HQUSACE), under the Structural Engineering Research Program. Messrs. C. C. Hamby and Edward E. Schilling, Design Branch, USAED, Vicksburg, were the project monitors under the general supervision of Mr. Charles Bradshaw, Chief, Design Branch.

The work was performed at the U.S. Army Engineer Waterways Experiment Station (WES) by Dr. Robert M. Ebeling, Interdisciplinary Research Group (IRG), Computer-Aided Engineering Division (CAED), Information Technology Laboratory (ITL), Dr. Reed L. Mosher, Acting Chief, CAED, Mr. Kevin Abraham, Scientific and Engineering Applications Center, CAED, and Dr. John F. Peters, Soil and Rock Mechanics Division, Soil Research Center, Geotechnical Laboratory. Messrs. John Hendrix and Joe Jenkins, ITL, provided invaluable assistance in processing the results of the computer analyses and preparing the figures for this report. This report was prepared by Drs. Ebeling and Mosher. Review commentary was provided by Messrs. Hamby and Schilling. Additional commentary was provided by Mr. Sam Stacy and Mr. George Sills, Foundation and Materials (F&M), USAED, Vicksburg, under the general supervision of Mr. Thomas Wayne Forest, Chief, Analytical Section, F&M. The work was accomplished under the general direction of Dr. Mosher and the general supervision of Dr. N. Radhakrishnan, Director, ITL.

At the time of publication of this report, Director of WES was Dr. Robert W. Whalin. Commander was COL Bruce K. Howard, EN.

Conversion Factors, Non-SI to SI Units of Measurement

Non-SI units of measurement used in this report can be converted to SI units as follows:

Multiply	By	To Obtain
degrees (angle)	0.01745329	radians
feet	0.3048	meters
inches	25.4	millimeters
kip-feet	1355.818	newton-meters
kips (force) per square foot	47.88026	kilopascals
kips (force) per square inch	6.894757	kilopascals
miles (U.S. nautical)	1.852	kilometers
pounds (force) per linear foot	14.5939	newtons per meters
pounds (force) per square foot	47.88026	pascals
pounds (force) per square inch	0.006894757	megapascals
pounds (mass) per cubic foot	16.01846	kilograms per cubic meter

1 Introduction, Project Description, Objectives, and Methods

Introduction

This report describes the soil-structure interaction investigation of the performance of the lock at Lock and Dam No. 1 on Red River Waterway under present operating conditions. Also included is a discussion of the potential performance of the lock and dam after construction of a reinforced soil retaining wall to relieve silt loading on the lock. Lock and Dam No. 1 on the Red River Waterway has experienced a serious sediment problem since its completion in 1983. Sediments are being deposited during periods of high water at a much higher rate and to a greater level than anticipated during the design of the project. There are four major areas of the siltation that affect the operation of the lock: the upstream and downstream approaches, the riverside lock wall, and the lock chamber. The placement of rock dikes and other hydraulic changes have somewhat alleviated the siltation problem in the lock approaches. However, the sediments deposited against the riverside lock wall have created a very costly maintenance problem.

The silt buildup against the lock wall is significantly higher than that assumed in the design of the lock. During a high-water period in the Spring of 1985, silt deposits against the riverside lock wall were 14 ft[1] higher than assumed in the design of the wall. This roughly corresponds to 2 ft below the high-water level at the time. No damage to the lock was observed. However, before the river returned to normal level, the silt was removed. Since the navigation structure has not experienced even a

[1] A table of factors for converting non-SI units of measurements to SI units is presented on page xviii.

10-year flood, it is anticipated that this will be a continuing problem resulting in an extremely high maintenance cost.

In a recent study, the U.S. Army Engineer District (USAED), Mobile, considered eight concepts for a permanent solution to this problem. Three of these concepts were considered feasible and were developed to the feature design memorandum (FDM) stage (USAED, Mobile 1988); a concrete I-wall, a reinforced soil retaining wall, and silt removal as warranted. It was concluded that the reinforced soil retaining wall, referred to as a reinforced soil berm in this report, has the best potential for a permanent solution with little or no maintenance required after its placement. This additional study was initiated to investigate the interaction between the proposed reinforced soil berm, the U-frame lock, and their foundations.

The design of a reinforced soil retaining wall on most projects is accomplished using conventional force-equilibrium procedures. This method of analysis is sufficient for the evaluation of the stability of proposed reinforcement layout(s) and the evaluation of the overall stability of the reinforced soil retaining wall and its foundation. However, with the placement of a reinforced soil berm adjacent to the lock, these conventional analysis techniques are unable to provide sufficient information to satisfactorily evaluate the performance of the reinforced soil berm with regard to its interaction with the lock and their combined interaction with the surrounding soil. To ensure that the berm would accomplish its mission, a soil-structure interaction evaluation was conducted using state-of-the-art finite element techniques.

Project Description

Site

The Red River Lock and Dam No. 1 is located in Catahoula Parish, Louisiana, Figure 1, in a 1.7-mile-long cutoff between river miles 42.6 and 51.1 on the Red River. It is approximately 9 miles upstream from the confluence of the Red and Black Rivers and 5 miles downstream from the settlement of Brouillete (Figure 2). The 1.7-mile-long cutoff, shown in plan view (Figure 3), shortened the waterway by 8 miles with the elimination of an oxbow meander, (Figure 1). It is the first in a series of locks and dams to provide navigation for barge traffic between the Mississippi River and Shreveport, LA.

River

The Red River has its origin in the plains of New Mexico and flows through Texas, Oklahoma, Arkansas, and Louisiana where it empties into

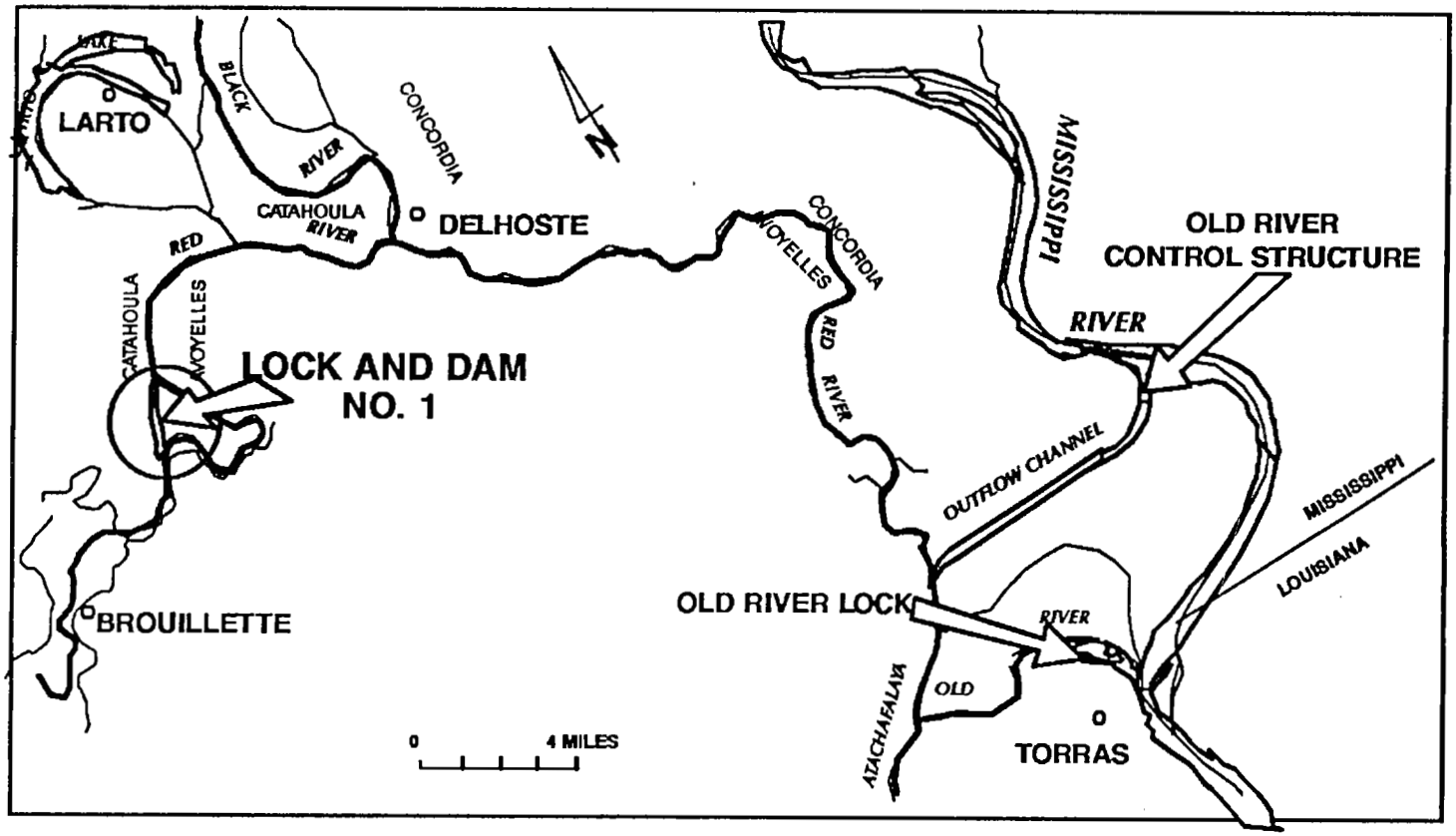

Figure 1. Project site location

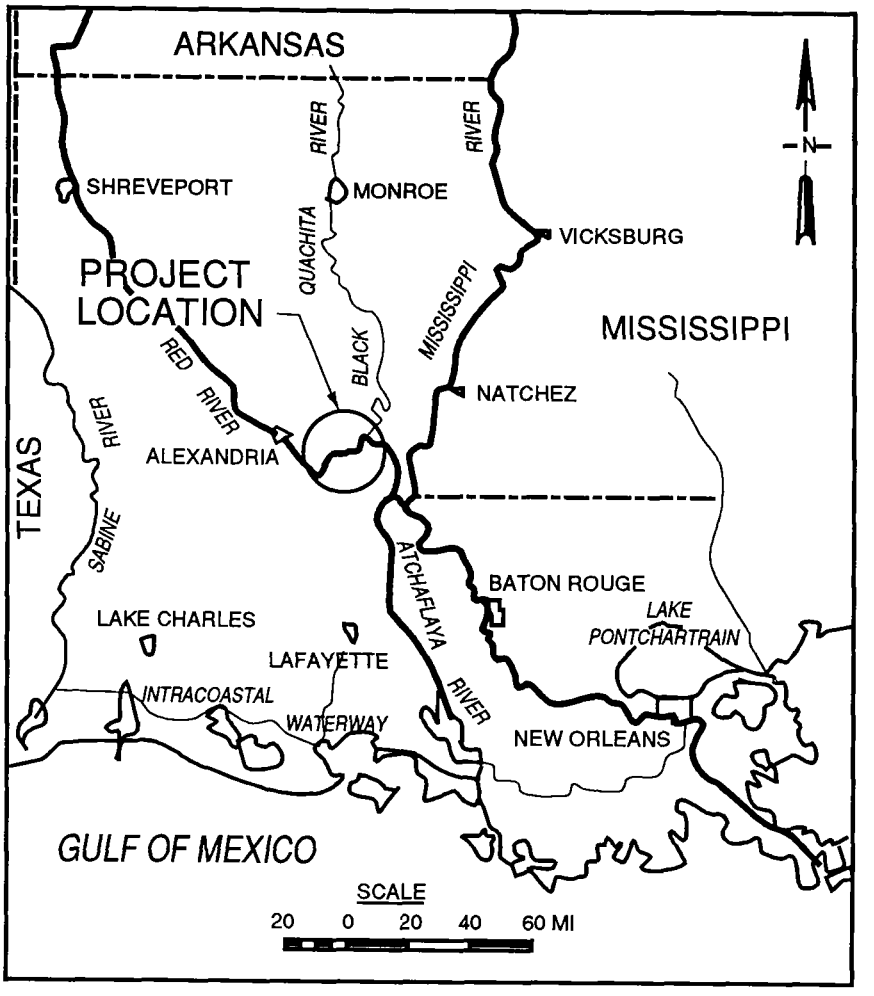

Figure 2. Vicinity map

the Atchafalaya River. It's name reflects the rusty color of the suspended sediment carried from the iron rich soils of the Red River Valley.

Lock

Construction of Red River Lock and Dam No. 1 was started in 1977 and completed in 1983. The soils-founded U-frame lock has an 84- by 785-ft chamber, pintle to pintle. The U-frame is a monolithic structure consisting of 18 lock monoliths (Figure 4). Figure 5 shows a cross-section through the lock monolith no. L-10, located midway along the chamber at station 4+12L. The lock is 83.5 ft tall. The tops of the lock walls are at el 60.5 ft[1] and the base of the lock is at el -23. The base slab

[1] Unless stated otherwise, all elevations (el) cited herein are in feet referred to National Geodetic Vertical Datum (NGVD) of 1929.

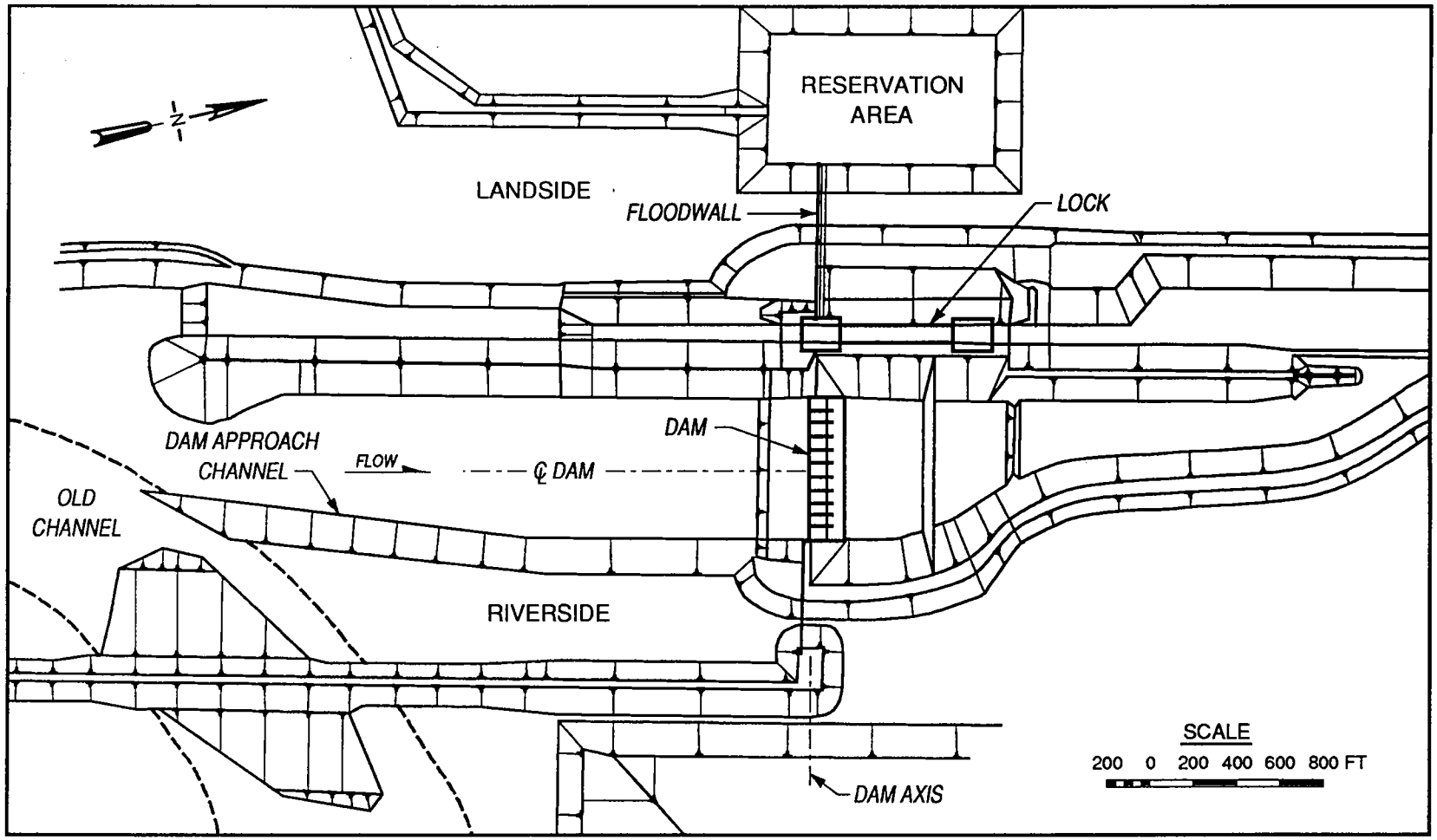

Figure 3. Plan view of Red River Lock and Dam No. 1

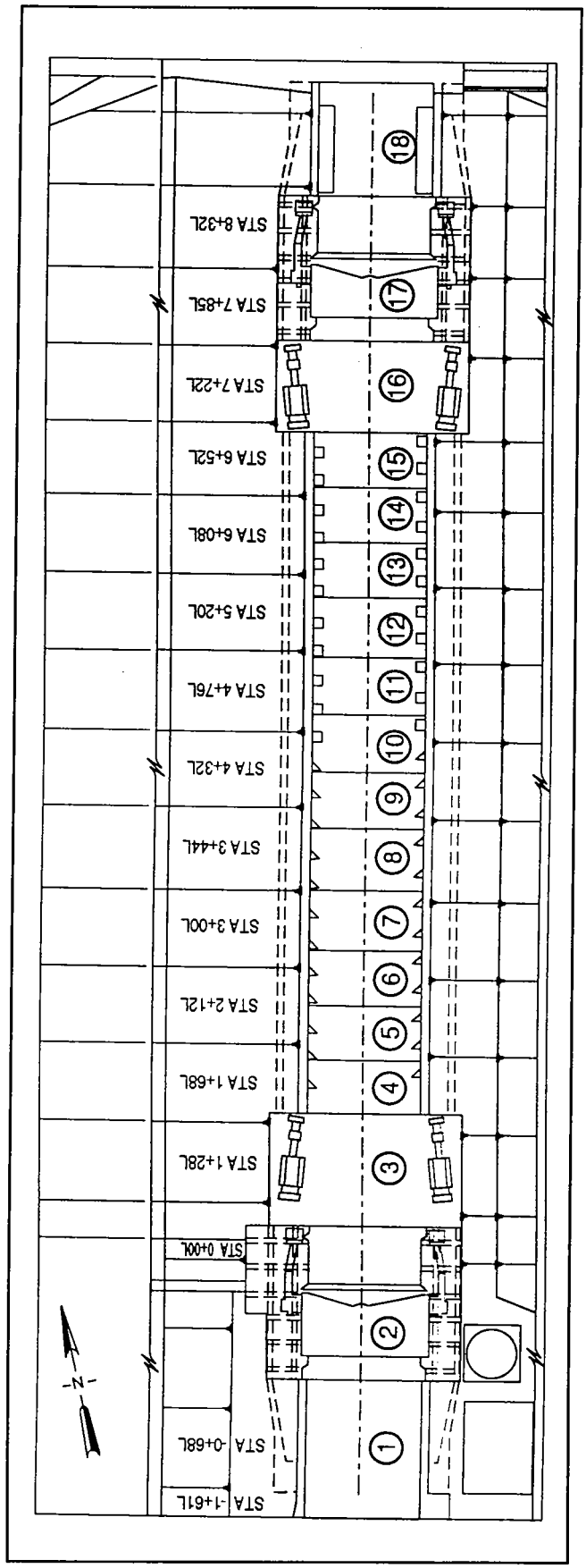

Figure 4. Plan view of lock monolith numbers

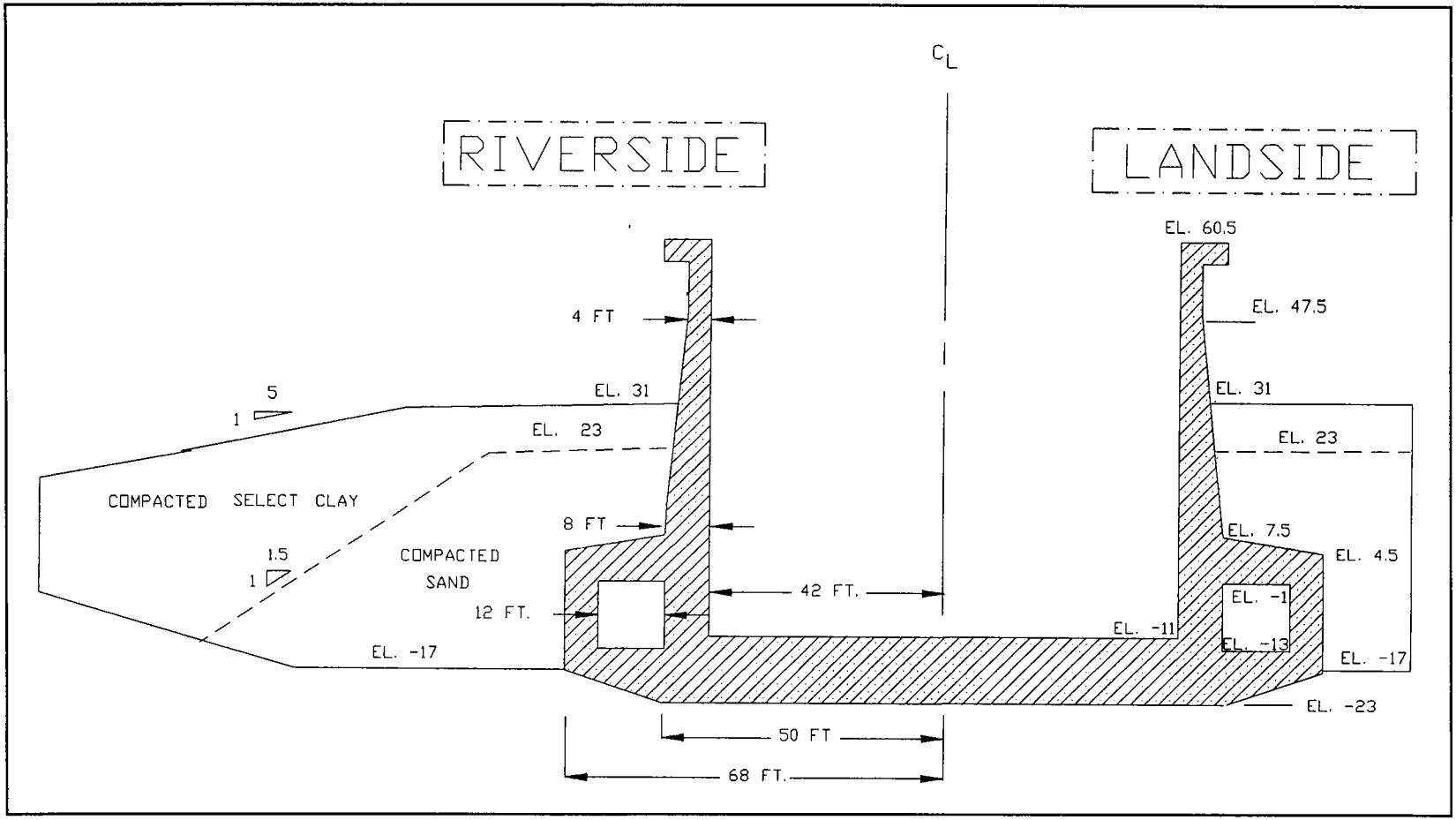

Figure 5. Cross section through lock monolith no. L-10

is 12 ft thick with the chamber floor at el -11. The lock is symmetrical about its center line and has a maximum width equal to 136 ft, as measured from the outside culvert walls. Each side has a 12-ft-square culvert, formed by 8-ft-thick interior and 6-ft-thick exterior culvert walls. The tapered stem walls are 8 ft wide at el 7.5, directly above the culvert, and they decrease in thickness to 4 ft at el 47.5. Above el 5, the stem wall thickness is a constant 4 ft. The U-frame structure is constructed with compacted sand and select compacted clay backfill on each side of the culvert and stem walls to el 31. The riverside backfill slopes away from the lock on a 1V to 50H slope for a lateral distance equal to 50 ft, beyond which the slope increases to 1V to 5H into the new river channel.

Geology

The geology at the site of Red River Lock and Dam No. 1 is described in section number 7 of Design Memorandum No. 9 (USAED, New Orleans 1977). The following two paragraphs are excerpts from this section.

The site is located within the Gulf Coastal Plain Province near the western edge of the Mississippi River Floodplain. The immediate area is characterized by natural levees, backswamps, oxbow lakes, and the ridge and swale topography of meander scars. The natural levees provide local relief of about 10 ft above the surrounding point bars and swamps. Elevations along the levee crests are approximately 50 ft.

Only the sedimentary history from the end of the Pleistocene Epoch is pertinent to this site. As sea level rose from a low of about 450 ft below the present level, an episode of aggregation by braided streams ensued which ended 4,000 to 5,000 years ago. This episode resulted in the deposition of the large quantities of sand and gravel comprising the substratum deposits. As sea level reached its present stand, the braided condition of the Mississippi River and its tributaries gave way to a meandering pattern. This change started from the south and had probably reached the north to the site area 4,000 to 4,500 years ago. Since that time, the Mississippi River has occupied several entrenched channels starting with the Maringouin Course and including parts of the present courses of the Red and Black rivers, Bayou Cocodrie, and Bayou des Glaise. As the Mississippi River shifted its channel, the Red and Arkansas Rivers adjusted their courses to the changing base levels. These adjustments caused the three rivers to transverse near or through the site of Lock and Dam No. 1 during the last 4,500 years. At present, sediments are being deposited in the area only during high stages of the Red River.

Foundation conditions

The subsurface conditions at the site are described in detail in Design Memorandum No. 9 (USAED, New Orleans 1977). A series of 125 general type borings and fourteen 5-in. undisturbed borings were made over the

entire site prior to excavation for the channel and structures. A plan view of the boring locations is shown in Figure 6. The approximate location of the new river channel lies along the section labeled L-L′ in this figure. Geologic sections were developed from the information provided by these soil borings. Figure 7 presents the preconstruction geologic sections along three sections perpendicular to the center line of the lock and looking upstream: section E-E′ through the upstream entrance of the lock and along the center line of the dam, geologic section D-D′ midway along the axis of the lock, and geologic section C-C′ through the downstream exit of the lock. The dam and lock structures are presented in these figures at their postconstruction positions. Those soil borings along the center line of the lock used in the development of the three geologic cross sections E-E′, D-D′, and C-C′ of Figure 7 are shown in Figures 8, 9, and 10, respectively. The variation in water content with elevation and the ranges for the Atterberg Plastic Limits and Liquid Limits with elevation are also shown. The site is delineated by four distinct soil strata: the natural levee, the point bar deposit, the backswamp deposit, and the substratum. Within the region in which the lock was constructed, the elevation of the ground surface prior to construction was at a nearly constant el 50, and the delineation between the natural levee and point bar deposit was approximately el 30. The top elevation of the substratum is approximately at el -50 relative to the lock and dam and for most of the new river channel. The thicknesses of the Point Bar and Backswamp deposits vary due to the traversing of the site by tributaries(s) to the Mississippi or Red Rivers during the last 4,000 years.

The deepest deposit is the substratum and comprises mainly sand with some gravel present. The uppermost deposit, the natural levee, is almost exclusively categorized as a fat clay (CH) by its Atterberg Limit values. Between these two deposits lie the Point Bar Deposit and Backswamp Deposit. The Point Bar is predominantly a silt deposit, with regions of silty sand and poorly graded sand deposits. The Backswamp Deposit consists predominantly of CH clays, but also contains interbedded layers of lean clays (CL), silts, silty-sands, and sands. The degree of heterogeneity within the Point Bar Deposit and Backswamp Deposit varies with location.

Geologic section D-D′, Figure 11, is the approximate location of monolith no. 10 (Figure 4) and is midway along the lock chamber. Three of the soil borings used in the development of the geologic section D-D′ of Figure 11 are shown in Figure 12. The Backswamp Deposit is more heterogeneous within the region at the base of the lock for geologic section D-D′ than for geologic sections E-E′ and C-C′. The center line borings shown in Figures 8, 9, and 10 show the Backswamp Deposit to be more heterogeneous midway along the lock chamber (geologic section D-D′) than at the upstream and downstream ends (geologic sections E-E′ and C-C′).

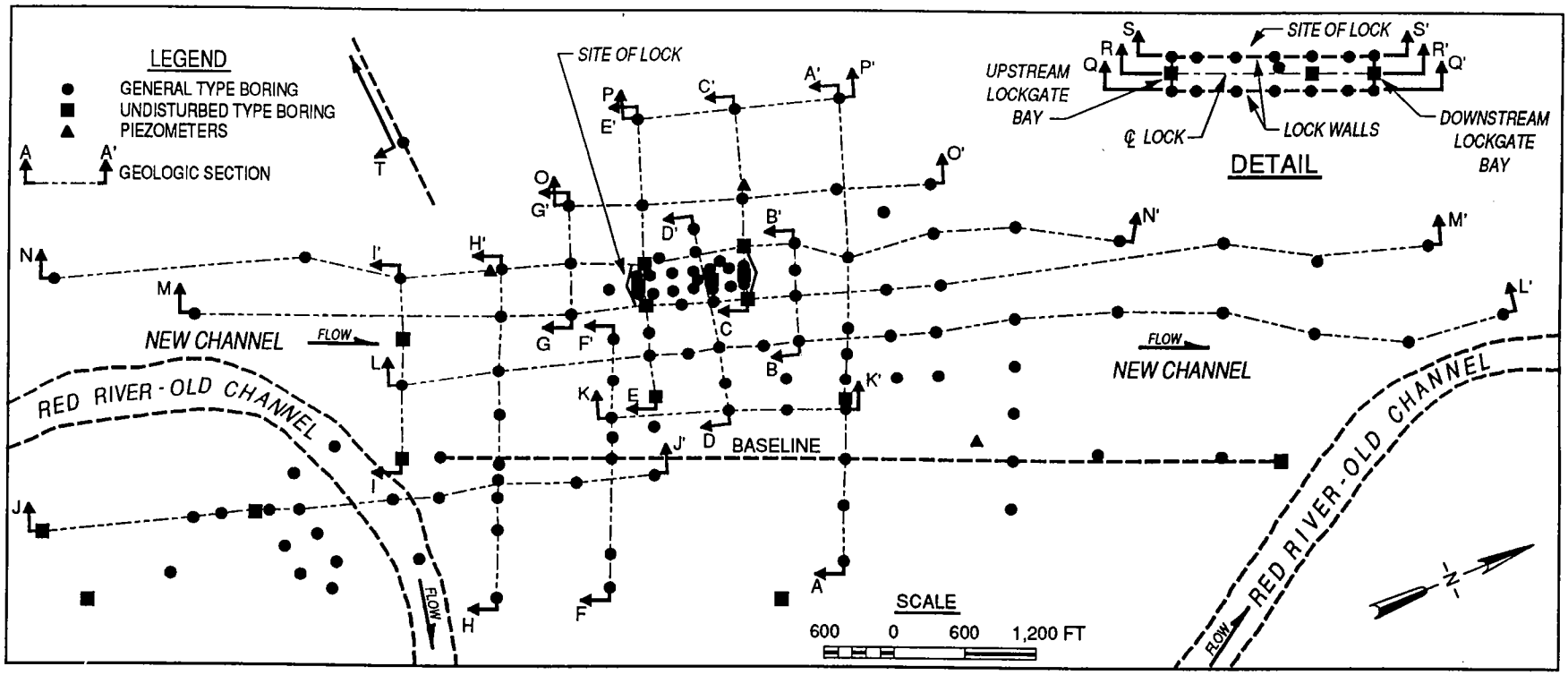

Figure 6. Plan view of locations of borings made at site prior to construction

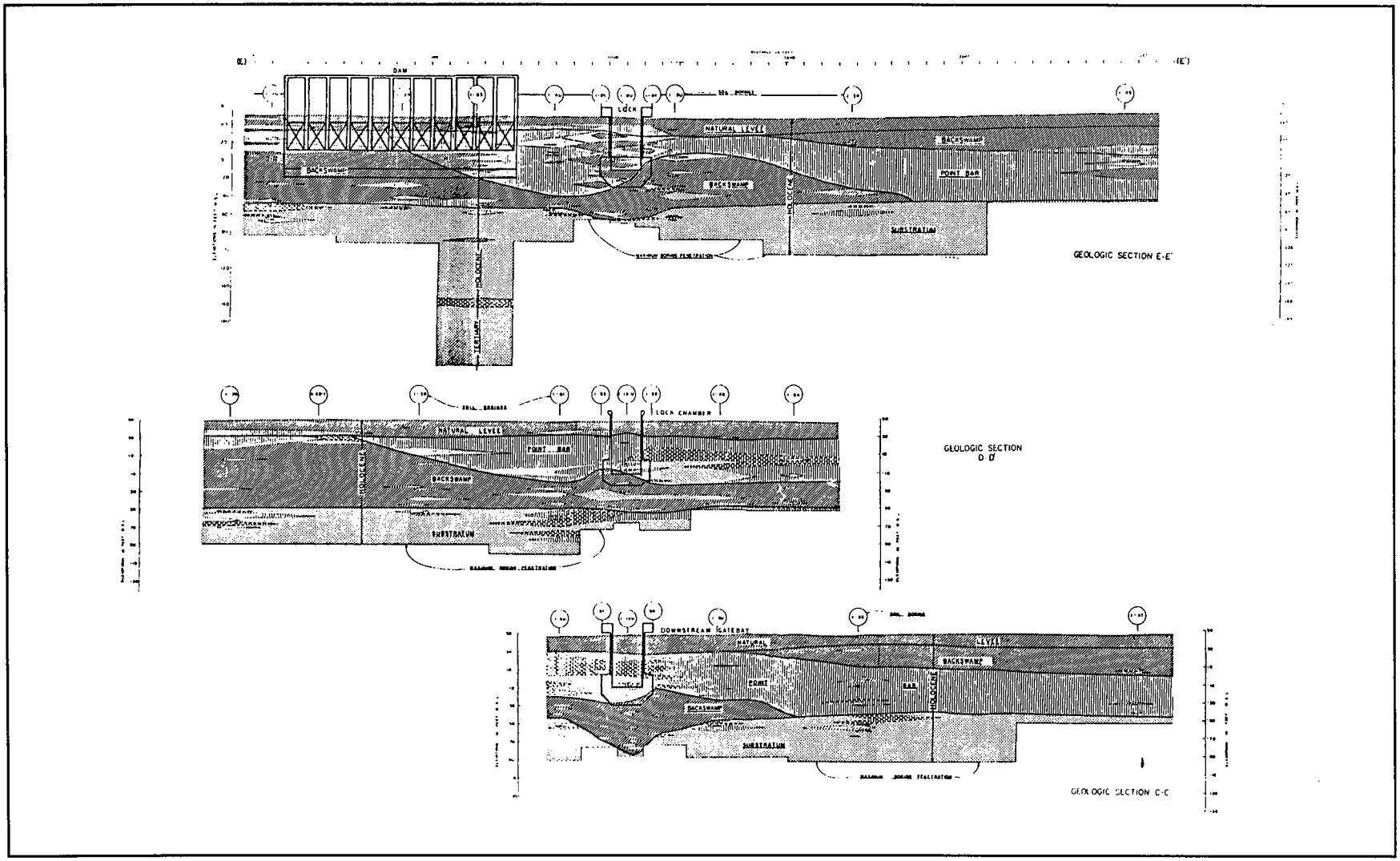

Figure 7. Geologic profiles C-C′, D-D′, and E-E′, looking upstream

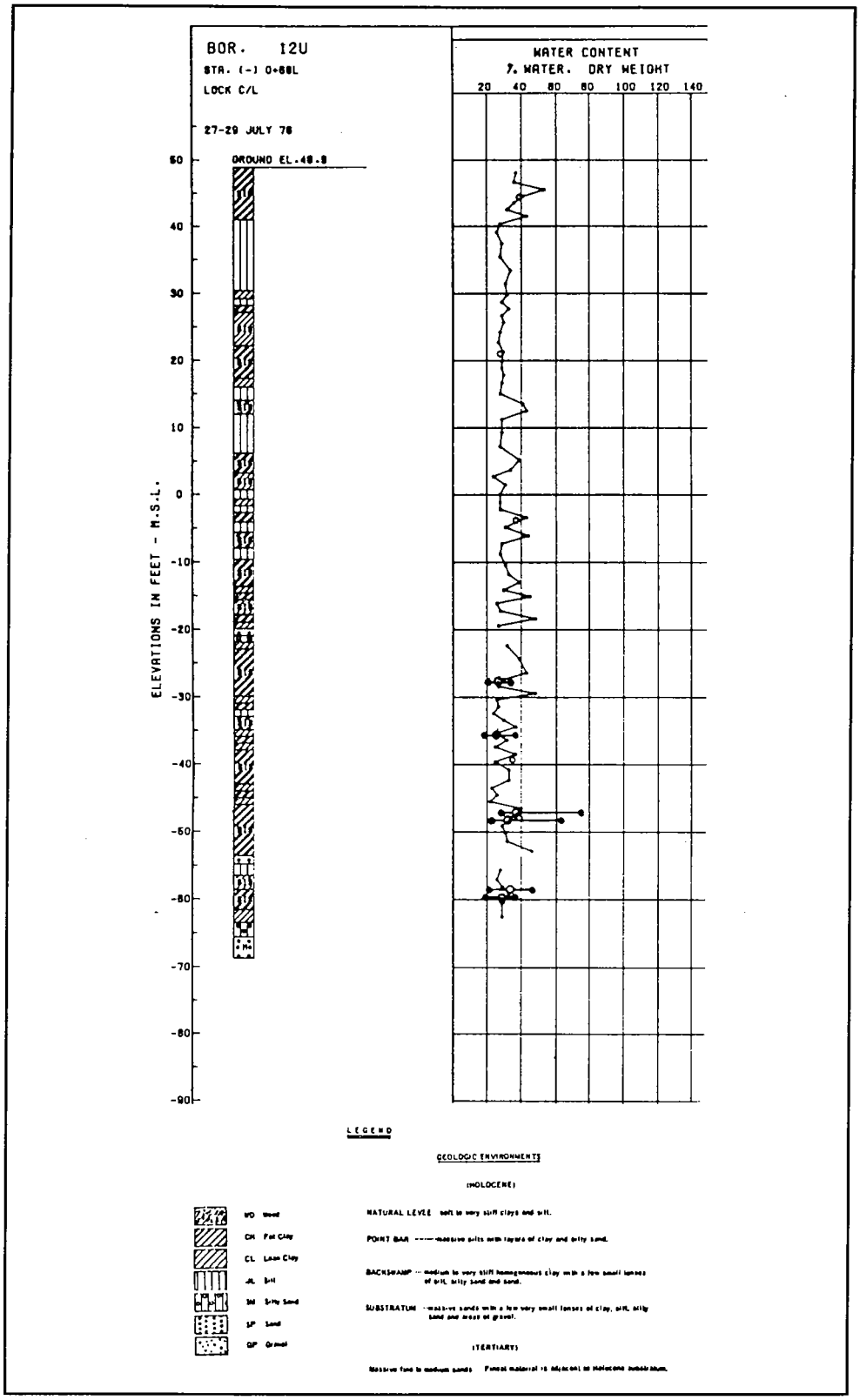

Figure 8. Boring 12U, center line of lock, water contents, and Atterberg Limits, cross section E-E′

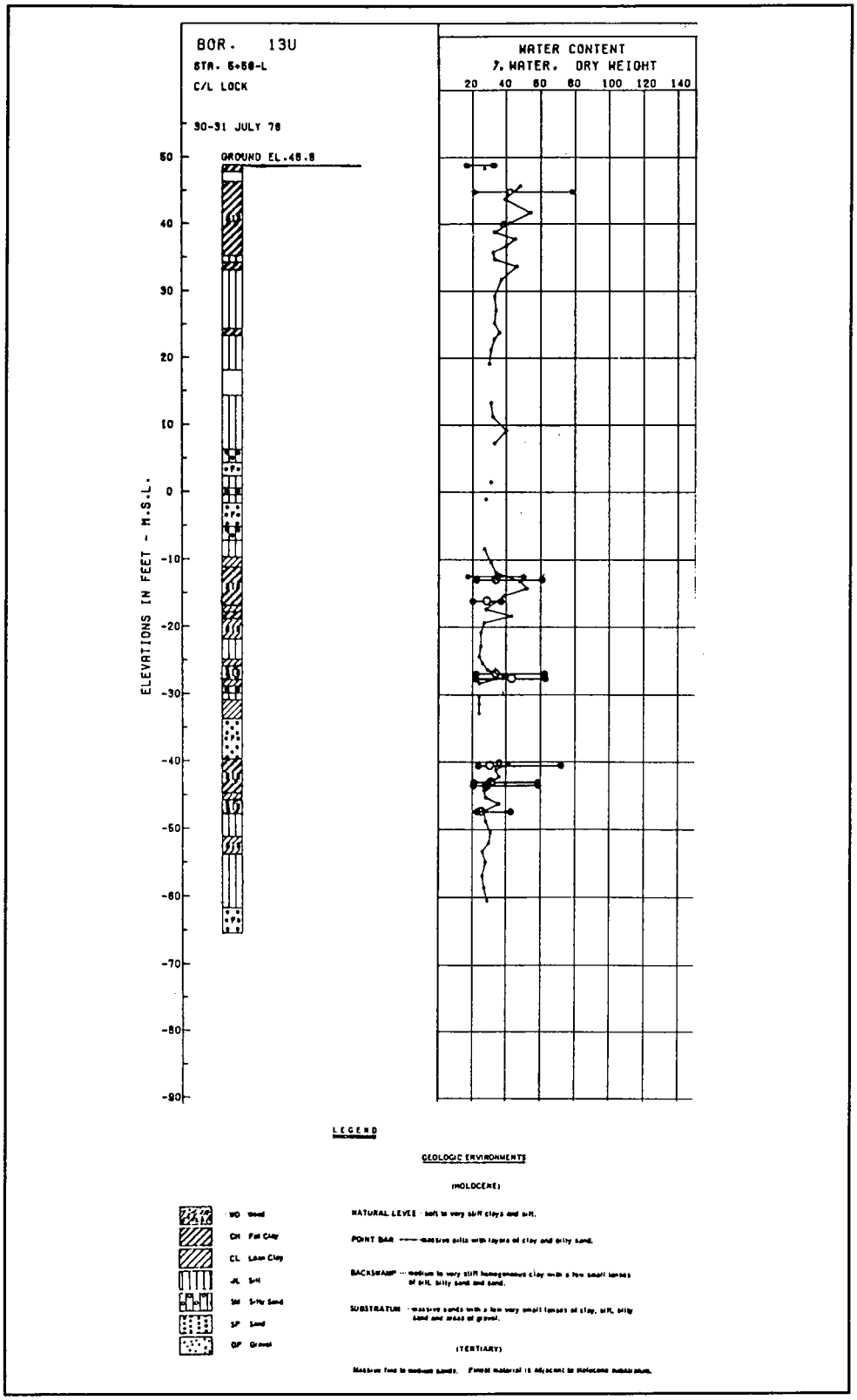

Figure 9. Boring 13U, center line of lock, water contents, and Atterberg Limits, cross section D-D′

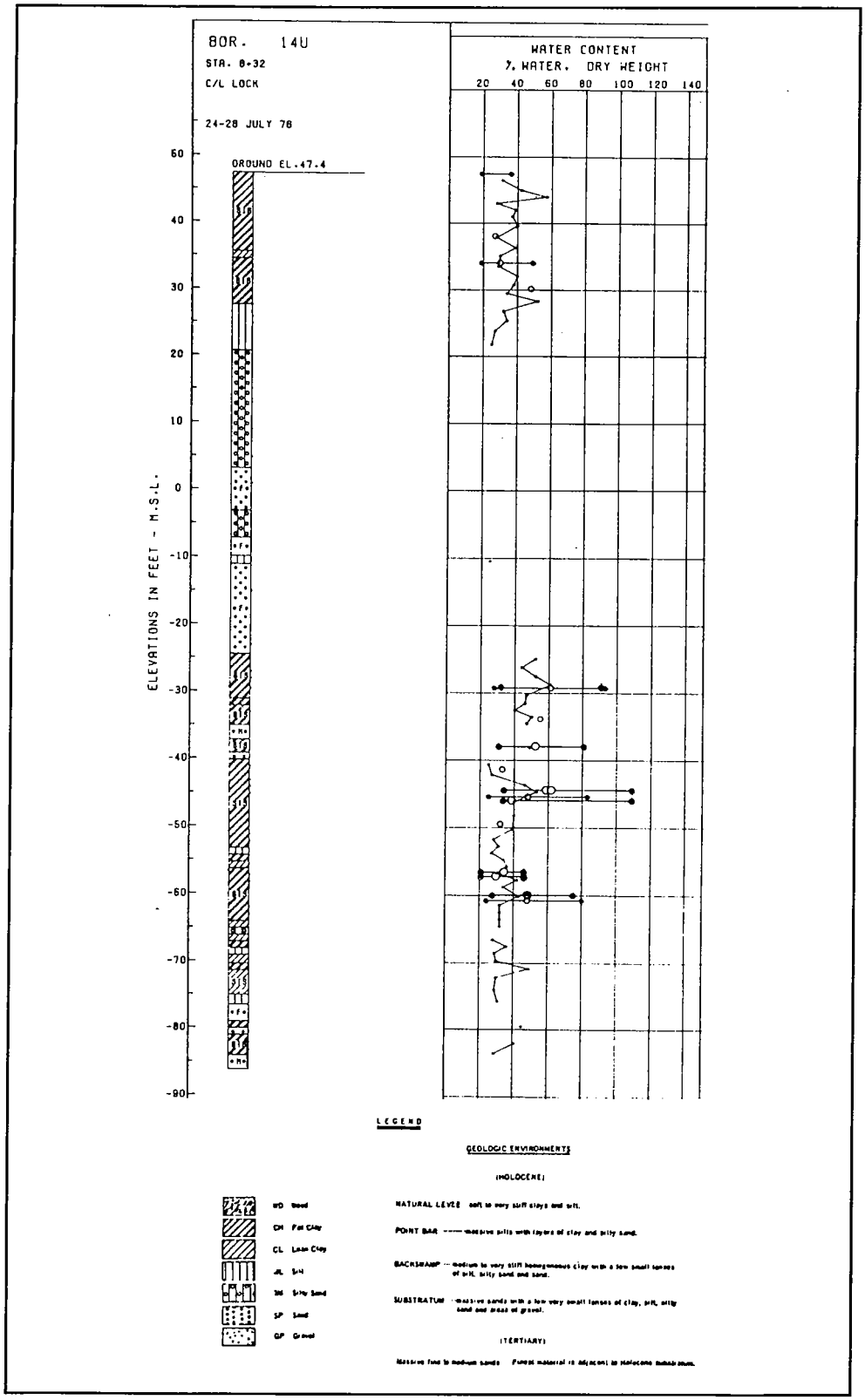

Figure 10. Boring 14U, center line of lock, water contents, and Atterberg Limits, cross section C-C′

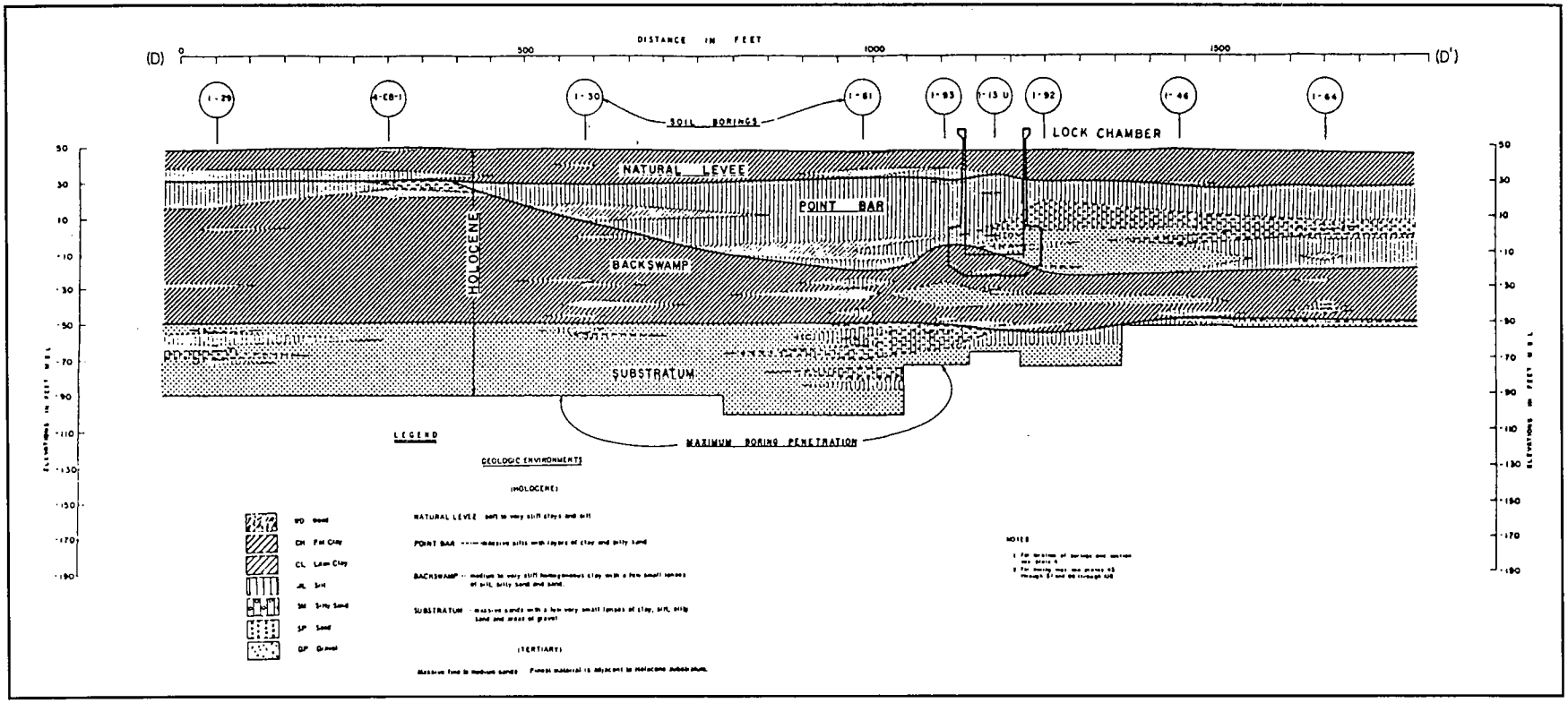

Figure 11. Geologic profile D-D'

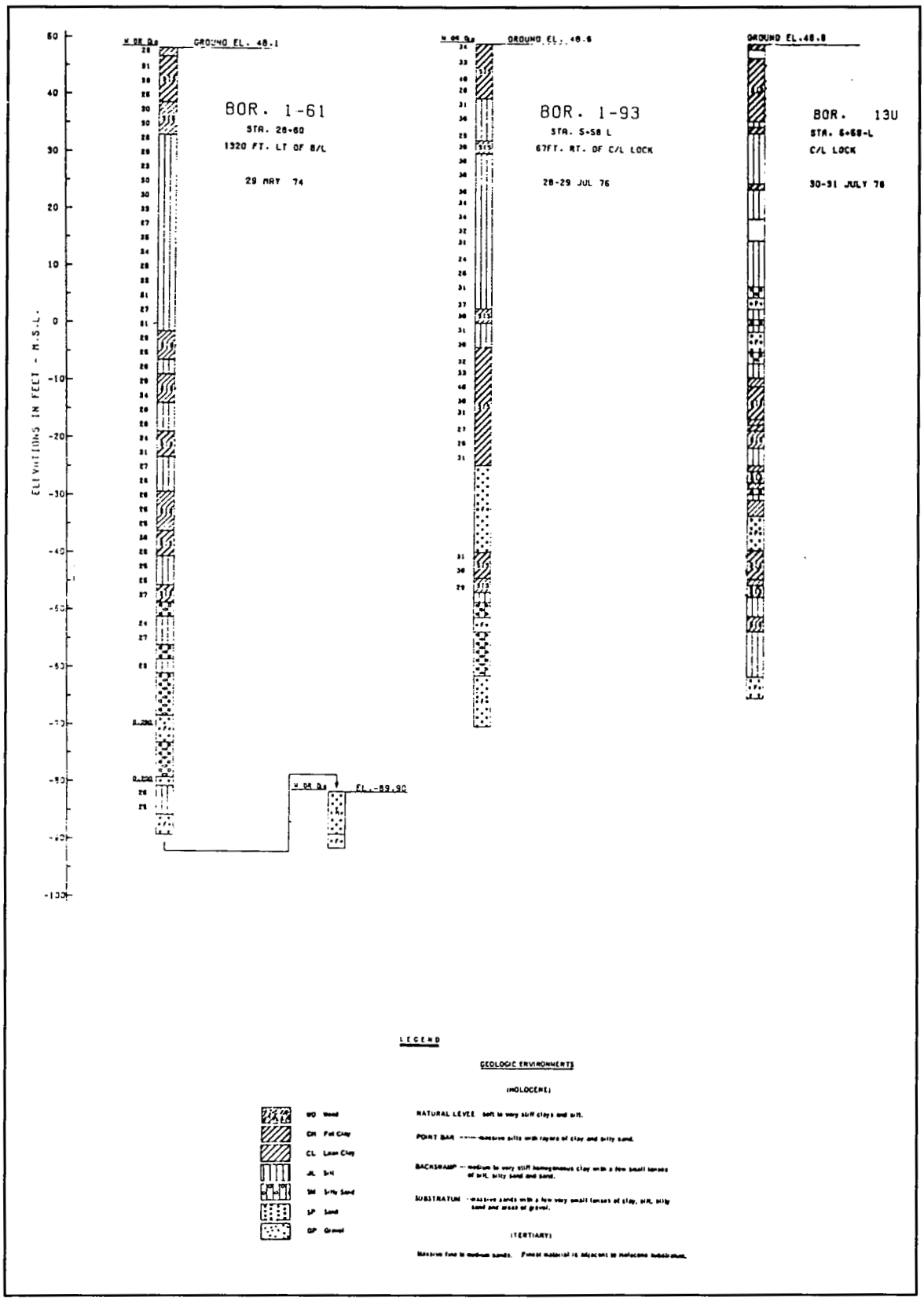

Figure 12. Borings 1-61, 1-93, and 13U, along geologic profile D-D′

Study Objectives

The principal objective of the study described in this report is to assess potential lock performance with the construction of a reinforced soil berm adjacent to the riverside lock wall. The intent of this structure is to provide a permanent solution to the problem of siltation against the lock. Because of the nature of the problem the conventional analysis techniques, which are based upon the equations of equilibrium and used in the design of the reinforced soil berm, are unable to provide sufficient information to satisfactorily evaluate performance of this type of structure with regard to its interaction with the lock and the surrounding foundation soil strata. The evaluation of the soil-structure interaction is being preformed using the finite element method and a state-of-the-art analysis procedure.

The results of this study depict the behavior of the lock, the reinforced soil berm, and the foundation soil strata when subjected to various loading conditions occurring during the operational life of the structure. Lock behavior is presented in terms of earth pressures and base pressures; mobilized friction angle along the exterior of the lock; earth pressure coefficients; displacements of the lock, backfill, and foundation; and bending moments within the lock structure. The reported earth pressure coefficients include both horizontal and vertical forces. The deformations of the reinforced soil berm, the magnitude of forces developed within the layers of reinforcement, and the stress level developed within the soil phase of the reinforced berm are also presented. The changes in stresses and displacements at several points within the soil foundation are followed through the course of lowering of the water table at the site, excavation, construction of the lock and backfilling, construction of the berm, operation of the lock, and flood stages of the river.

Lock Monolith Analyzed

Lock monolith no. L-10, shown in Figure 5, is evaluated in the soil-structure interaction study. This monolith is located midway along the chamber at station 4+12L. The corresponding geologic section at this location, section D-D′, is shown in Figure 11. This monolith was selected for study for two reasons: it is a representative section midway along the lock chamber, and field instrumentation is located at this section. The existence of field instrumentation data provides the opportunity to assess the accuracy of the model used in the analysis. Specifically, the accuracy of the nonlinear finite element model is established by comparing the earth pressures and base pressures computed by the finite element analyses to those measured on the walls and the base of the lock.

Analysis Description

The two-dimensional soil-structure interaction finite element computer program SOILSTRUCT is used to assess the behavior of the lock by simulating the sequence of lock construction and backfilling, as well as the various water and silt loadings applied to the structure. This aspect of the procedure of analysis is important because the stress-strain response of soil is nonlinear and stress-path dependent. Experience with previous soil-structure interaction studies has shown that to compute accurate values of stresses and displacements within the soil foundation, soil backfill, and the lock, the sequence of the construction operation at the site must be followed in the analysis. The modeling of the construction, backfilling, and loadings during the course of the analyses is done in a series of increments. This allows the constitutive model to simulate the nonlinear stress-strain soil response during each sequence of loadings.

Another important SOILSTRUCT feature is the ability to allow for the relative movement between the soil and the structure using interface elements. This feature is of great importance for accurately computing the normal earth pressures and shear stresses acting on the lock walls. Unlike conventional equilibrium procedures, this procedure does not require the use of predetermined earth distributions applied to the lock but allows for the development of these stresses through the soil-structure interaction that occurs during construction of the lock, backfilling, and water and/or silt loadings. This procedure of analysis has been successfully used in the past for a wide variety of soil-structure interaction problems and structures, including the evaluation of Port Allen and Old River locks (Clough and Duncan 1969).

Sequences of analyses

The soil-structure interaction evaluation of Red River Lock and Dam No. 1 was conducted in two phases. The first phase consisted of an evaluation of the behavior of lock monolith no. 11, it's backfill, and it's foundation during all stages of lock construction and for four operational load cases. Stages of construction discussed in this report include after lowering the water table at the site, after excavation, and upon completion of lock construction and backfilling. The computed results for four operational load cases for which instrumentation data are available were then analyzed and the results compared to the measured earth pressure measurements. One of these operational load cases includes silt loads acting on the lock. This provides the opportunity to verify the accuracy of the nonlinear finite element model and establish a baseline for the assessment of the response of the lock to the construction of the reinforced wall and their interaction during siltation.

The second phase of the analysis consisted of a series of soil-structure interaction analyses with the construction of the reinforced soil berm and

the response of the lock, soil foundation, and berm-to-water-and-silt loadings.

In addition to the finite element analyses, the variation of internal bending moments within the U-frame lock was computed using the computer program CUFRAM (Dawkins 1987) for select load cases. CUFRAM is a frame analysis program developed explicitly for the analysis of a U-frame lock. These analyses were used as verification of the computed values for the bending moments developed from the finite element stress distributions within the lock.

Finite elements

In this study, three types of SOILSTRUCT elements were used in the finite element model of lock monolith no. L-10: quadrilateral, interface and bar elements. The quadrilateral elements were used to model the lock, backfill, and the soil foundation. Interface elements were used to model the region between the soil and the lock. Bar elements were used to model the reinforcement within the soil berm in the phase 2 studies.

The soil and lock were modeled by use of a two-dimensional, plain strain, subparametric, quadrilateral element, QM5, which is defined by four nodes at the corners of the element. The shape functions of the QM5 element are of the linear variety along the boundary, with reduced integration for the shear terms. The QM5 element was developed to improve the bending behavior of the basic four-node element and eliminate the need for using higher-order elements in "bending" cases (Doherty, Wilson, and Taylor 1969). Bending is the primary means by which U-frame locks respond to water loads and soil loads. The four corner nodes have 2 degrees of freedom (DOF) each. Two additional internal element DOF's are located at the center of the element. The DOF's are generated within the computer program when the local stiffness matrix is formulated.

In the finite element model of the U-frame lock and the soil backfill, interface elements were placed along the exterior face of the lock between the soil and concrete structure. The interface element employed by SOILSTRUCT is the four-node, 0-thickness element developed by Goodman, Taylor, and Brekke (1968). It allows for controlled relative movements along the interface between the backfill and lock wall or between the soil foundation and the base of the lock. The importance of the use of interface elements on the computed results in soil-structure interaction studies has been demonstrated for a number of structures, including the analyses of Port Allen and Old River locks by Clough and Duncan (1969).

A third type of SOILSTRUCT element used in the phase 2 studies of the behavior of a reinforced soil berm constructed riverside of the lock is a one-dimensional bar element. The bar element is used to model the reinforcement per linear foot within the berm. The formulation of the element is similar to a truss member which responds to loading in tension

or compression along the line of the member. Details regarding the features of the soil reinforcement model using bar elements and its implementation in the analyses are described in Chapter 3 of this report.

Nonlinear soil model

Soils have a nonlinear stress-strain response to loading. This type of behavior is captured in SOILSTRUCT by combining a nonlinear constitutive model with an incremental analysis procedure, as described by Duncan and Chang (1970). Details regarding the SOILSTRUCT computer program are described by Ebeling, Peters, and Clough (1990). This particular type of nonlinear model is the most widely used in finite element studies involving soils or soil-structure interaction because of its relative simplicity and its ability to model key aspects of the soil response.

The constitutive model is shown in Figure 13 with a stress-strain response to loading being either primary loading or unload/reload behavior. For primary loading, the stress-strain curve is represented by a nonlinear, hyperbolic curve, the shape of which is dependent upon both the confining stress and the Mohr-Coulomb strength parameters of the soil. During unloading or reloading, the soil behavior is approximated by a linear response. Stress-strain response by primary loading is distinguished from unload/reload response by comparing the magnitude of the current total deviator stress to the maximum value of deviator stress attained during any of the previous stage(s) of loading. Soil responds to loading along the unload/reload stress-strain curve when the current deviator stress is less than any prior maximum value; otherwise, it responds to loading in a nonlinear fashion along the primary loading curve of Figure 13 until failure is reached.

In the soil model, the strength of the soil is defined by the conventional Mohr-Coulomb criterion, with the soil strength parameters specified by the friction angle and the cohesion. If the stresses in an element are equal to or exceed those allowed by the Mohr-Coulomb limits, the modulus is set to a very low value so that the element will not take on any additional shear stresses; however, the hydrostatic stresses can be increased. Additional details regarding the incremental construction procedure of analysis and the stress-strain model for the soil elements are given in Appendix A.

Soil-to-Lock Interface Model

Interface elements are used to allow for relative movement between different material regions, such as between the soil backfill and the lock wall. The constitutive model, as formulated by Goodman, Taylor, and Brekke (1968), is defined by two parameters, an interface normal stiffness, and an interface shear stiffness. To prevent the sides of the interface element from overlapping one another, the value of interface normal

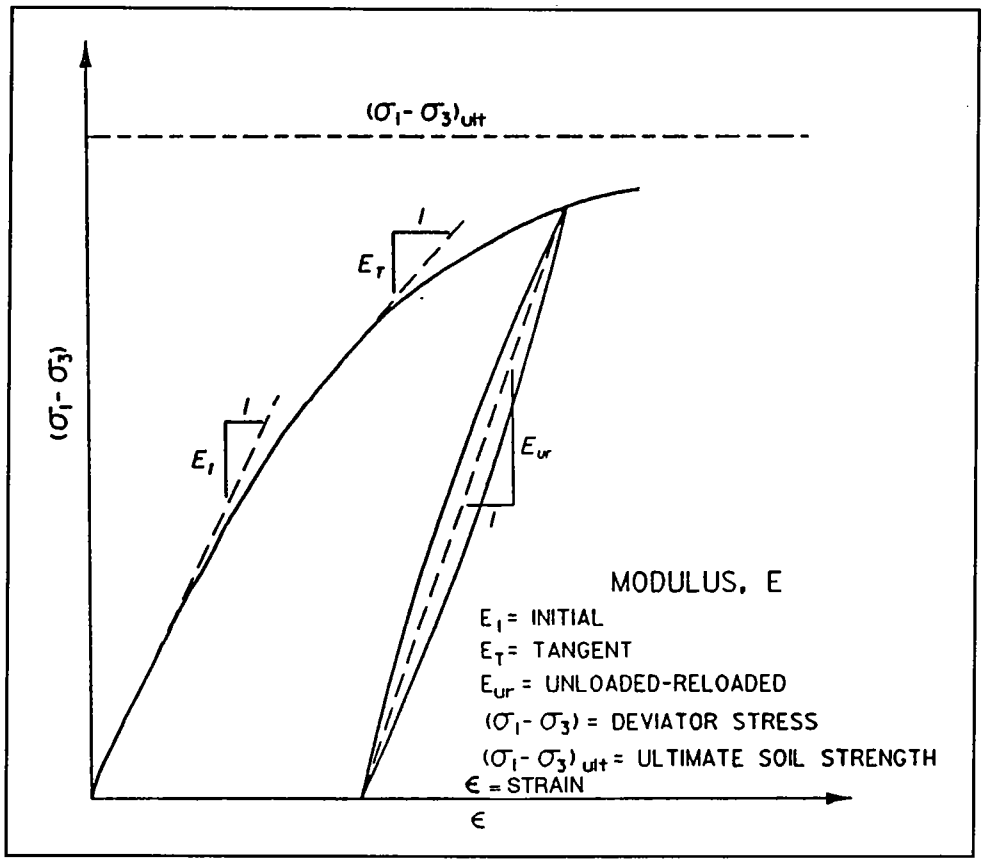

Figure 13. Hyperbolic representation of stress-strain curve for soil

stiffness is set to a high value in SOILSTRUCT. Extensive soil to concrete interface direct shear tests conducted by Clough and Duncan (1969) and Peterson, Kulhawy, Nucci and Wasil (1976) have shown the shear stress-relative shear displacement to be nonlinear. In fact, extensive tests using a varity of soils have shown the shape of this curve to be similar to the nonlinear stress-strain response of soils discussed in the previous section. This observation led Clough and Duncan (1969) to propose a hyperbolic curve for the shear stress versus relative shear displacement relationship shown in Figure 14.

The shear stiffness for the interface depends upon the normal stress on the interface and the strength along the soil to concrete interface. The interface strength is defined in terms of the Mohr-Coulomb criterion. If the shear stress in an interface element equals or exceeds those allowed by the Mohr-Coulomb limits, the shear modulus is set to a very low value so that the element will not take on any additonal shear stresses. Further details regarding the model for the interface elements are given in Appendix A.

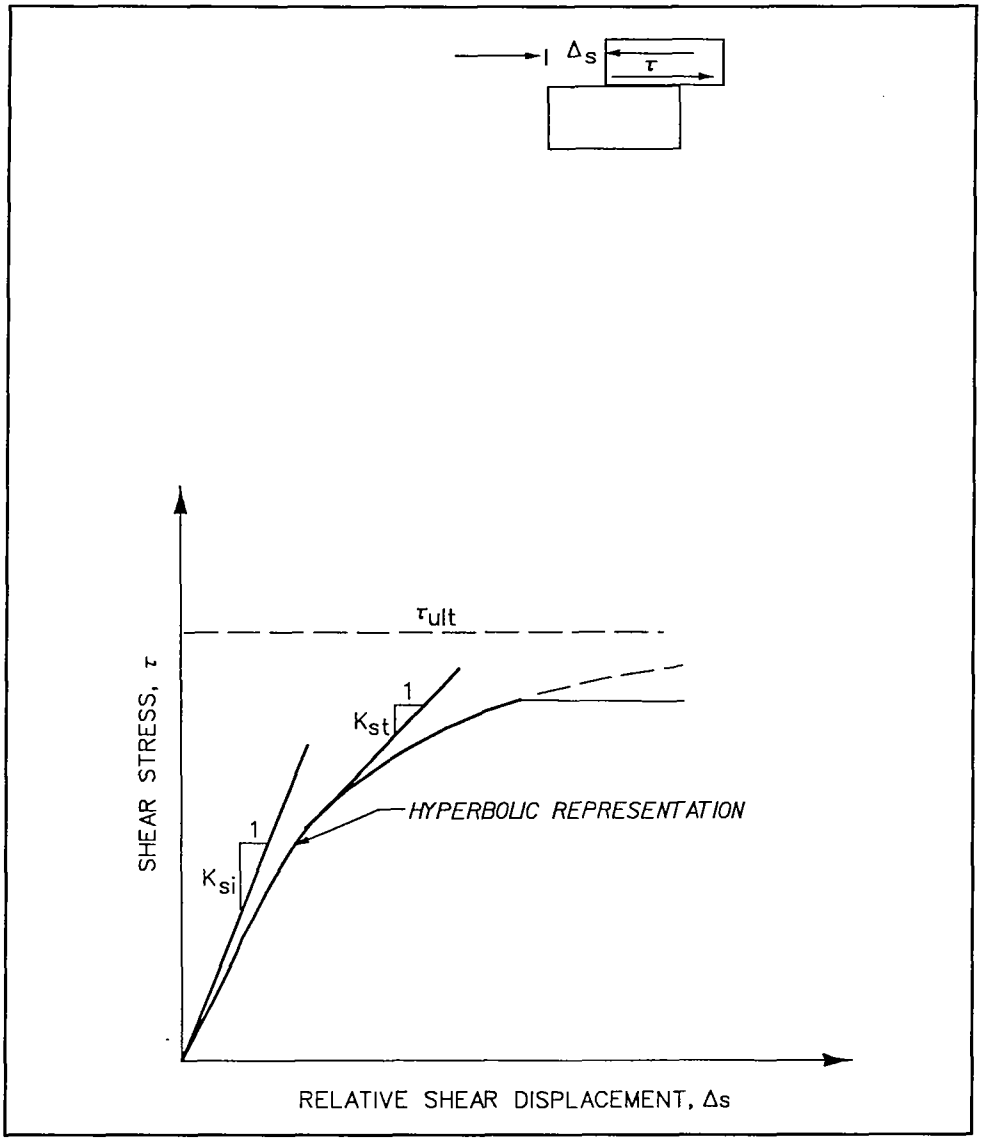

Figure 14. Hyprobolic representation of interface shear stress-relative shear displacement curve

Soil material parameters

The material properties and hyperbolic parameters assigned to the soil foundation and soil backfill are listed in Table 1. Drained properites were specified in the analyses after considering the time required for excavation of the site and construction of the lock, heterogeniety and thickness, and permeability of the foundation strata. The soil properties were obtained from laboratory test data, as described in Ebeling, Mosher, and Abraham (1991) or were estimated based upon published data found in the reports by Clough and Duncan (1969) and Duncan, Byrne, Wong, and Mabry (1978). These values are appropriate for the conditions existing at lock monolith no. L-10. Due to the heterogeniety of the Backswamp

Table 1
Drained Hyperbolic Stress-Strain and Strength Parameters

Location	Soil Type[1]	Unit Weight (lbs/ft^2)	Strength Parameters		Hyperbolic Parameters						Comments
			C′ (tons/ft^2)	ϕ′ (degrees)	K	n	K_{UR}	K_B	m	R_F	
											Avg. D_r = 48%
Foundation	Point Bar Sands, SP	117	300	31	330	0.6	500	300	0.2	0.7	
	Point Bar Silty Sands, SM	117	300	33	330	0.6	500	300	0.2	0.7	
	Point Bar Silts, ML	117	300	33	330	0.8	500	300	0.2	0.7	
	Backswamp Deposit	115	300	28	90	0.8	360	100	0.2	0.7	
	Substratum Sand,. SP	122	0	33	1,160	0.5	1,750	600	0.2	0.7	
											Avg. D_r > 71% by SPT correlation
Backfill	Compacted Sand, SP	122	300	35	500	0.5	600	150	0.2	0.7	D_r > 85%
	Compacted Selected Clay, CL and CH	112	300	30	120	0.8	250	110	0.2	0.7	Greater than 95% Relative Compaction
Reinforced Soil	Sand, SP	122	0	34	500	0.5	600	150	0.2	0.7	

[1] According to the ASTM Soil Classification System (ASTM 1990)

Equations for soil stress - strain model

$$E_i = K \cdot P_A \cdot (\sigma_3 / P_A)^n \qquad E_{UR} = K_{UR} \cdot P_A \cdot (\sigma_3 / P_A)^n$$

$$E_t = E_i (1 - R_F \cdot SL)^2 \qquad BULK = K_B \cdot P_A \cdot (\sigma_3 / P_A)^m$$

$$SL = (\sigma_1 - \sigma_3) / (\sigma_1 - \sigma_3)_{FAILURE} \qquad P_A = atmospheric\ pressure$$

Deposit, the Point Bar Deposit, and the size of elements employed in the mesh, the material characterization listed in Table 1 may not be applicable for some locations along the lock. This detail is discussed in Chapter 4 of this report.

Lock material parameters

The lock structure is assumed to behave in a linear elastic manner. The two values for the elastic material constants of the concrete are a Young's modulus equal to 3×10^6 psi (4.32×10^8 psf) and a Poisson's ratio equal to 0.2.

Interface material parameters

The material properties and hyperbolic parameters assigned to the soil to lock interface elements are listed in Table 2. Interface properties were estimated based upon soil-to-concrete interface direct shear tests conducted and published by Clough and Duncan (1969), Peterson, Kulhawy, Nucci and Wasil (1976) and Potyondy (1961). The soil-to-concrete cohesion values were set equal to zero for all interface regions. The value of interface normal stiffness is set equal to 1×10^8 pcf within SOILSTRUCT.

Table 2
Interface Parameters

Interface Region	Soil Type	Interface Friction Angle, deg	K_j[1]	n_i[1]	R_{fi}[1]
Stem	Compacted Select Clay	30	1×10^4	0.8	0.9
Stem and Culvert	Compacted Sand	35	1×10^4	0.8	0.9
Base	Backswamp Deposit	28	1×10^4	0.8	0.9

[1] Definitions may be found in Appendix A, page A2, of this report.

Equations for Interface Model

$$k_{st} = k_{si}(1 - R_{fi}SL_i)^2$$

$$k_{si} = K_j \gamma_w \left(\frac{\sigma_n}{p_a}\right)^{n_i}$$

$$SL_i = \tau/\tau_{failure}$$

Organization of Documentation

The contents of this report are presented in chronological order according to the progression of work accomplished. The study was divided into two categories, material characterization of the site and the analysis of lock monolith no. L-10. The results from the material characterization study, conducted prior to the analyses which are discussed in this report, are presented in a companion report titled "Numerical Material Characterization of Red River Lock and Dam No. 1 Site" by Ebeling, Mosher, and Abraham (1991). The values for all of the material parameters assigned to all the soil strata and structural materials in the analyses are summarized in this report. The results from all analyses are presented in this report. The analyses were divided into two phases. The first phase involved the development and analysis of a model of lock monolith no. L-10, its backfill and soil foundation to predict performance of the lock to four loading conditions for which instrumentation results exist. A description of the history of lock monolith no. 10 construction and backfilling is presented in this section. This work phase also involved the reduction of the field data recorded at lock monolith no. L-10 for four operational load cases. One of the four load cases includes siltation at the lock during the flood in the Spring of 1985. These results are discussed in Chapter 2 of the report.

Phase 2 involved the development and analysis of the model used to predict field performance of the lock and the soil foundation with the construction of a reinforced soil berm riverside of the lock and the response of the lock and foundation to several water and silt load cases. These results are presented in Chapter 3. The material properties assigned to the reinforcement as well as the layout of the reinforcement within the soil berm are described. Also included in this section is a discussion of the factors which may contribute to variations in the response of the lock and soil foundation based on those results computed for lock monolith no. L-10. These factors include the variation in the soil foundation conditions along the length of the lock and time for consolidation of the foundation soils. A discussion of the difference in the computed magnitudes of settlement obtained using one-dimensional settlement theory as compared to those obtained using two-dimensional finite element results is also presented.

Chapter 4 presents a summary of the results from the phases 1 and 2 studies, the conclusions, and design recommendations for the reinforced soil berm. Several design details to be addressed during the course of the design of the reinforced berm are listed.

Appendix A describes the use of the bar element in SOILSTRUCT to simulate the reinforcement within the soil berm.

2 Results of the Phase 1 Studies - Comparison to Field Instrumentation Measurements

This chapter describes the results of the phase 1 soil-structure interaction analyses of lock monolith no. 10 during its construction and operation. The objective of the Phase 1 study was to assess the accuracy of the non-linear finite element model so that it could be used with confidence in the Phase 2 assessment of the potential performance of the proposed reinforced berm. The phase 1 study consisted of modeling the initial state of stress prior to construction, dewatering and excavation of the site, construction of the lock, listed as stages A through D in Table 3, and operation of the lock at key river levels.

Table 3
Phase 1 Finite Element Analyses - Construction Stages

Construction Stage	Description
A	Initial state of stress prior to construction
B	Lower water table at site
C	Excavate site of New River Channel and Lock
D	Lock construction and backfilling

The finite element results are presented in terms of stresses and displacements within the soil foundation, soil backfill, and the lock at all stages of loading. These results are reported for tests conducted after the completion of each stage of loading. The variation in moments within the lock were computed using the resulting stress distributions from the finite element analyses. For comparison purposes, the distributions of moments within the lock were computed using the program CUFRAM for one of

the operational load cases. CUFRAM is a frame analyses program specifically developed for the computation of the moment distribution within a U-frame lock given internal and external water table elevations and applied earth and base pressure distributions.

The results of dewatering and excavation are presented first. They are followed by the presentation of the comparison of the finite element results for construction of the lock and placement of the surrounding backfill with the instrumentation measurements. Finally, the comparisons are presented between the finite element results and three key operational conditions.

Instrumentation at Lock Monolith No. 10

A wide variety of instrumentation was installed at Red River Lock and Dam No. 1 during the construction of these structures. The types of instruments include Casagrande open-tube piezometers, Carlson PE-50 stress meters, strain gages and resteel strain gages, concrete stress meters, inclinometers, surface monuments, reference bolts, and stainless steel plates. Details regarding the instrumentation, installation and measurements are discussed in detail in the reports by Anderson and Vanadit-Ellis (1987) and Vanadit-Ellis, Hall, and Graham (1988). During this study, data from the various instruments were reviewed and an assessment was made regarding the quality of the instrumentation data for each of the comparisons. Due to incomplete measurements and/or conflicting information from different instrumentation, the measurements provided by the stress meters and the piezometers were judged to be the most complete, reliable, and the most useful to this study. Therefore, the measurements from the Casagrande open-tube piezometers and Carlson PE-50 stress meters are also presented in the following sections in discussions of the results of the phase 1 analyses.

The layouts of the stress meters, SPM, within the backfill and along the base of lock at stations 4+12L and 4+10L, respectively, are shown in Figures 15 and 16. A total of 17 stress meters were placed along the foundation of lock monolith no. 10 prior to its construction. During backfilling, four pressure meters were placed along the riverside culvert wall and three pressure meters were placed along the landside culvert wall. Two pressure meters were placed along the top of each of the two culverts, and three pressure meters were placed along each of the riverside and landside stem walls, located immediately above the culverts.

Figure 17 shows the layouts of the piezometers, *P*, at monolith no. 10. Seven piezometers were placed within the foundation along the base of the lock, and six piezometers were placed within the backfill, three along the riverside, and three along the landside of the lock.

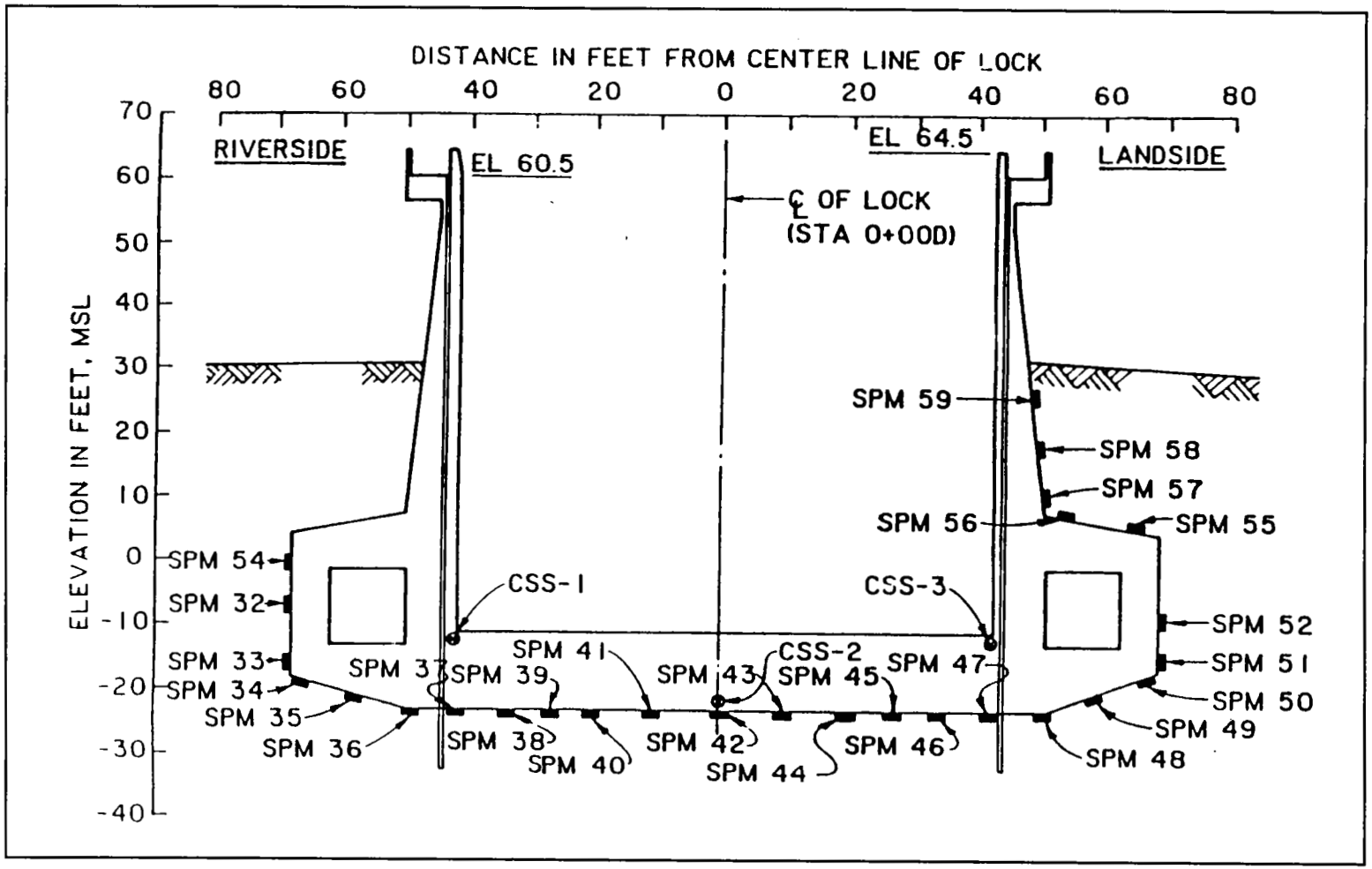

Figure 15. Layout of stress meters at lock monolith no. 10, station 4+12L

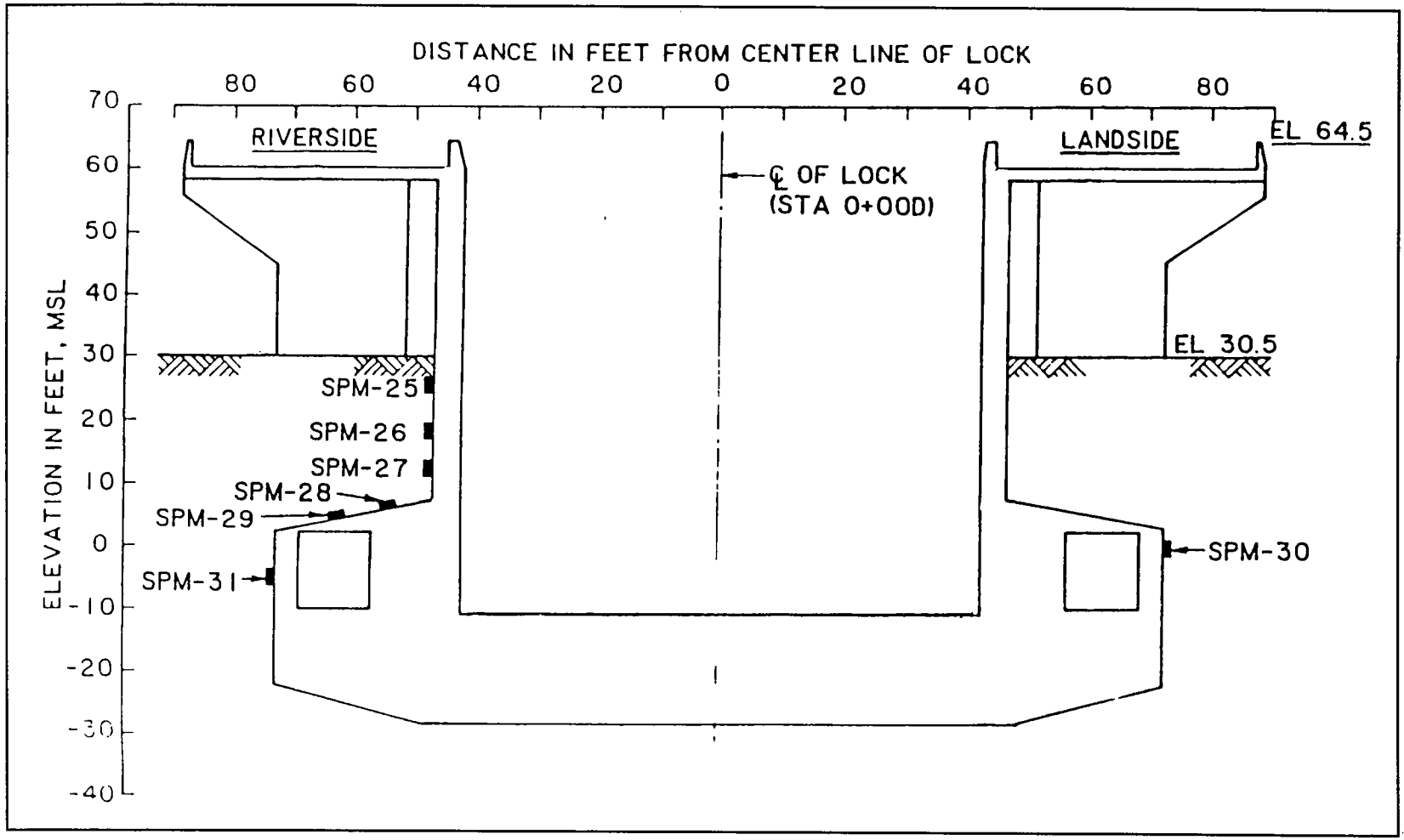

Figure 16. Layout of stress meters and piezometers at lock monolith no. 10, station 4+10L

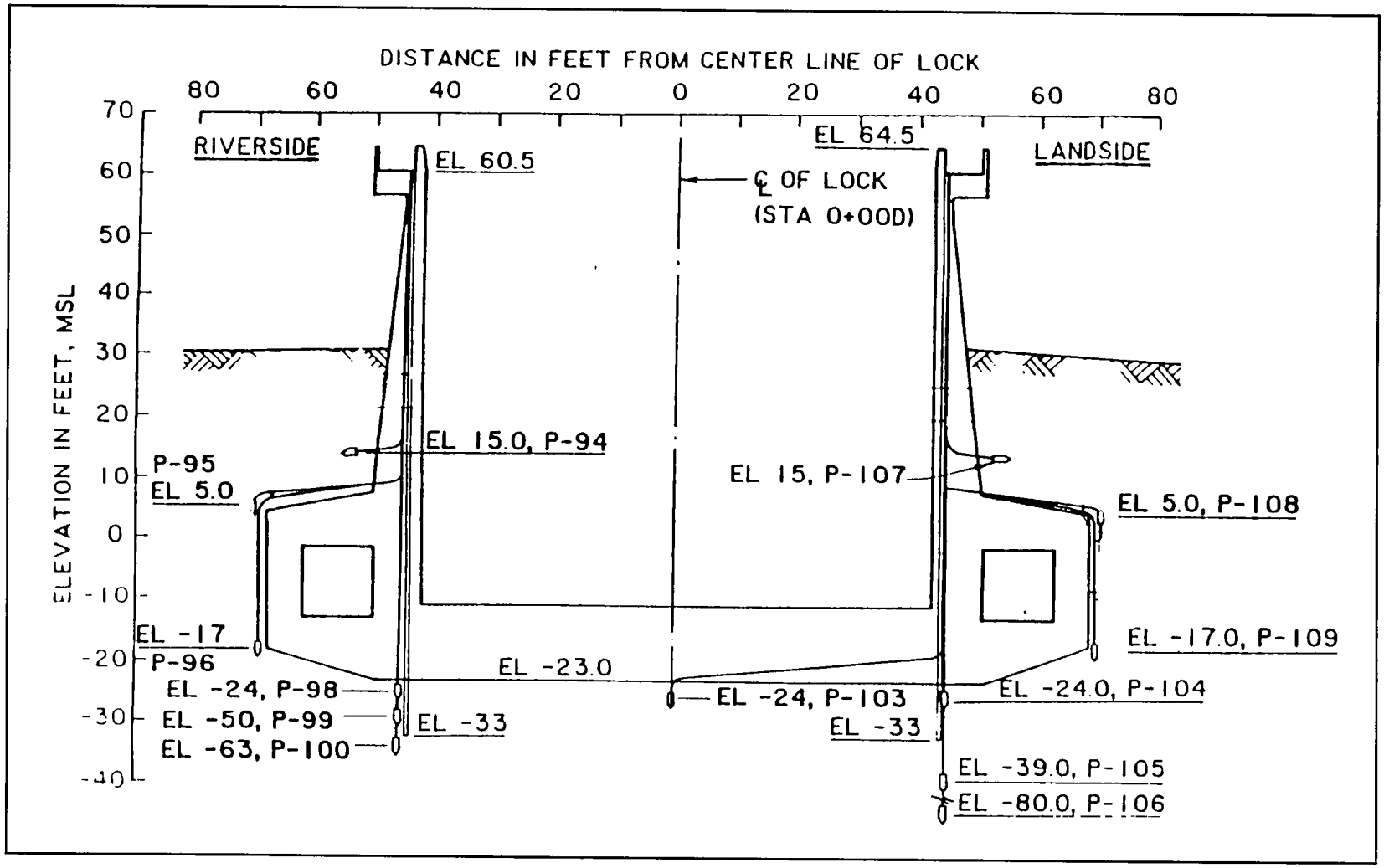

Figure 17. Layout of piezometers at lock monolith no. 10, station 4+12L

The objective of the phase 1 study was to assess the accuracy of the results from the finite element analyses. This was accomplished by subjecting the finite element model to a set of water and silt loads which were consistent with those existing at lock monolith no. 10 on days for which instrumentation records were available. The site conditions existing at the lock on 4 days between September 1983 and April 1985 were specified in the finite element analyses. On the dates selected, the water and silt elevations at the lock represent key load cases for the lock. The first set of instrumentation measurements that are compared with the results from the finite element analyses were recorded 22 September 1983, after completion of the construction of the lock and backfilling and prior to flooding of the lock and the new river channel. Since no instrumentation was placed prior to the completion of the dewatering and excavation of the lock site, no comparisons could be made between instrumentation and the results and previous stages of the finite element analyses. Comparisons are also made for the three key operational load cases listed in Table 4. The first operational load case was recorded on 30 September 1984 when the river was at a low water level. The second operational load case was recorded on 1 January 1985 when the river was at a high water level. The third operational load case was recorded on 4 April 1985 when the river was at a high water level and siltation was occurring along the river channel and against the lock walls.

Table 4
Phase 1 Finite Element Analyses - Operational Load Cases

Case No.	Description	Date of Field Instrumentation Measurement
1	Lower pool at el 11	30 September 1984
2	Lower pool at el 40	1 January 1985
3	Silt loading	4 April 1985

Dewatering and Excavation

The finite element analyses modeling the lowering of the water table and excavation of the site of the lock and new river channel are discussed in this section. These loading cases correspond to construction stages A, B, and C listed in Table 3. The objective of these first three series of analyses is to develop an effective stress regime within the soil foundation that is consistent with that existing in the field **after excavation**. To reach this stress state, simplifying assumptions regarding the moduli assigned to the soil foundation elements were made. These assumptions affected the magnitude of the **computed displacements** for these first three series of

analyses. In general, these assumptions will result in larger computed displacments than would be expected to occur in the field. These assumptions will have minimal effect upon the effective stress regime calculated in these series of analyses and prior to construction of the lock. An additional requirement for the constitutive model of the soil is that the finite elements representing the soil retain the memory of previous maximum values of effective stresses because of the difference in stress-strain behavior during unloading (and reloading), as compared to primary loading. This affects both the magnitude of horizontal effective stresses computed and the magnitude of future computed displacements.

The effective stresses existing within the four soil strata prior to excavation, referred to as the initial condition in this report (stage A), are influenced by several factors. These factors include both current and previous site conditions, among which are; (a) the history of deposition and erosion of the strata, (b) the current elevation of the water table, and (c) past fluctuations in the groundwater table. Values for the horizontal effective stress are especially sensitive to effective stress history. The effective stress history of a soil sample is determined by comparing the resulting preconsolidation pressure, obtained from consolidation tests, to the current effective vertical stress existing in the field at the elevation from which that soil sample was obtained. The preconsolidation pressure for a soil sample is the maximum vertical effective stress the sample has ever experienced. This comparison was made using the results of consolidation tests on both backswamp clay deposit samples and natural levee deposit samples, reported in Design Memorandum No. 9 (USAED, New Orleans 1977).

The range in preconsolidation pressures computed from the results of one-dimensional consolidation tests on 30 natural levee deposit and backswamp deposit clay samples are plotted in Figure 18. The soil samples are classified as either CL or CH clays. They were obtained from 15 undisturbed borings conducted prior to excavation at the lock site. The initial total overburden pressure is also shown in this figure. The majority of the preconsolidation pressure values for the backswamp clay deposit samples recovered between el -23, the elevation at the base of the lock, and el -50, indicating the preconsolidation pressure value to be nearly equal to the total overburden pressure. Computations of the effective overburden pressure using the water table elevations observed during the 5 years of monitoring prior to excavation indicates that the Backswamp Clay Deposit is overconsolidated. Low river levels during previous years is one explanation for the high values of preconsolidation pressures. The data from the river gages show the river elevation can fluctuate tens of feet during the course of a single season. During the 5 years of monitoring, the river gage data show the river varied from a low elevation equal to 5 ft to a maximum value greater than the initial ground surface elevation at the site (el 50). The observation wells installed within the substratum sands prior to excavation show the water table at the site of the lock reflects changes in the river levels within a few weeks. Because of the need to introduce an appropriate effective stress history in the soil model, the details regarding

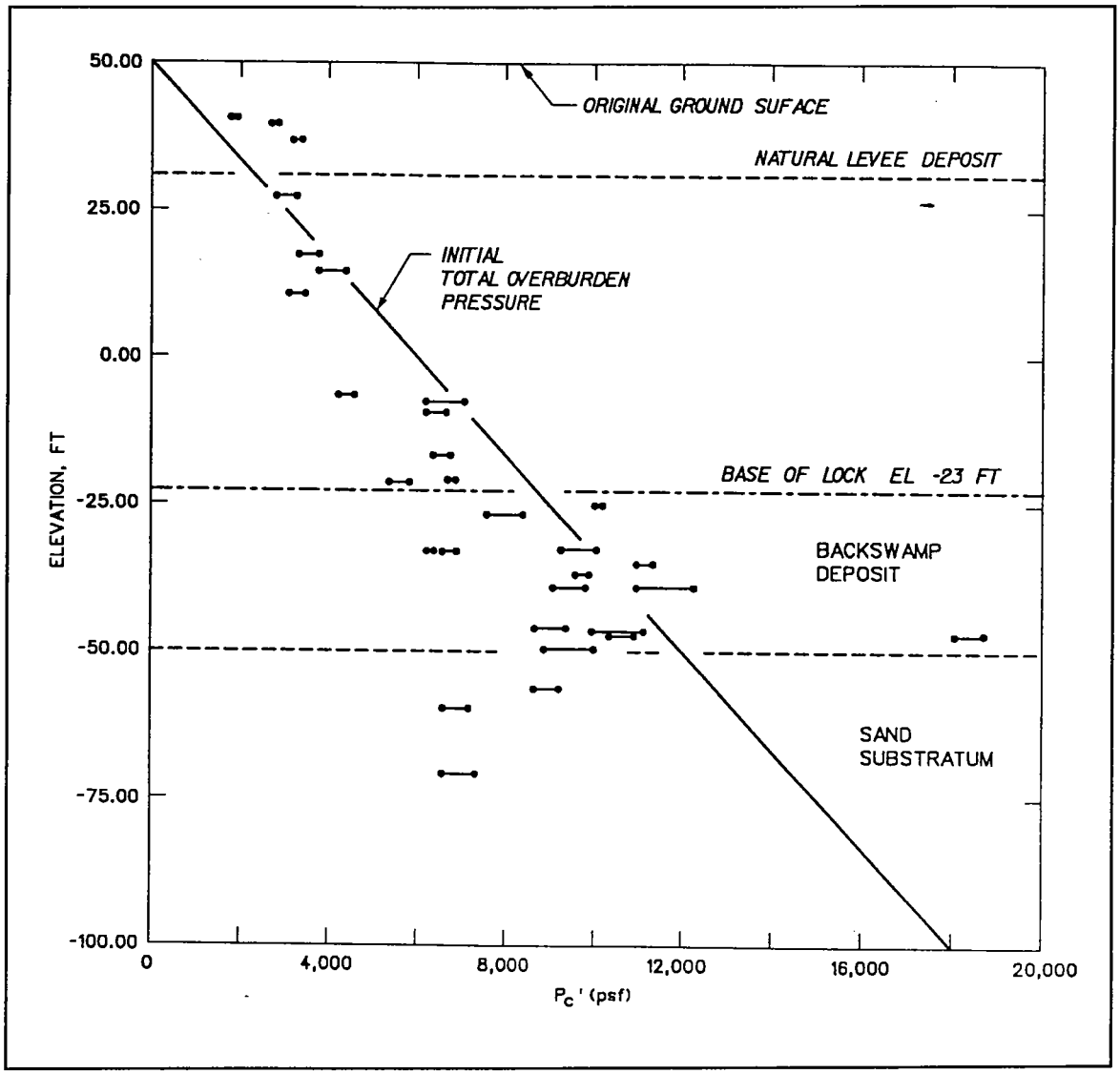

Figure 18. Range in preconsolidation pressures from consolidation tests on clay samples

the lowering of the water table and excavation in the finite element analysis were altered from the actual excavation schedule used in the field. The details of the finite element analyses are discussed in detail for these construction stages, stages A through C, in the following sections.

Construction Stage A - Initial State of Stress Prior to Construction

The geologic section D-D′ (Figure 11) corresponds to the location of lock monolith no. 10 and is modeled in the analysis. The finite element mesh of this cross section is shown in Figure 19. The mesh consists of

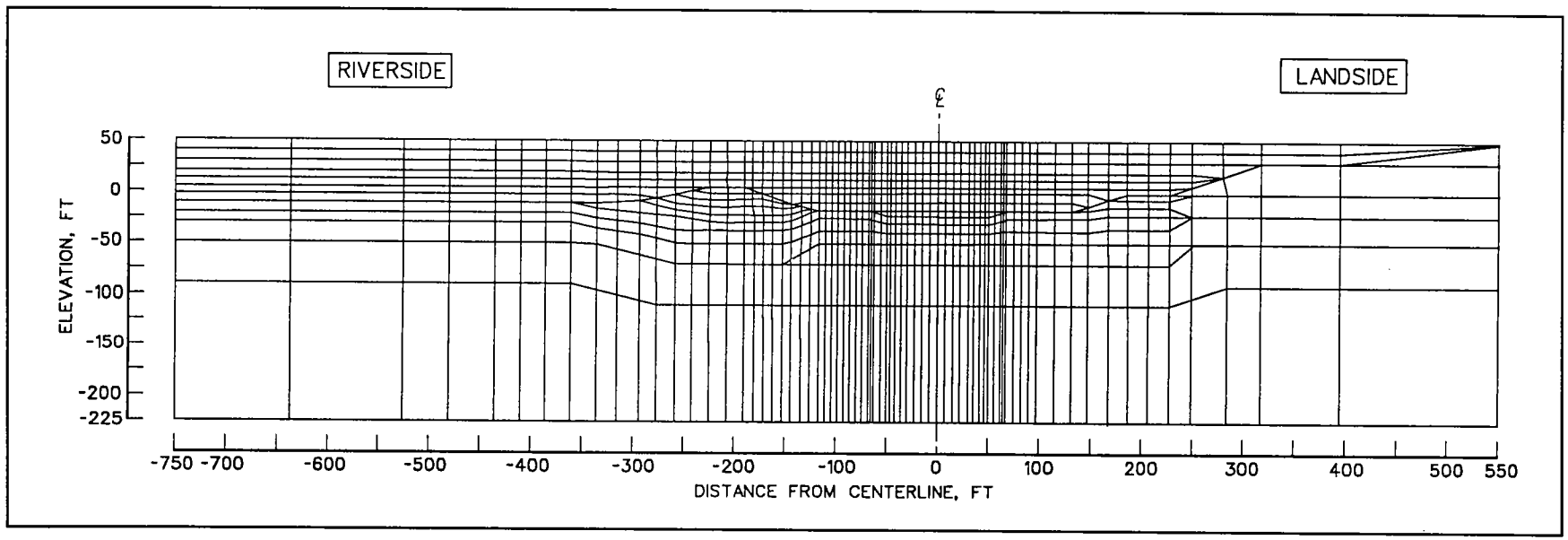

Figure 19. Initial finite element mesh prior to excavation at section D-D′

1,016 two-dimensional elements and 1,081 nodes. It is 1,300 ft long, extending 750 ft riverside from the center line of the lock and 550 ft landside of the center line. The mesh is 275 ft tall with the top of the mesh corresponding to the initial ground surface at el 50. The base elevation is -225 ft and is located within the substratum sands. The nodes along the sides of the mesh are limited to vertical displacements, while those along the base of the mesh are fixed against horizontal and vertical displacements. The four material property regions for this mesh are shown in Figure 20, with the corresponding material properties listed in Table 1. The initial water table is assigned to el 40.

The initial effective stresses were computed for the soil elements by use of the gravity turn-on method of analysis incorporated within the program SOILSTRUCT. During this computation, total unit weights were assigned to the soil elements above the water table, and submerged unit weights were assigned to those elements below the water table. The displacements of the nodes were set equal to zero.

The computed major principal effective stress for the elements was equal to the vertical effective stress and equal in value to the effective weight of submerged soil assuming hydrostatic pore water pressures. Figure 21 shows the variation in magnitude and orientation of the initial major principal effective stress valves of select elements within the lock foundation. Those elements for which the major principal effective stress values are shown in Figure 21 define the ground surface after excavation (stage C). These elements underwent the greatest changes in stresses during the course of the analyses.

Figure 22 shows the locations of five sections for which the variation in the ratio of horizontal effective stress to vertical effective stress, K_h*, with elevation is monitored throughout the analysis of the excavation. Figures 23 through 27 show the values of K_h* for the initial gravity turn-on analysis at the end of lowering of the groundwater and at the end of the excavation for the five sections shown in Figure 22. The value of K_h* after the gravity turn-on analysis is nearly constant within each stratum. These initial values for K_h* are equal to 0.68 for the natural levee and backswamp clay deposits, 0.67 for the point bar silt deposit and 0.54 for the sand substratum.

Construction Stage B - Lower Water Table

The water table was lowered in a series of 10 increments from el 40 to -35 during construction stage B (Figure 28). The computed settlements due to lowering of the water table are given in Figure 29 for select nodal points. These nodes define the ground surface after completion of the excavation (stage C). The computed settlement for the nodes identified in Figure 29 range in value from 7 to 9 in. Figure 30 shows the variation in magnitude and orientation of the computed major principal effective

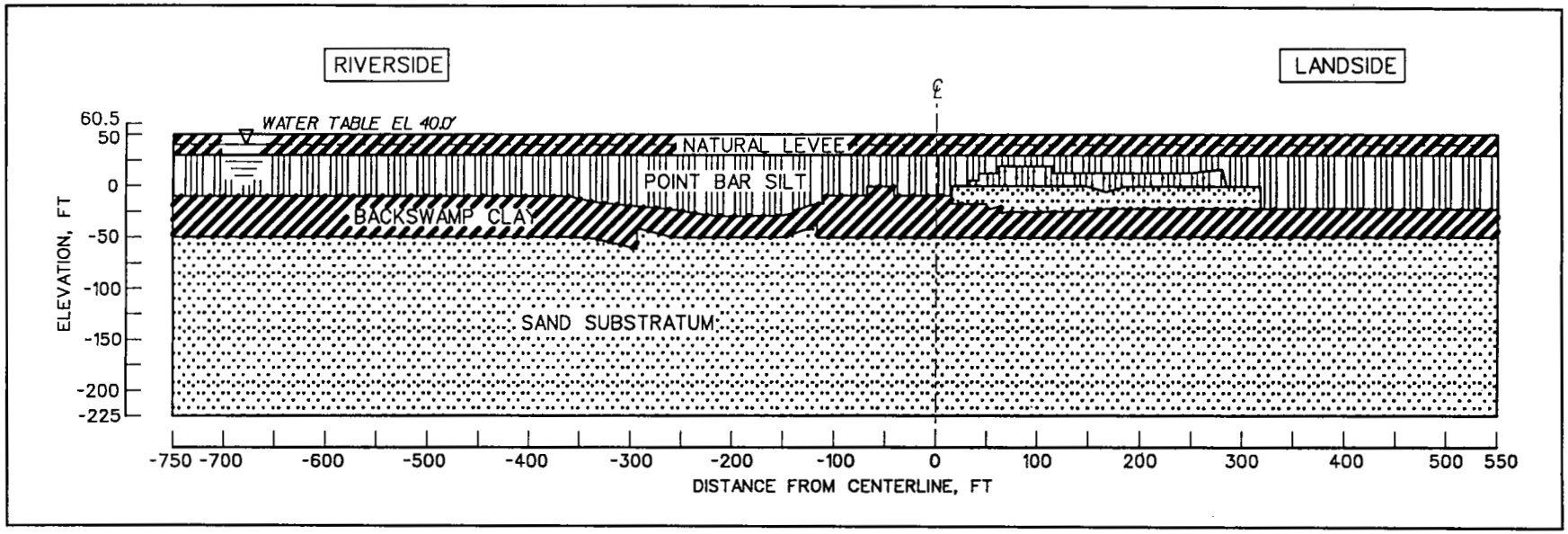

Figure 20. Material regions corresponding to initial finite element mesh - water table at el 40

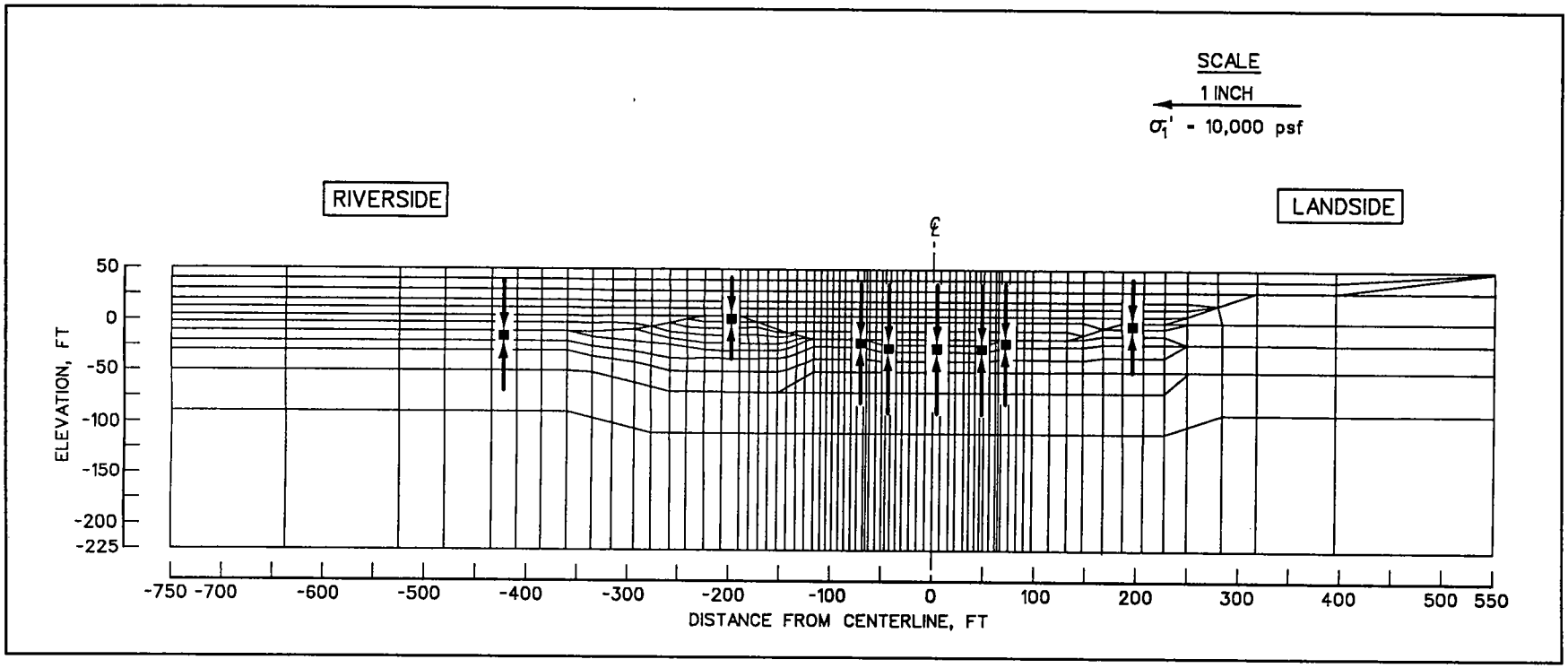

Figure 21. Initial major principal effective stresses for select foundation elements

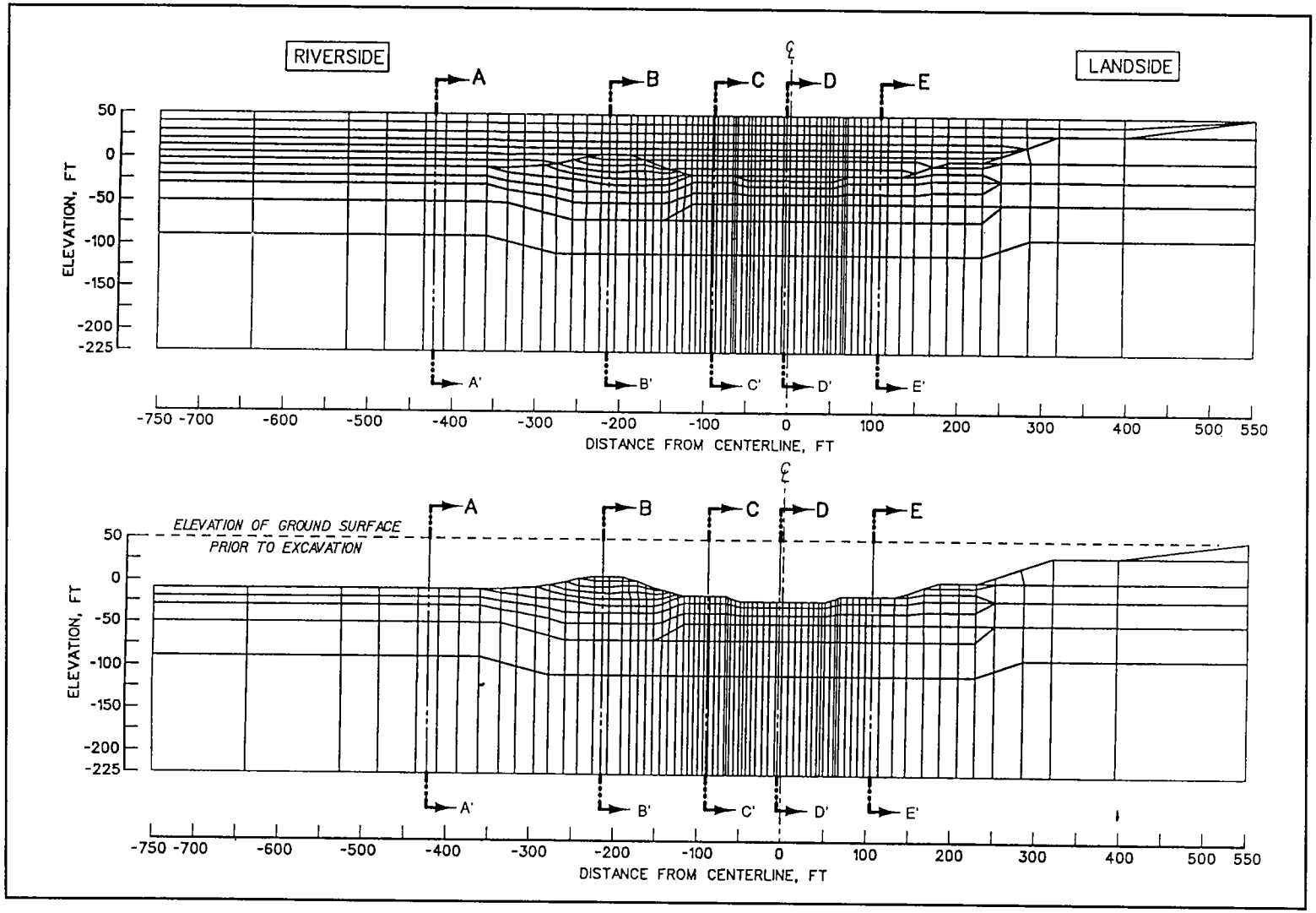

Figure 22. Five sections along which variation K_h^* with depth is computed

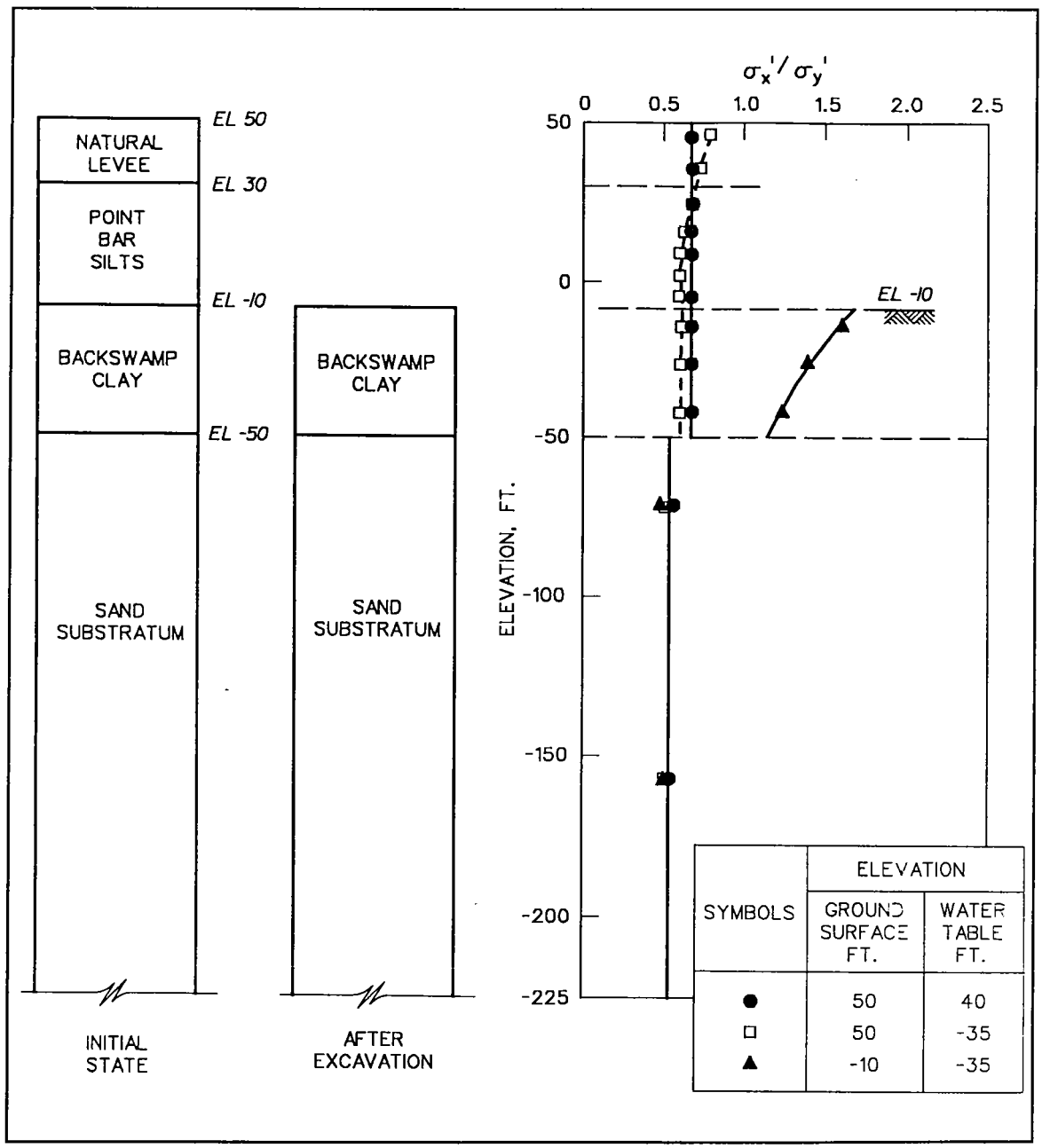

Figure 23. Ratio of effective horizontal stresses to effective vertical stresses along section A-A′

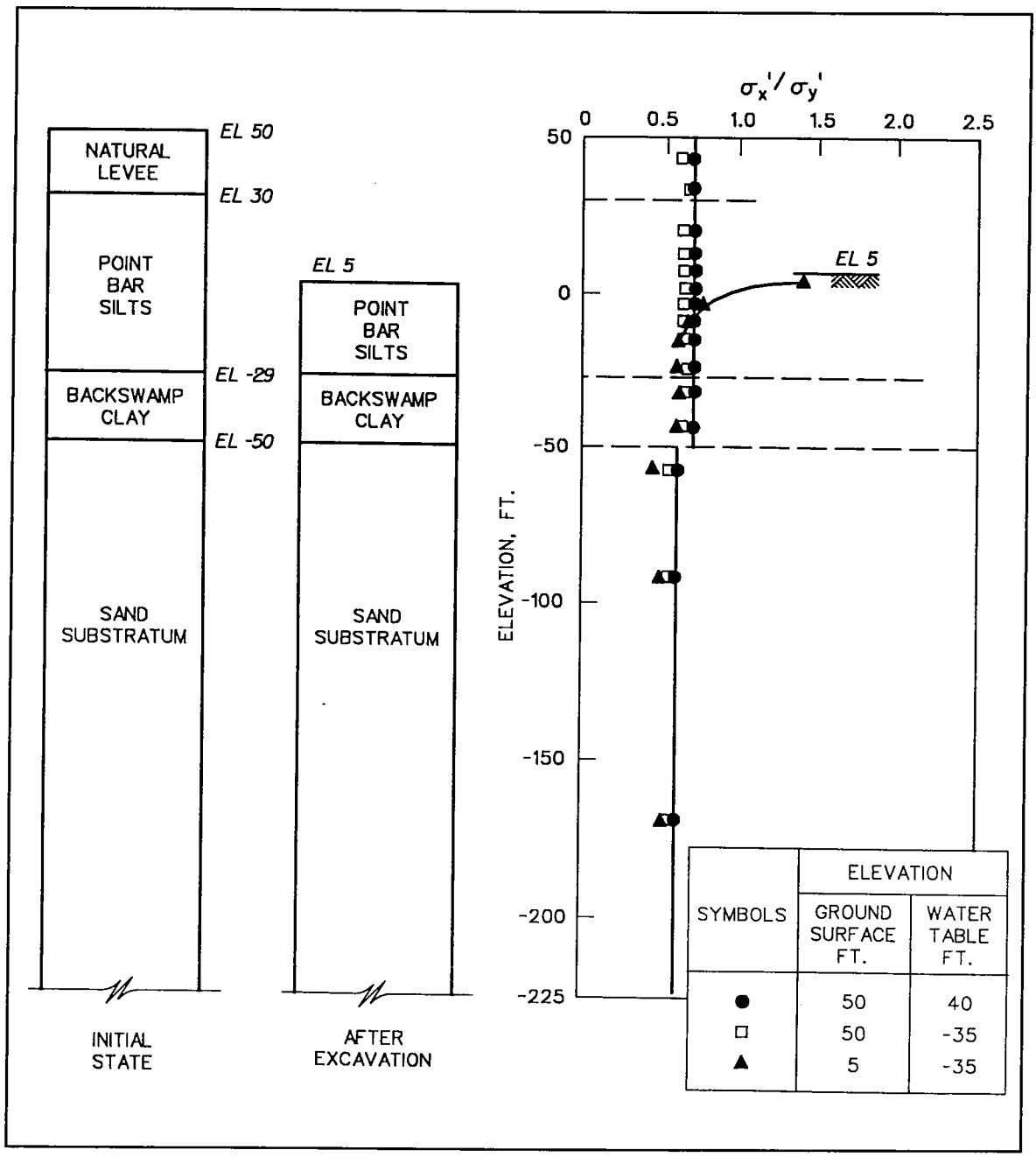

Figure 24. Ratio of effective horizontal stresses to effective vertical stresses along section B-B′

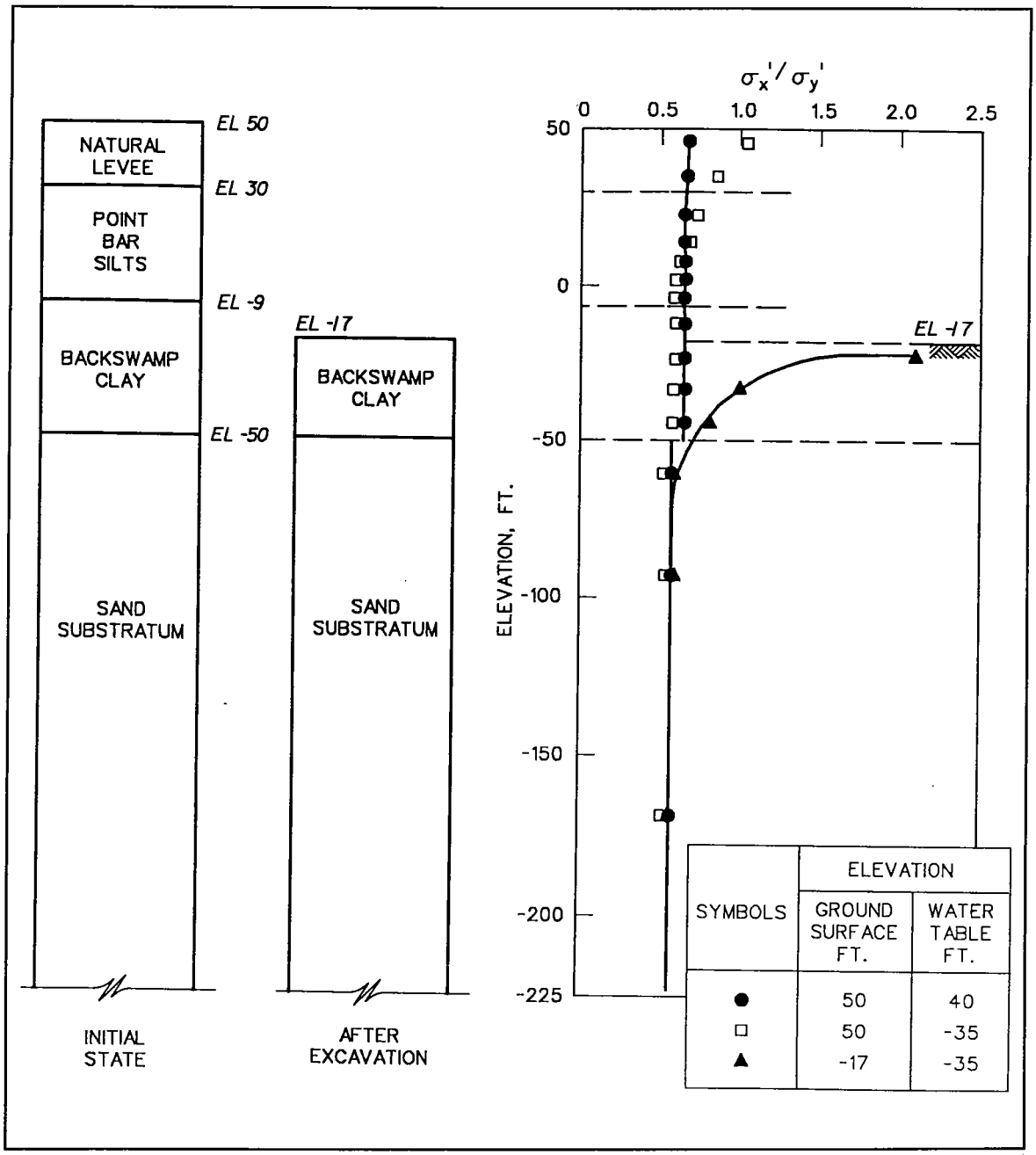

Figure 25. Ratio of effective horizontal stresses to effective vertical stresses along section C-C′

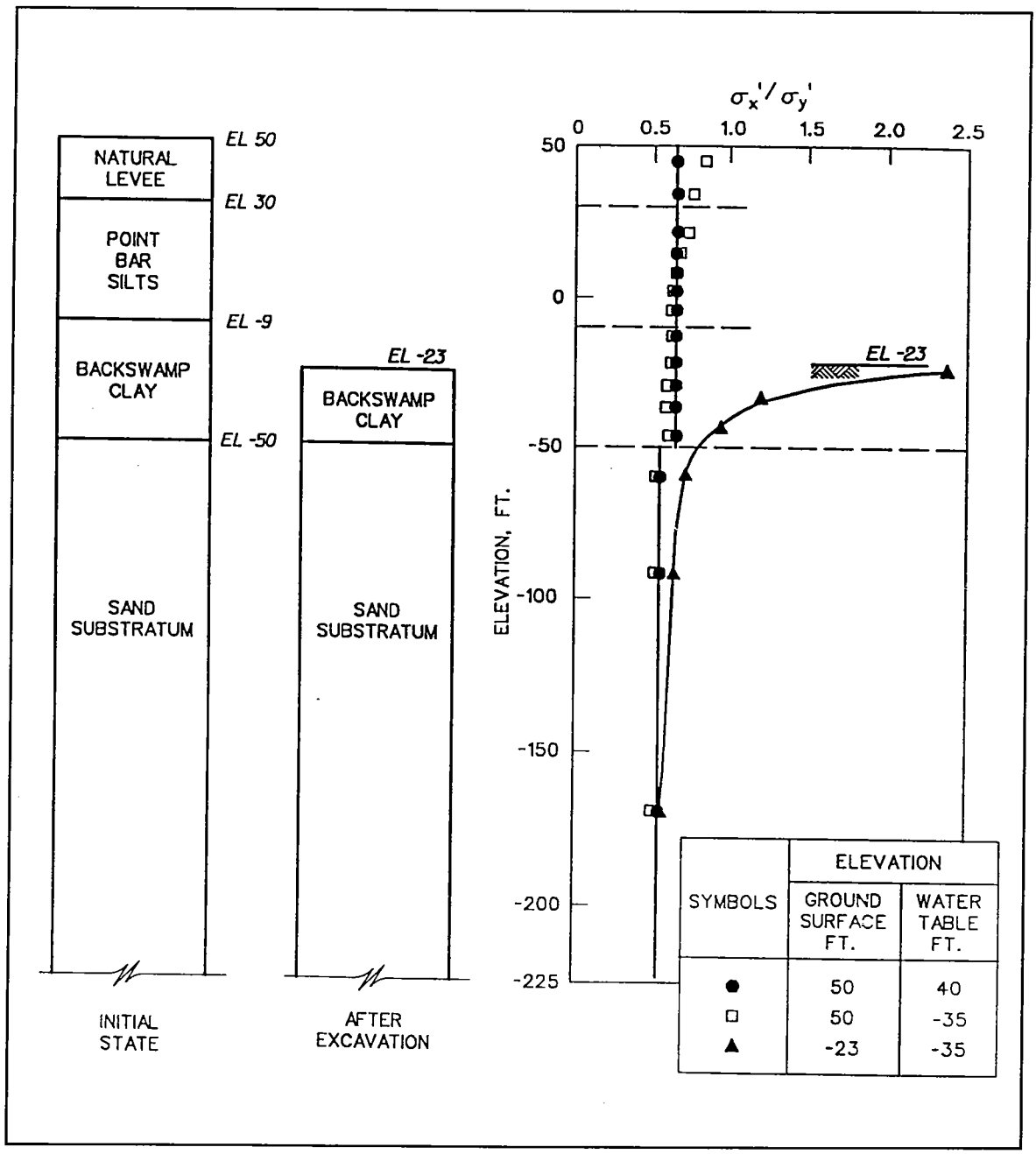

Figure 26. Ratio of effective horizontal stresses to effective vertical stresses along section D-D′

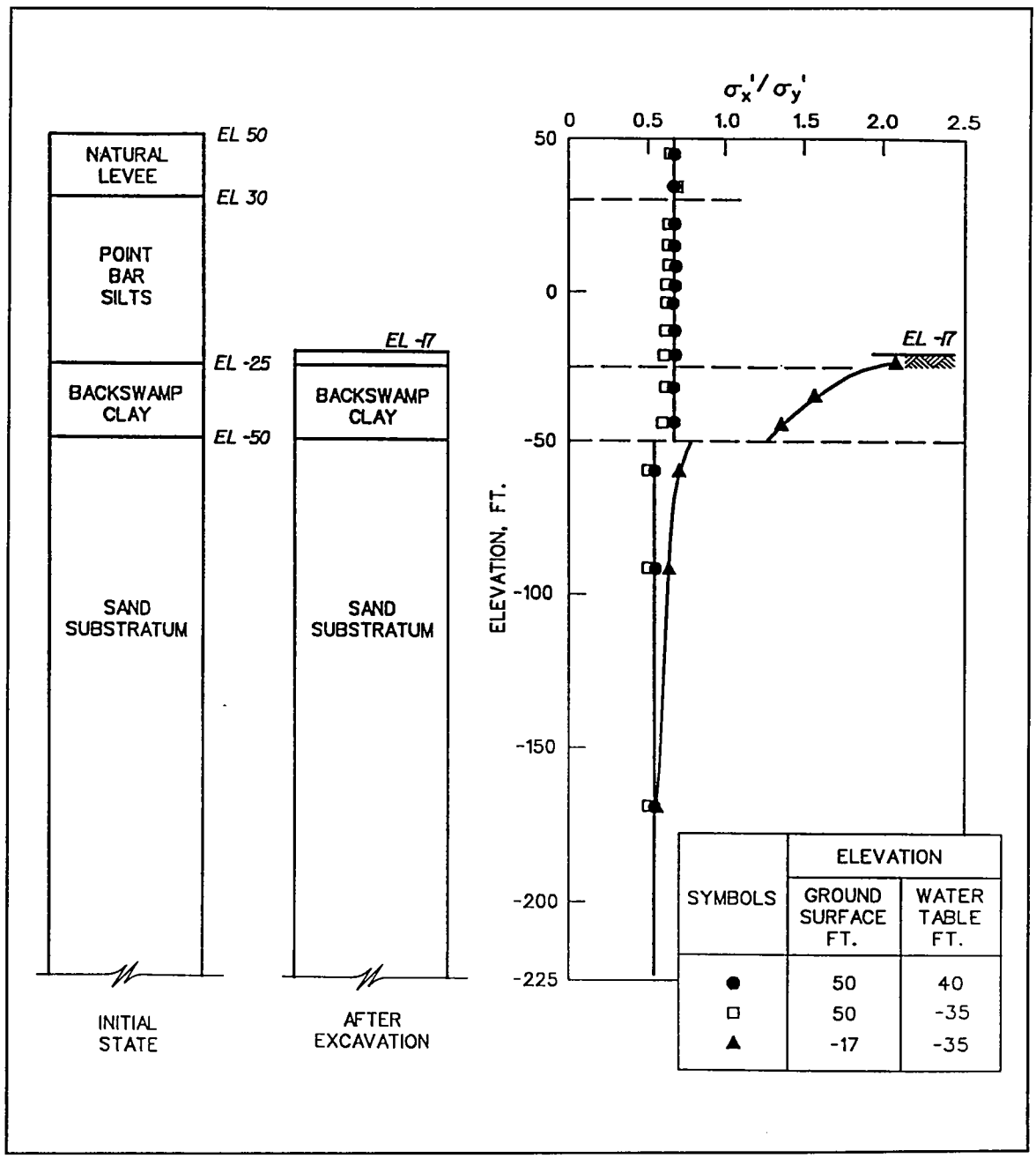

Figure 27. Ratio of effective horizontal stresses to effective vertical stresses along section E-E′

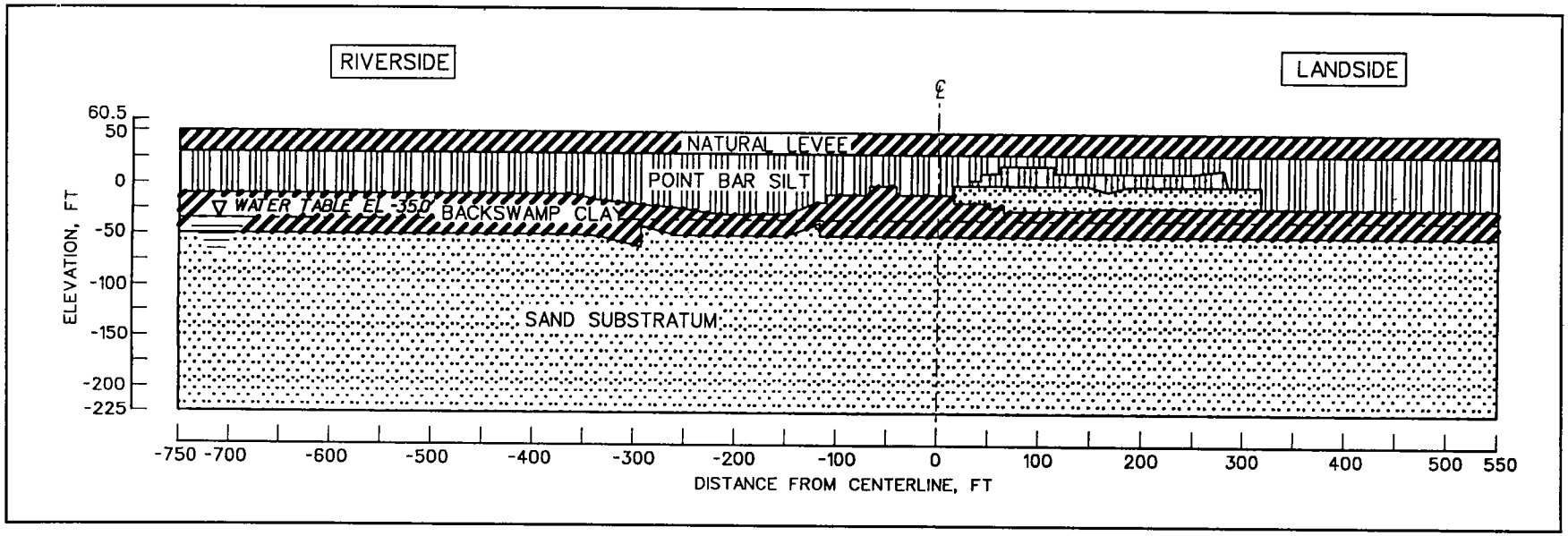

Figure 28. Material regions corresponding to the initial finite element mesh - water table at el -35

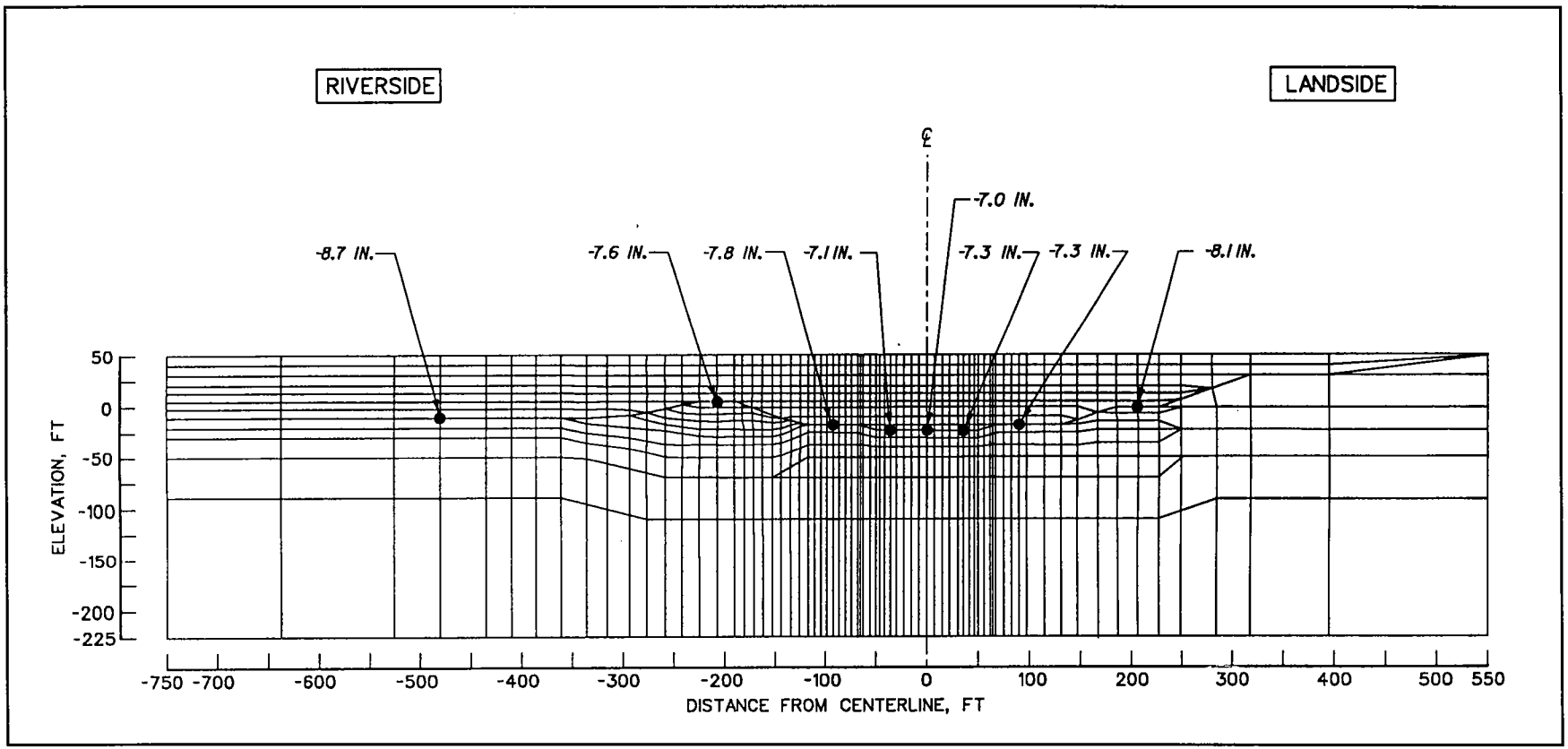

Figure 29. Vertical displacements of select nodal points after lowering the water table from 40 to -35 ft assuming complete dissipation of excess pore water pressures

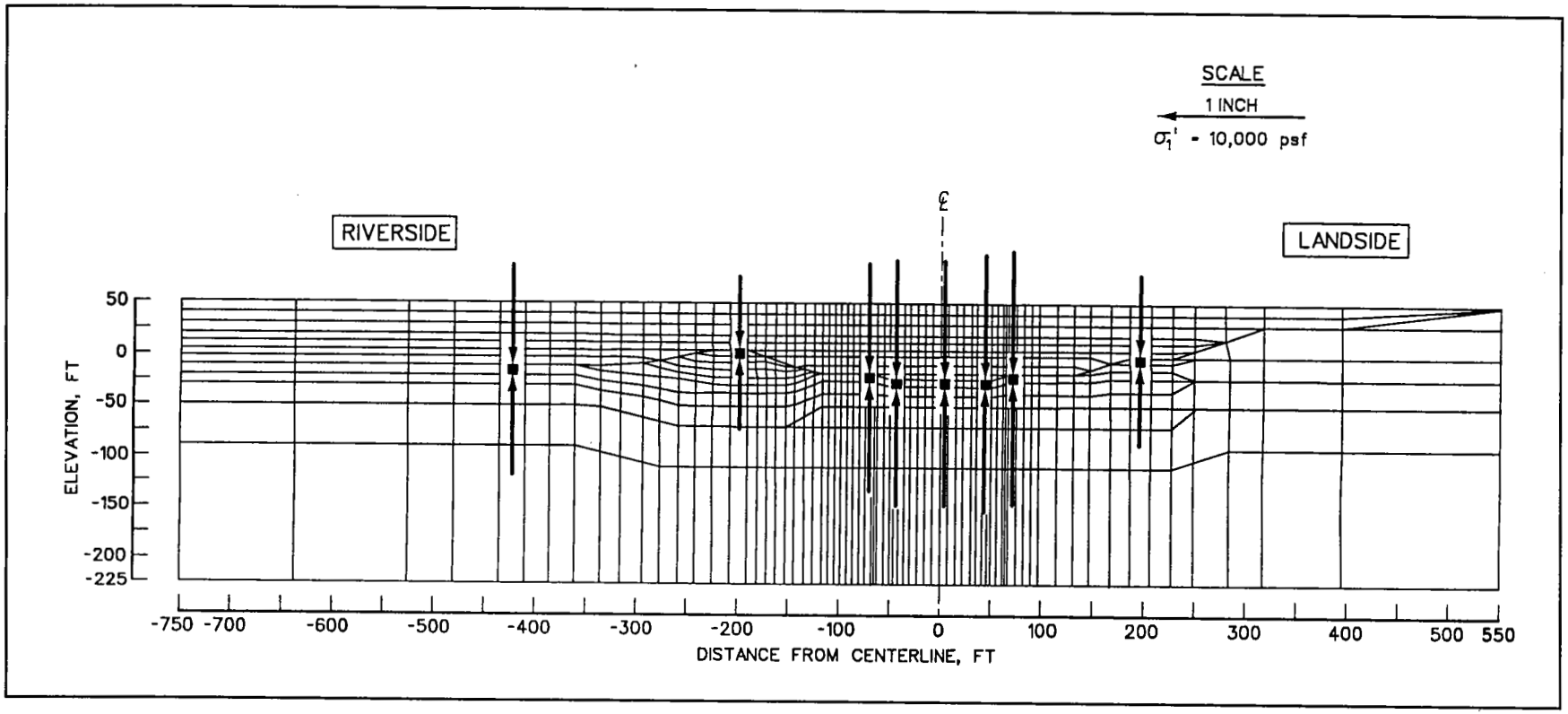

Figure 30. Major principal effective stresses for select foundation elements after lowering water table from 40 to -35 ft

stresses of the select elements within the lock foundation that were previously discussed in association with Figure 21. The major principal effective stresses again corresponded to the vertical effective stresses and increased in magnitude by a factor of 2 with the lowering of the water table. Since primary loading is maintained during this series of loadings, the values of K_h* for the four strata are nearly equal to the same values that were computed initially (Figures 23 through 27).

Construction Stage C - Excavation

The site of the lock and new river channel was excavated in a series of nine stages using SOILSTRUCT with the water table maintained at el -35. The deepest excavation occurred at the site of the lock where the ground surface was lowered 73 ft, from an initial el 50 to a final el -23. The final elevation at the new river channel was equal to -10 ft, a 60-ft-deep excavation. The finite element mesh of this cross section after completion of the excavation is shown in Figure 31. The material property regions are shown in Figure 32. The computed vertical displacements were upward, consistent with unloading of the foundation by the removal of the overburden. The heave for select nodal points is given in Figure 33. These are the same nodes whose displacements as a result of the lowering of the water table were given in Figure 29. The rebound computed at these nodes ranged from 2 to 4 in., depending upon the location of the node. The magnitudes of the computed values of heave were less than the magnitudes of the values of settlement during lowering of the water table by a factor of 2 to 3.

Figure 34 shows the computed values of major principal effective stresses and their orientations for the same elements for which results from construction stages A and B analyses were discussed previously. Comparisons with the values reported in Figures 21 and 30 show a substantial decrease in the magnitude of major principal effective stress for the elements and a significant reorientation of principal planes. This response is consistent with expected behavior with the removal of overburden during excavation, not unlike the development of stress regimes within an overconsolidated deposit. After excavation, the newly exposed elements have the smallest values for major principal stress and have undergone the largest rotation of principal planes when compared to the results for the foundation elements with greater overburden. For example, at the location of the center line of the lock, the horizontal plane corresponds to the plane on which the major principal stress acts. The magnitude of the rotation of principal planes from vertical diminished with depth below the newly exposed surface. In addition, for a newly exposed surface that was inclined, the principal stress vectors of the shallow depth elements were parallel to the slope of the ground surface (Figure 34).

Figures 23 through 27 show the variation in the magnitude of K_h* with depth. For a given elevation, K_h* increased in value as a result of the

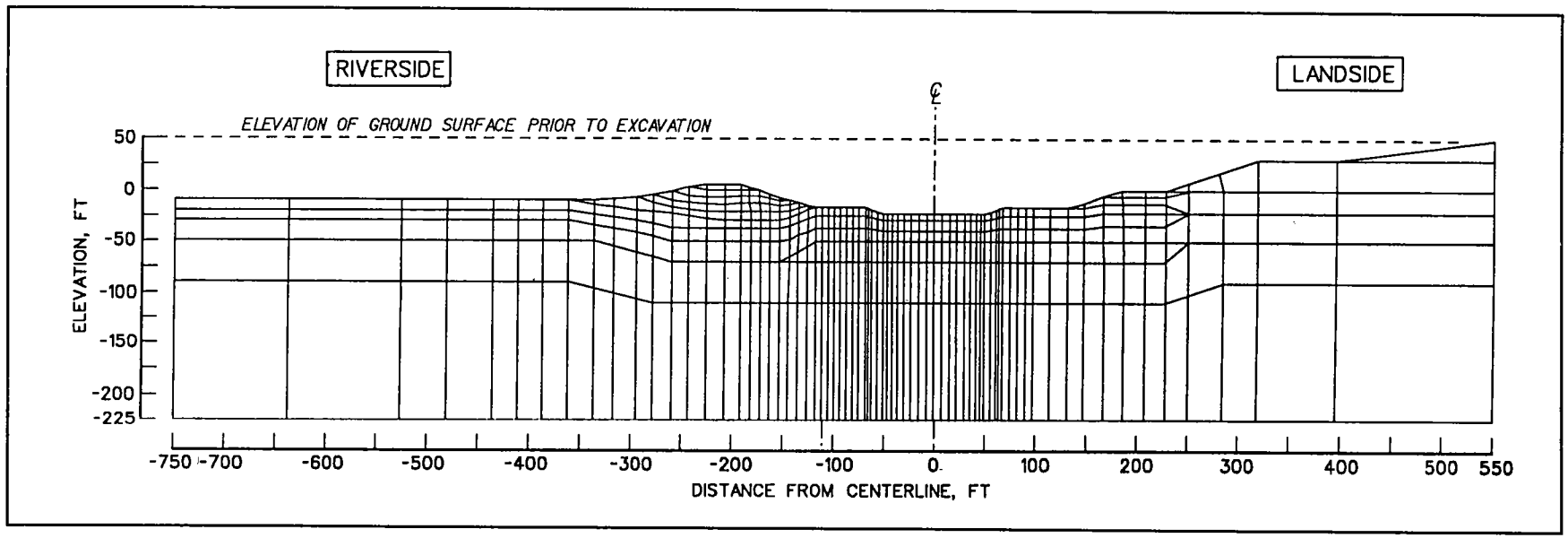

Figure 31. Finite element mesh after excavation

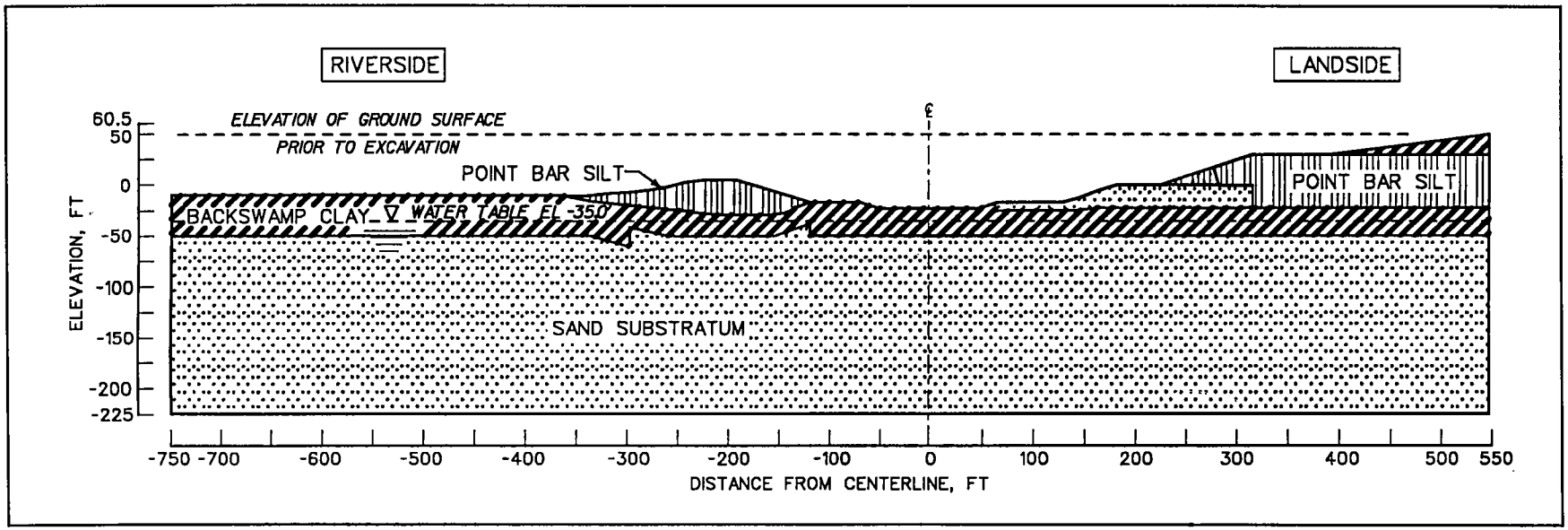

Figure 32. Material regions corresponding to finite elment mesh after excavation - water table at el -35

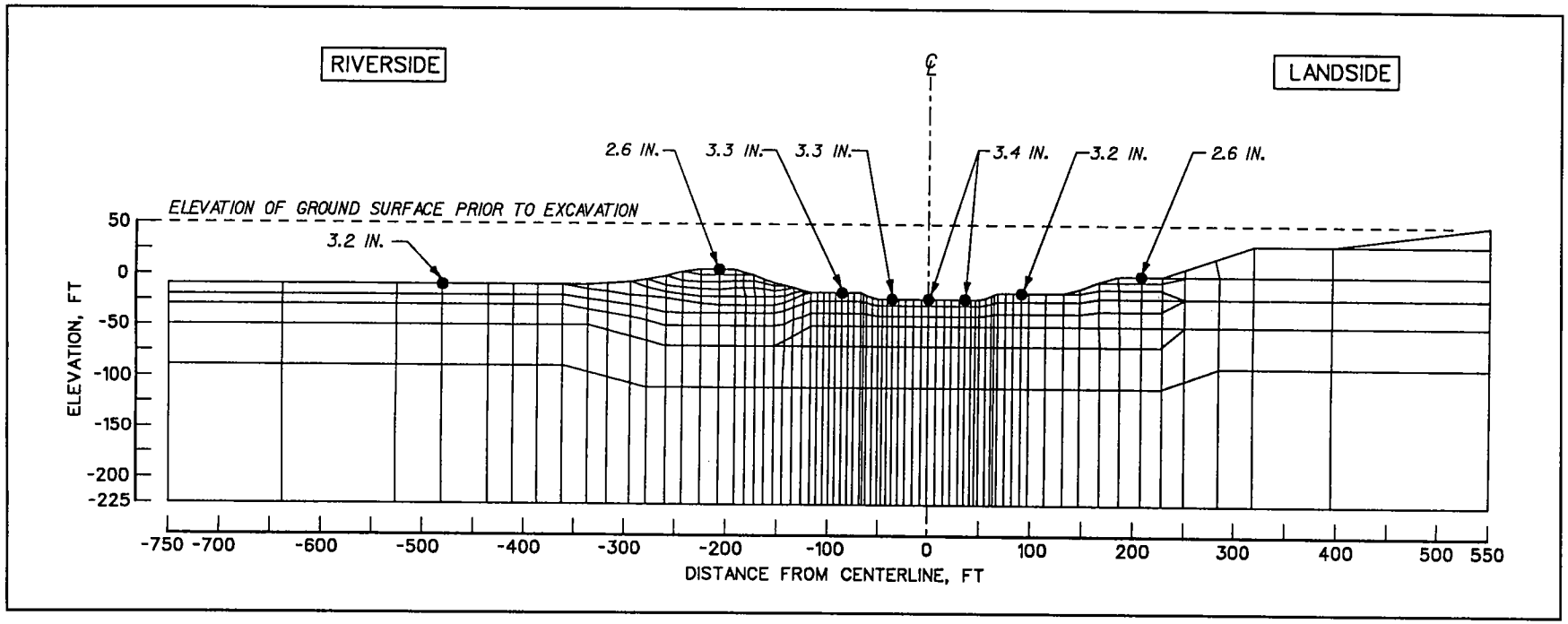

Figure 33. Vertical rebounds at select nodal points due to excavation assuming complete dissipation of excess pore water pressures

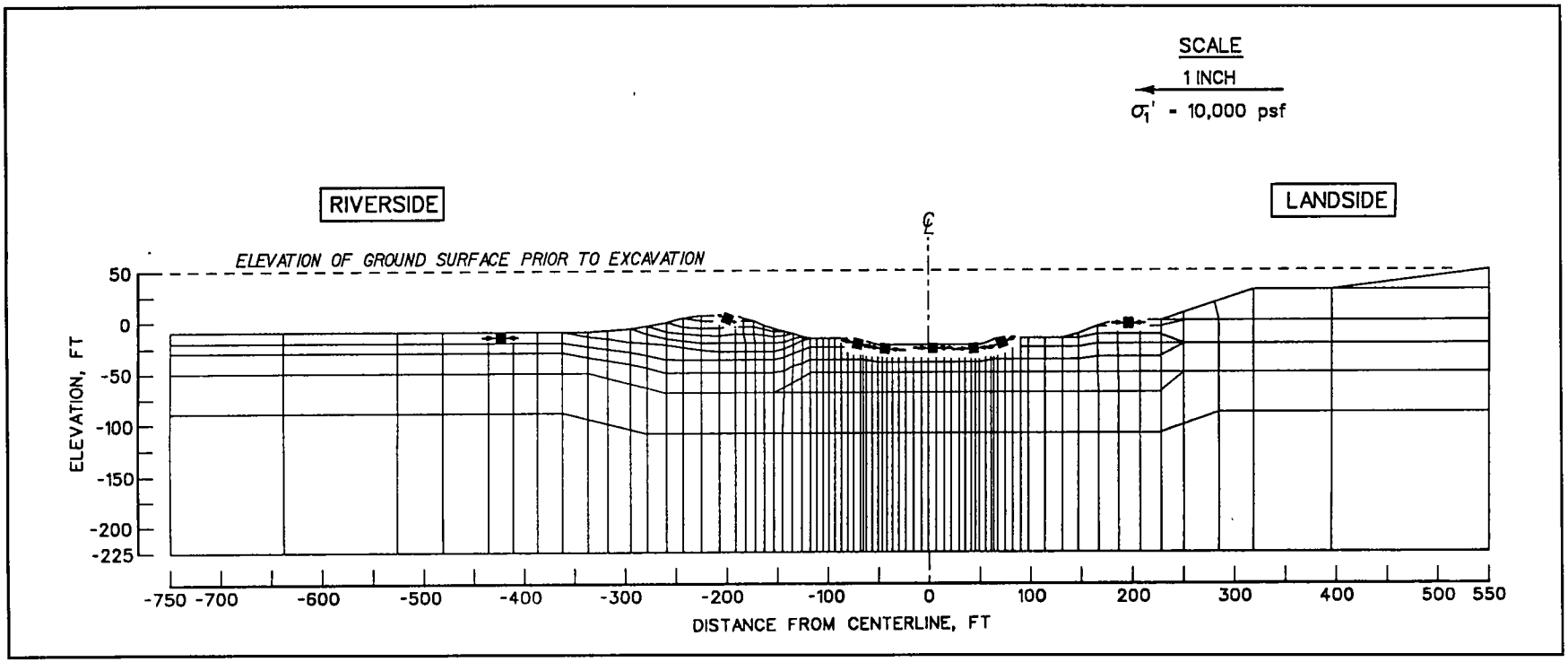

Figure 34. Major principal effective stresses for select foundation elements after excavation

removal of overburden pressures during excavation of the soil. Secondly, the values of K_h* decreased with depth within each soil stratum. The increase in value of K_h* at a given elevation is due to two factors: the initial value of effective stress prior to excavation (after construction stage B), and the magnitude of the stress release that occured during excavation. Since the removal of overburden pressure resulted in a decrease in effective stress within the foundation soil, the overconsolidation ratio (OCR) for the foundation soils increased. Empirical correlations between values of K_h* and OCR indicate that the value of K_h* increased with increasing values of OCR. The largest OCR values within the foundation corresponded to the locations of the largest values for K_h*, below the newly exposed surfaces after excavation. For example, Figure 26 shows that directly below the center line of the lock (el -26.5) K_h* increased in value from 0.62 (stage B) to 2.4 (stage C). The decrease in rate of increase in K_h* values with depth was caused by a decrease in the value of OCR with depth, largely because the initial value of effective stress prior to excavation (stage B) increased in value with depth. Lastly, the value of K_h* varied with material type, as shown in these figures.

Changes in the values of effective stress during construction may also be described using stress paths. Stress paths are loci of points describing the states of stress on the plane of maximum shear, in terms of p' (the average of the major and minor effective principal stress) and q (the maximum shear stress). Stress paths provide insight into the current stress state relative to those corresponding to failure and to those stress states corresponding to previous stages of construction. Figure 35 lists the relationships between Mohr Coulomb failure criteria and the corresponding parameters used to describe stress paths at failure, labeled the K_f line in this figure. The effective stress paths are computed for 12 of the foundation elements identified in Figure 36. The outline of the lock and backfill to be constructed later in the analysis is also shown in Figure 36. Table 5 lists the 11 stress path point numbers and the corresponding load cases. Their stress paths are shown in Figures 37 through 48. Stress path point numbers 1 through 4, respectively, correspond to construction stages A through D discussed in this section. Stress path point numbers 5 through 11 correspond to load cases associated with the construction of a reinforced berm and subsequent silt loadings, which are discussed in Chapter 3 of this report.

The stress path for the backswamp deposit element 761 is shown in Figure 37. This element is located below the center line of the lock at el -26.5. Stress point no. 1 corresponds to the initial stress state prior to construction (stage A). Lowering of the water table from el 40 to el -35 (stage B) increases both the effective confining stress and shear stress, as shown by stress point no. 2 (p' = 6,575 psf and q = 1,560 psf). After excavation (stage B), described as stress point no. 3 in this figure, the newly exposed ground surface is at el -23. The values of confining pressures and shear stresses are significantly reduced. The values for p' and q decreased to 681 psf and to -276 psf, respectively. At this stage of unloading, the value for the maximum shear stress is plotted negative on the stress

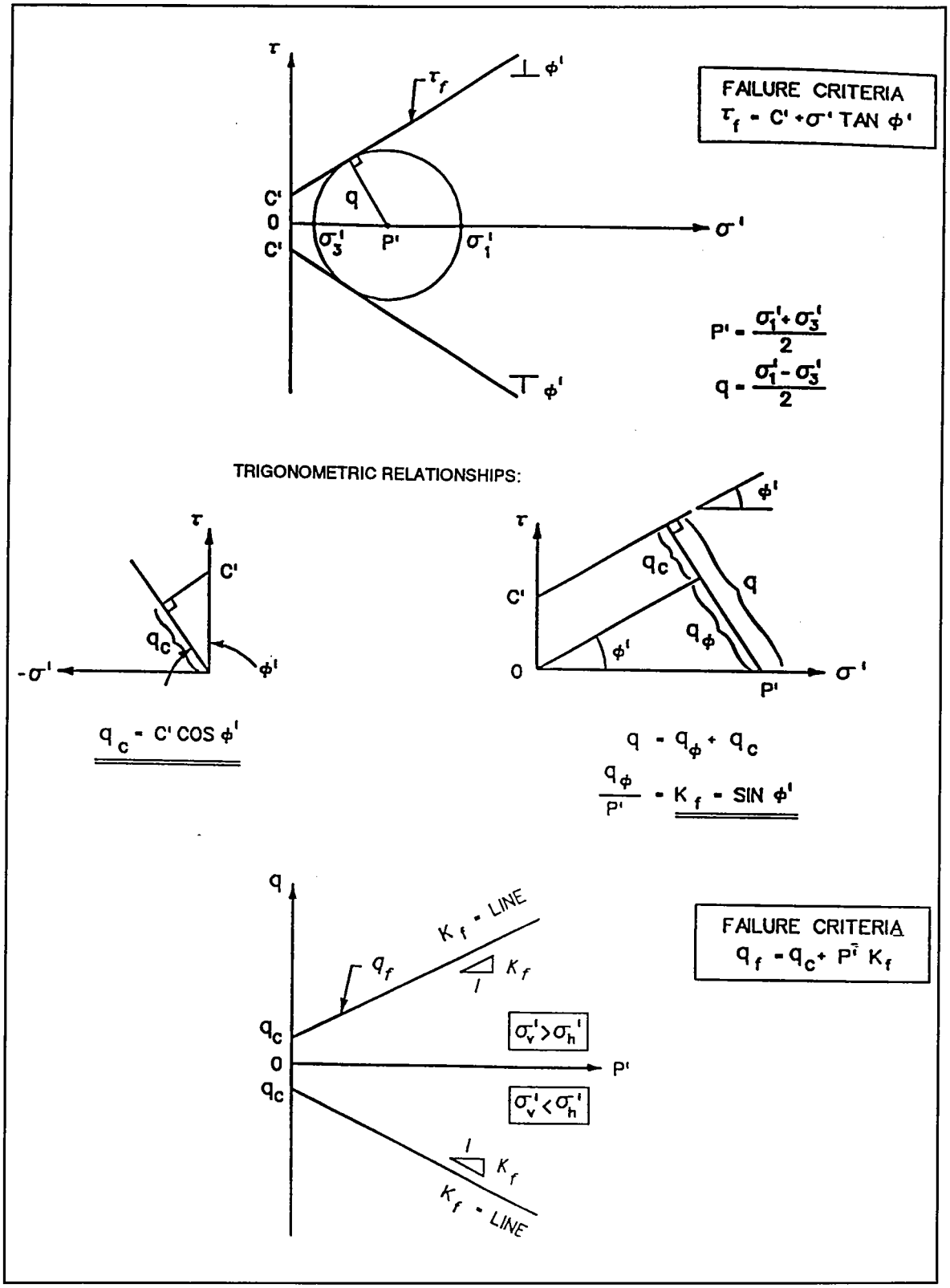

Figure 35. Relationships between Mohr-Coulomb failure criteria and parameters used to describe stress paths

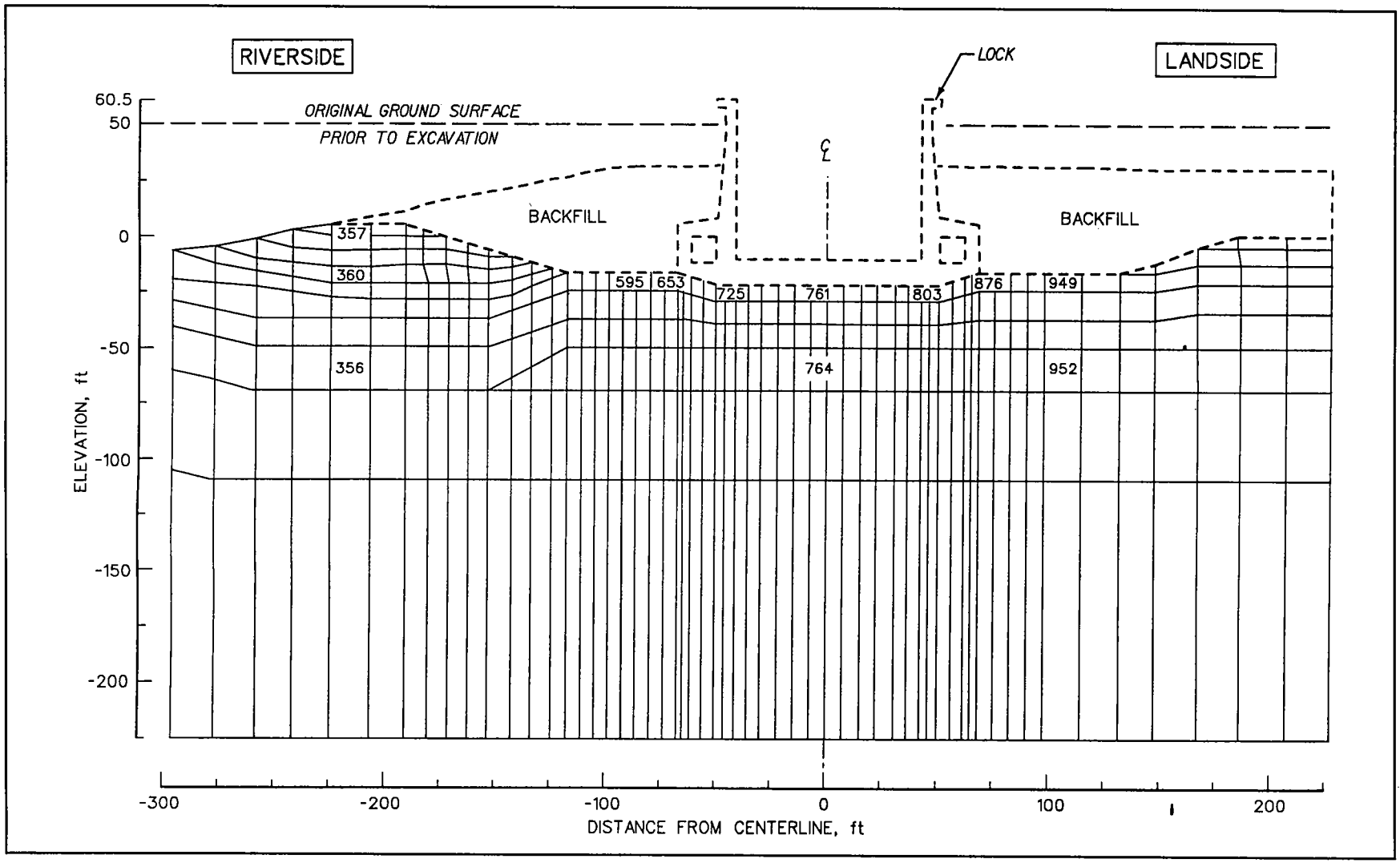

Figure 36. Locations of finite elements within foundation for which stress paths were computed

Table 5
Descriptions of Load Cases for Stress Path Point Numbers

Stress Path Point No.	Description	Water Table el, ft	River el, ft	Pool in Lock el, ft	Riverside Silt el, ft
1	Initial stress state	40	—	—	—
2	After lowering water table	-35	—	—	—
3	After excavation	-35	—	—	—
4	After construction of lock and backfilling	-35	—	—	—
5	Flood site	11	11	11	—
6	Excavate for riverside reinforced berm	11	11	11	—
7	Construct reinforced berm	11	11	11	—
8	Submergence of reinforced berm	60.5	60.5	60.5	—
9	Deposition of 10 ft of riverside silt on reinforced berm	60.5	60.5	60.5	55
10	Lowering river elevation and pool in lock	4	4	40	55
11	Lowering pool in lock	4	4	4	55

Note: — indicates no data available.

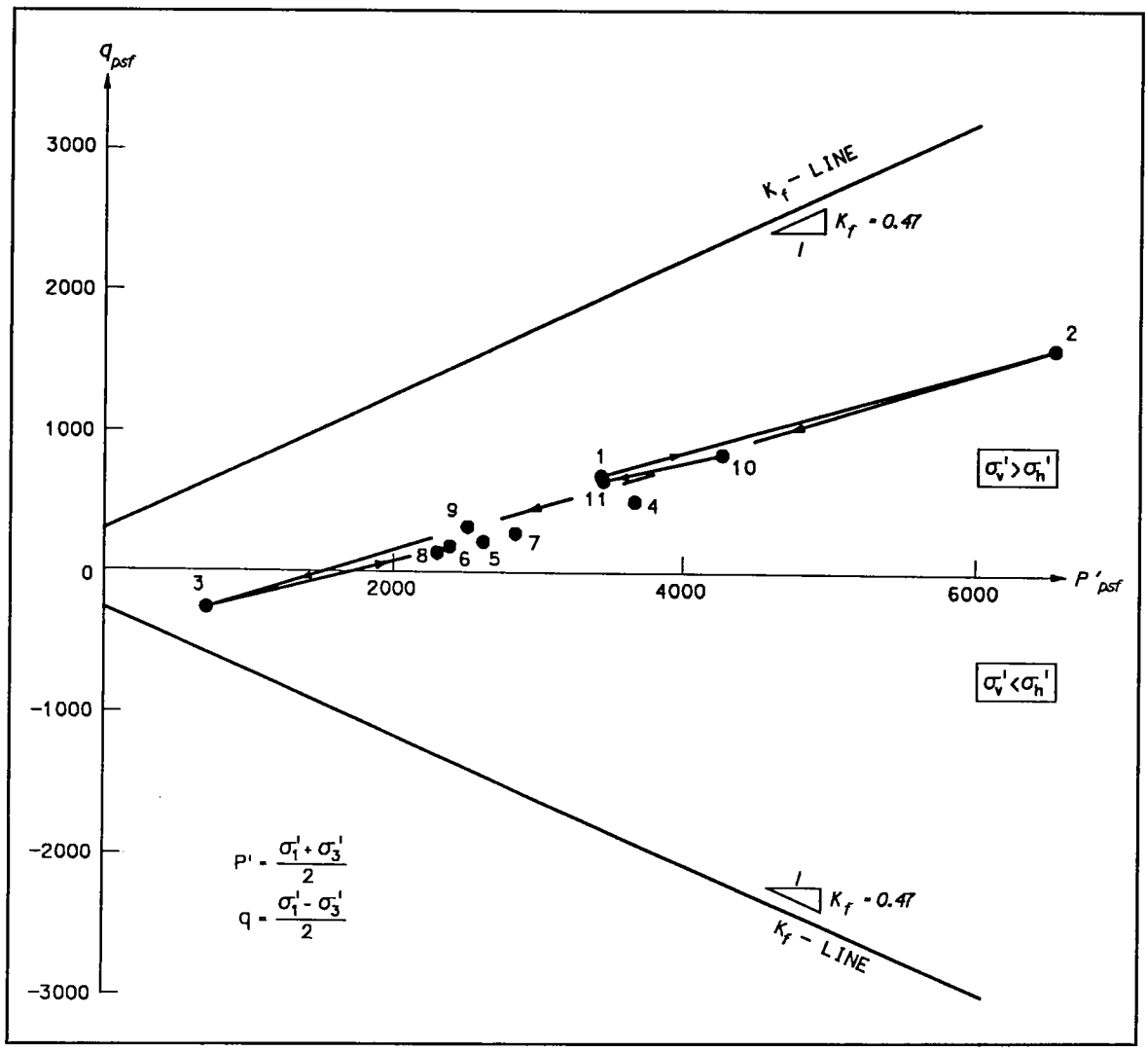

Figure 37. Stress paths for backswamp deposit element 761, below center line of lock at el -26.5

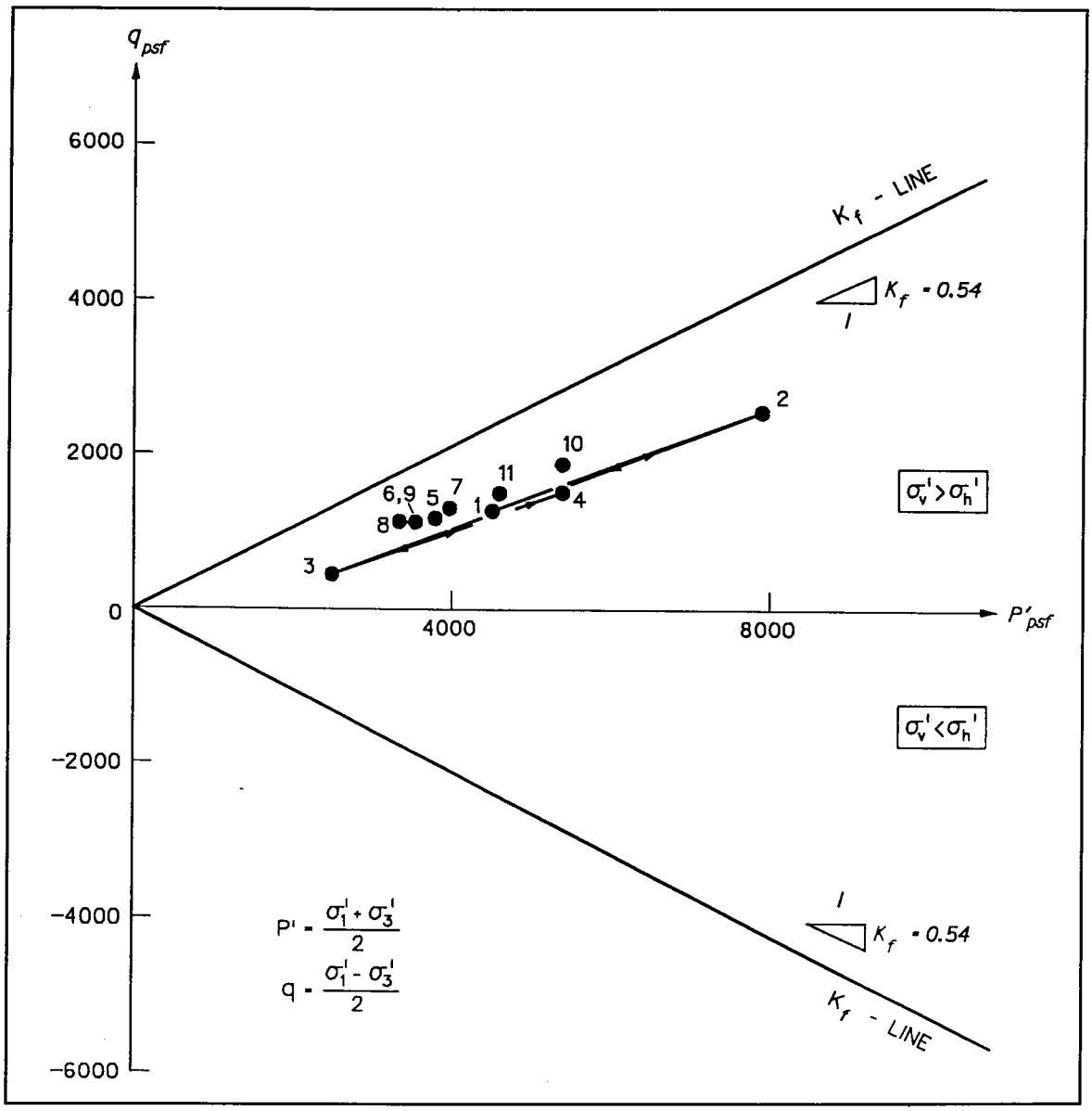

Figure 38. Stress paths for sand substratum element 764, below center line of lock at el -60

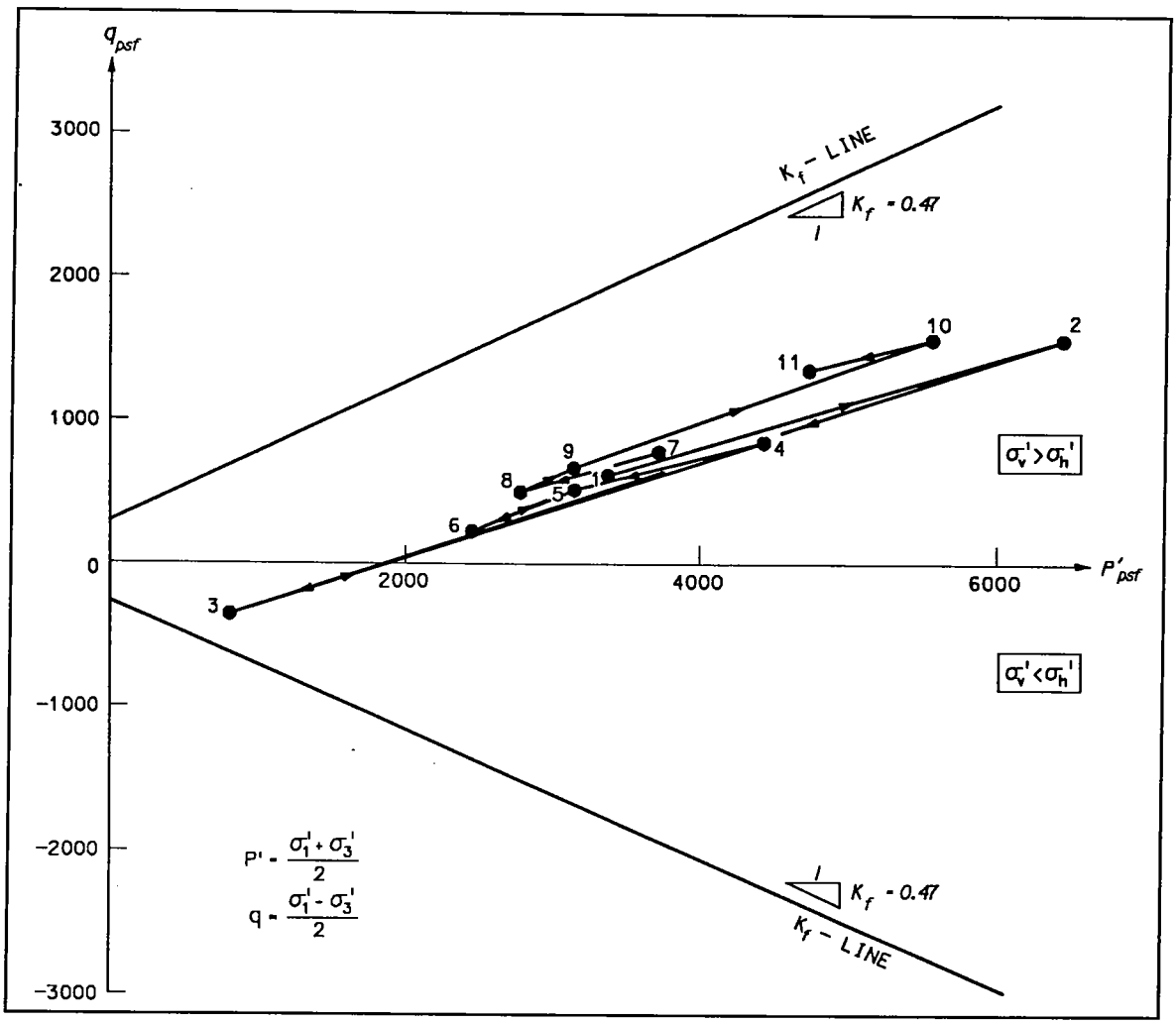

Figure 39. Stress paths for backswamp deposit element 725, below riverside stem at el -26.5

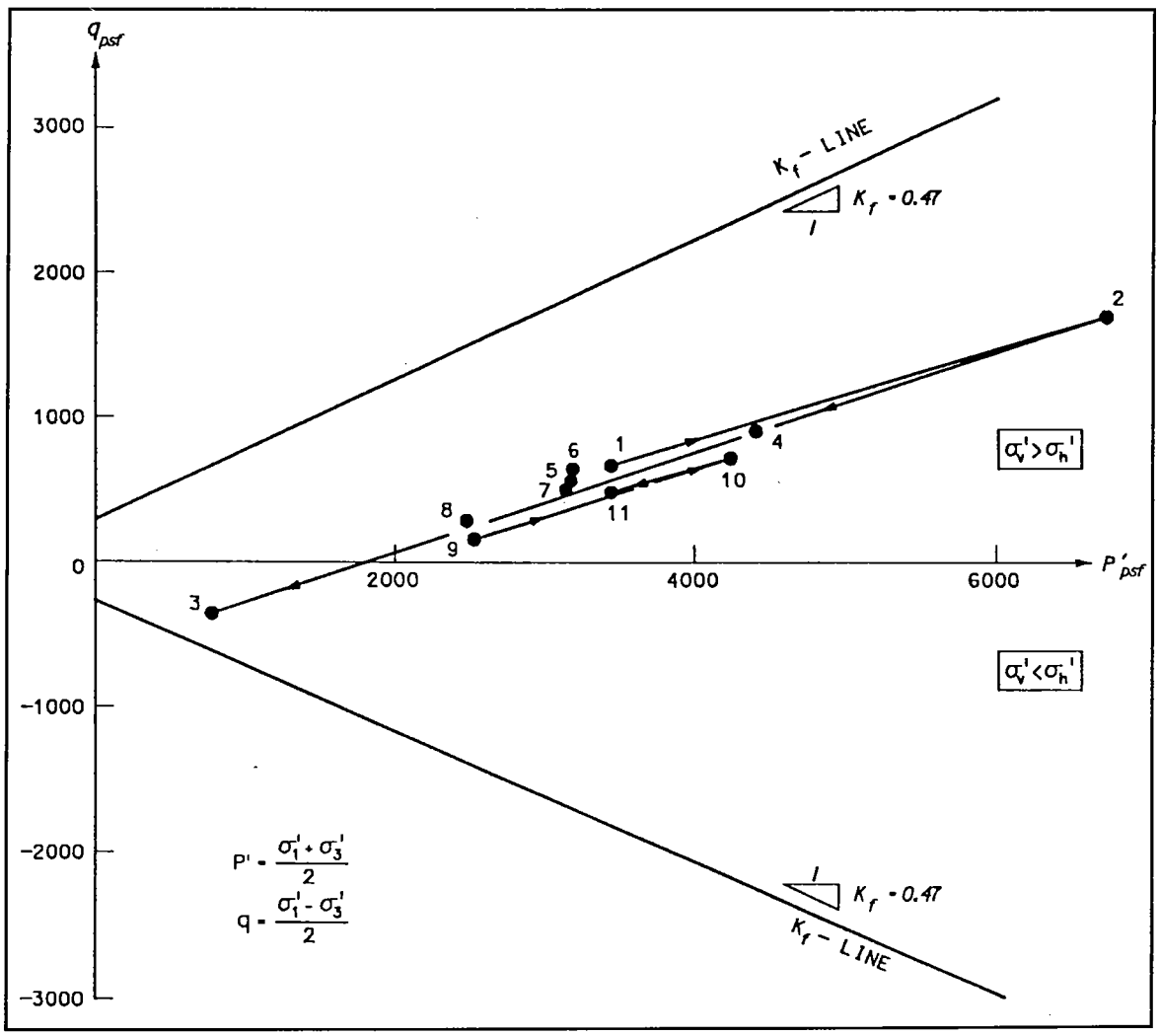

Figure 40. Stress paths for backswamp deposit element 803, below landside stem at el -26.5

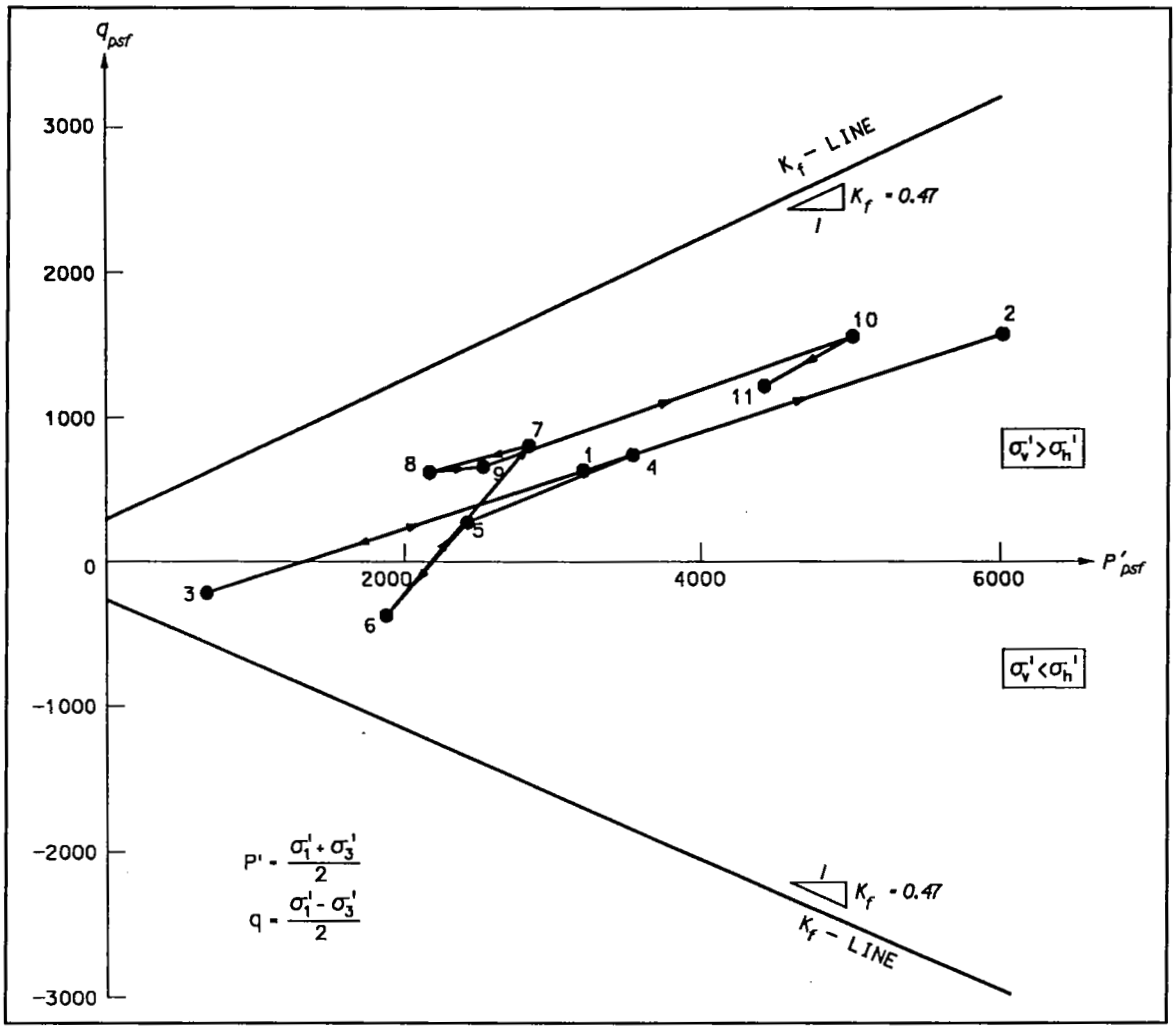

Figure 41. Stress paths for backswamp deposit element 653, adjacent to corner of river-side culvert at el -20

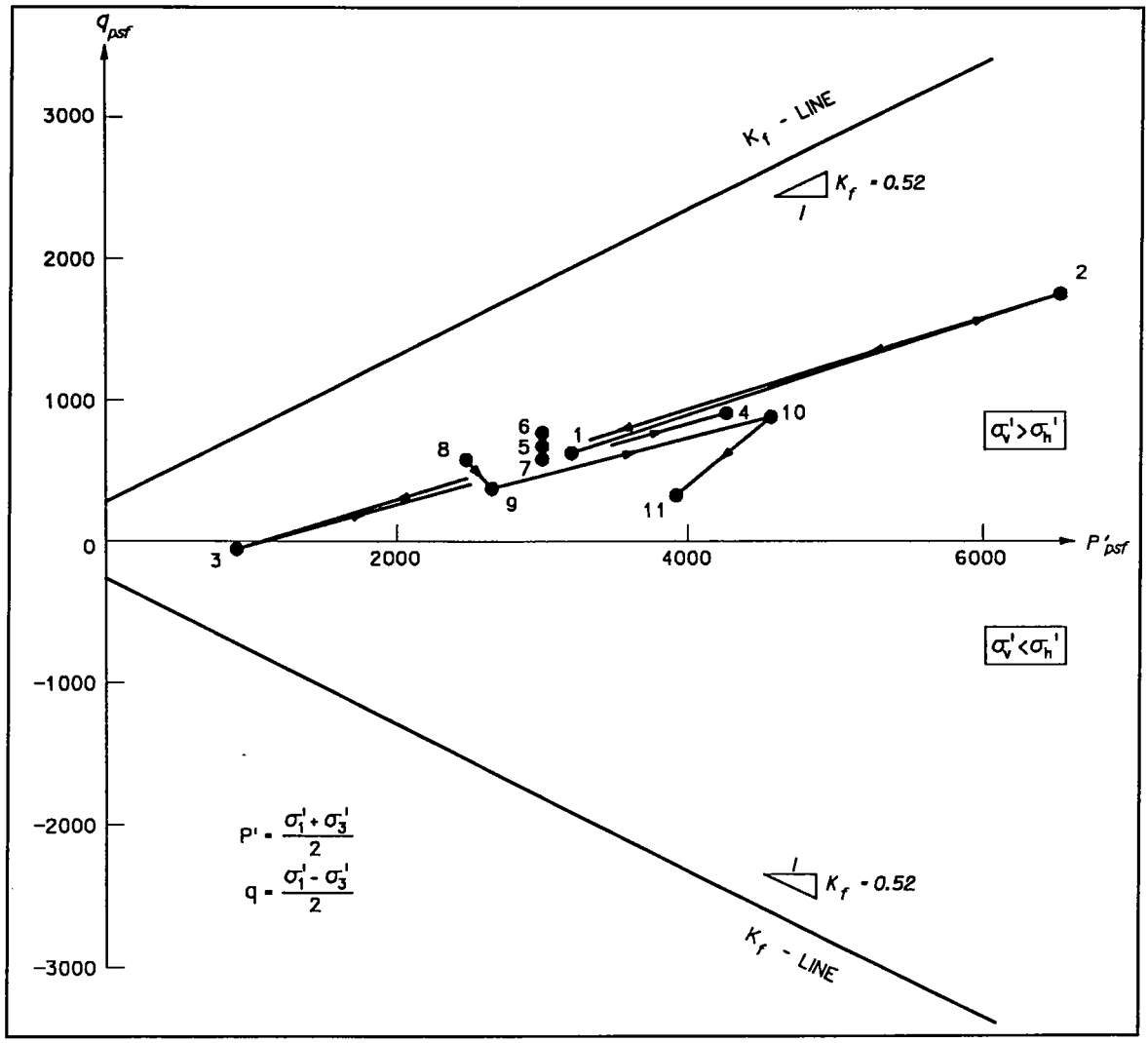

Figure 42. Stress paths for backswamp deposit element 876, adjacent to corner of land-side culvert at el -20

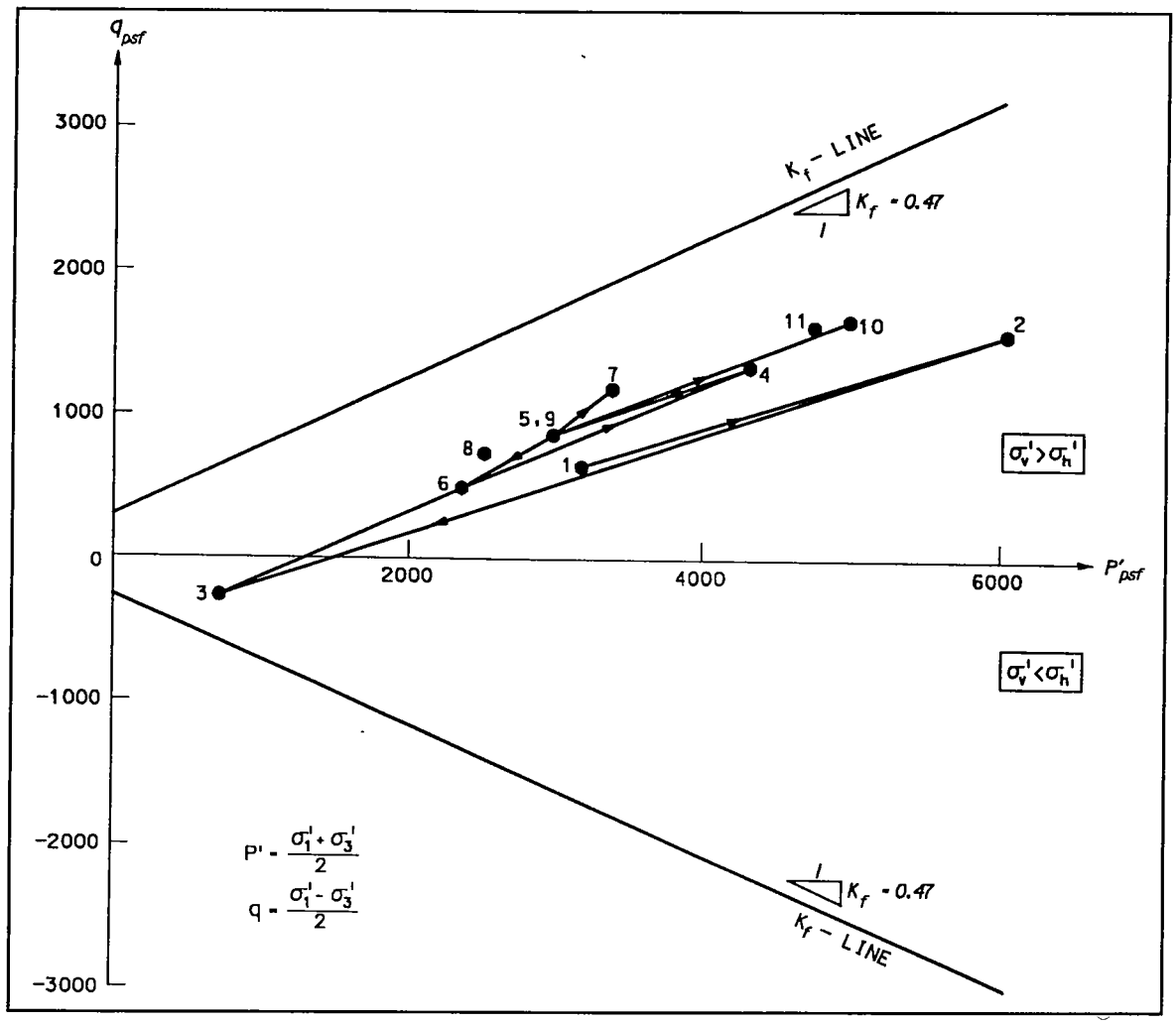

Figure 43. Stress paths for backswamp deposit element 595, 21 ft riverside of culvert at el -20

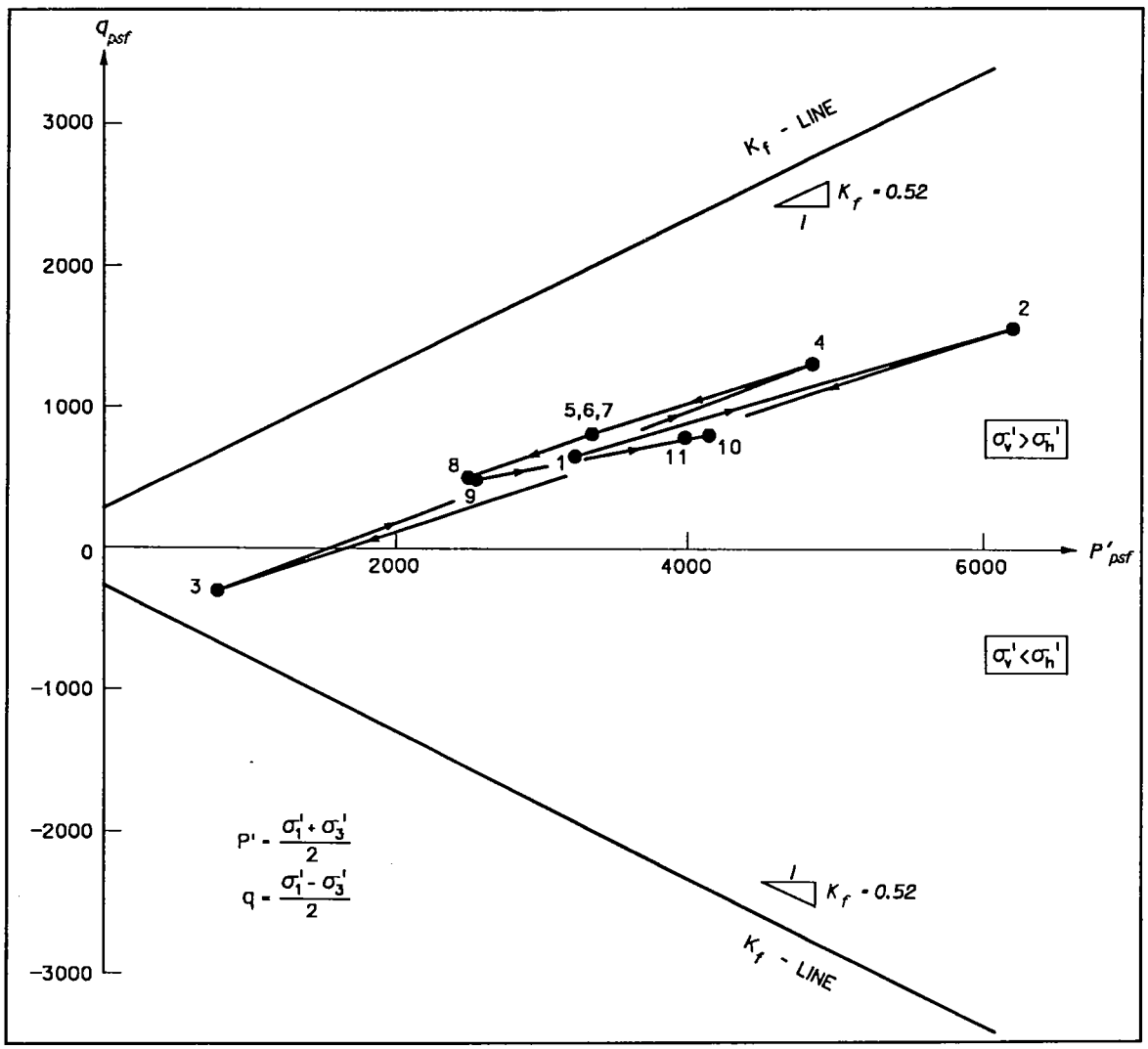

Figure 44. Stress paths for point bar sand element 949, 38 ft landside of culvert at el -20

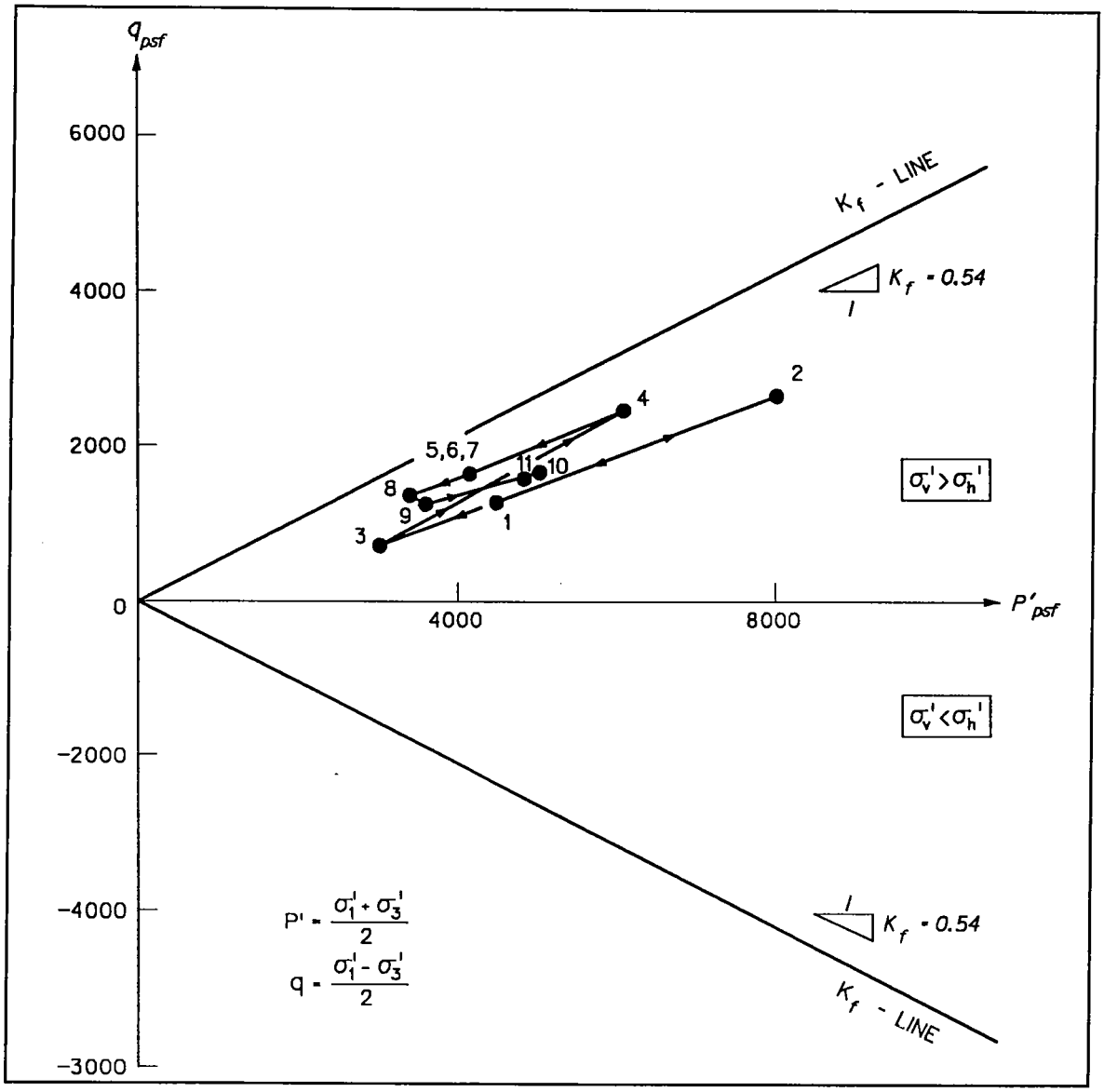

Figure 45. Stress paths for sand substratum element 952, 38 ft landside of culvert at el -60

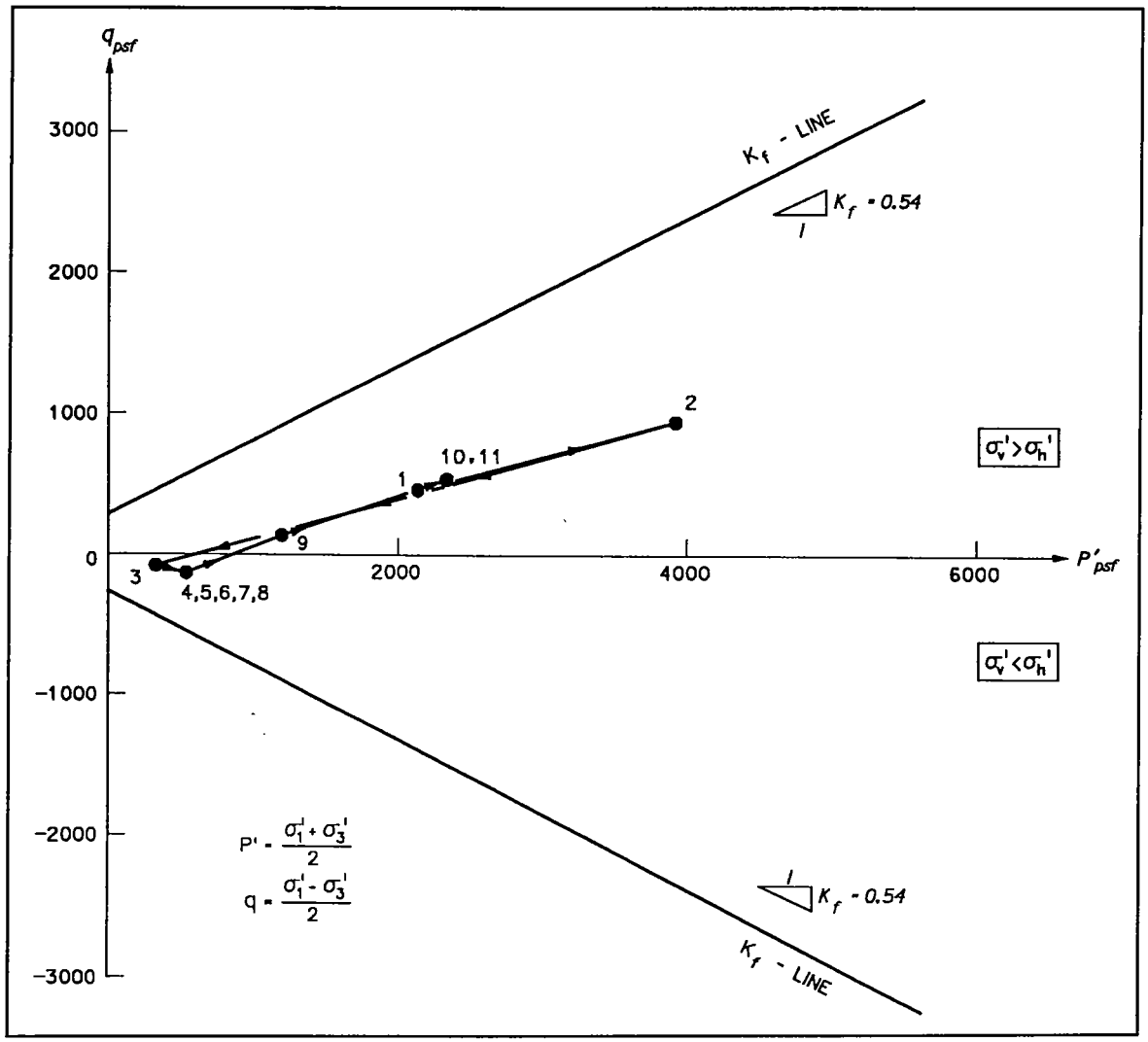

Figure 46. Stress paths for point bar silt element 357, 216 ft riverside of center line of lock at el 2

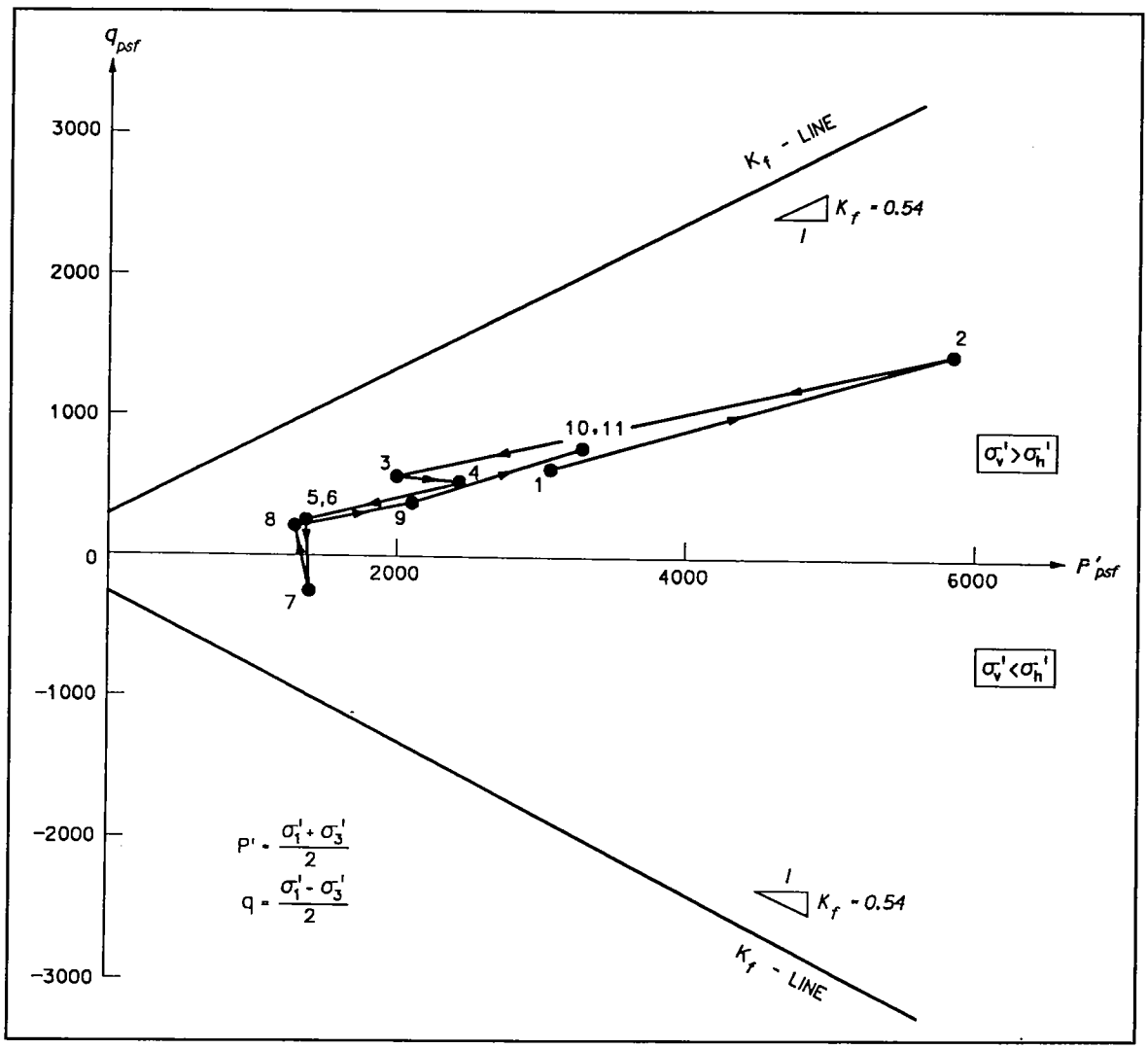

Figure 47. Stress paths for point bar silt element 360, 216 ft riverside of center line of lock at el -18

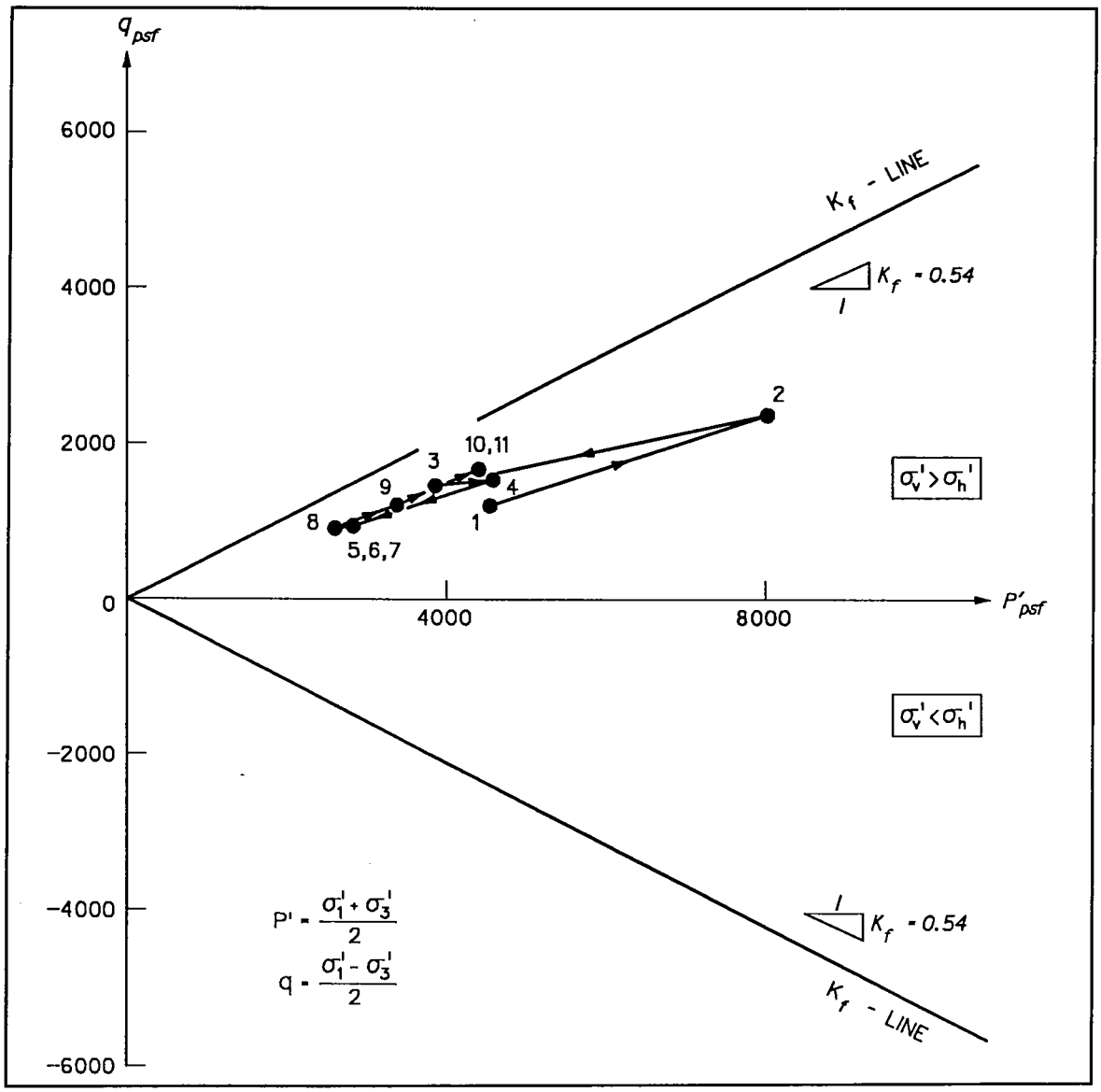

Figure 48. Stress paths for sand substratum element 356, 216 ft riverside of center line of lock at el -60

path, because the value of the horizontal effective stress within element 761 is larger than the value of vertical effective stress. This was previously discussed in association with the K_h* results shown in Figure 26. This behavior is in contrast to that for the substratum sand element 764 (Figure 38), also located along the center line at el -60. The changes in stresses during construction were greater for this element, but due to the confining pressure effects provided by the location of element 764's being deeper within the foundation than element 761, the horizontal effective stress was always less than the vertical effective stresses for all three construction stages. Lastly, the stress states for both elements were well below the K_f line which corresponded to stress states at failure. These strength parameters corresponded to drained foundation conditions for which the loadings were assumed to be applied at a sufficiently slow rate to preclude generation of excess pore water pressures. This is in contrast to short term loadings, during which the loading rates are faster than the soil is able to dissipate the generated excess pore water pressures. Undrained strength and undrained stress-strain response are appropriate for this situation.

The stress paths for the foundation elements 725 and 803, located immediately below the riverside and landside stem walls, are shown in Figures 39 and 40, respectively. Their stress paths are similar to those of the center line element 761 for the three construction stages (stress points no. 1 through 3). The negative value for the maximum shear stress after excavation (point no. 3) plots negative on the stress path because the value of the horizontal effective stress is greater than the value of vertical effective stress.

The stress paths for the foundation elements 653 and 876, located below the culvert walls of the lock at el -21, are shown in Figures 41 and 42, respectively. After excavation, the ground surface is at el -17. The element 653 and 876 stress paths, points no. 1 through 3 in the figures, are similar to those for the newly exposed elements shown in Figure 37 and Figures 39 and 40. This is also true for the stress paths for the newly exposed foundation elements 595 and 949, shown in Figures 43 and 44, respectively. The centers of these elements are also at el -21 and will be located below the sand backfill.

The stress path for element 952 shown in Figure 45, modeling the deeper substratum sands at el -60, again shows the influence of higher confining pressures on the computed stress paths, as compared with the stress path for element 949 at el -21 (Figure 44). The horizontal effective stress is always less than the vertical effective stress for all three construction stages. The stress path for element 949 is similar to the stress path for element 764, also at el -60 (Figure 38).

Figures 46 through 48, respectively, show the stress paths for the point bar silt elements 357 and 360 and sand substratum element 356. These elements are located 216 ft riverside of the lock center line at el 2, -18, and -60, respectively. The elevation at the surface of the newly exposed Point

Bar Deposit after completion of excavation is equal to 5 ft. The centers of these elements lay near the center line of a mound of foundation material that will buttress the backfill on the riverside of the lock (Figure 36). Element 357 exhibits a stress path that is similar to that observed for other newly exposed shallow cover elements for the three construction stages (Figure 46). An increase in overburden or confining pressure shifts the stress paths upward and to the right, as shown by the results for elements 357, 360, and 356 (Figures 46, 47, and 48).

The effective stress paths for the twelve foundation elements shown in Figures 37 through 48 show that under drained loading conditions the shear strength within the foundation is not fully mobilized during any of the three construction stages. Secondly, the changes in stresses during construction are greater for elements deeper within the foundation. Lastly, an increase in overburden pressure contributes to a shift in the stress paths that is upward and to the right.

Lock Construction and Backfilling

Excavation of the site was followed by the construction of the lock and the placement of backfill surrounding the lock. The outline of lock monolith no. 10 and backfill is shown in Figure 49, superimposed on a closeup view of the finite element mesh for the soil foundation after completion of the excavation of stage C. Details regarding lock and backfill dimensions and final elevations are shown in Figure 5. Notes regarding the progress of the construction taken by the USAED, New Orleans, field engineers provided information regarding the chronology of construction. The chronology of lock monolith no. 10 construction and backfilling is shown in Figure 50. The first lift of the base slab was poured in August of 1981. Construction of the base slab and culverts to el 7.5 preceded backfilling. Placement of backfill adjacent to the riverside and landside culvert walls of the lock began at el -17 in December 1981. Placement progressed on both sides of the lock simultaneously. The elevation of the backfill on each side of the lock never differed by more than 2 ft. Construction of lock monolith no. 10 and backfilling were completed by April 1983. The finite element analysis modeling the construction of the lock, referred to as construction stage D, follows the actual sequence of lock construction and backfilling for monolith no. 10 (Figure 50).

The finite element analyses through construction stage C result in effective stresses computed within the foundation, accounting for both the preconsolidation of the foundation that occurred prior to site excavation and the preconsolidation due to the removal of overburden during excavation. Both factors resulted in a stress-strain response for the foundation elements controlled by the unload-reload relationships during the modeling of the lock construction and backfilling.

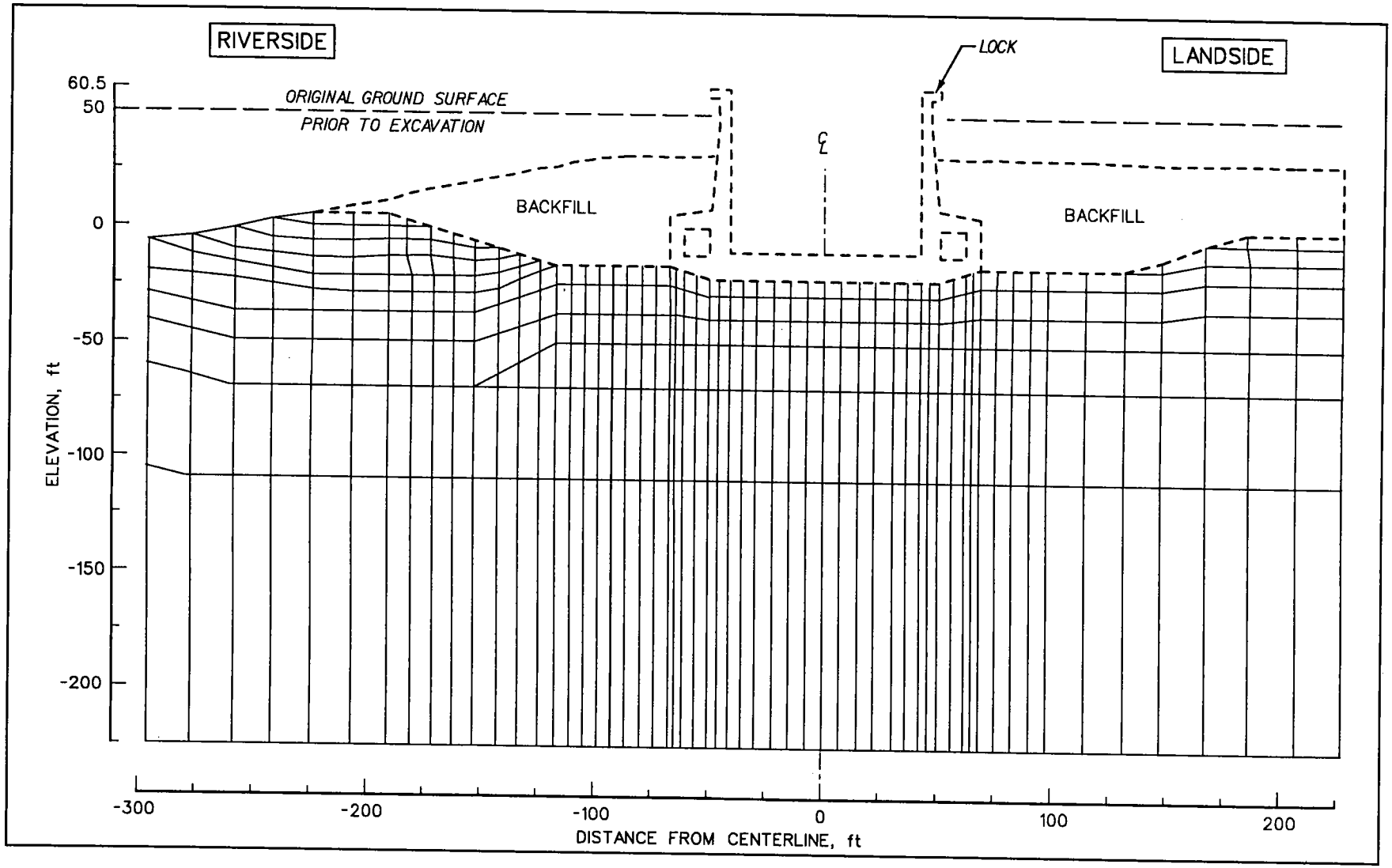

Figure 49. Outline of lock monolith no. 10 and backfill superimposed on finite element mesh of foundation

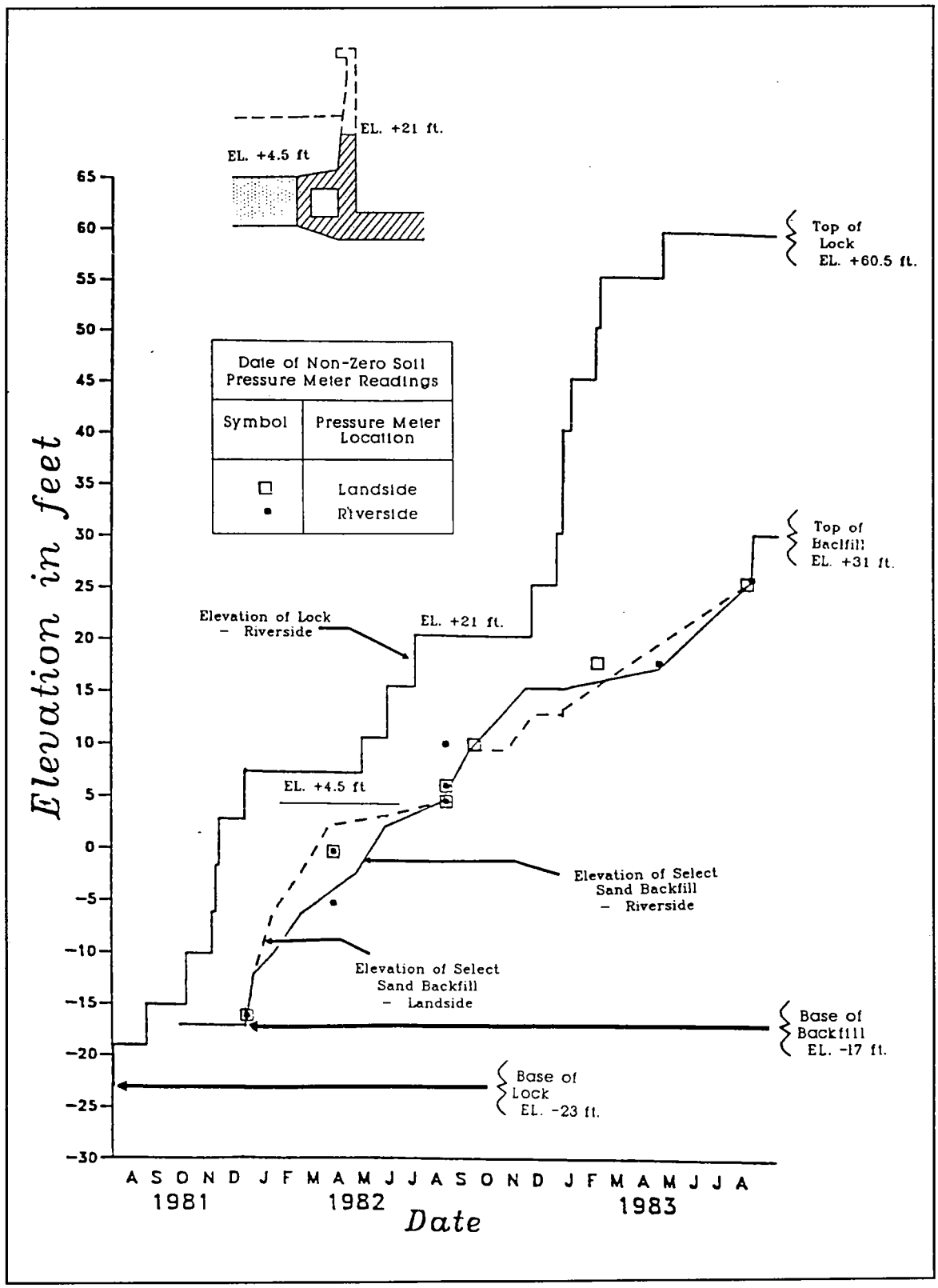

Figure 50. Chronology of lock construction and backfilling of lock monolith no. 10

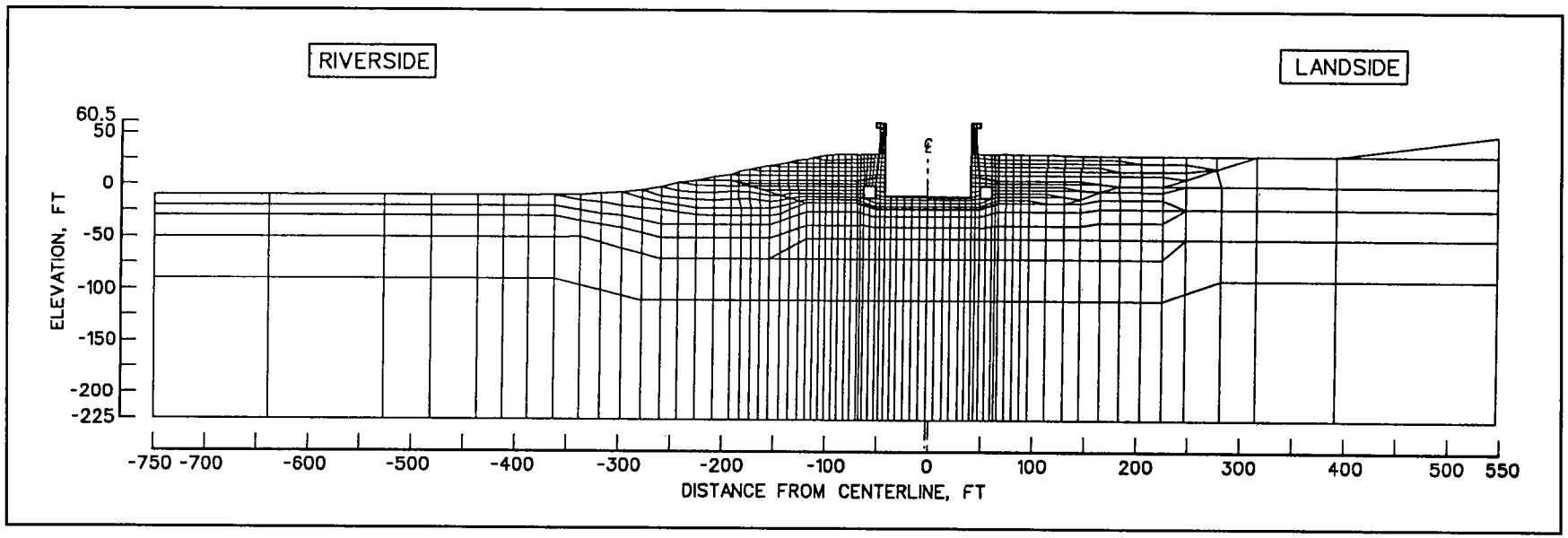

Figure 51. Finite element mesh after lock construction and backfilling

Finite Element Model for Lock Construction

The post construction finite element mesh of the lock and backfill is shown in Figure 51. The elements modeling the soil foundation were the same as those shown in Figure 31. The mesh consisted of 1,152 elements and 1,257 nodes. The lock was modeled by 206 elements and the backfill and soil foundation by 991 elements. Sixty interface elements were placed between the base of the lock and the foundation and between the lock walls and the backfill. The material property regions for this mesh are shown in Figure 52, with the assigned material properties listed in Table 1. The water table was maintained at el -35 during the course of lock construction and backfilling. A closeup view of the finite element mesh for the lock and surrounding backfill is shown in Figure 53, and the material property regions for the mesh are shown in Figure 54. The 83.5-ft-tall lock was modeled using 27 rows of elements. The base of the lock was modeled using four rows of elements through the depth of the lock. The stem walls, culvert walls, and the top of the culverts were modeled using pairs of elements. There was a transition in the number of rows of elements used to model the base within the region of the culverts. The number of rows of elements used was reduced from four to two. The backfill was modeled using 13 layers of 3.7-ft-high elements. In the stage D finite element analyses, construction of the lock and the placement of the backfill were modeled in 25 load increments. The sequence for the progression of the construction in the analysis is the same as that outlined in Figure 50.

Comparison of Lock Construction Analysis to Instrumentation Measurements

The results from the incremental finite element analyses and instrumentation measurements both showed that significant soil-to-structure interaction occurred early in the construction of the lock. For example, Figure 55 shows the change in total normal pressures along the base of the lock after placement of the first 5 ft of backfill adjacent to the chamber walls from the stress meter measurements and computed in the analyses. At this stage of lock construction, the base is in place and the culverts are completed to el 7.5. The instrumentation measurements were recorded on 1 December 1981 and 30 January 1982. Both the finite element analyses and the instrumentation measurements showed a decrease in normal pressure at both corners along the base of the lock. One explanation for this behavior is that the placement of the backfill, whose weight acted as an applied pressure on the foundation, caused the compressible foundation to settle not only directly below the fill but also below the corners of the culverts. Subsequent stages of the lock construction and backfill placement analyses showed that interactions continued to occur between the regions throughout the analyses.

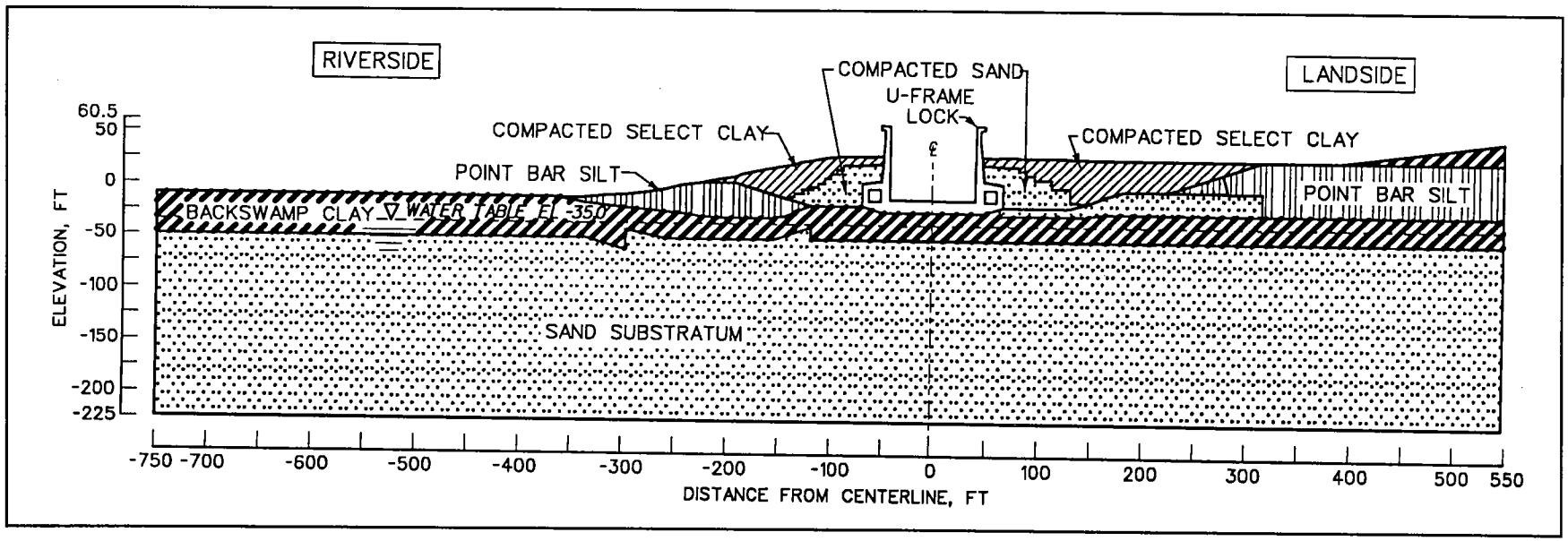

Figure 52. Material regions corresponding to the finite element mesh after lock construction and backfilling - water table at el -35

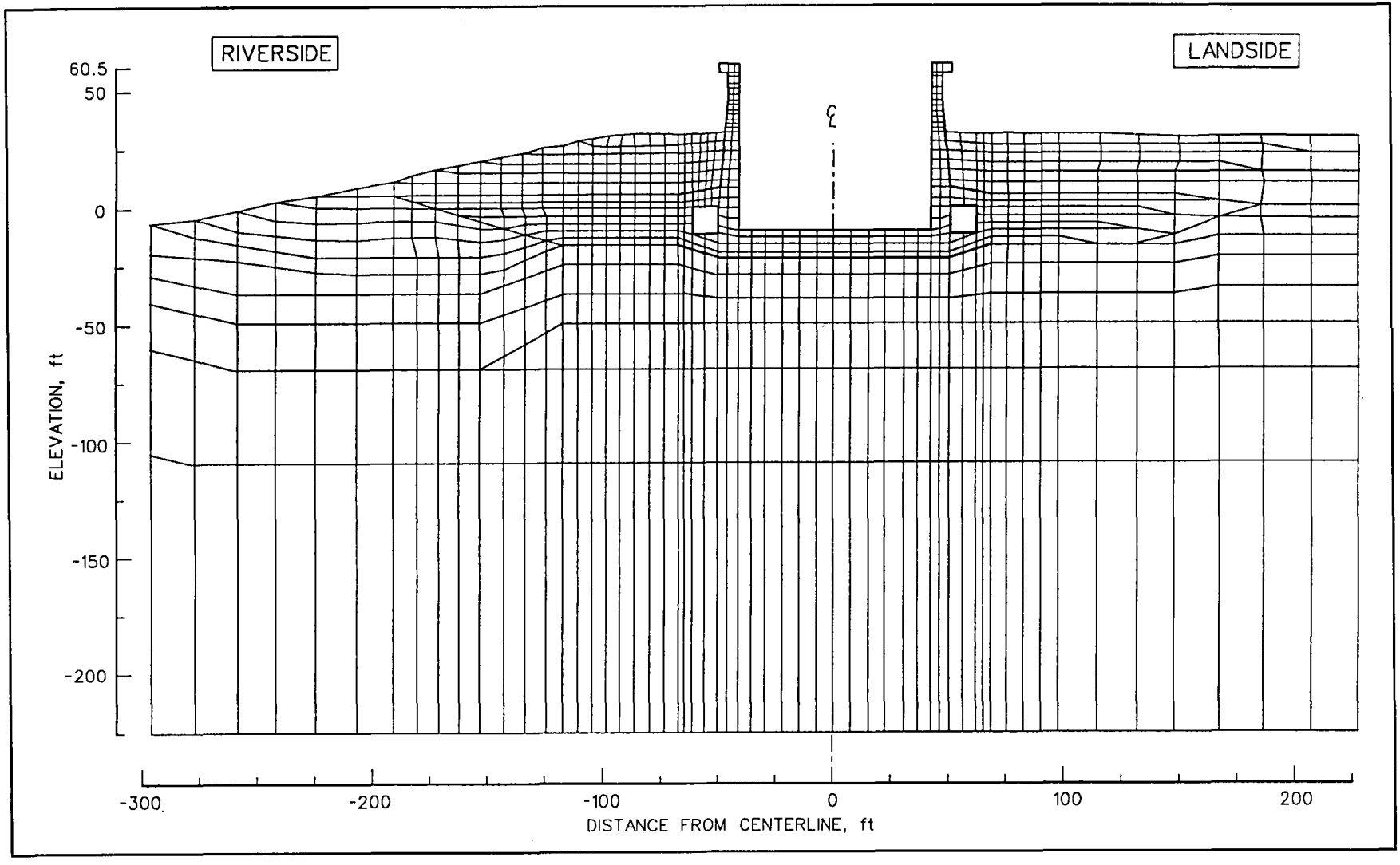

Figure 53. View of finite element mesh modeling lock monolith no. 10

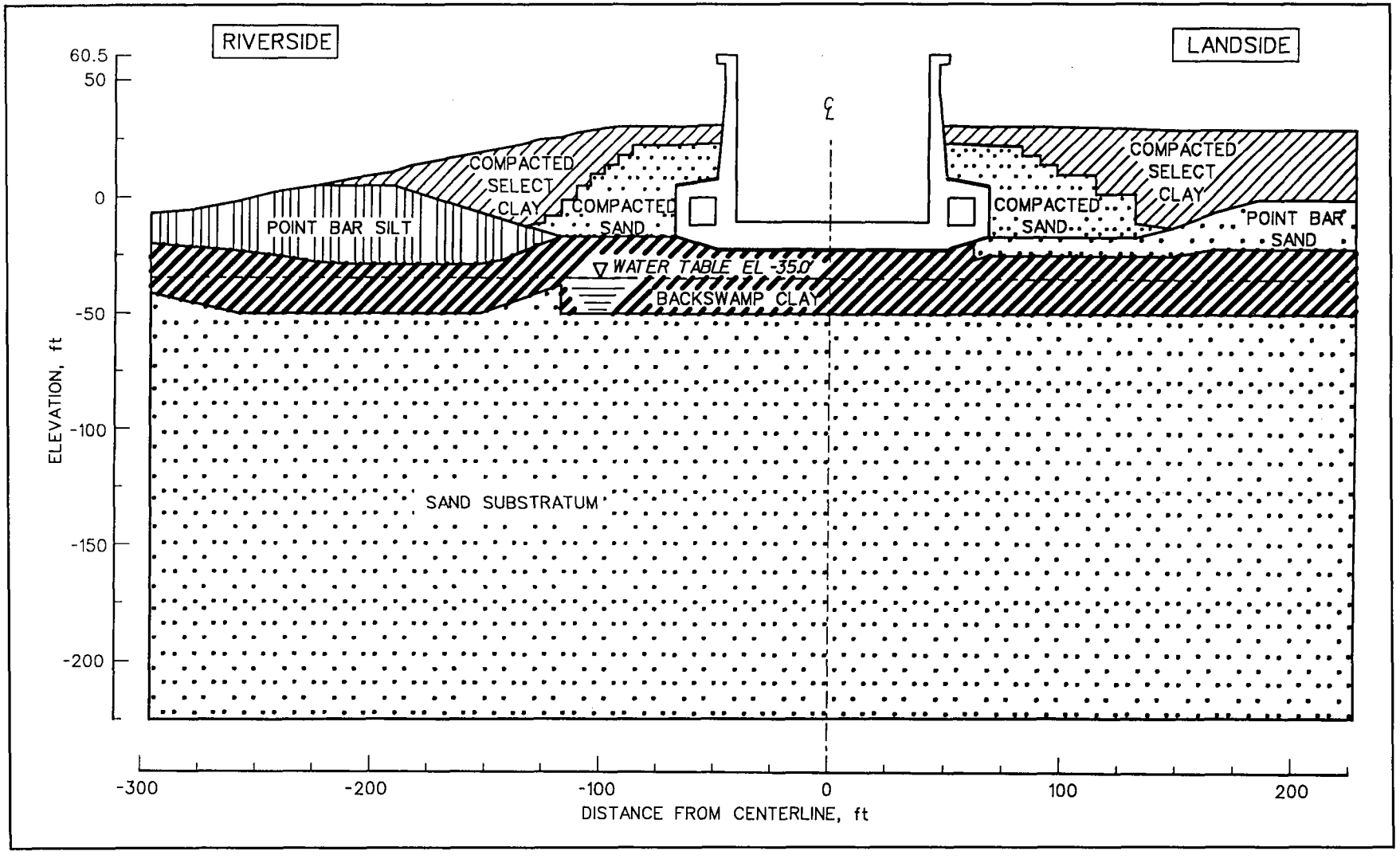

Figure 54. Material regions corresponding to finite element mesh modeling lock monolith no. 10

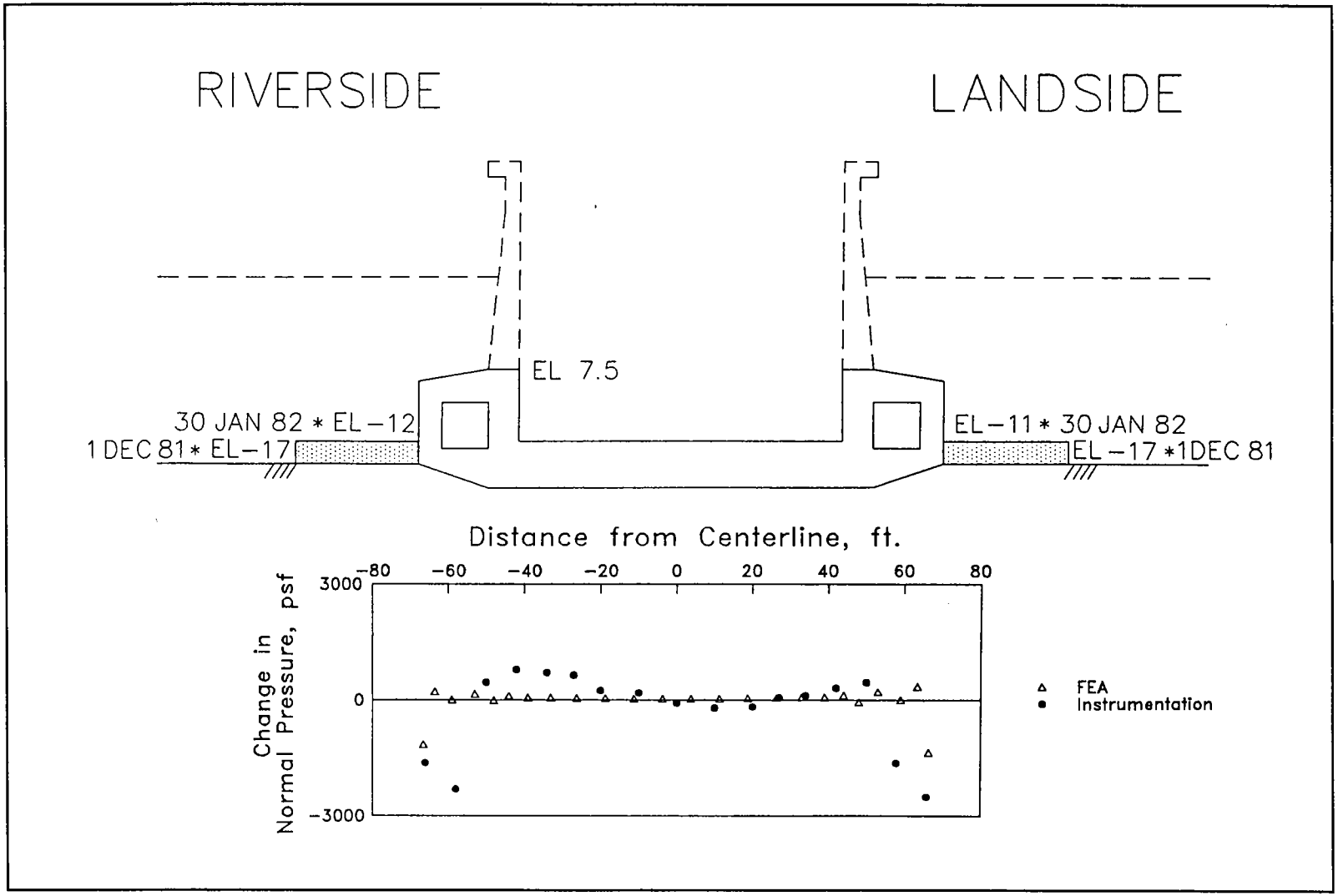

Figure 55. Comparison of changes in effective normal base pressures after placement of 5 ft of backfill

Computed settlements of the foundation due to lock construction and backfilling are given in Figure 56 for select nodal points. These nodal points define the surface of the foundation, prior to lock construction, and are the same nodes whose displacements after lowering of the water table and excavation were discussed in Figures 29 and 33, respectively. The computed settlement below the center line of the lock was 2.1 in. and below the center lines of the riverside and landside backfills were 2.6 and 2.5 in., respectively. The values for computed nodal displacements within the backfill regions away from the lock showed that the magnitude of the settlement decreased as the thickness of backfill placed decreased.

Figure 57 shows the computed values of major principal effective stresses and their orientations for the same foundation elements for which values of principal effective stress were discussed after the completion of construction stages A, B, and C. Comparisons with the values computed after the completion of the excavation stage C and reported in Figure 34 show both a substantial increase in the magnitude of principal effective stress and a significant reorientation of principal planes for these elements. This response is consistent with expected behavior with the construction of the lock and the placement of backfill. In general, the orientations of principal stresses after lock construction and backfilling correspond to the primary direction of loading for each of the foundation elements. For example, the two pairs of foundation elements located immediately below the two culverts reflect the influence of unsymmetrical loadings due to lock construction and backfilling. At the center line of the lock, the change in stress is symmetrical about the center of the element and the principal effective stress corresponds to the vertical effective stress, as is the case for the shallow foundation element 200 ft landside of the center line.

Figure 58 shows the computed normal pressures along the base of the lock and along the riverside and landside culvert walls and stem walls and the stress meter measurements of 22 September 1983. No pore water pressures were recorded by the piezometers along the base or within the backfill at this stage of construction. The computed base pressures were symmetrical about the center line and in the shape of an inverted saddle. The greatest computed pressure was 5,500 psf and was located below the stem walls. Below the center line of the lock, the base pressure was 3,800 psf. The lowest values for the base pressures normal to the lock were computed below the outside corners of the culverts and were 3,600 psf (riverside) and 3,200 psf (landside). One factor contributing to the lower values computed below the corners of the culverts was the settlement of the foundation due to the placement of backfill adjacent to the culverts, as discussed previously and shown in Figure 55. The computed normal pressures acting on the walls increased with depth below the surface of the backfill, and the pressures acting on both sides of the lock were equal in magnitude at a given elevation. The results from 22 September 1983 stress meter measurements were in agreement with the finite element results, considering the trend of the instrumentation measurements and discounting erroneous data.

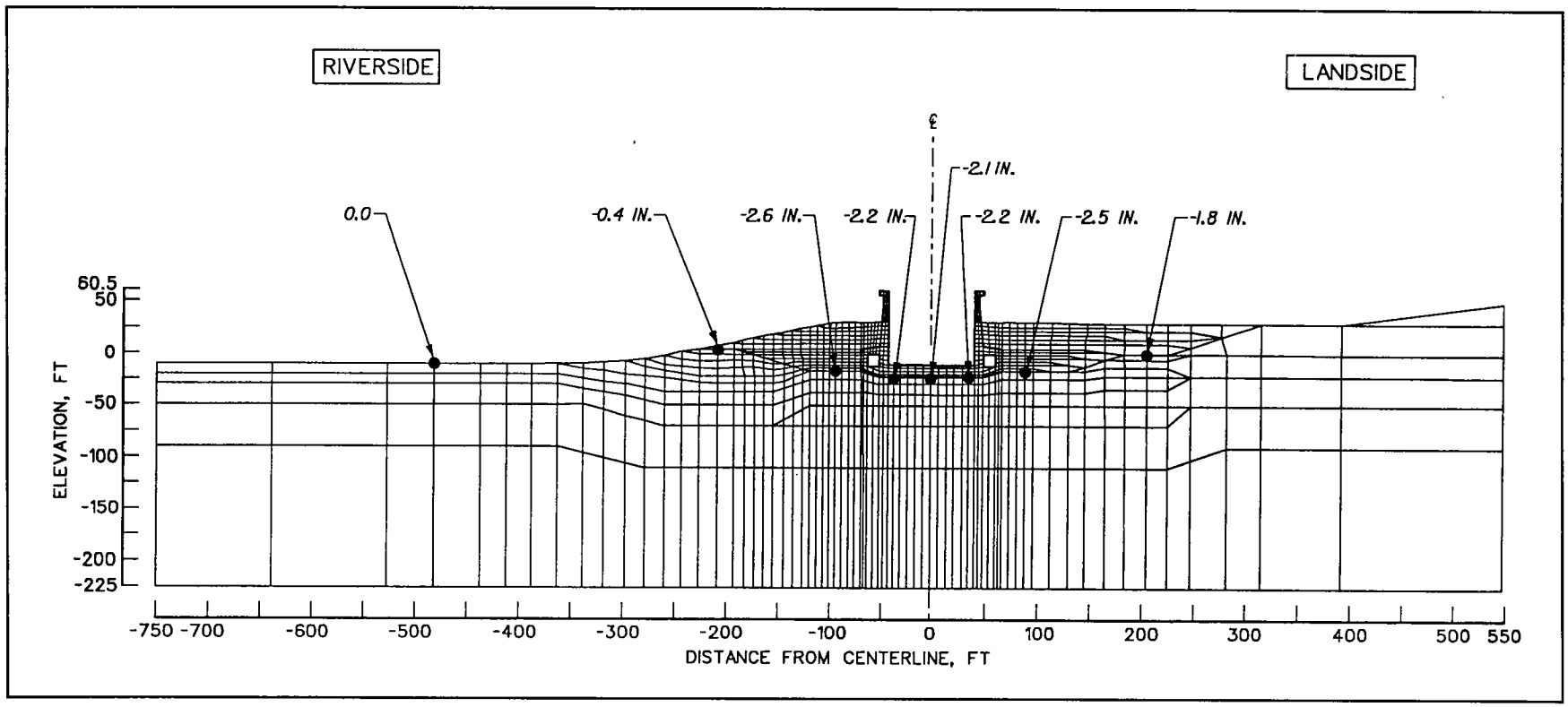

Figure 56. Vertical displacements of select nodal points due to construction of lock and placement of backfill

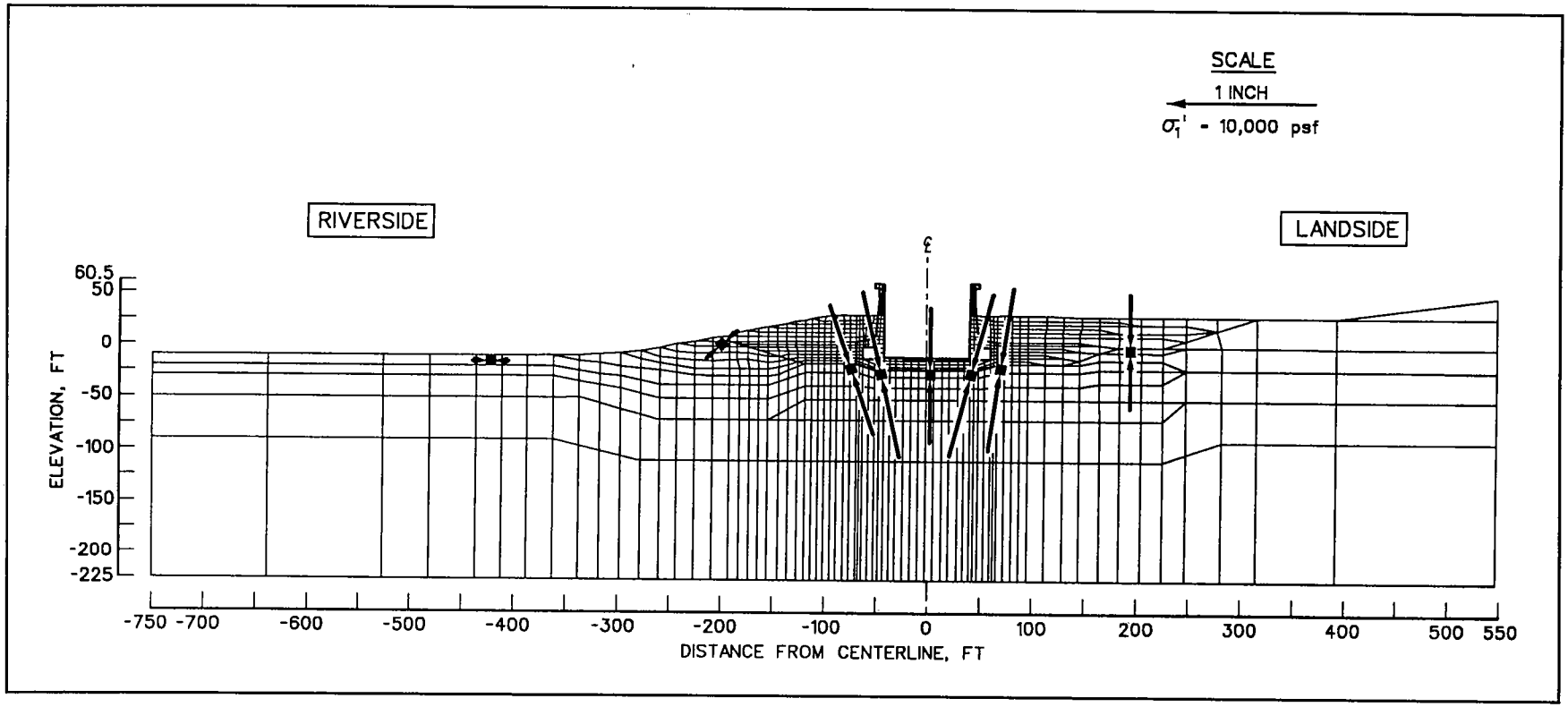

Figure 57. Major principal effective stresses for select foundation elements after construction of lock and placement of backfill

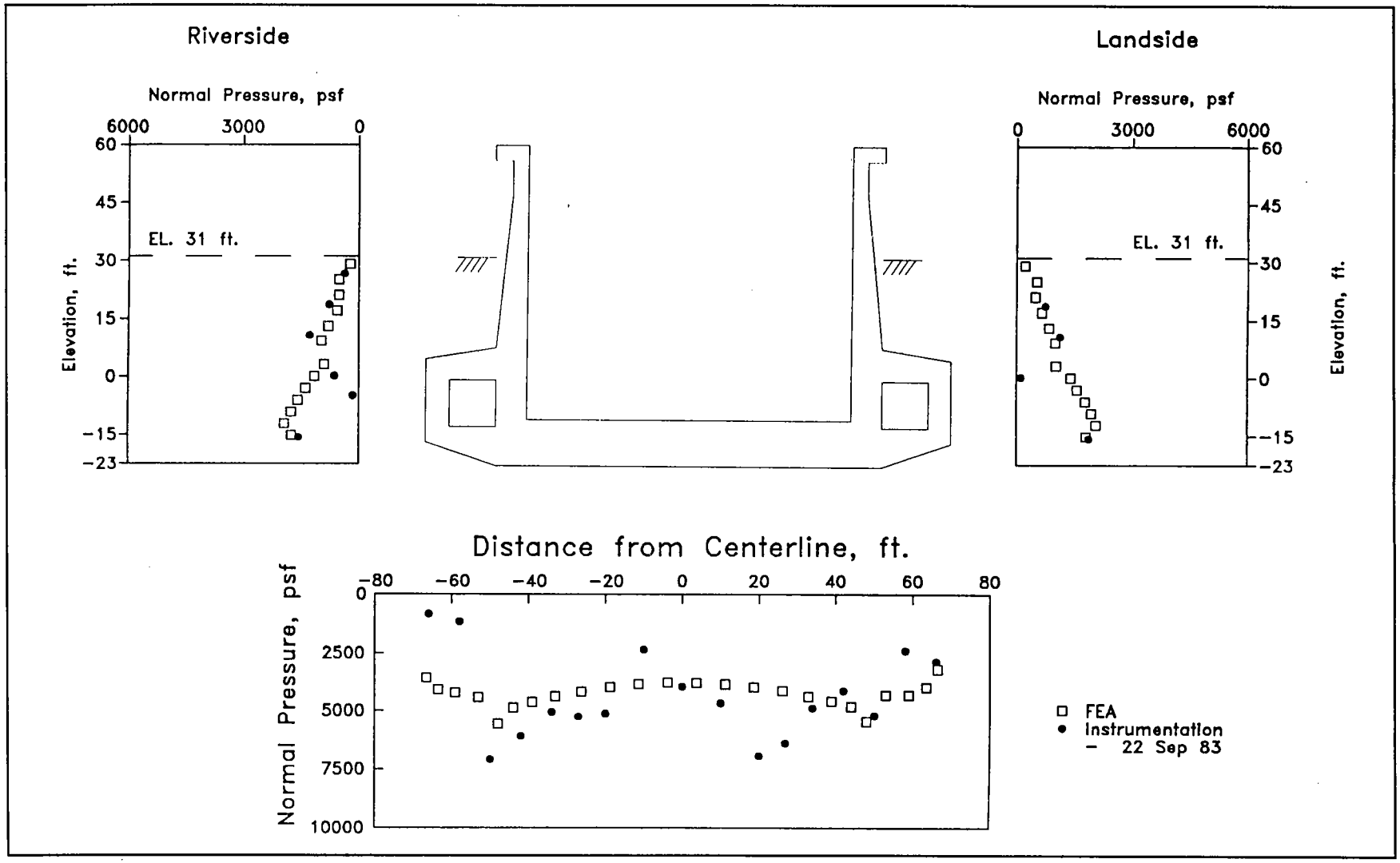

Figure 58. Normal pressures after lock construction and placement of backfill

In addition to normal stresses, shear stresses were also computed to be acting along the lock walls and the base of the lock. Since shear stresses usually act downward along the surface of a wall, as was the case in this analysis, they are referred to as the drag, or downdrag. These drag forces are a result of either differential settlement within the backfill or the movement of the backfill relative to the lock. In this loading case, downdrag resulted from the differential settlement of the soil during the backfilling adjacent to the lock. In loading cases discussed in later sections of this report, the drag forces may act upward, depending upon the movement of the lock relative to the backfill.

The computed values for the shear stresses along the interface between the lock and the foundation and the lock and the backfill are presented in terms of the mobilized friction angles, δ_{mob}, and are shown in Figure 59. The value of δ_{mob} can be expressed as follows:

$$\tan \delta_{mob} = \frac{\tau}{\sigma_n'} \tag{1}$$

where

τ = computed value of shear stress

σ_n' = computed value of effective normal stress

Along the base of the lock, the largest value of δ_{mob} was computed below the stem walls and was 9 deg riverside and 6 deg landside. Below the center line of the lock, δ_{mob} decreased to nearly 0.

The variation in mobilized friction angle along the walls with elevation was distinguishable from those computed values that occurred along the stem walls, above el 7.5 (Figure 5), and computed values that occurred along the vertical culvert walls. Along the riverside stem wall, δ_{mob} increased from a value equal to zero at el 29, to a value equal to 20 deg at el 17. Then δ_{mob} decreased in value to 12 deg at el 9. The greatest value of mobilized friction angles were computed as 30 deg at the top of the riverside culvert wall. At el -15.5, δ_{mob} decreased in value to 17 deg. A similar trend was observed along the landside stem and culvert walls. Maximum values for δ_{mob} were 16 deg at el 17 along the stem wall and 28 deg at the top of the culvert wall.

Computed variations in horizontal earth pressure coefficient, K_h, with elevation after the completion of lock construction and the placement of backfill are shown in Figure 60. K_h is the ratio of the horizontal effective stress, σ_x', on the lock wall to the effective overburden pressure. The effective overburden pressure equaled the difference between the total overburden pressure and the pore water pressure. The total overburden pressure was computed as the total weight of a 1-ft-square column of soil above a given elevation. When the river was above el 31, the elevation of the

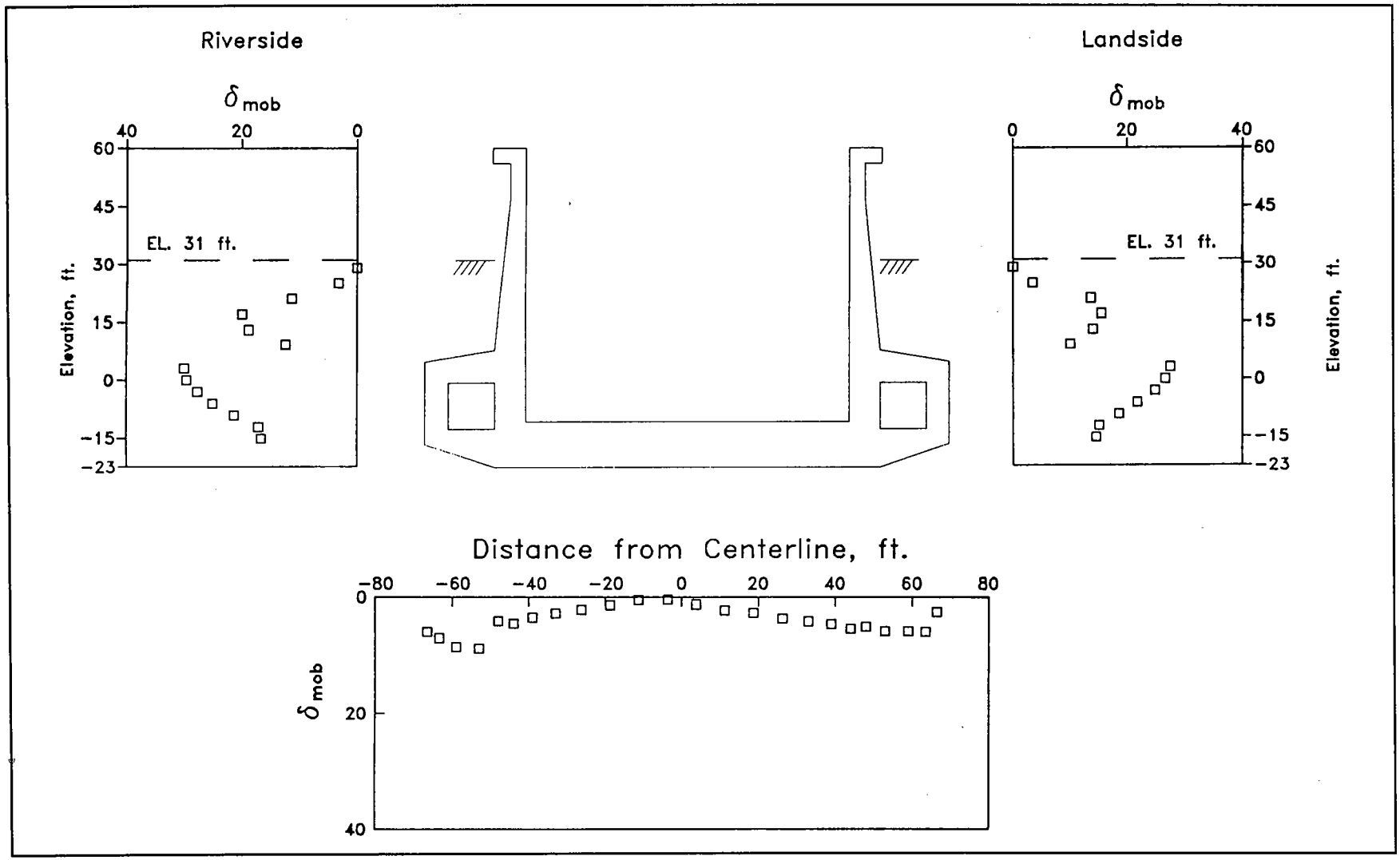

Figure 59. Mobilized friction angles along exterior of lock after lock construction and placement of backfill

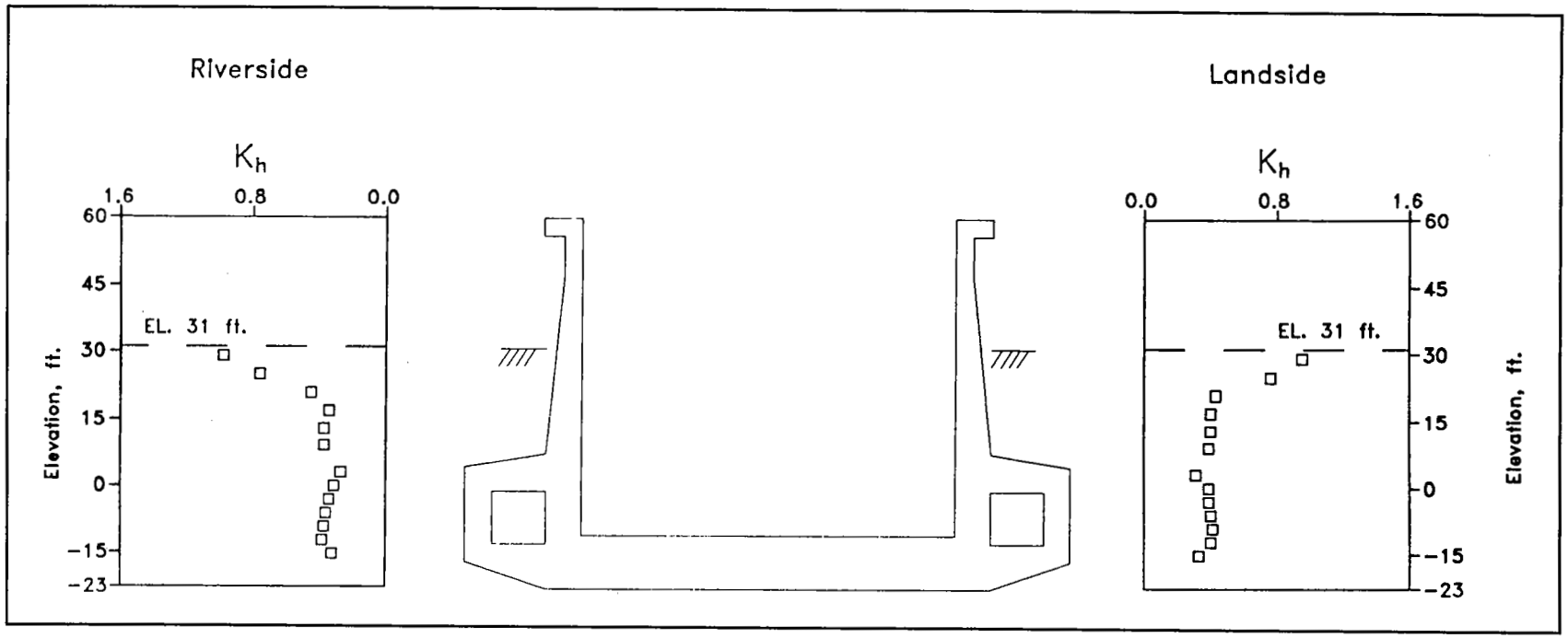

Figure 60. Horizontal earth pressure coefficients, K_h, after lock construction and placement of backfill

backfill adjacent to the lock walls, the weight of the water was also included in the computation of the total overburden pressure. The value of K_h decreased with decreasing elevation along the stem walls and was nearly constant along the culvert walls (Figure 60). The maximum K_h value was 0.98 at el 29, and the minimum value was 0.34 at el 17 along the riverside stem wall. The average K_h values are given in Table 6 for the different backfills placed against the riverside and landside stem walls and culvert walls. The average value for K_h within the select compacted clay backfill was 0.87, and the average value for K_h within the compacted sand backfill adjacent to the stem wall was 0.38 (Table 6). K_h was nearly constant, averaging 0.35 along the riverside culvert wall. The computed distribution for K_h with elevation landside of the lock was the same as that computed riverside of the lock. The average values for K_h within the compacted sand backfill landside of the stem wall and culvert wall were higher than those computed riverside of the lock by 0.03 and 0.05, respectively.

Table 6
Average Values of Horizontal and Vertical Earth Pressure Coefficients after Construction of Lock and Placement of the Backfill

Backfill Region	Backfill Material	Riverside K_h	Riverside K_v	Landside K_h	Landside K_v
Stem	Compacted select clay	0.87	0.02	0.86	0.02
Stem	Compacted sand	0.38	0.10	0.41	0.10
Culvert	Compacted sand	0.35	0.15	0.40	0.15

Variations in the vertical (shear) earth pressure coefficient, K_v, with elevation are shown in Figure 61 after the completion of lock construction and the placement of backfill. K_v is the ratio of the vertical shear stress, τ_{xy}, to the effective overburden pressure. A positive K_v value implies that τ_{xy} acts downward along the lock walls. Along the riverside stem wall, K_v increased from zero at el 29 to 0.13 at el 13. K_v then decreased to 0.08 at el 9. The greatest value for the vertical earth pressure coefficient was 0.18 at the top of the riverside culvert wall. There was a slight decrease in the value of K_v to 0.17 at el -15.5. A similar trend was observed along the landside stem and culvert walls. Maximum values for K_v were 0.11 at el 17 along the stem wall and 0.19 at the top of the culvert wall. The average values for K_v were 0.02 for the compacted select clay adjacent to the stem walls and 0.10 and 0.15 for the compacted sand adjacent to the stem walls and culvert walls, respectively. The distribution of K_v shown in Figure 61 appears similar to the distribution of δ_{mob} in Figure 59. This is not surprising since the factors that affect the values of δ_{mob} also affect those of K_v.

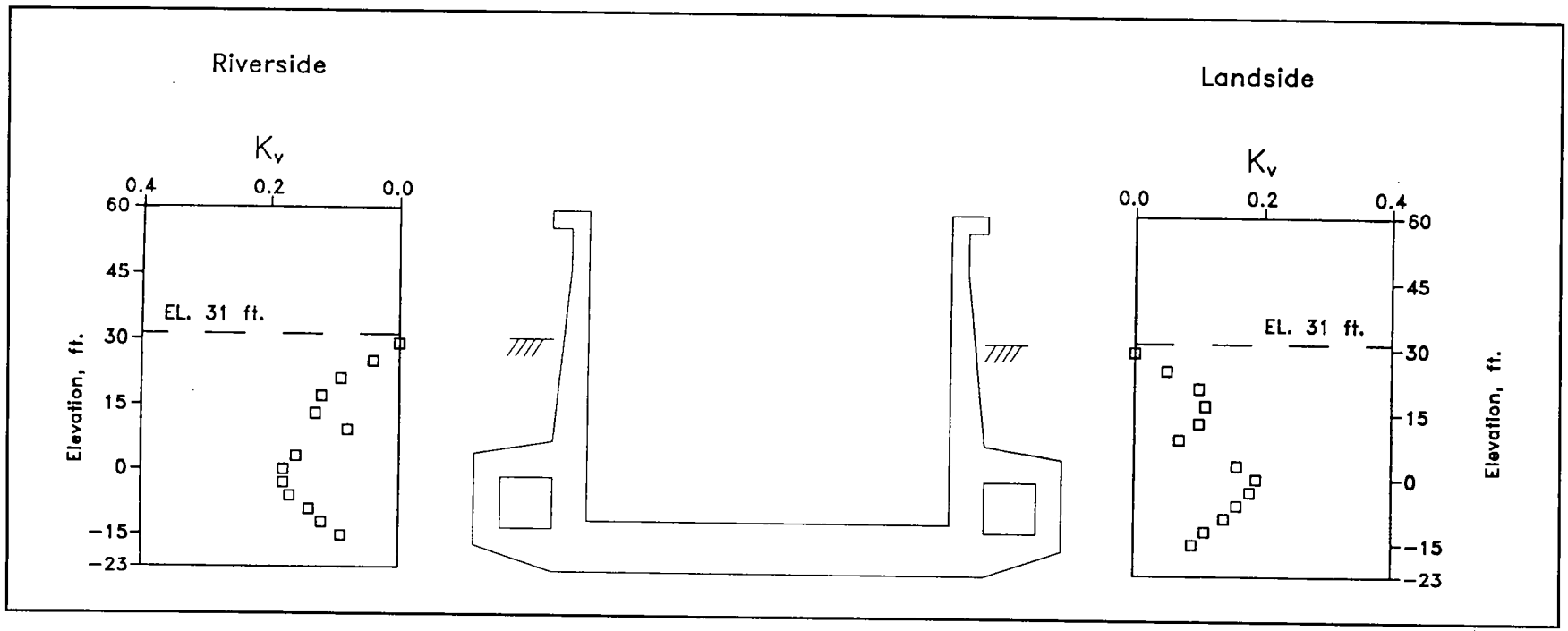

Figure 61. Vertical earth pressure coefficients, K_v, after lock construction and placement of backfill

Stress paths for the foundation elements identified in Figures 36 and 62 are shown in Figures 37 through 48. Stress path point no. 4 corresponds to the completion of lock construction and backfilling (Table 5). In general, these stress paths are upward and to the right. Although there is a corresponding increase in shear stress with an increase in confining pressure, the slope of the stress paths shown in these figures is less than the slope of the K_f - line. Thus, the mobilized shear strength within these foundation elements are less for stress point no. 4 than that for stress point no. 3 (after excavation), due to the increased confinement of the foundation by the lock and backfill. The exceptions are elements 357 and 360, riverside of the backfill. The changes in the stress paths for these elements reflect the lateral thrust toward the river channel by the newly placed backfill.

Stress paths for the newly placed backfill elements identified in Figure 62 are shown in Figures 63 through 69. The stress paths for six of seven backfill elements are upward and to the right, similar to the stress paths for most of the foundation elements shown in Figures 37 through 48. The exception is backfill element 471, whose stress path is shown in Figure 68. It's stress path is downward and to the right, reflecting the lateral thrust of the adjacent backfill. Although there is a corresponding increase in shear stress with an increase in confining pressure for all of the elements, the slopes of the stress paths are less than the slope of the K_f - line.

Figure 70 shows the stress distributions normal to the cross sections of the lock after the completion of lock construction and the placement of backfill. Section A-A is adjacent to the riverside stem wall 39 ft from the center line of the lock, and section B-B is 3.75 ft riverside of the center line. The stress distribution along section B-B is nearly linear and varies from a tensile normal stress equal to -93.5 ksf at el -11, the floor of the lock, to a compressive normal stress equal to 97.5 ksf at el -23, the base of the lock. The stress distribution normal to section B-B is converted to an equivalent moment about the midelevation of the base slab of the lock using the flexure formula. The corresponding moment computed about el -17 is -2,147 kip-ft. The negative sign reflects the tensile normal stress at the base of the lock.

The normal stress distribution along section A-A is bilinear, in contrast with the linear distribution along section B-B (Figure 70). The normal stress along section A-A varies from a tensile normal stress equal to -33.5 ksf at the floor of the lock to a compressive normal stress equal to 26.5 ksf at the base of the lock. One factor contributing to the difference in the shape of the stress distribution normal to section A-A when compared with that for section B-B is the influence that shear along the base of the lock has on the distribution of stresses within the lock. The greatest value of shear acting along the base occurs below the stem walls (Figure 59), which is adjacent to section A-A. The magnitude of this shear boundary condition diminishes as the center of lock is approached, as does the difference in slope along the two sections of the normal stress

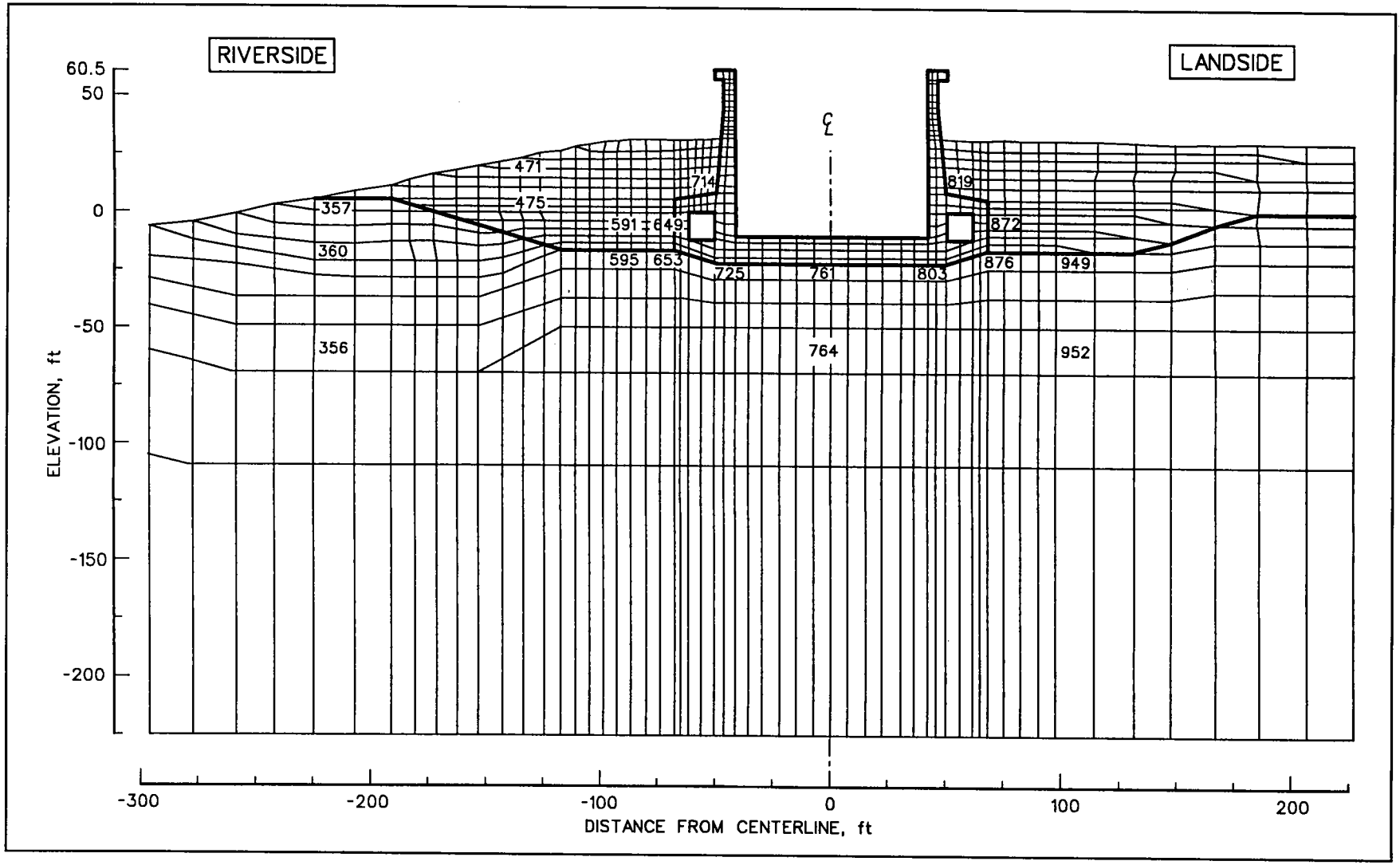

Figure 62. Locations of finite elements within foundation and backfill for which stress paths were computed

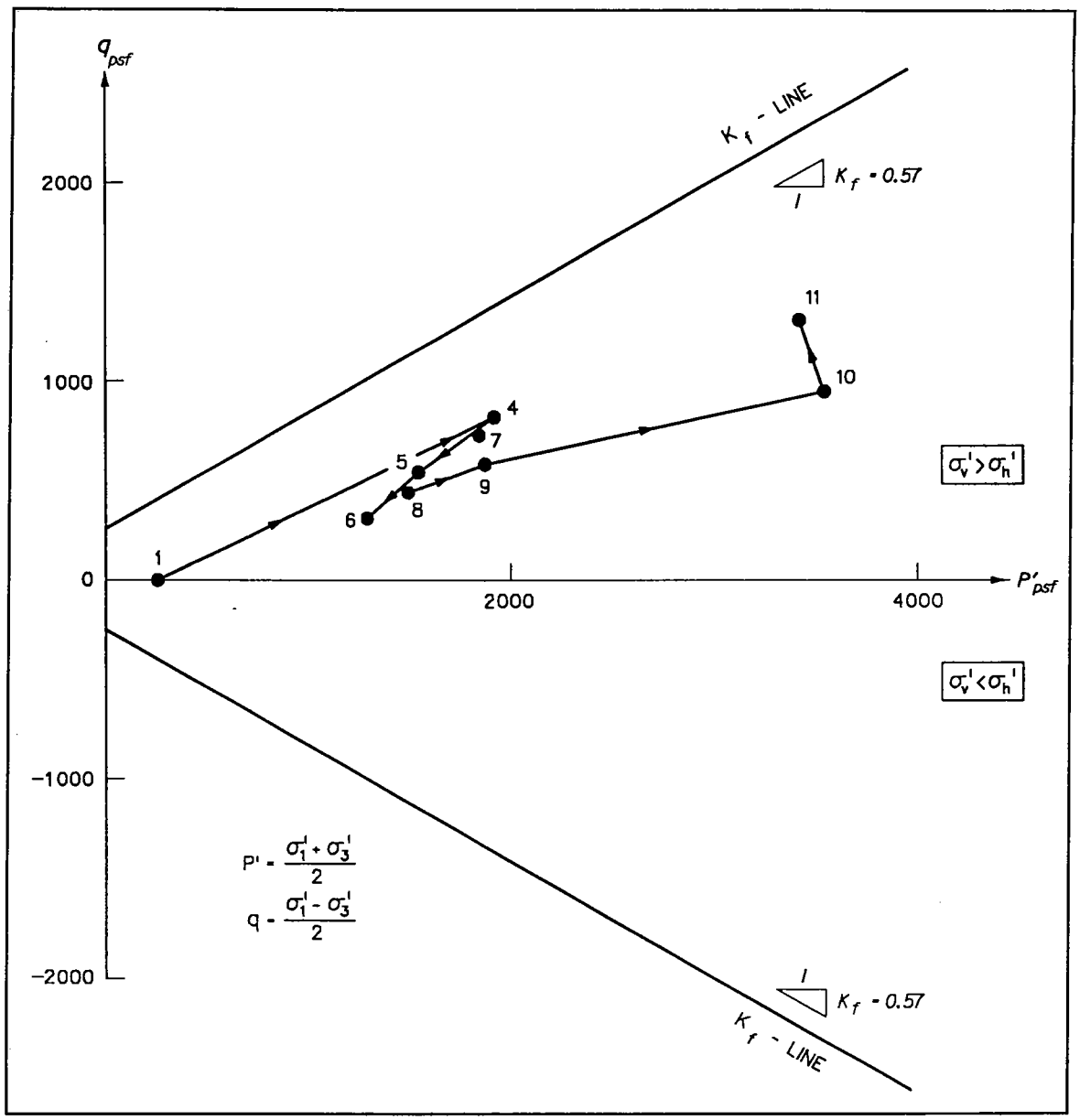

Figure 63. Stress paths for compacted sand backfill element 649, adjacent to riverside culvert at el -6

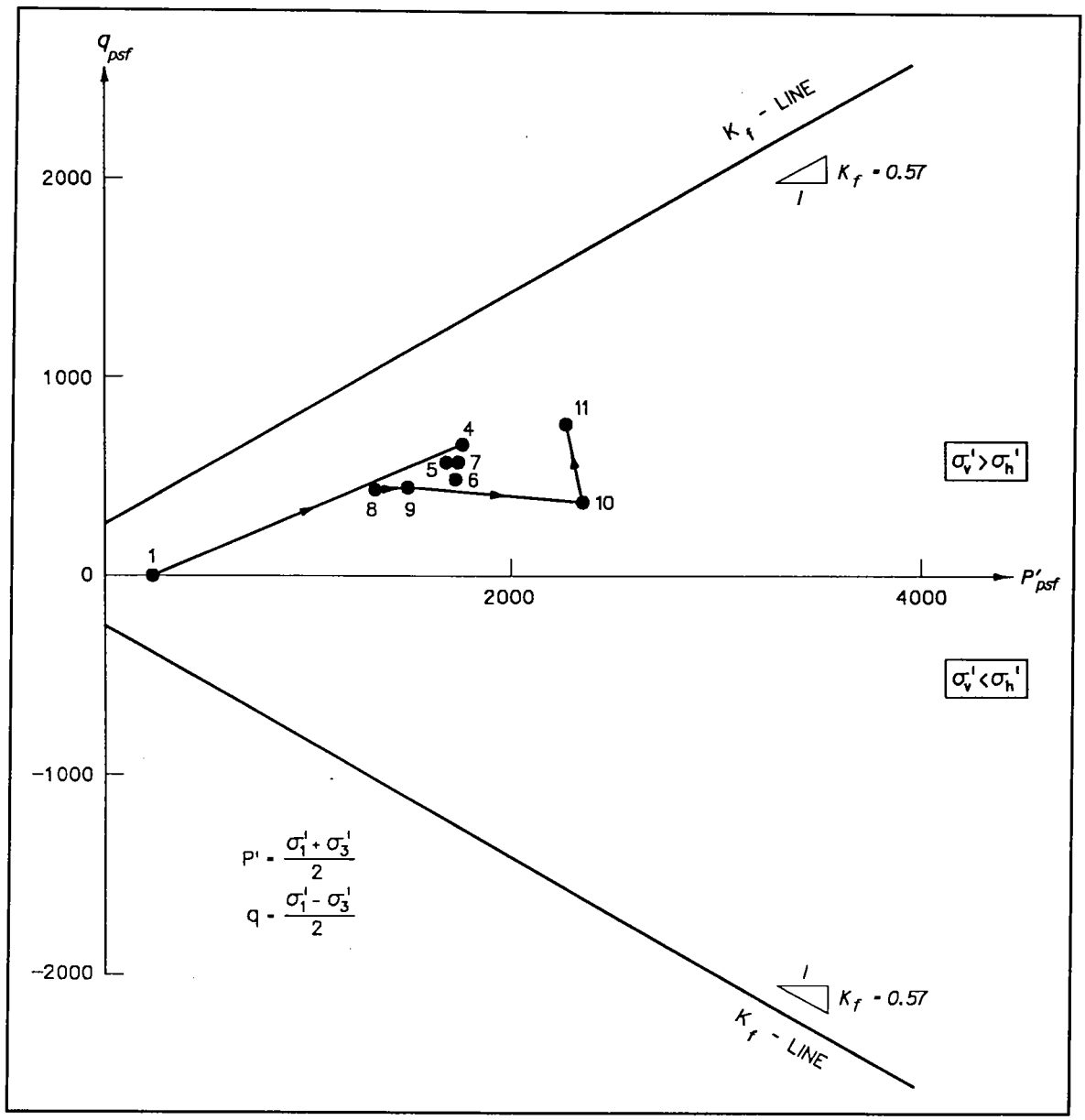

Figure 64. Stress paths for compacted sand backfill element 872, adjacent to landside culvert at el -6

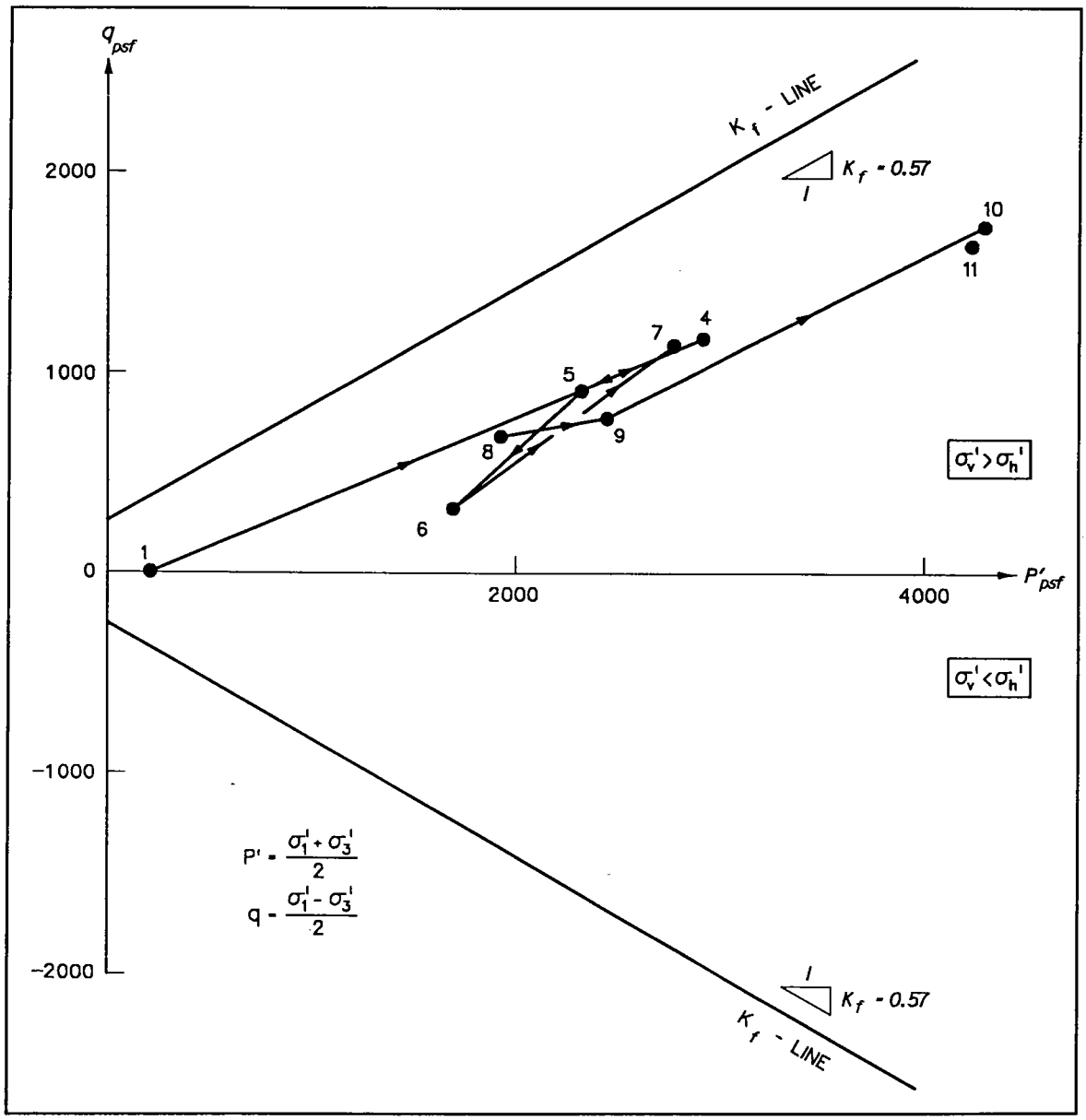

Figure 65. Stress paths for compacted sand backfill element 591, 21 ft riverside of culvert at el -6

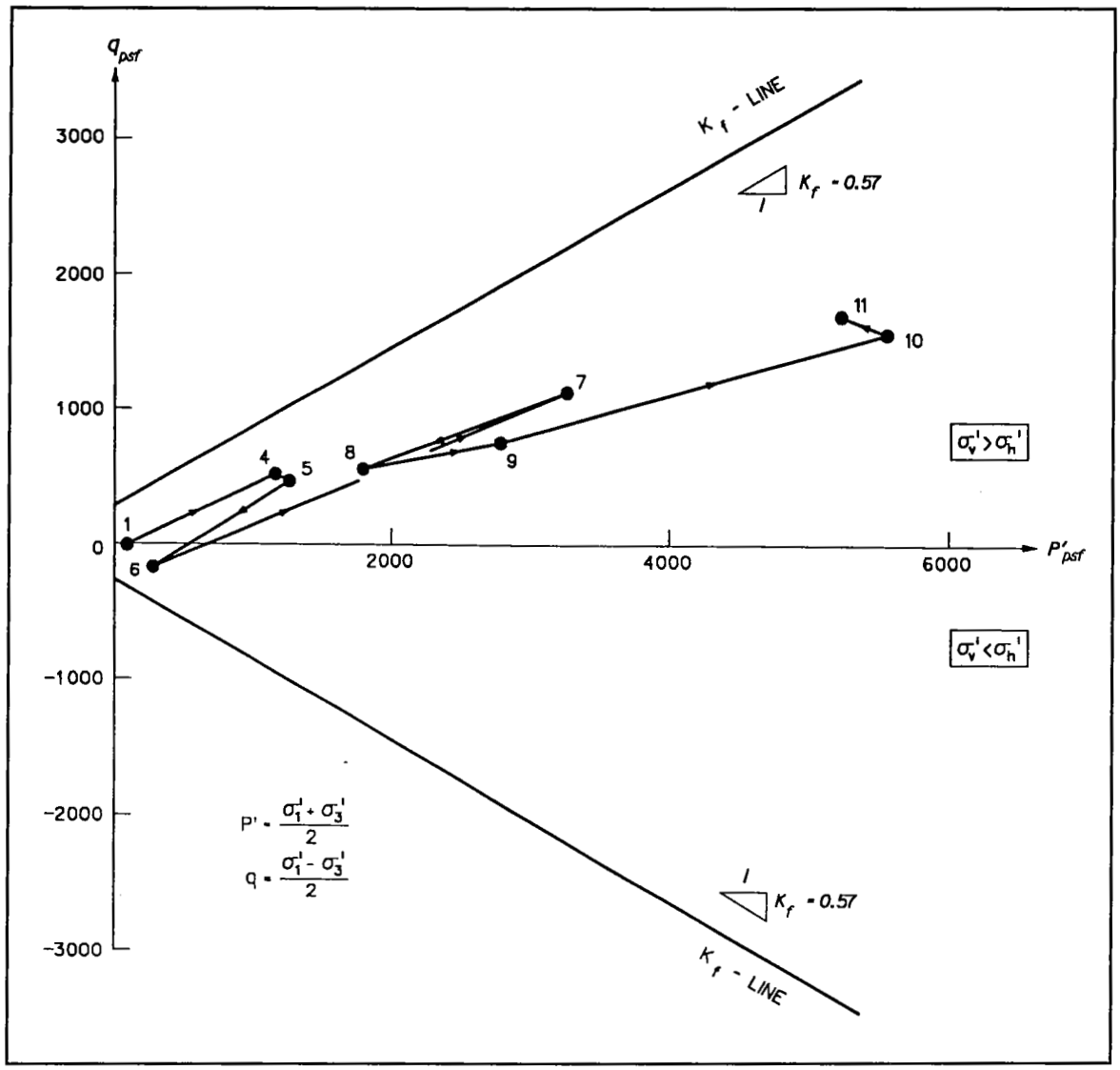

Figure 66. Stress paths for compacted sand backfill element 714, adjacent to riverside stem wall at el 13

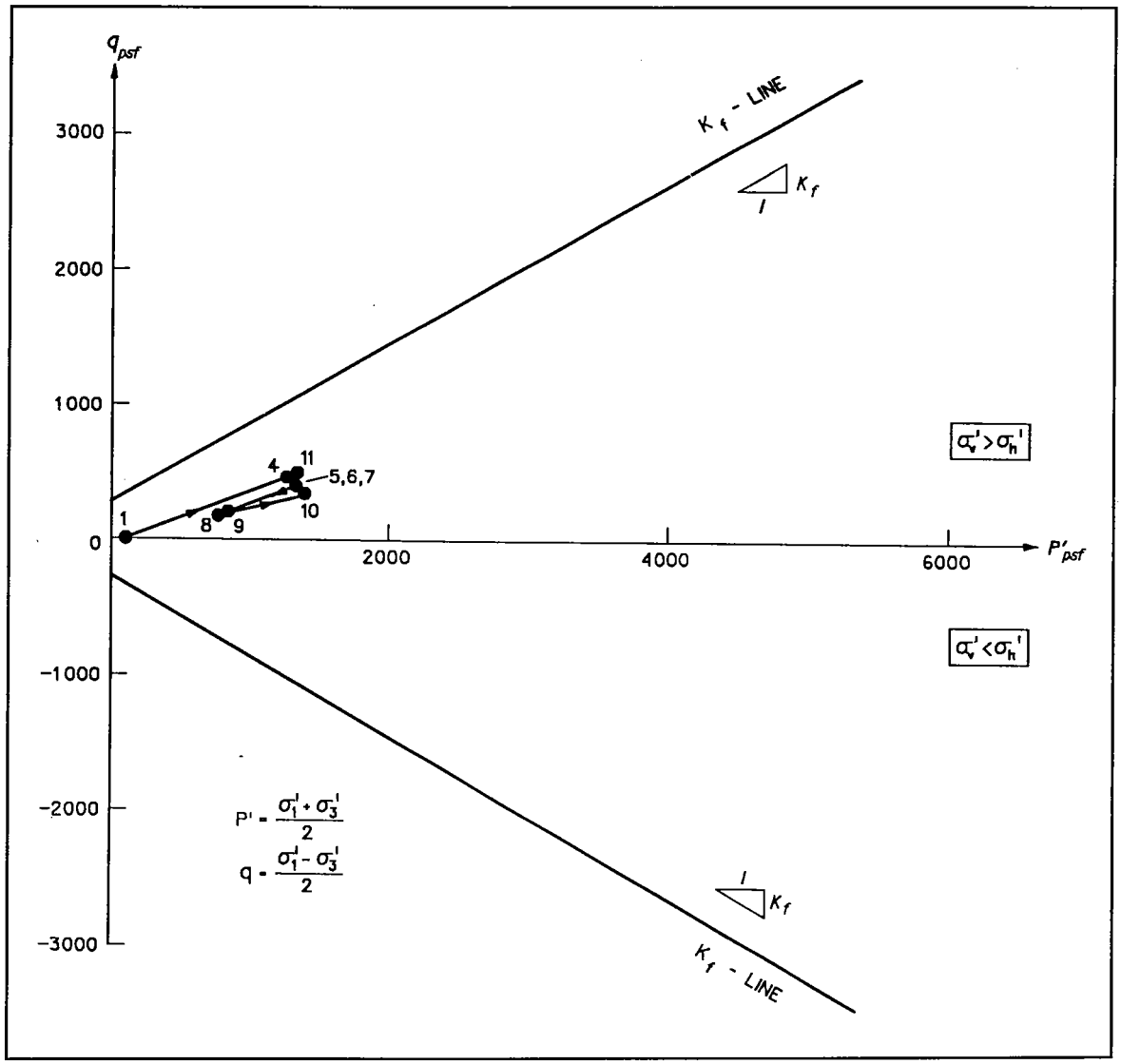

Figure 67. Stress paths for compacted sand backfill element 819, adjacent to landside stem wall at el 13

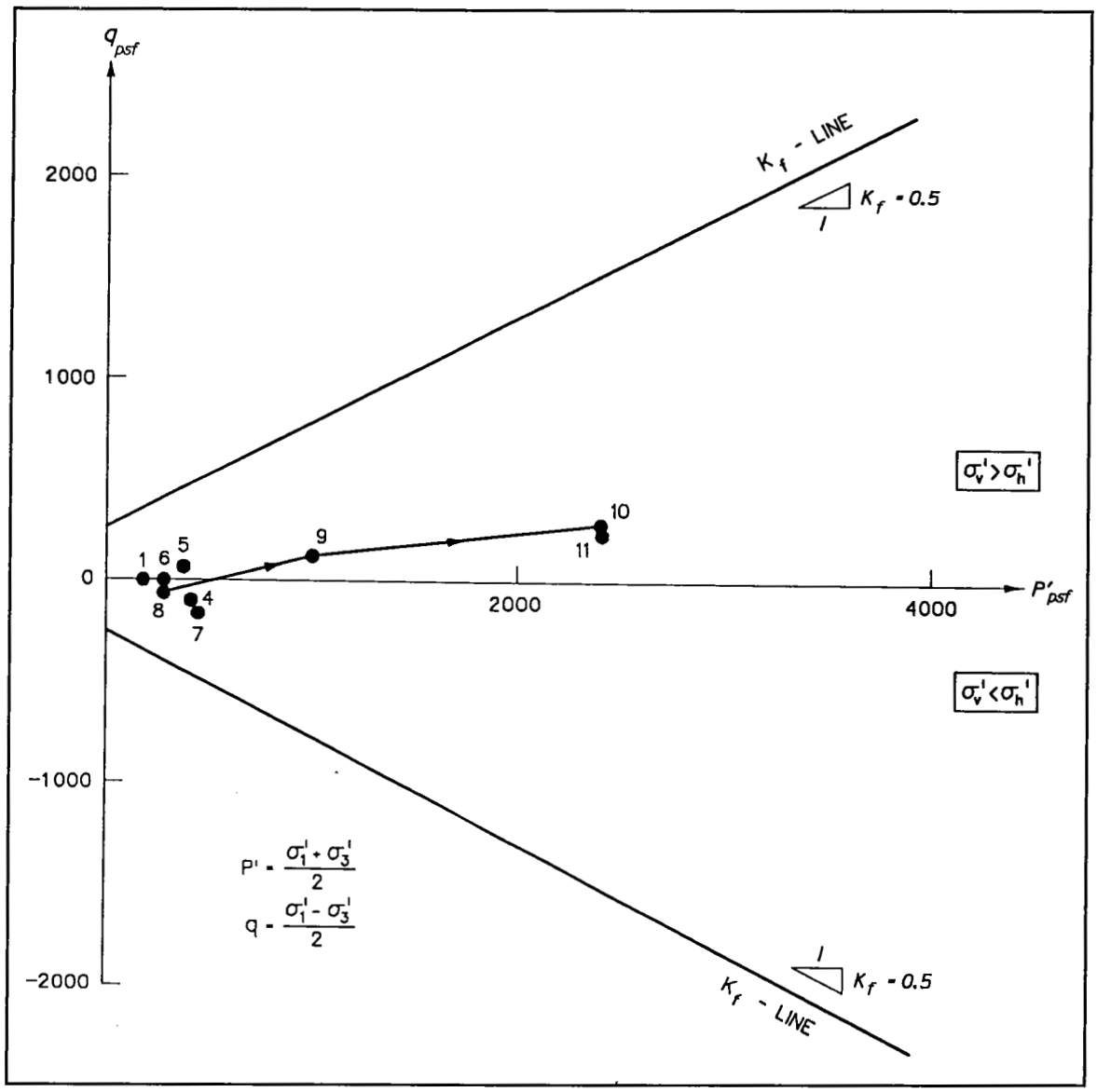

Figure 68. Stress paths for compacted select clay backfill element 471, 80 ft riverside of stem wall at el 20

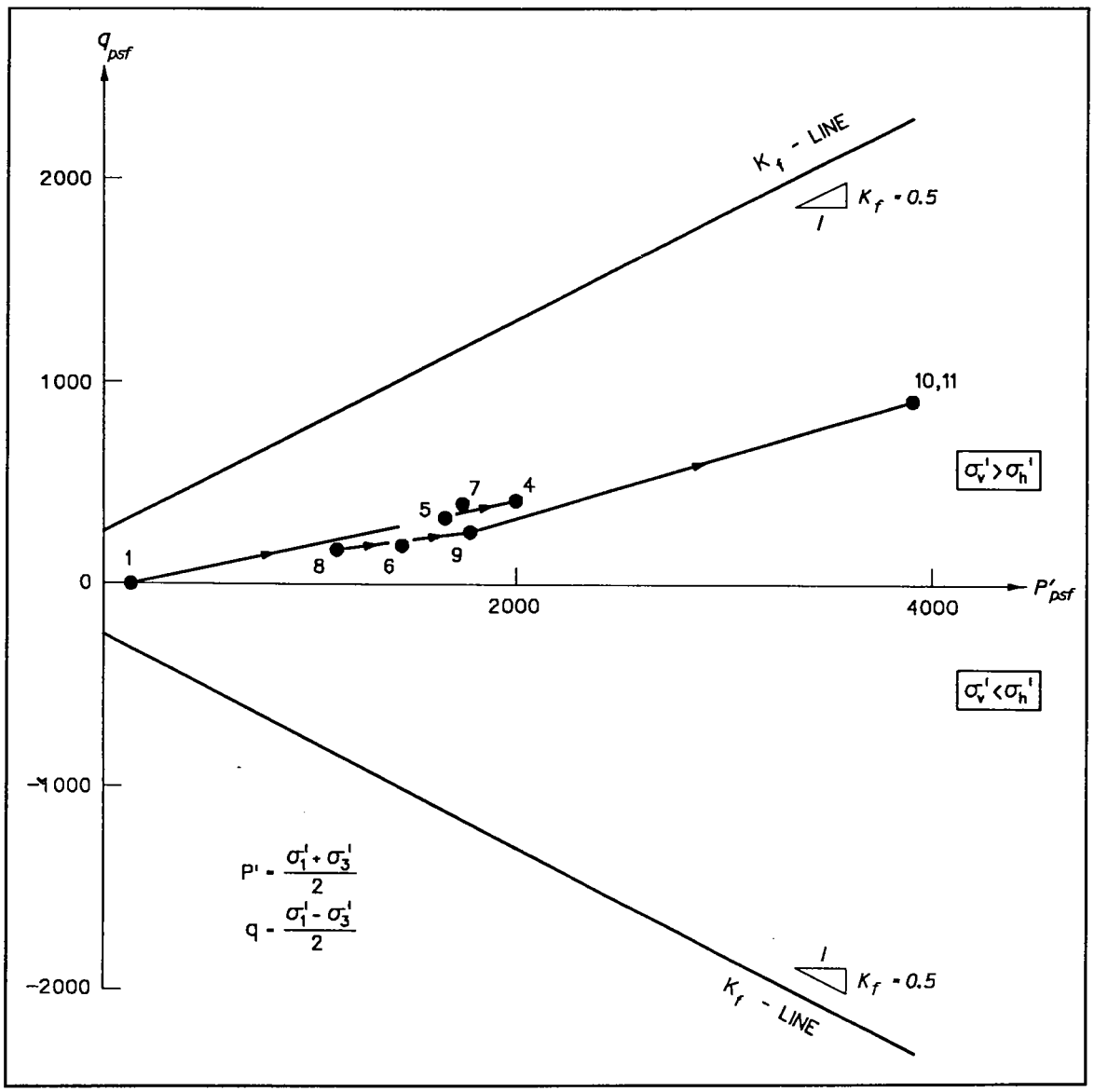

Figure 69. Stress paths for compacted select clay backfill element 475, 80 ft riverside of stem wall at el 3

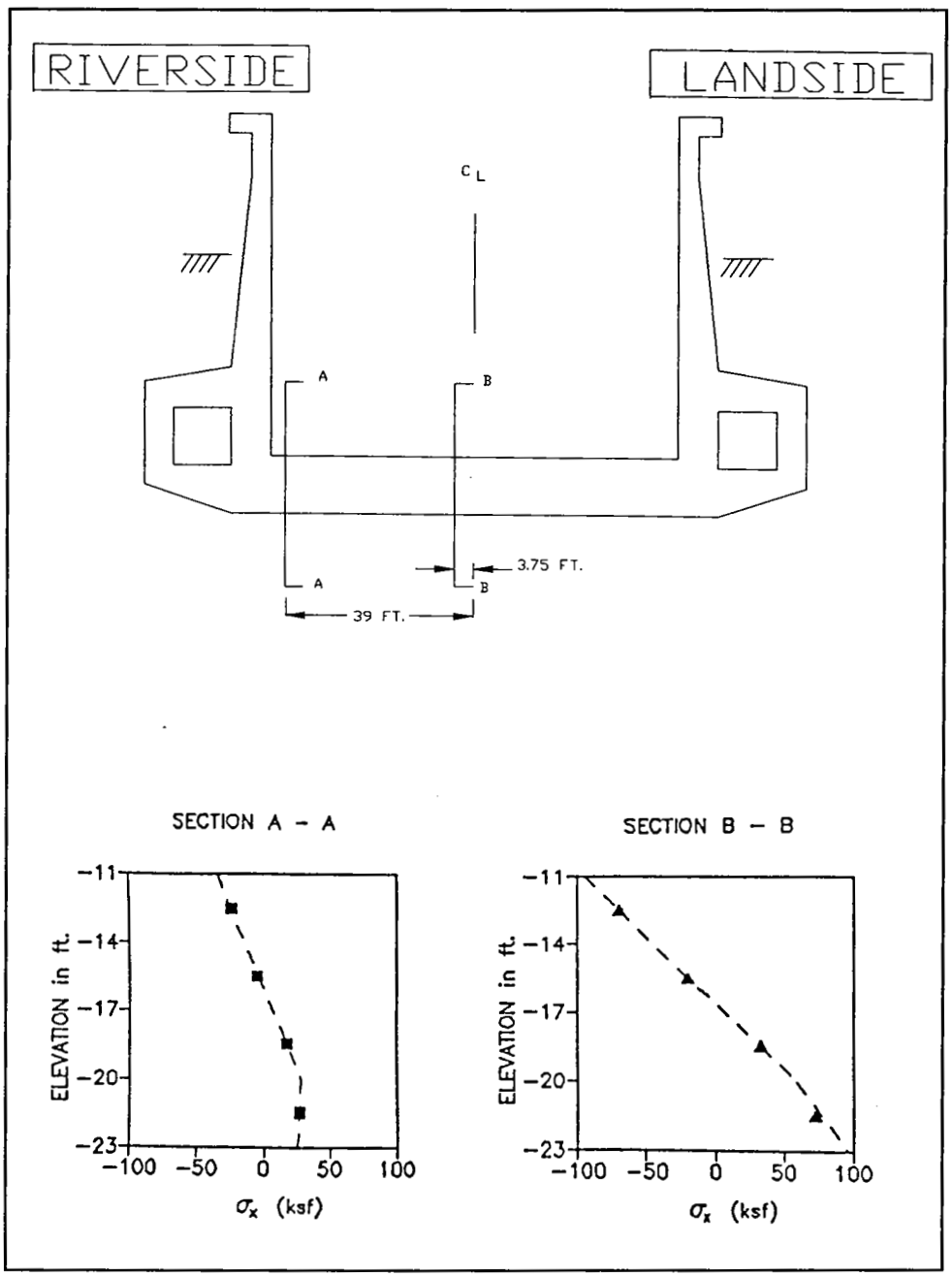

Figure 70. Stress distributions across two sections within lock after lock construction and placement of backfill

distributions. The corresponding moment computed at section A-A is -741 kip-ft. The value for the moment at section A-A is less than the value for the moment at section B-B by a factor of 3.0. This procedure was also used to compute the equivalent moments for each of the cross sections for the remaining groups of elements comprising the base of the lock and the pairs of elements comprising the culverts and the stem walls.

Figure 71 shows the resulting distribution of factored moments computed within the lock along with the design moment capacity distributions. The moments are computed from the finite element stresses and multiplied by a factor of 2.21. This factor reflects the extreme load case and is equal to the products of 1.3, the factor applied to hydraulic structures, and 1.7, the factor applied to live loads. The design moment capacity distributions were developed for each of the members comprising the lock using a yield strength of reinforcement steel equal to 60 ksi. The results of the finite element analysis after lock construction and backfilling indicate that the top of floor for the entire base slab is in tension. The largest factored moment, -4,745 kip-ft was computed along the base at the center line of the lock. Due to the earth pressures acting along the stem walls, the chamber sides of the stem walls are in compression. The maximum values for the factored moments computed within the stem walls was equal to 195 kip-ft and occurs at el 9.25. As expected, the values for the factored moments at all locations with the lock are all well below those for the design moment capacity for this loading case. A factored moment value that is less than the design moment capacity value indicates that the moment capacity for that structural member is not fully utilized at that location within the lock.

Key Operational Load Cases

This section of the report discusses the results from three finite element analyses and compares these results with the instrumentation measurements recorded at lock monolith no. 10 during its operation. The three operational load cases consisted of a low pool elevation condition (Case 1), a high pool elevation condition (Case 2) and a high pool elevation condition with silt loading against the lock walls (Case 3).

Case 1: Comparison of analysis with 30 September 1984 instrumentation measurements

This section discusses the first of three finite element analyses of operational load cases (listed as Case 1 in Table 4) and compares these computed results with the instrumentation measurements recorded at the lock on 30 September 1984. This analysis considers the response of the lock, backfill, and foundation to water loadings. These analyses were performed using the finite element mesh shown in Figures 51 and 53. The

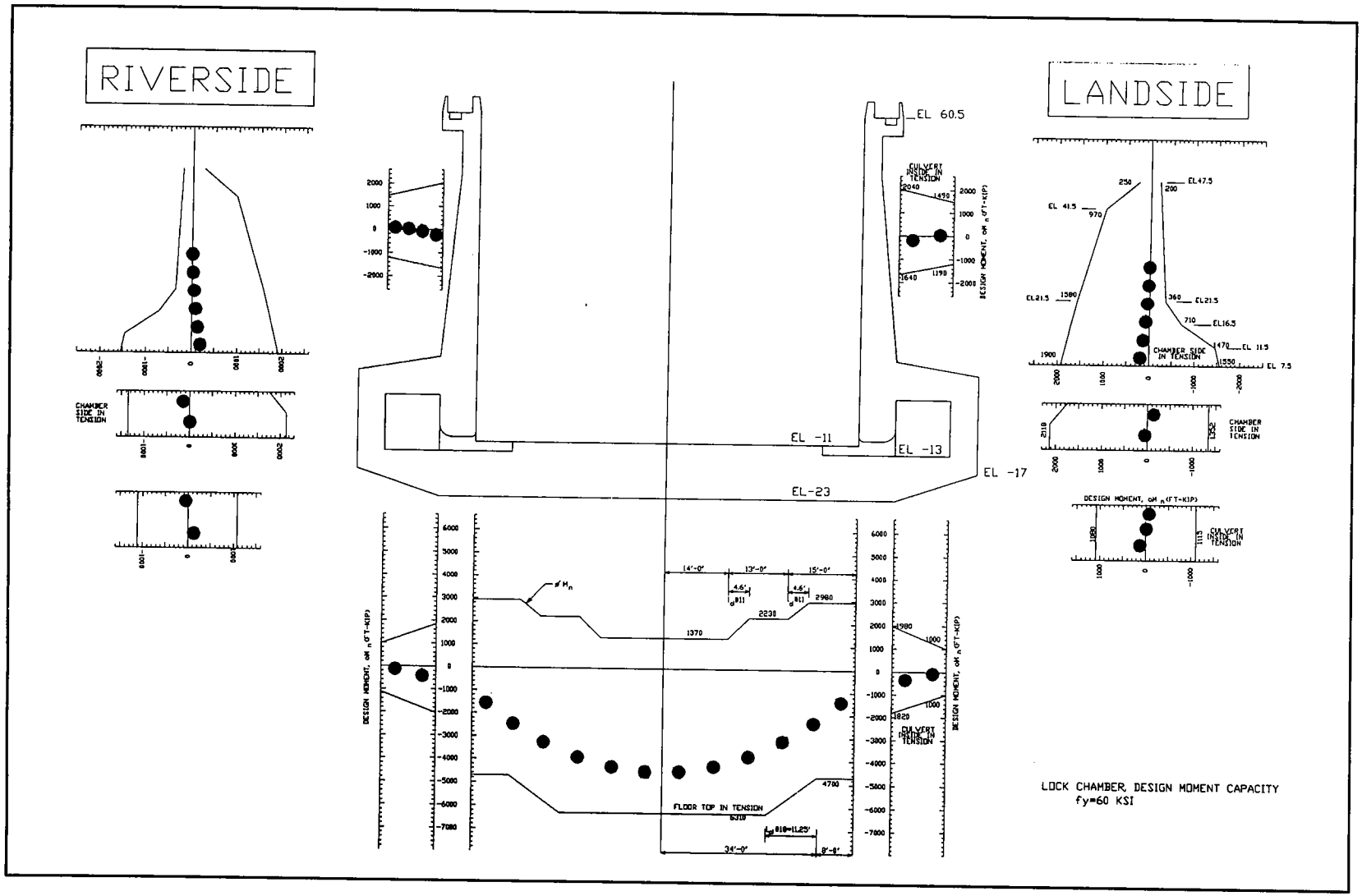

Figure 71. Distribution of factored moments after lock construction and placement of backfill and design moment capacity

computed stresses and displacements within the mesh after construction of the lock and backfilling were the initial values for this series of analyses.

On 30 September 1984, the river in the new channel downstream of the dam and adjacent to the lock, referred to as the lower pool in subsequent sections, is at el 11. The piezometers within the backfill and immediately below the foundation of lock monolith no. 10 indicated a piezometric head ranging in value from el 26 to 31, with the majority of the measurements at el 31. The response of the lock to two different pool elevations in the chamber of the lock are reported; one analysis with a pool el 11 and the second analysis with a pool el 35.

The water level within the foundation and within the backfill was raised from el -35 to the ground surface of the backfill in 23 increments during this series of finite element analyses. Corresponding boundary water pressures were applied to the base of the lock and along the lock walls. The water table within the soil that formed the new river channel was raised from el -35 to the lower pool elevation, 11 ft. The lock chamber and culverts were flooded in two stages. The first stage raised the pool to el 11 and the second stage raised the pool to el 35. The effects of the pool on the lock were modeled through the incremental application of hydrostatic boundary water pressures applied normal to the internal faces of the chamber walls and chamber floor and to the internal faces of the walls, ceiling, and floor of the two culverts. Five load increments were used to raise the pool in the lock from the floor of the lock (el -11) to el 11, followed by an additional 6 increments to raise the pool in the lock to el 35.

Figure 72 shows the two sets of computed total normal pressures along the base of the lock and along the riverside and landside culvert walls and stem walls for the pool elevations in the lock at els 11 and 35 and the 30 September 1984 stress meter measurements. Both analyses resulted in computed base pressures which were symmetrical about the center line and in the shape of an inverted saddle, as was observed at the end of the lock construction analysis. The greatest total normal pressures were computed to be 5,400 and 5,700 psf below the riverside and landside stem walls, respectively, for the water level in the lock at el 11. Below the center line of the lock, the total base pressure was 4,950 psf. The lowest values for the total pressures normal to the base of the lock were computed below the outside corners of the culverts and were 4,100 psf. All base pressures increased in value by nearly 800 psf with the raising of the pool elevation by 24 ft to el 35 in the second analysis. The computed total normal pressures acting on both sides of the lock were equal at a given elevation for both of the analyses. The computed values of total pressures normal to the walls were slightly greater with pool el 35 in the lock than when the water was at el 11. The five total normal pressure measurements from the five Carlson PE-50 stress meters located along each of the culvert walls were less than the water pressure measurements. Therefore, they were considered erroneous. The measurement from these instruments, identified as SPM-54, SPM-32, SPM-33, and SPM-51 in Figure 15

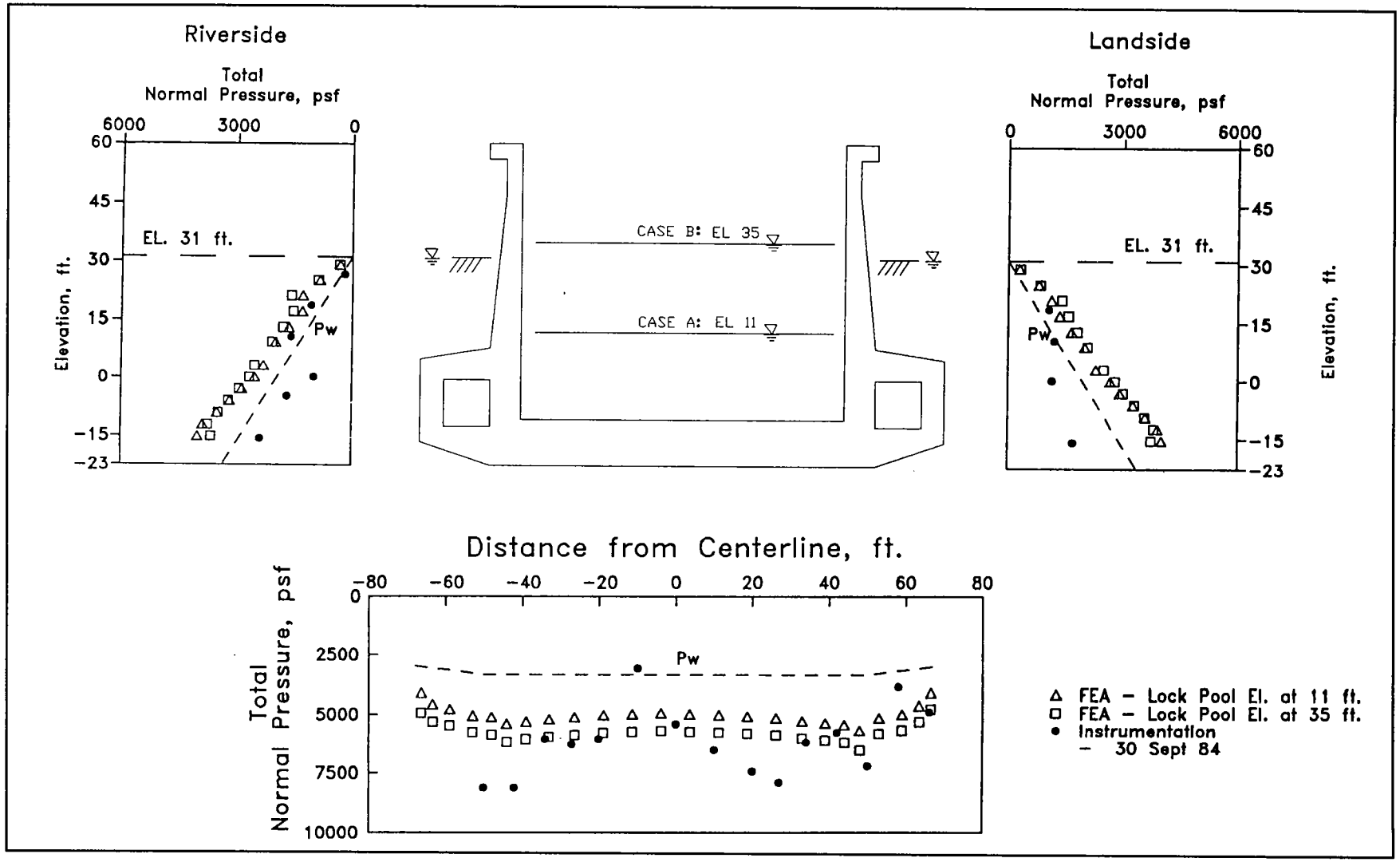

Figure 72. Total normal pressure - river at el 11, pool in lock at els 11 and 35

and SPM-30 in Figure 16, will not be used during the evaluation of the finite element results for the three operational load cases. Lastly, the total normal pressures computed along the base and lock walls after the pool in the lock was raised to el 35 were in closer agreement with the 22 September 1983 stress meter measurements.

Figure 73 shows the two sets of computed effective normal pressures for the pool elevations in the lock at el 11 and 35. The instrumentation measurements shown in this figure are the difference between the 30 September 1984 stress meter measurements and the piezometer measurements. The results are not shown for those stress meters with measurements less than the piezometer measurements since this would imply tensile effective stress values. The values for the effective normal pressures shown in this figure are equal to the difference between the total normal pressures and the pore water pressures, reported in Figure 72. The greatest effective normal pressures were 2,100 and 2,300 psf below the riverside and landside stem walls, respectively, for pool el 11 ft. Below the center line of the lock, the effective base pressure was 1,600 psf. The lowest values for the effective base normal pressures were computed below the outside corners of the culverts and were 1,100 psf. The values for the two sets of effective base pressures are in the shape of an inverted saddle and differ by 800 psf because of the 24-ft difference in pool elevations between the two analyses. The effective pressures normal to the walls for pool el 35 in the lock were slightly greater than those computed for pool el 11. The effective normal pressures computed after raising the pool in the lock to el 35 are shown in Figure 73 and are in closer agreement with the 30 September 1984 stress meter measurements.

The values of shear stresses computed along the lock walls and base are presented in Figure 74 in terms of the mobilized friction angles. The resulting distributions of δ_{mob} along the base were nearly the same for both pool elevations. The greatest values of δ_{mob} were computed below the stem walls and were 9 deg below the riverside stem wall and 7 deg below the landside stem wall. Below the center line of the lock, δ_{mob} decreased to nearly 0.

Along both stem walls, δ_{mob} was 0 from el 17 to the top of the backfill at el 31. Between el 7.5 and 17, δ_{mob} was less than 7 deg along both sides of the lock for both lock pool elevations. This reduction in downdrag along the stem walls is attributed to the seepage force within the backfill as a result of the submergence of the backfill. This seepage force acts as an uplift force and is in a direction opposite to those downward acting forces developed in previous stages of the analyses. The greatest difference between the values of mobilized friction angle for the two pool elevations occurred along the culvert walls. Along the culvert walls and between el -17 and -2, δ_{mob} averaged 28 deg for lock pool el 11. An increase in the lock pool elevation to 35 ft resulted in a decrease in the average values for δ_{mob} to 14 deg. The increased weight of water, acting downward along the floor of the chamber, was countered by both an increase in the effective base pressures and a updrag force acting upward

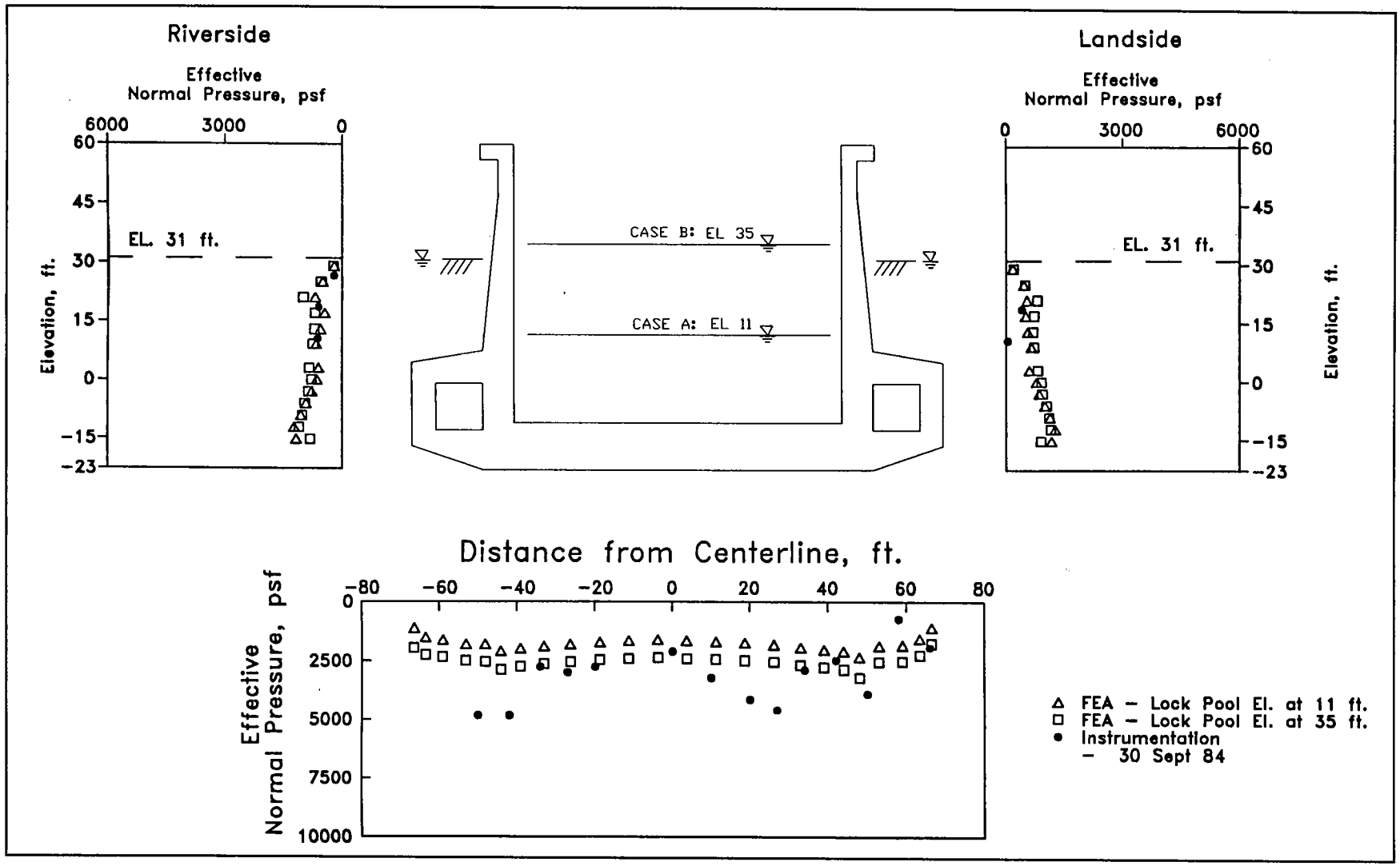

Figure 73. Effective normal pressures - river at el 11, pool in lock at els 11 and 35

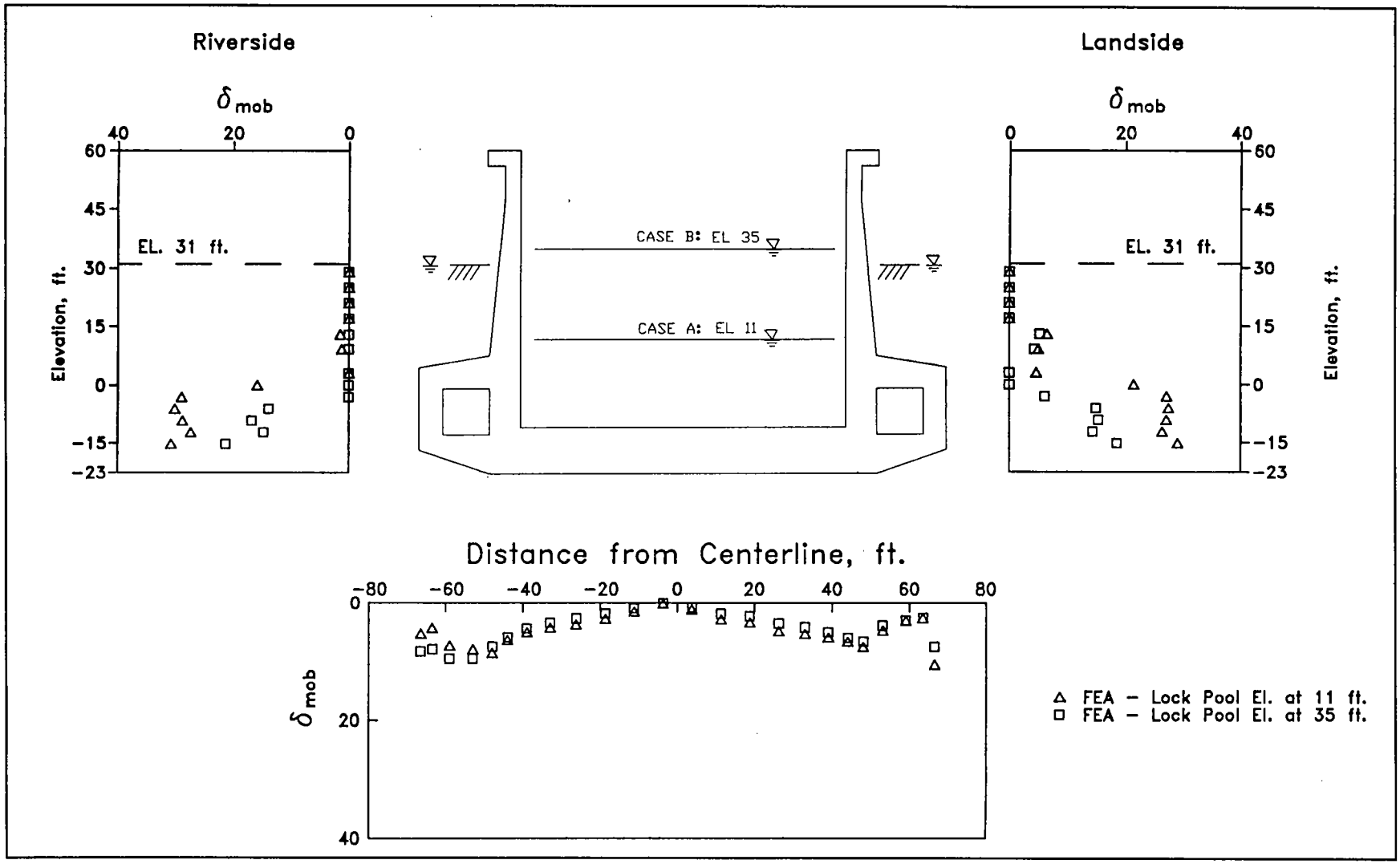

Figure 74. Mobilized friction angle along exterior of lock - river at el 11, pool in lock at els 11 and 35

along the exterior faces of the culvert walls. This updrag force along the culvert walls acted counter to the direction of the downdrag force that developed during backfilling against the lock. The reduced values for downdrag resulted in reduced values for δ_{mob}.

The variation in horizontal earth pressure coefficient with elevation is shown in Figure 60. This figure shows that the value of K_h decreases with decreasing elevation along the stem walls and is nearly constant along the culvert walls for both lock pool elevations. The maximum K_h value was 1.7 at el 29 and decreased with decreasing elevation to 0.51 at el 9 along the riverside stem wall for a lock pool at el 11. At this lock pool elevation, the maximum value of K_h landside of the lock was 1.45, which was 0.25 less than the riverside value. The average K_h values are given in Table 7 for the different backfills placed against the riverside and landside stem walls and culvert walls. The average value for K_h within the select compacted clay backfill was 1.59, and the average value for K_h within the compacted sand backfill adjacent to the riverside stem wall was 0.71 (Table 7). Along the riverside culvert wall, K_h was nearly constant, averaging 0.41. The computed distribution for K_h with elevation landside of the lock is similar to that computed along riverside of the lock. The average values for K_h within the compacted select clay and compacted sand backfill landside of the stem wall and culvert wall were 1.4, 0.66, and 0.45, respectively. These average values for K_h were higher than the average values computed after construction of the lock and backfilling due to the submergence of the backfill. During submergence, the seepage force acting on the soil reduced the effective confining pressure. This reduction in effective confining pressure resulted in the overconsolidation of the soil. Empirical correlations between values of K_h and the overconsolidation ratio indicate that K_h increased with the magnitude of overconsolidation.

Figure 75 also shows the distribution in values of K_h for lock pool el 35. The distribution of K_h is similar for both analyses. Slightly greater values were computed for K_h along the stem walls for the higher lock pool elevation, but along the culvert walls the values for K_h were virtually the

Table 7
Average Values of Horizontal and Vertical Earth Pressure Coefficients - River at El 11, Pool in Lock at El 11

Backfill Region	Backfill Material	Riverside K_h	Riverside K_v	Landside K_h	Landside K_v
Stem	Compacted select clay	1.59	0	1.4	0
Stem	Compacted sand	0.71	0.01	0.66	0.03
Culvert	Compacted sand	0.41	0.18	0.45	0.2

Elevation of river: 11 ft
Elevation of pool in lock: 11 ft
Phreatic surface: 11-ft ground surface

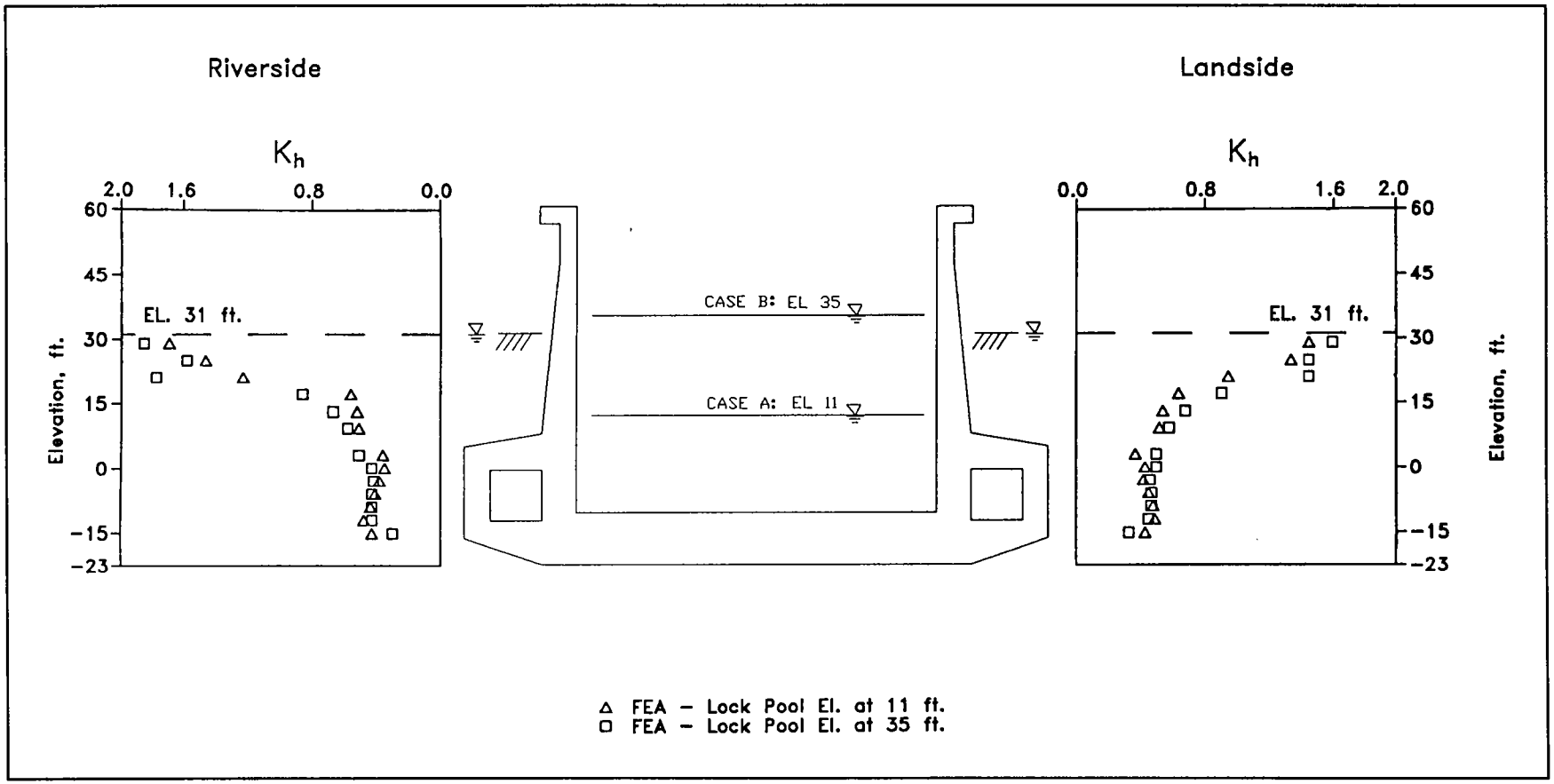

Figure 75. Horizontal earth pressure coefficient, K_h, - river at el 11, pool in lock at els 11 and 35

same at any given elevation. The average values for K_h within the compacted select clay and compacted sand backfill riverside of the stem wall and culvert wall were 1.73, 0.97, and 0.43, respectively (Table 8). The average values of K_h for the three zones landside of the wall were 1.53, 0.91, and 0.47, respectively.

Table 8
Average Values of Horizontal and Vertical Earth Pressure Coefficients - River at El 11, Pool in Lock at El 35

Backfill Region	Backfill Material	Riverside K_h	Riverside K_v	Landside K_h	Landside K_v
Stem	Compacted select clay	1.73	0	1.53	0
Stem	Compacted sand	0.97	0	0.91	0.03
Culvert	Compacted sand	0.43	0.07	0.47	0.08

Elevation of river: 11 ft
Elevation of pool in lock: 35 ft
Phreatic surface: 11-ft ground surface

Figure 76 shows that the vertical (shear) earth pressure coefficients are 0 or nearly 0 along the riverside and landside stem walls for both pool elevations. The largest value for K_v was 0.25 at el -12 for both culvert walls with the lock pool at el 11. The average values of K_v were 0.01 and 0.18 for the compacted sand adjacent to the riverside stem walls and culvert walls, respectively (Table 7). The average values of K_v along the landside wall were greater than those along the riverside wall by 0.02.

At pool el 35, the maximum value for K_v was 0.13 and occurred along both culvert walls at el -9. The average values for K_v, listed in Table 8, were 0 and 0.07 for the compacted sand adjacent to the riverside stem walls and culvert walls, respectively. The average landside K_v values were greater than those along the riverside and equaled 0.03 and 0.08 for the two compacted sand regions. Reduced values of K_v at culvert walls are to be expected with increasing lock pool elevations since the additional weight of water in the chamber reduces the magnitude of downdrag forces developed along the culvert walls.

Figure 77 shows the two distributions of factored moments computed within the lock and the design moment capacity distributions for the two pool elevations. The results of the finite element analyses indicate that along 88 percent of the 84-ft-wide base slab, the top of the floor is in tension when the chamber pool is at el 11. When the chamber pool was raised to el 35, the entire top of the floor is computed to be in tension. The greatest factored moment was computed at the center line of the lock and was -2,550 kip-ft at a lock pool elevation of 11 ft. The value of the factored moment computed at the center line of the lock decreased by

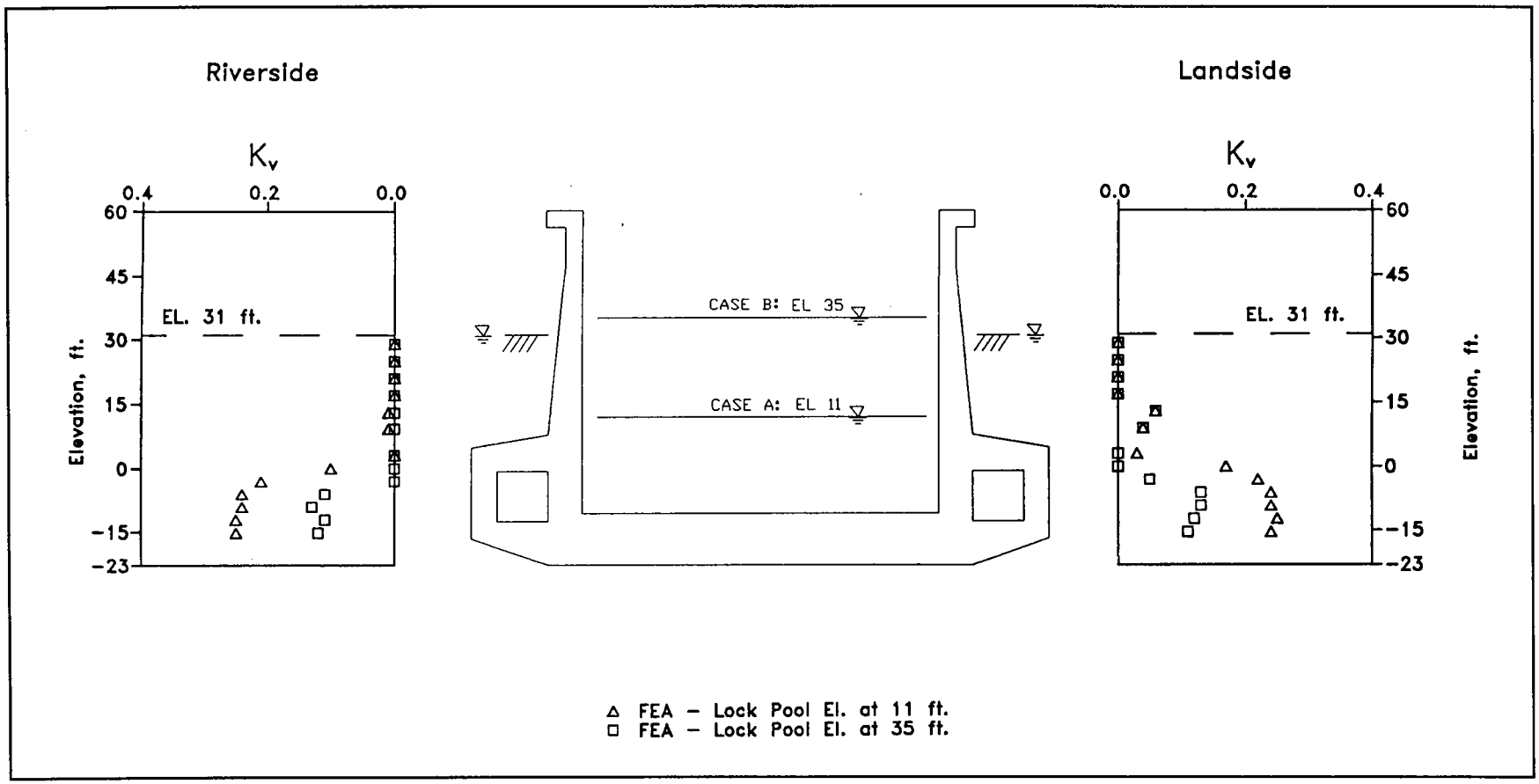

Figure 76. Vertical earth pressure coefficient, K_V, - river at el 11, pool in lock at els 11 and 35

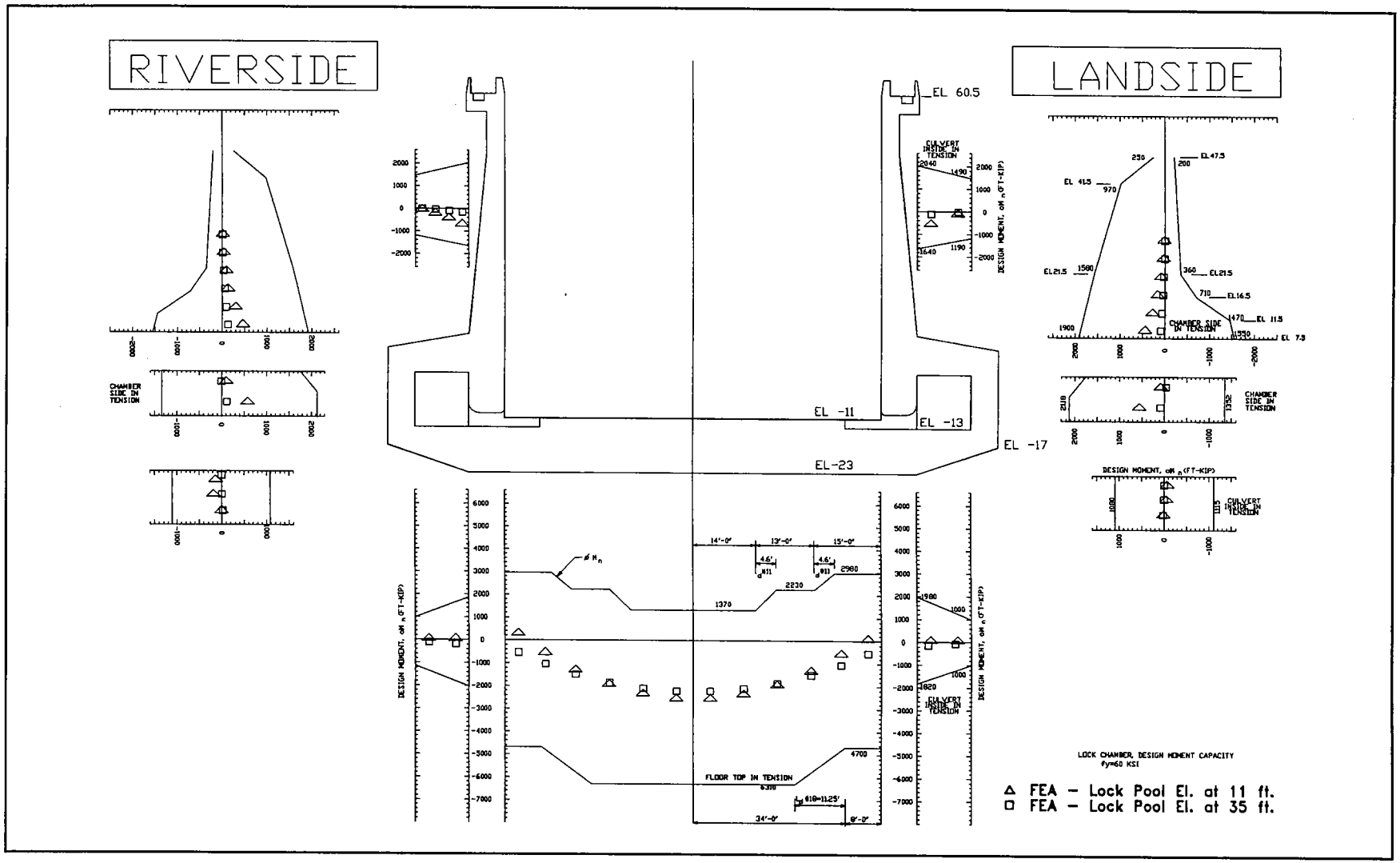

Figure 77. Distribution of factored moments and the design moment capacity - river at el 11, pool in lock at els 11 and 35

14 percent when the chamber pool was raised 24 ft, and equaled -2,200 kip-ft. These maximum values for the factored moments are equal to about one-half the maximum value computed for operational load Case 1. Because of the earth and water pressures acting along the stem walls, the chamber sides of the stem walls were in compression at both pool elevations. With the chamber pool at el 11, the maximum values for the factored moments computed within the stem walls at el 9.25 were 460 kip-ft at the riverside stem wall and 440 kip-ft at the landside stem wall. When the pool elevation was raised by 24 ft, the increase in the lock chamber water pressures countered the backfill pressures acting along the exterior face of the stem walls and thereby reduced the moments within the stem walls. When the pool was raised to el 35, the computed values for the riverside and landside factored moments at el 9.25 were less by factors equal to 3.7 and 4.5, respectively. Lastly, the values for the factored moments at all locations within the lock are all well below the values for the design moment capacities for both pool elevations.

Case 2: Comparison of analysis with 1 January 1985 instrumentation measurements

This section discusses the results from a high pool elevation operational load case (Case 2 in Table 4) and compares these computed results for the mesh shown in Figure 51 to the instrumentation measurements recorded at the lock on 1 January 1985. The computed stresses and displacements within the mesh after construction of the lock and backfilling are the initial values for this series of analyses.

On 1 January 1985 the lower pool was at el 40. The piezometers within the backfill and immediately below the foundation of lock monolith no. 10 indicated a piezometric head equal to elevations ranging in value from 34.5 to 35 ft. The response of the lock to a pool elevation in the chamber of the lock equal to 40 ft is reported.

The water level within the soil foundation and within the soil backfill was raised from el -35 to 35 in 34 increments during this series of finite element analyses. Boundary water pressures, corresponding to an elevation of 35 ft, were applied to the base of the lock and along the lock walls embedded in backfill. From el 31 to 40, hydrostatic water pressures corresponding to el 40, the elevation for the lower pool, were applied to the stem walls of the lock. The 5-ft difference in head between the river head and the piezometric head was applied as a boundary pressure normal to the surface of the soil regions. The pool in the lock was raised to el 40 in 16 increments through the incremental application of hydrostatic boundary water pressures applied normal to the internal faces of the lock and culverts.

The computed base pressure distribution of the total normal pressures (Figure 78) are in the shape of an inverted saddle. The maximum values of total normal pressure were computed below the riverside and landside

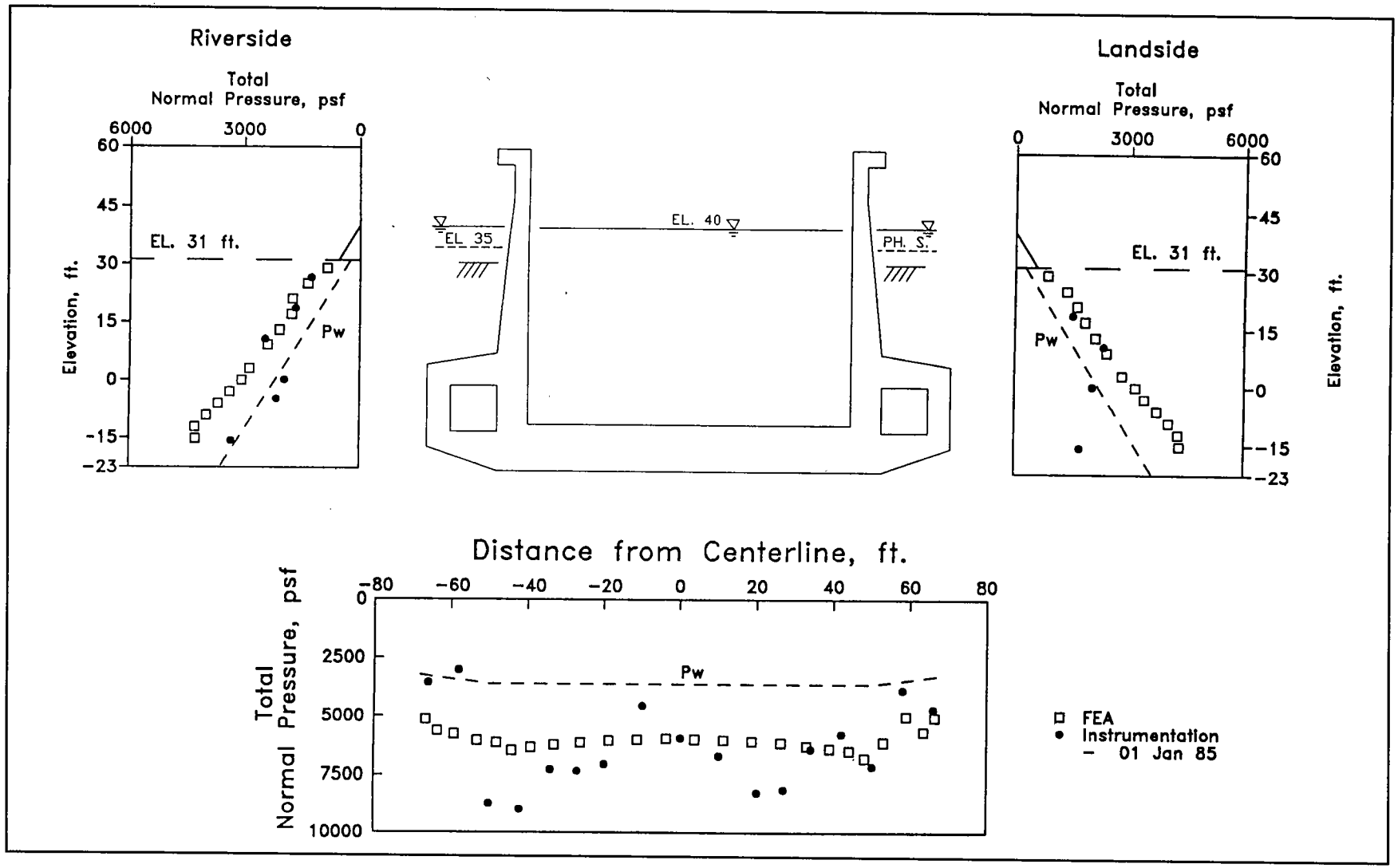

Figure 78. Total normal pressures - lower pool and pool in lock at el 40, phreatic surface at el 35

stem walls and were 6,500 and 6,800 psf, respectively. Below the center line of the lock, the total base pressure was 6,000 psf. The lowest values for the total pressures normal to the base of the lock were computed below the outside corners of the culverts and were 5,100 psf at both corners. The values of computed total normal pressures acting along both sides of the lock were approximately equal. The four stress meter measurements located along the culvert walls were erroneous because their recorded values were less than the corresponding water pressures at those same elevations. The computed results were in agreement with the instrumentation measurements along the base and along the stem walls for 1 January 1985.

Figure 79 shows computed effective normal pressures and the instrumentation measurements computed as the difference between the 1 January 1985 stress meter measurements and the piezometer measurements shown in Figure 78. The greatest effective normal pressures were computed as 2,850 and 3,200 psf below the riverside and landside stem walls, respectively. Below the center line of the lock, the effective base pressure was 2,350 psf. The lowest values for the effective base normal pressures were computed below the outside corners of the culverts and equaled 1,800 psf. As expected, the magnitudes of the effective pressures normal to the stem walls and culvert walls increased in value with decreasing elevation. The effective normal pressures computed after the lower pool and the pool in the lock were raised to el 40 were in agreement with the 1 January 1985 stress meter measurements.

The values of the mobilized friction angles computed along the lock walls and base are presented in Figure 80. The values of δ_{mob} are of the same magnitudes and distribution as those computed in previous analyses. The greatest values of δ_{mob} were 9 deg below the riverside stem wall and 6 deg below the landside stem wall. The magnitudes and distribution of δ_{mob} along both stem walls were essentially the same. The value for δ_{mob} was zero for the upper 10 ft of backfill, which is the same value computed within this region for Case 1. Along the culvert walls and between els -2 and -17, δ_{mob} averaged 20 deg.

The variation in K_h with elevation is shown in Figure 81. This figure shows the value of K_h decreasing from a maximum value of 1.15 along the riverside stem wall at el 29 to 0.5 at el 9. The average K_h values are given in Table 9 for the different backfills placed against the riverside and landside stem walls and culvert walls. K_h is a nearly constant value of 0.45 along the riverside culvert wall (Table 9). The average value of K_h within the select compacted clay backfill was 1.17, and the average value for K_h within the compacted sand backfill adjacent to the riverside stem wall was 0.68 (Table 9). The distribution of K_h with elevation along the landside wall was virtually the same as that computed for the riverside wall. The average values for K_h within the compacted select clay and compacted sand backfill landside of the stem wall and culvert wall were 1.12, 0.64, and 0.47, respectively. These values for K_h are nearly equal to the average values computed along the riverside wall.

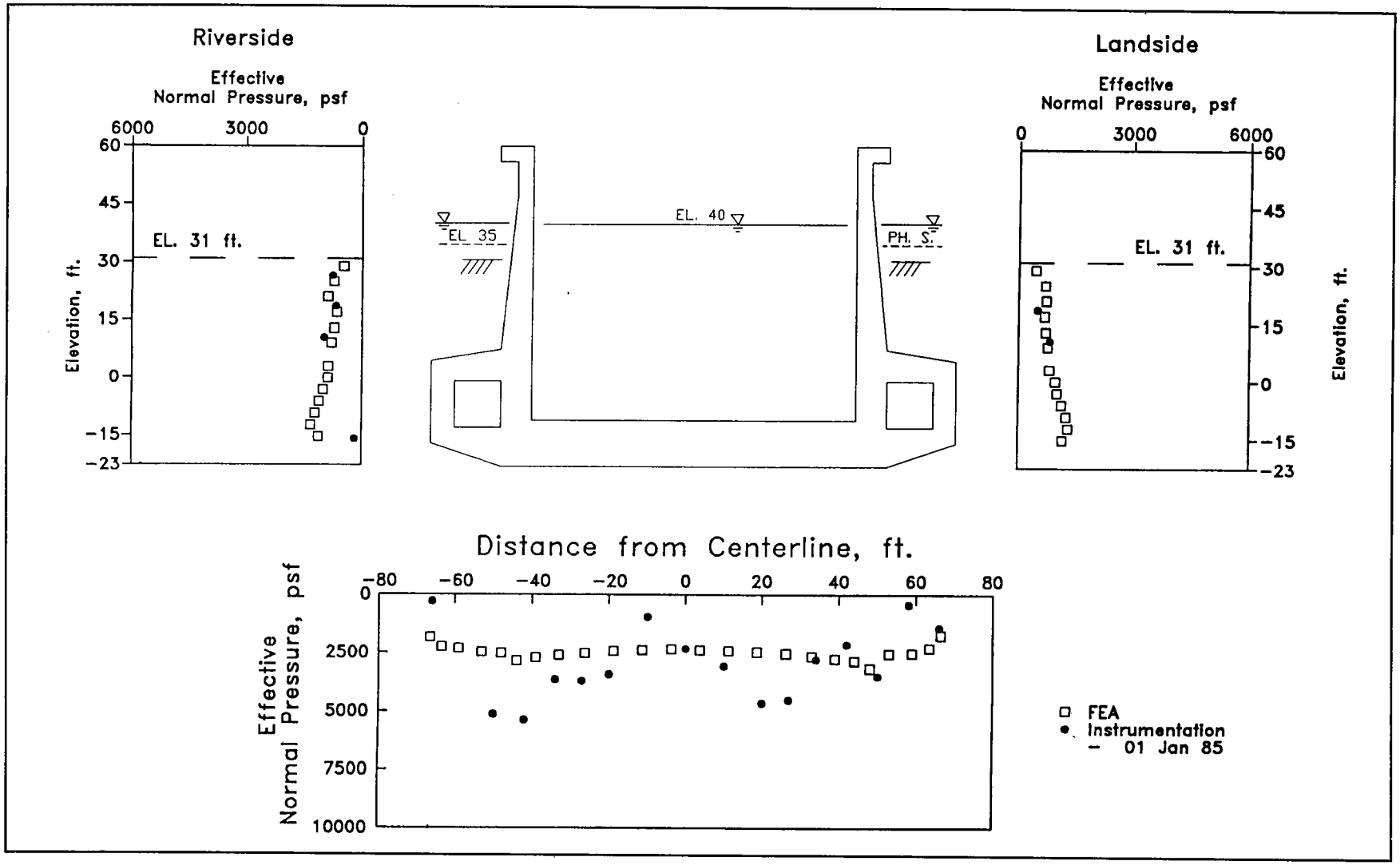

Figure 79. Effective normal pressures - lower pool and pool in lock at el 40, phreatic surface at el 35

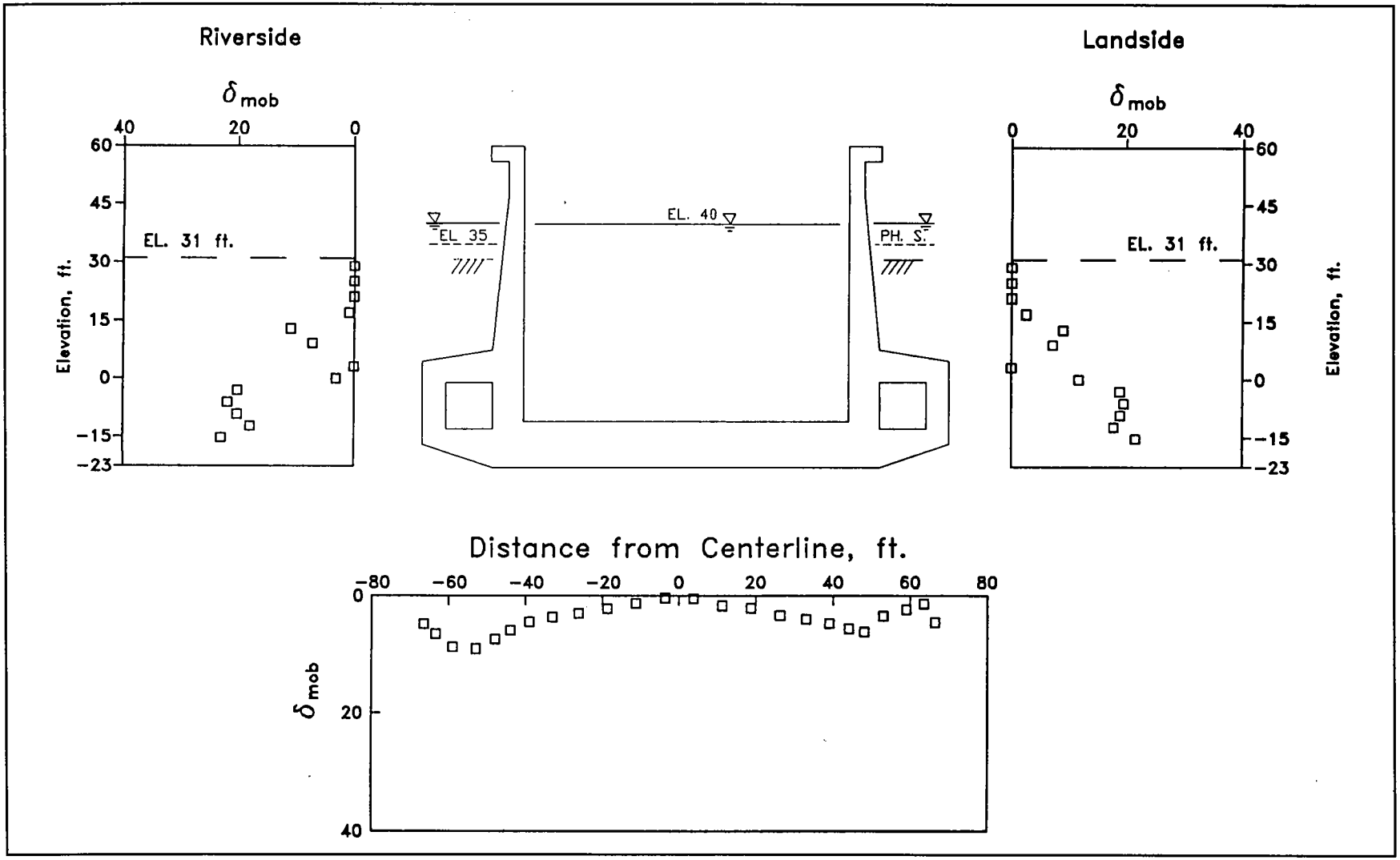

Figure 80. Mobilized friction angles along exterior of lock - lower pool and pool in lock at el 40, phreatic surface at el 35

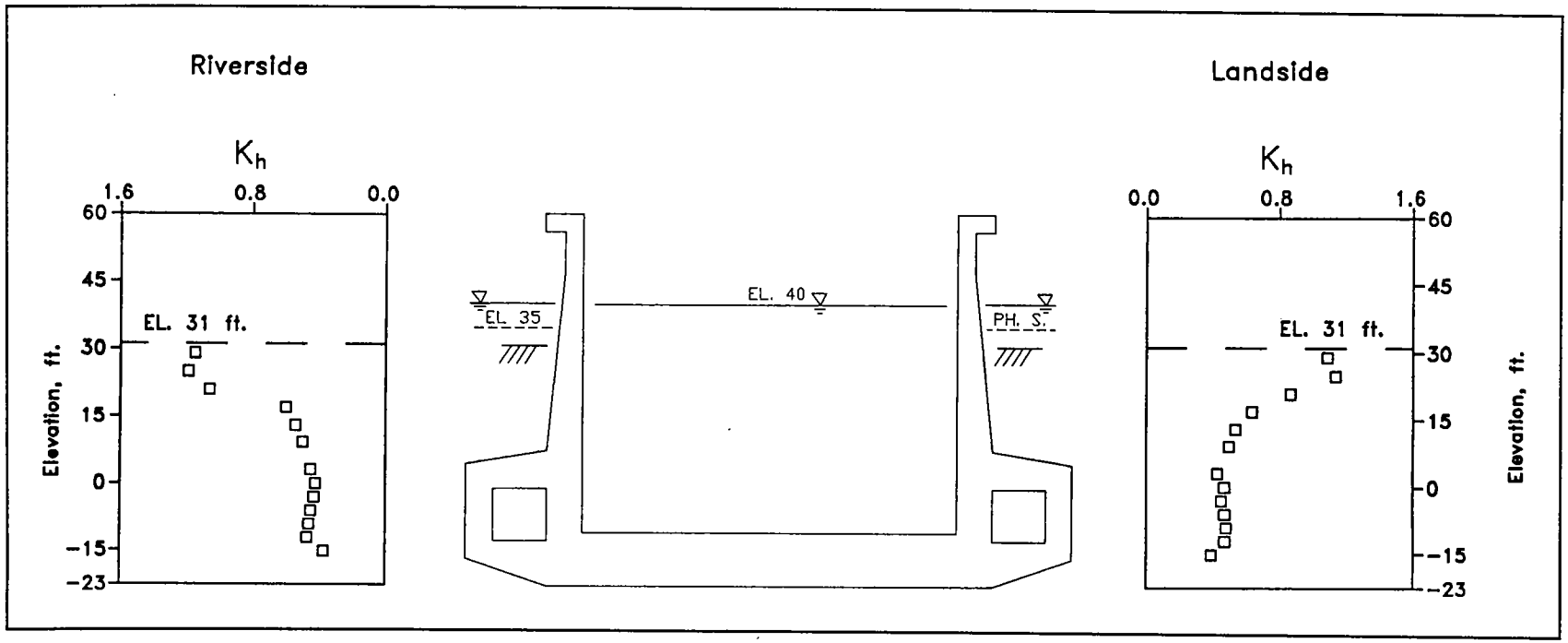

Figure 81. Horizontal earth pressure coefficient, K_h, - lower pool and pool in lock at el 40, phreatic surface at el 35

Table 9
Average Values of Horizontal and Vertical Earth Pressure Coefficients - Lower Pool and Pool in Lock at El 40, Phreatic Surface at El 35

Backfill Region	Backfill Material	Riverside K_h	Riverside K_v	Landside K_h	Landside K_v
Stem	Compacted select clay	1.17	0	1.12	0
Stem	Compacted sand	0.68	0.05	0.64	0.05
Culvert	Compacted sand	0.45	0.12	0.47	0.13

Elevation of river: 40 ft
Elevation of pool in lock: 40 ft
Phreatic surface: 35 ft

Figure 82 shows a K_v value of 0 within the first 10 ft of backfill. The greatest value for K_v was computed at el -6 along the culvert walls and was 0.18. The average values for K_v were 0.05 and 0.12 for the compacted sand adjacent to the riverside stem walls and culvert walls, respectively (Table 9).

Figure 83 shows the distributions of factored moments computed within the lock and the design moment capacity distributions. The results of the finite element analyses indicated that along the entire base slab, the top of the floor slab was in tension. The greatest factored moment was computed at the center line of the lock and was -2,350 kip-ft. The maximum value for the factored moment was within the range of maximum values computed for operational load Case 1 and about one-half the maximum value computed at the end of construction. The chamber sides of the stem walls were in compression, as was the case for the previous analyses. At el 9.25, the factored moments computed within the stem walls were 322 kip-ft at the riverside stem wall and 300 kip-ft at the landside stem wall. The values for the factored moments at all locations with the lock were all well below the values for the design moment capacity.

Case 3: Comparison of analysis with 4 April 1985 instrumentation measurements

The last of the three operational load case analyses of the mesh shown in Figure 51 considers the case of silt loading against the lock that occurred during the Spring of 1985. The results of this series of finite element analyses are compared to the instrumentation measurements recorded at the lock on 4 April 1985.

During the high-water period in the Spring of 1985, silt was deposited to depths ranging from a few feet to tens of feet against both the riverside lock wall and along the surface of the riverside backfill. The thickness of

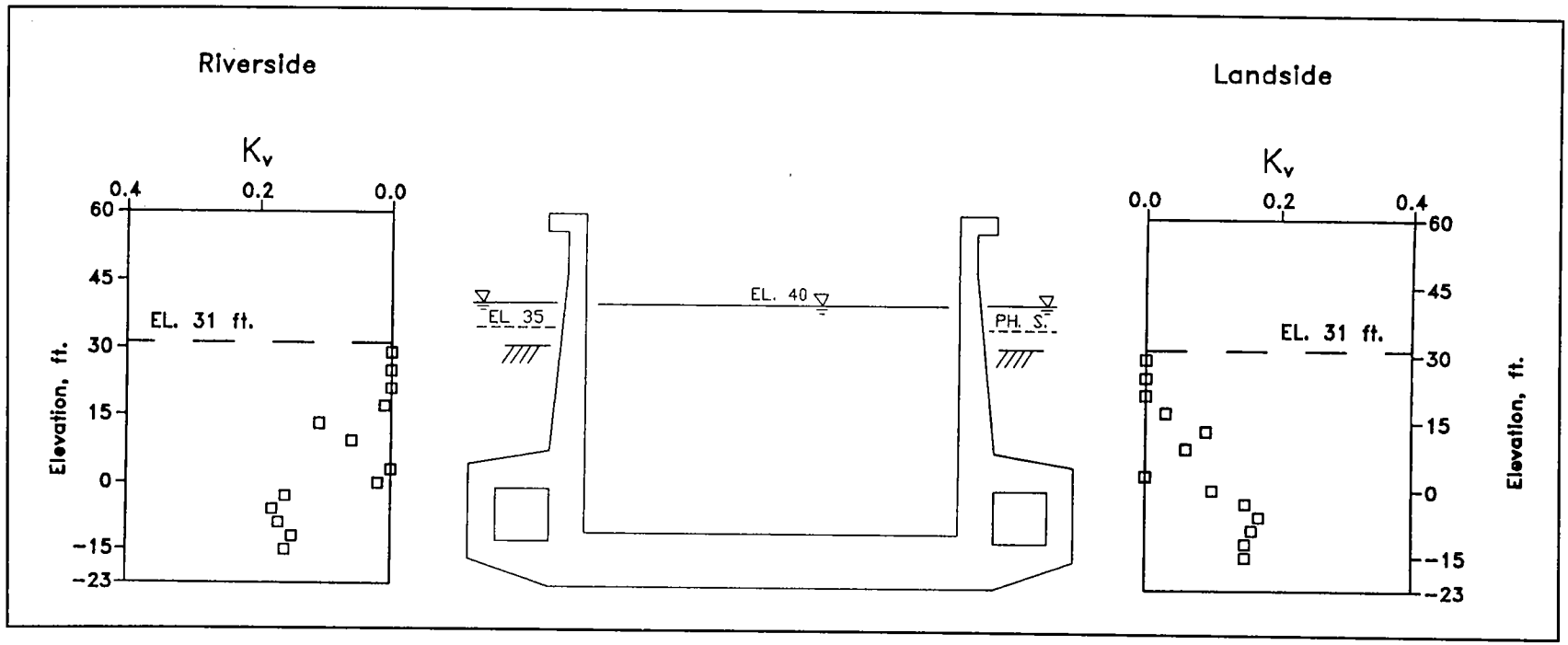

Figure 82. Vertical earth pressure coefficient, K_v, - lower pool and pool in lock at el 40, phreatic surface at el 35

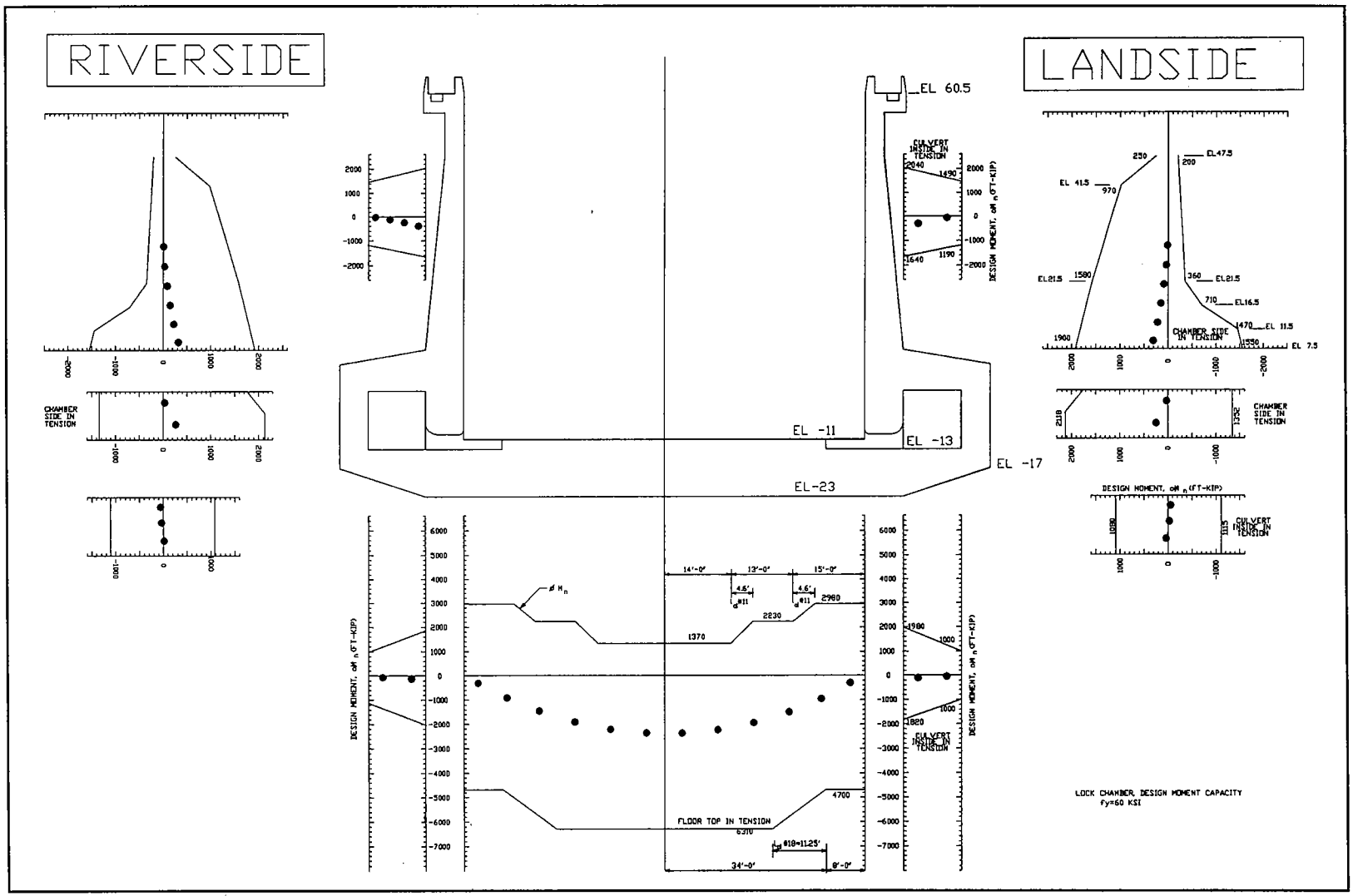

Figure 83. Distribution of factored moments and design moment capacity - lower pool and pool in lock at el 40, phreatic surface at el 35

the silt varied with both the station along the lock and with location along the backfill. Three field surveys were conducted riverside of lock monolith no. 10 during the month of April, and one was conducted during the month of May by the U.S. Army Corps of Engineers. The measurements recorded on 4 April 1985 and shown in Figure 84 represent the extreme of the four silt loads that were recorded at monolith no. 10. On this date, the thickness of the riverside silt deposited against the stem wall was 7 ft. Along the top of the backfill, the thickness of riverside silt increased with increasing distance from the wall. The maximum thickness of silt along the top of the backfill was 11 ft at a distance of 40 ft from the face of the stem wall. The width of the top of the riverside backfill equals 50 ft. Along the sloping face of the backfill, the thickness of the silt ranged from a minimum of 10 ft at the top corner of the backfill to a maximum of 20 ft at a distance of 130 ft from the stem wall. The silt thickness along the sloping face of the backfill was greater than that along the top of the backfill because the slopes of the deposited silt were less steep than the face slope of the riverside backfill (5H:1V). Approximately 2 ft of silt had been deposited on the landside of monolith no. 10 by this date.

On 4 April 1985, the elevation of both the upper and lower pools was 45 ft. The piezometers within the backfill and immediately below the foundation of lock monolith no. 10 indicated a piezometric head equal to elevations ranging in value from 41.5 to 42.5 ft, with a majority of the measurements equal to 41.5 ft. The response of the lock to the silt loadings shown in Figure 84 and a pool elevation in the chamber of the lock equal to 45 ft is reported in the following paragraphs.

The initial values of computed stresses and displacements are those computed after construction of the lock and backfilling. The water level within the soil foundation and within the soil backfill was raised from el -35 to el 45 in 40 increments during this series of analyses. Boundary water pressures, corresponding to el 41.5, were applied to the base of the lock and along the lock walls embedded in backfill. From els 31 to 45, hydrostatic water pressures were applied to the riverside stem walls of the lock. Effective boundary pressures, corresponding to the siltation shown in Figure 84, were applied normal to the stem walls and normal to the surface of the backfill. The 3.5-ft difference in head between the river and the piezometric head was applied as a boundary pressure normal to the surface of the soil regions. The pool in the lock was raised to el 45 in 18 increments through the incremental application of hydrostatic boundary water pressures applied normal to the internal faces of the lock and culverts.

The computed base pressure distribution shown in Figure 85 is more uniform than the base pressures computed after construction of the lock and backfilling and in the operational load Cases 1 and 2. The computed maximum values of total normal pressures were 7,100 psf below the riverside stem wall and 7,200 psf below the landside stem wall. Below the center line of the lock, the total base pressure was 6,500 psf. The lowest values for the total pressures normal to the base of the lock were computed below the outside corners of the culverts and were not equal due to

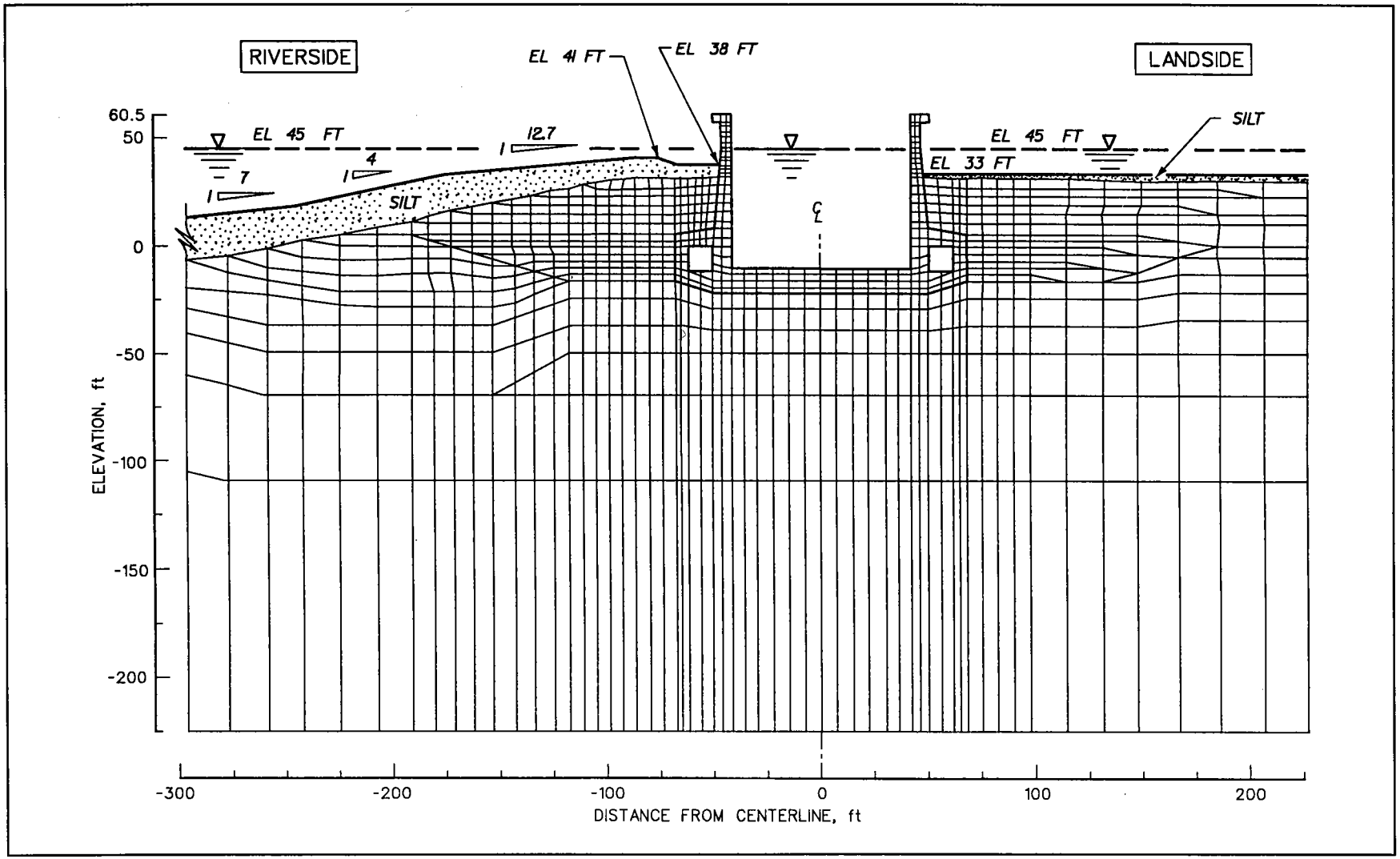

Figure 84. Silt deposition at lock monolith no. 10 on 4 April 1985

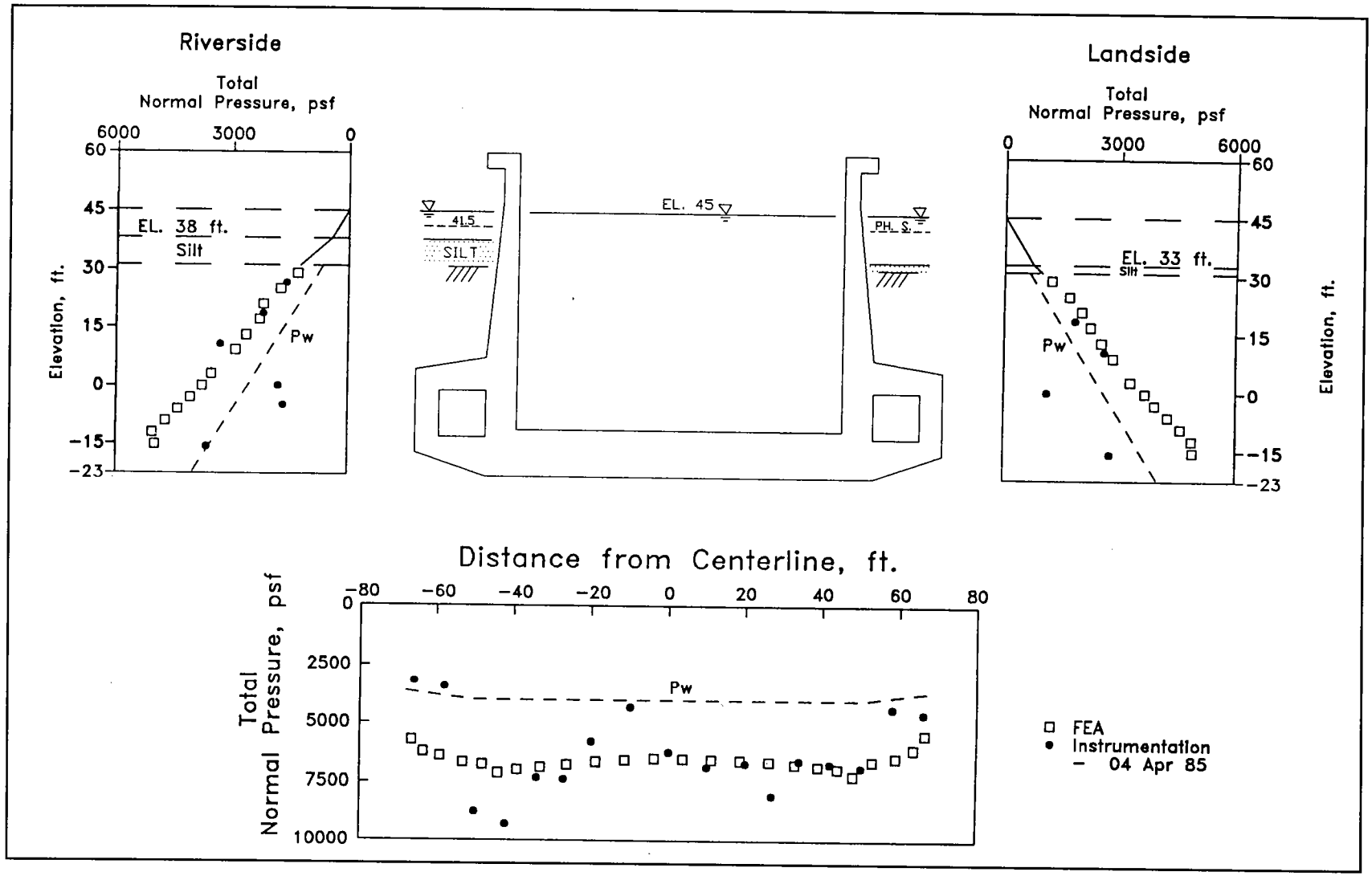

Figure 85. Total normal pressures after deposition of 7 ft of riverside silt against lock with river and pool in lock at el 45

the heavier silt loads riverside of the lock. The base pressures below the riverside and landside corners differed by 300 psf and were 5,750 and 5,450 psf, respectively. Due to the weight of the riverside silt, the values of total normal pressures computed along the riverside wall were greater than those computed along the landside wall. The four stress meter measurements located along the culvert walls were erroneous, because their recorded values were less than the corresponding water pressures at those same elevations. The computed results are in agreement with the instrumentation measurements for 4 April 1985.

Figure 86 shows the effective normal pressures computed along the base of the lock and along the stem and culvert walls. The instrumentation measurements equaled the difference between the 4 April 1985 stress meter measurements and the piezometer measurements from Figure 85. The computed effective base pressure distribution is more uniform than the distributions of effective base pressures computed in the three previously discussed operational load cases. The greatest effective normal pressures were 3,100 and 3,200 psf below the riverside and landside stem walls, respectively. Below the center line of the lock, the effective base pressure was 2,500 psf. The lowest values for the effective base normal pressures were computed below the riverside and landside corners of the culverts and were 2,050 and 1,750 psf, respectively. The values for the effective pressures normal to the riverside walls were greater than those along the landside walls due to the unsymmetrical silt loads. The effective normal pressures computed after application of the water and silt loadings were the same as the 4 April 1985 stress meter measurements.

Figure 87 shows the values of δ_{mob} computed along the lock walls and base. Due to the lateral thrust of the riverside silt loads, the computed values for δ_{mob} along the base were greater for the riverside of the center line than for the landside of the center line. The greatest value of δ_{mob} was 10 deg below the riverside lock wall. Values of δ_{mob} along the base and landside of the center line of the lock were of the same magnitude and distribution as those computed in previous analyses. The weight of the silt resting on the riverside backfill resulted in larger settlements within the backfill and, consequently, greater downdrag forces. These greater downdrag forces along the riverside lock wall were reflected in the greater δ_{mob} values, as compared with the values computed along the landside lock wall. For example, at el 29 and within the compacted select clay backfill, the riverside and landside values for δ_{mob} were 11 and 0 deg, respectively. Within the compacted sand at el 13, the riverside and landside values for δ_{mob} were 17 and 11 deg, respectively. Along the riverside culvert, the δ_{mob} values were about 2 deg greater than those computed along the landside culvert wall.

The variation in K_h with elevation is shown in Figure 88. This figure shows K_h values to be more uniform with elevation along the riverside stem wall than those along the landside stem wall. A maximum K_h value of 0.82 was computed between els 20 and 25 within the backfill along the riverside stem wall, as compared with a maximum K_h value of 1.06 at the

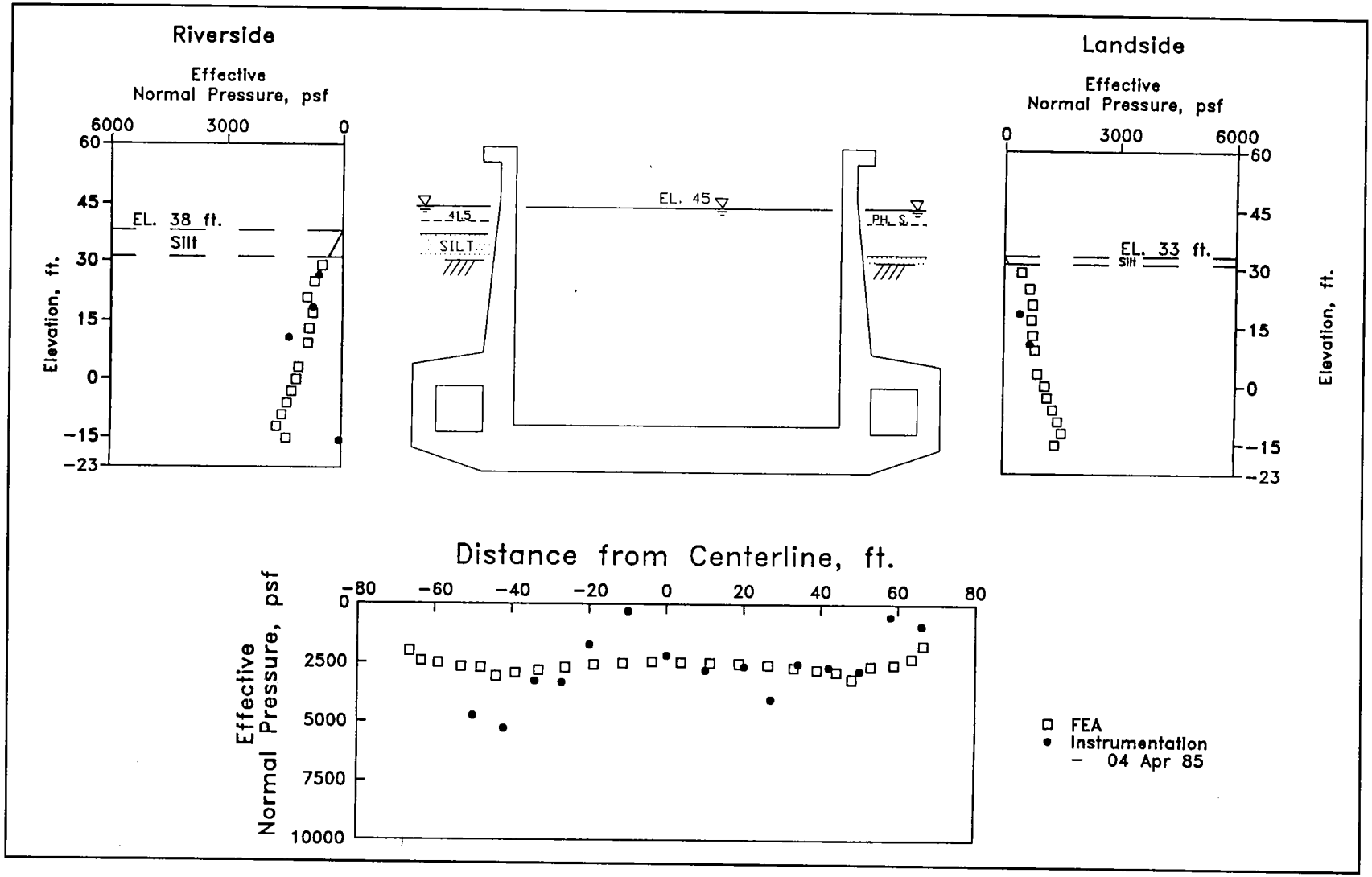

Figure 86. Effective normal pressures after deposition of 7 ft of riverside silt against lock, river and pool in lock at el 45

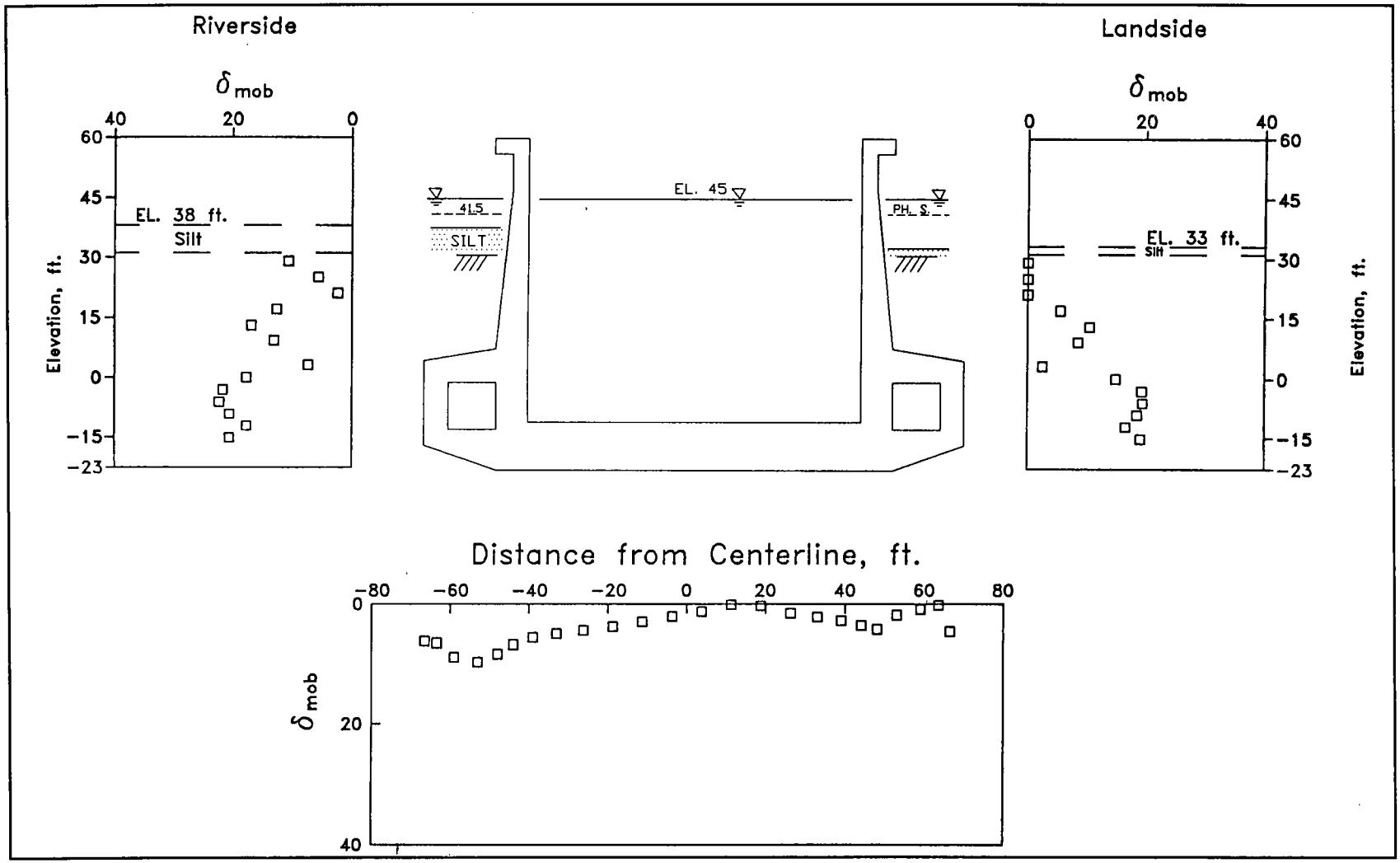

Figure 87. Mobilized friction angle along exterior of lock after deposition of 7 ft of riverside silt against lock, river and pool in lock at el 45

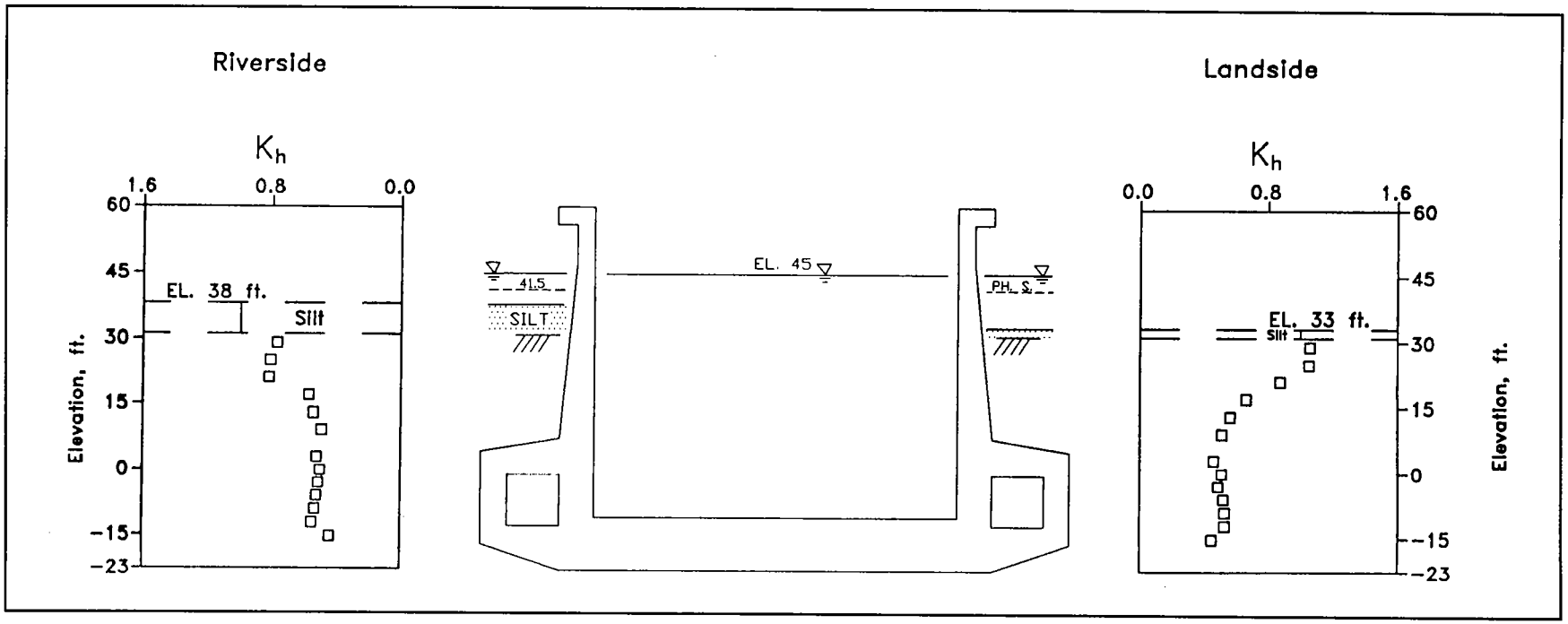

Figure 88. Horizontal earth pressure coefficient, K_h, after deposition of 7 ft of riverside silt against lock, river and pool in lock at el 45

top of the landside backfill. The average K_h values are given in Table 10 for the different backfills placed against the riverside and landside stem walls and culvert walls. K_h was a nearly constant value of 0.52 along both culvert walls (Table 10). The average value for K_h within the select compacted clay backfill was 0.79, and that within the compacted sand backfill adjacent to the riverside stem wall was 0.61 (Table 10). The average values for K_h within the compacted select clay and compacted sand backfill landside of the stem wall were 1.06 and 0.65, respectively.

Table 10
Average Values of Horizontal and Vertical Earth Pressure Coefficients after Deposition of 7 Ft of Riverside Silt Against Lock, River and Pool in Lock at El 45

Backfill Region	Backfill Material	Riverside K_h	Riverside K_v	Landside K_h	Landside K_v
Stem	Compacted select clay	0.79	0.12	1.06	0
Stem	Compacted sand	0.61	0.11	0.65	0.06
Culvert	Compacted sand	0.52	0.17	0.52	0.14

Elevation of river: 45 ft
Elevation of pool in lock: 45 ft
Elevation of riverside silt: 38 ft

The variation in K_v values with elevation is shown in Figure 89. The greater K_v values along the riverside stem wall reflect the effects of silt loads on the magnitude of downdrag forces which developed. The greatest value for K_v was computed at el 13 and was 0.16 along the riverside stem wall as compared with a K_v value of 0.1 along the landside stem wall. The average values for K_v were 0.12, 0.11, and 0.17 for the compacted select clay and compacted sand adjacent to the riverside stem walls and culvert walls, respectively (Table 10). The average values for the three landside regions were 0, 0.06, and 0.14, respectively.

Figure 90 shows the distributions of factored moments computed within the lock along with the design moment capacity distributions. The results of the finite element analyses indicated that along the entire base slab the top of the floor was in tension. The greatest factored moment was computed at the center line of the lock and was -2,500 kip-ft, which is within the same range of maximum values computed for operational load Cases 1 and 2. The factored moment computed within the base 39 ft riverside of the center line was nearly less than half that computed 39 ft landside of the center line, i.e. -200 and -395 kip-ft, respectively. As in the previous two operational analyses, the chamber sides of the stem walls were in compression. The factored moment computed within the riverside stem wall at el 9.25 was 100 kip-ft greater than that computed within the landside stem wall (392 versus 292 kip-ft). The values for the factored

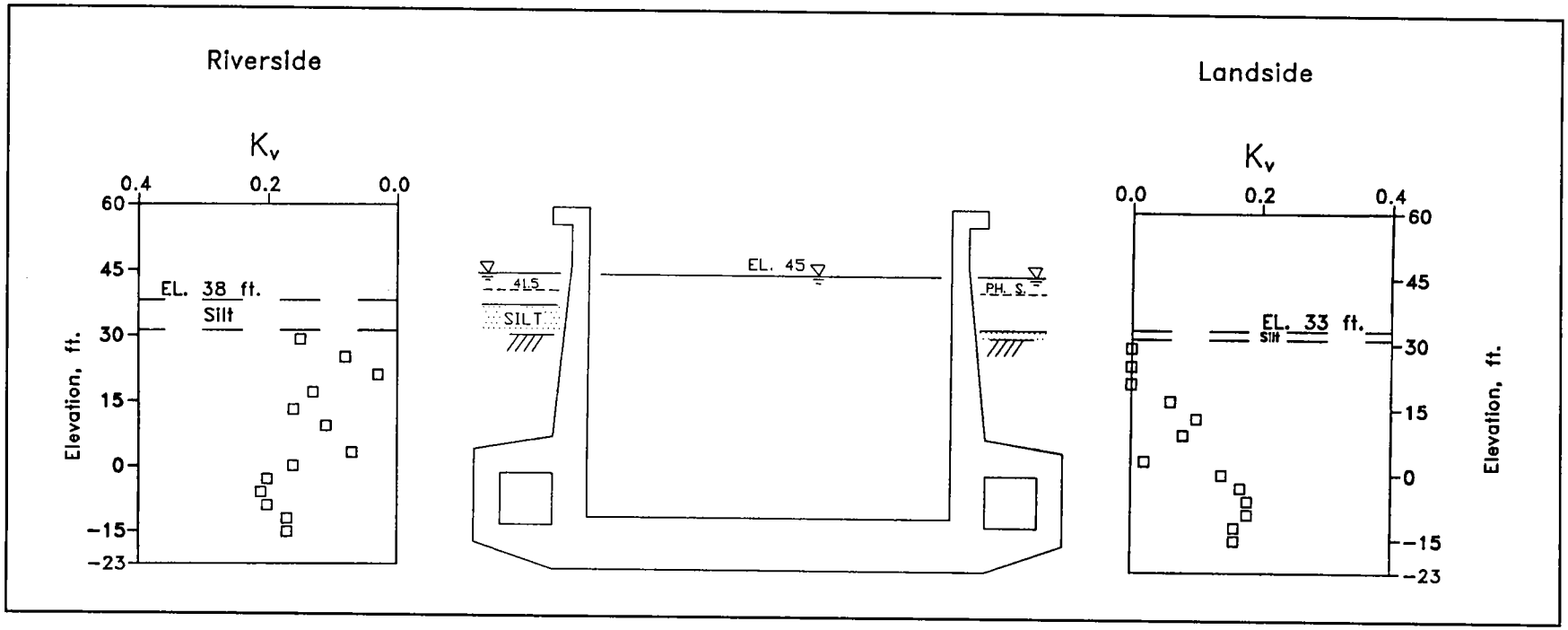

Figure 89. Vertical earth pressure coefficient, K_v, after deposition of 7 ft of riverside silt against lock, river and pool in lock at el 45

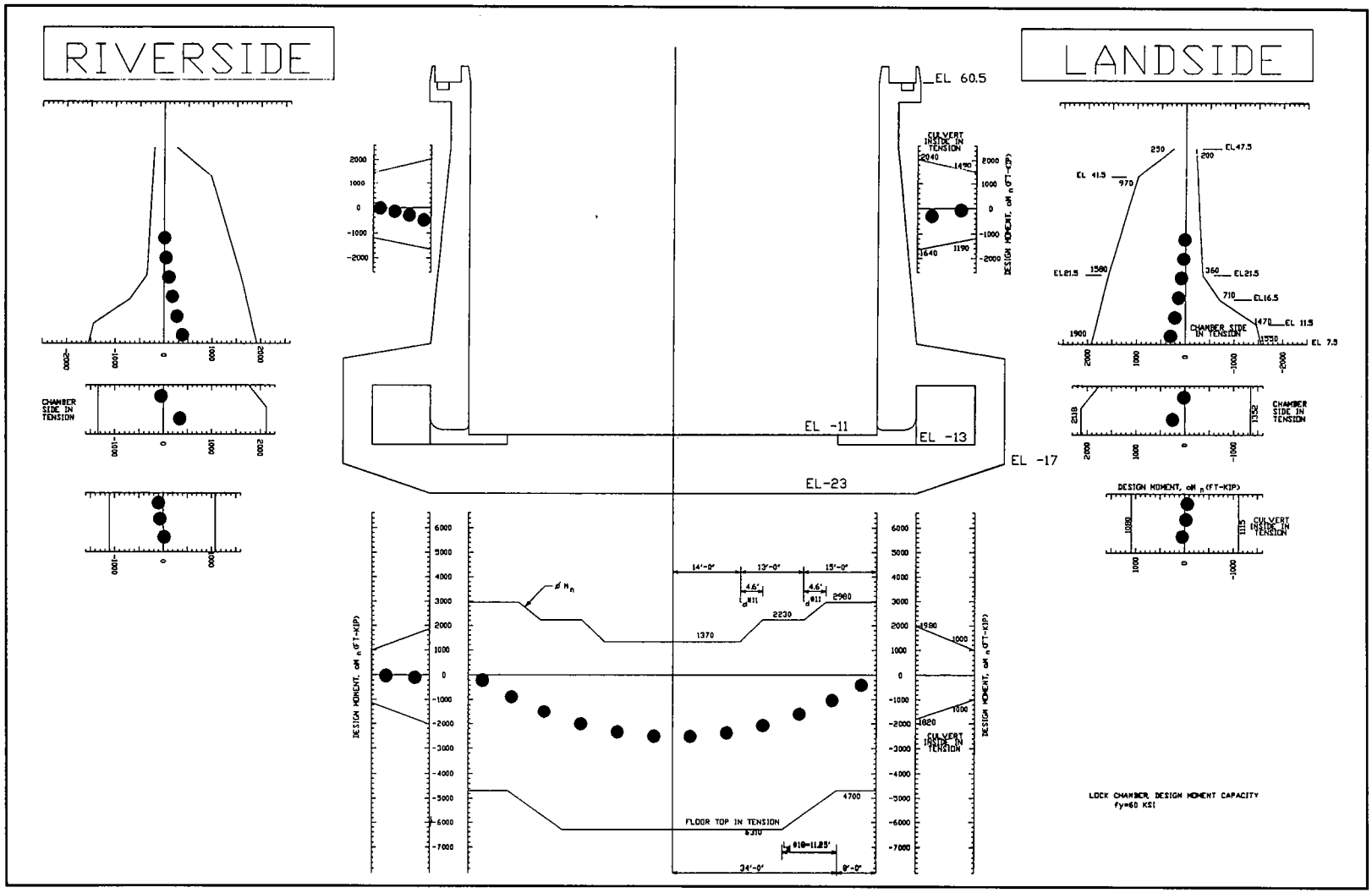

Figure 90. Distribution of factored moments and design moment capacity after deposition of 7 ft of riverside silt against lock, river and pool in lock at el 45

moments at all locations with the lock were all well below the values for the design moment capacity.

Figure 91 shows the results of a pair of CUFRAM analyses, compared with the distributions of factored moments within the lock from the results of finite element analyses. The earth and water pressures specified in the CUFRAM (Dawkins 1987) analyses were equal to those computed in the finite element analysis. The lock was analyzed twice, using the two extreme values for the rigid link factor, RLF, allowed within CUFRAM; i.e., RLF equal to 0 and RLF equal to 1.0. The resulting distributions of moments computed by two CUFRAM analyses were in agreement with each other, indicating that the RLF factor did not significantly influence the computed moments for this load case. The factored moments computed using CUFRAM confirmed the values for the factored moments computed from the finite element results.

Summary

Chapter 2 summarizes the results of two series of phase 1 soil-structure interaction analyses of lock monolith no. 10. The first series of analyses modeled the construction of the lock, while the second series of analyses modeled three operational load cases for which instrumentation measurements were available. In these series of analyses, an incremental, nonlinear finite element method of analysis was used to account for the complex soil-structure interaction occurring during the various stages of construction and during the operational load cases. Linear stress-strain response was presumed for the U-frame structure, while a nonlinear stress-strain response was considered in the model of the soil comprising the foundation and backfill. Drained soil parameters were specified for the soil in all of the finite element analyses.

The modeling of the four stages of lock construction and backfilling consisted of lowering the water table, excavating the river channel, dam and lock sites, and constructing the lock and dam and backfilling (Table 3). This first series of analyses culminated in a comparison between the results of the finite element analyses after completion of lock construction, backfilling, and the instrumentation measurements recorded at the lock on 22 September 1983, prior to flooding of the channel and lock. The three operational load cases included a low pool elevation condition (Case 1), a high pool elevation condition (Case 2), and a high pool elevation condition with silt loading against the lock walls (Case 3). The results of these analyses showed that: (a) there were three distinct regions of soil-to-structure interaction, i.e., the base, the culvert walls, and the stem walls, and (b) the response of the structure and the soil within these three regions depended upon the type of loading, its magnitude, and the direction from which it was applied. The following paragraphs summarize the computed soil-to-structure interaction along each of the three exterior surface regions of the lock and the internal response of the lock

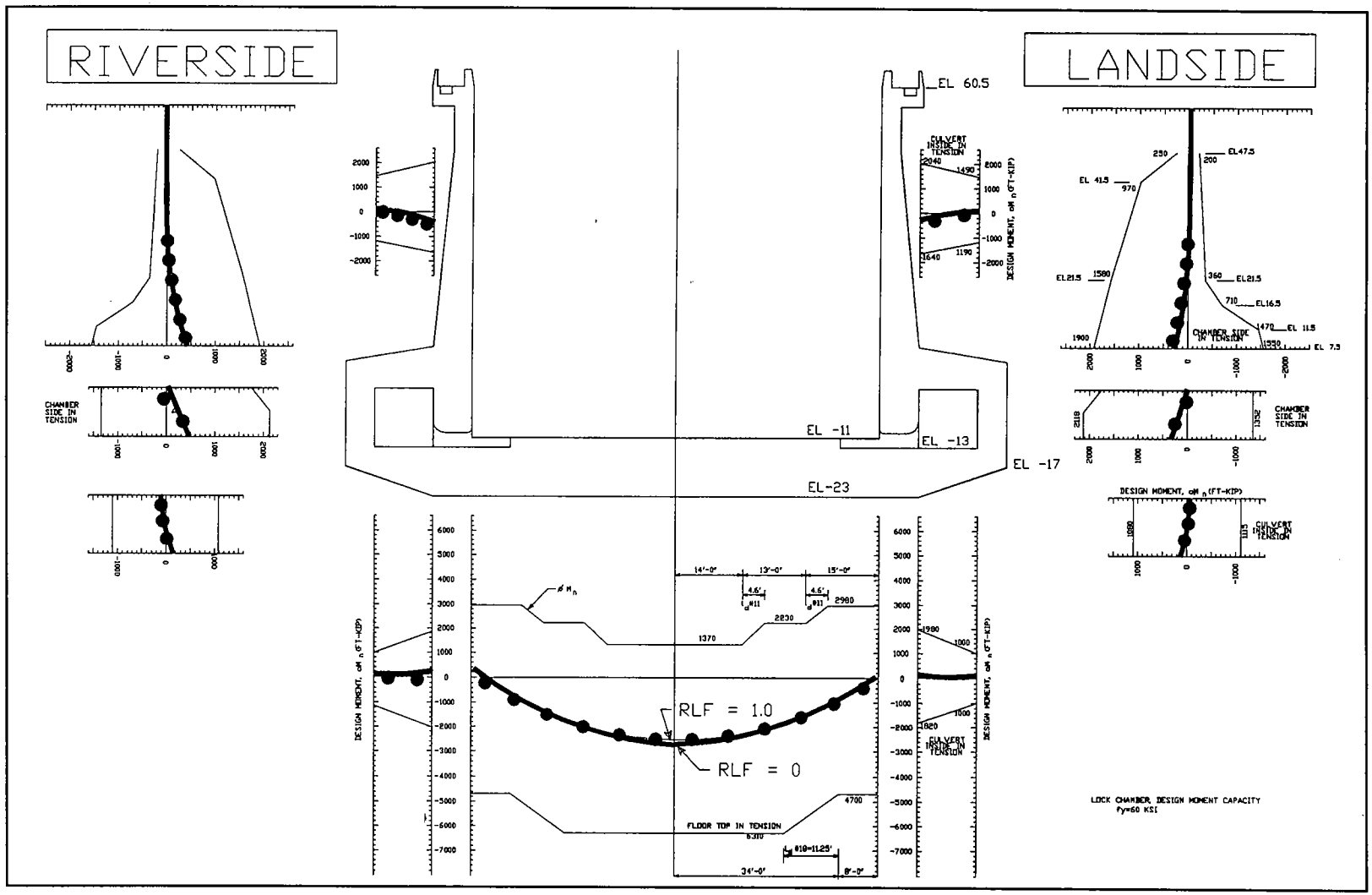

Figure 91. Distribution of factored moments, including CUFRAM results, after deposition of 7 ft of riverside silt against lock, river and pool in lock at el 45

after construction of the lock and backfilling and for the three operational load cases.

The computed total and effective normal pressure distributions for the four finite element analyses were in agreement with the instrumentation measurements recorded at the lock. The computed total and effective base pressure distributions for the first three analyses were in the shape of an inverted saddle, with a more uniform base pressure distribution computed for the third operational load case. Maximum base pressure values were computed below the stem walls of the lock, and minimum base pressure values were computed below the outside corners of the culverts. Due to the symmetry of the backfill geometry near the lock walls and the symmetry of the water loadings applied to both sides of the lock, the computed pressures along both the culvert and stem walls were in agreement for the first three analyses. The larger silt loads applied riverside of the lock in operational load Case 3 resulted in higher values for the riverside earth pressures than those computed along the landside lock wall.

The mobilized friction angles along the base were symmetrical about the center line, and the values of δ_{mob} were less than or equal to 10 deg after construction of the lock and backfilling and for the first two operational load cases. The maximum value of δ_{mob} was always computed below stem wall(s) and was nearly 0 at the center line of the lock. Maximum values for δ_{mob} were computed along the culvert walls ranged from 20 to 30 deg for the four analyses. The analyses of operational load Case 1 showed that an increase in the pool elevation in the lock chamber resulted in a component of drag force acting upward along the culvert walls, thereby reducing the corresponding values of δ_{mob} along this region. The riverside lateral silt loadings in Case 3 resulted in greater values of shear along the base of the lock, especially riverside of the center line. Therefore, δ_{mob} values were greater. In addition, the weight of the silt resting on the riverside backfill resulted in larger settlements within the backfill, increasing the magnitude of the downdrag forces on the face of the riverside stem wall.

Greater values of horizontal earth pressure coefficients were computed along stem walls than those computed along the culvert walls. The maximum values of K_h were computed at the surface of the backfill in the analyses. The range in average K_h values for the three geometrical and material regions riverside and landside of the lock walls are given in Table 11. The greater average K_h values occurred with the three operational load cases in which the backfill was submerged (Cases 1 through 3). This is consistent with empirical relationships that show that K_h increases with overconsolidation, brought about in these three analyses through the reduction in effective stress upon the submergence of the backfill.

The range in average values of vertical earth pressure coefficients for the three geometrical and material regions riverside and landside of the lock walls are summarized in Table 12. Since the values for K_v and δ_{mob}

Table 11
Range of Average Values of Horizontal Earth Pressure Coefficients - Four Operational Load Cases

Backfill Region	Backfill Material	Riverside Min	Riverside Max	Landside Min	Landside Max
Stem	Compacted select clay	0.87	1.73	0.86	1.53
Stem	Compacted sand	0.38	0.97	0.41	0.91
Culvert	Compacted sand	0.35	0.52	0.4	0.52

Table 12
Range of Average Values of Vertical Earth Pressure Coefficients - Four Operational Load Cases

Backfill Region	Backfill Material	Riverside Min	Riverside Max	Landside Min	Landside Max
Stem	Compacted select clay	0	0.02[1]	0	0.02
Stem	Compacted sand	0	0.11	0	0.1
Culvert	Compacted sand	0.07	0.17	0.08	0.2

1 For Operational Load Case 4, $(K_V)_{Max}$ = 0.12

both reflect the magnitude of the shear force, or equivalently, the drag force acting along the walls of the lock, the distribution in the values of these parameters along the stem walls and culvert walls were similar. Greater values of K_v were computed along the culvert walls than those computed for the stem walls. In addition, K_v along the culvert walls decreased in value with either the submergence of the backfill or as the elevation of the pool in the lock rose. The greater K_v values computed along the riverside stem wall, as compared with those values computed along the landside in the Case 3 analysis, were a result of the silt loads increasing the magnitude of downdrag forces along the riverside stem wall. The results of the finite element analyses indicated that along the entire base slab of the lock, the floor top was in tension for all analyses with the exception of one of the two operational load Case 1 analyses. For the Case 1 analysis with the elevation of the pool inside the lock equal to 11 ft, 88 percent of the base slab floor top was in tension. The distribution of computed stresses along each cross section through the centers of elements comprising the base, culverts, and stem walls of the lock were first converted to an equivalent moment acting at each cross section. Then the resulting equivalent moment value was factored by a value equal to 2.21. For all of the cases analyzed, the greatest factored moment was computed along the base and at the center line of the lock. After construction of the

lock and backfilling, the maximum moment was twice the magnitude of those computed in the three operational load cases. The values for the factored moments along the base, around the culverts, and along the stem walls of the lock were less than the design moment capacity values in all four analyses. In the unsymmetrical silt loading analysis (Case 3), the factored moment computed within a cross section through the base slab 39 ft riverside of the center line was less than half the value of the factored moment computed 39 ft landside of the center line.

The chamber sides of the stem walls were computed to be in compression in all four analyses. In the first three analyses, the factored moments at any given elevation within the riverside stem wall were nearly equivalent in value to those computed within the landside stem wall, due to the symmetrical loads about the center line of the lock. At el 9.25, the value of the factored moment computed within the riverside stem wall in operational load Case 3 was 33 percent greater than the value computed within the landside stem wall because of the riverside silt loads.

The CUFRAM analyses of lock monolith no. 10 to the earth and water pressures computed in operational load Case 3 indicated that the computed distribution of moments within the lock were independent of the value assigned to the rigid link factor. In addition, the factored moments computed using CUFRAM confirmed the values for the factored moments computed from the finite element results.

3 Results of the Phase 2 Studies - Reinforced Berm Analyses

Introduction

Siltation against the riverside lock wall that occurs during the seasonal high-water periods rises to elevations higher than those used in the design of the lock. Due to the frequency of high water and resulting silt deposition at the lock, it is anticipated that siltation against the walls will be a continuing problem resulting in an extremely high maintenance cost. A recent study by the USAED, Mobile, concluded that the construction of a reinforced soil berm adjacent to the riverside lock wall has the best potential for providing a permanent solution with little or no maintenance required after its placement. This part of the report assesses the potential performance of the lock after construction of a reinforced berm adjacent to the riverside lock wall. Due to the proximity of the proposed reinforced berm to the lock, significant soil-to-structure interactions will occur between the berm, the lock, the existing backfill, and the soil foundation. The evaluation of this interaction is performed by using the finite element method of analysis, because the conventional equilibrium method of analysis, used in the design of the reinforced soil berm, is unable to account for the interactions between these four regions. In Chapter 2 of this report, the incremental construction procedure was used to analyze the soil-to-structure interaction occurring at lock monolith no. 10 during its construction and operation. The computed results from the four series of finite element analyses of the lock to construction on three operational load cases were in agreement with the instrumentation data measurements at monolith no. 10. With the accuracy of the finite element model established in the phase 1 study, the phase 2 study of the berm-to-lock interaction proceeded. The results from this second group of analyses are described in this chapter of the report.

Descriptions of Cases Analyzed

The phase 2 berm-to-lock interaction analyses described in this chapter involve a series of incremental, nonlinear finite element analyses simulating the stages of berm construction, raising of the upper and lower pool levels, silt loading, and subsequent lowering of the pool levels. This series of phase 2 analyses has seven distinct stages, which are listed in Table 13 and shown in Figures 92 through 98. The initial state, prior to berm construction, at the cross section for lock monolith no. 10 is depicted in Figure 92. Assuming that the construction of the berm will occur during the dry season, the initial river elevation and the elevation of the pool in the lock were set at 11 ft as shown in Figure 92. The first stage of berm construction resulted in the partial excavation of the riverside backfill to the surface profile shown in Figure 93, followed by the construction of the reinforced berm, shown in Figure 94. The next four series of analyses corresponded to different water loads and silt loads applied to both the berm and lock.

The first loading stage after construction of the berm corresponded to a high-water condition at the lock, resulting in the submergence of the berm (Figure 95). In this series of analysis, the elevations of the river and the pool in the lock were raised from 11 ft to the top of the lock at 60.5 ft. The resulting interactions among the lock, berm, backfill, and foundation regions of the mesh were accounted for during the course of the analyses. Submergence of the berm was followed by the deposition of silt against

Table 13
Seven Stages of Phase 2 Finite Element Analyses

Description of Load Case	Elevation			
	Water Table ft	River ft	Pool in Lock ft	Riverside Silt ft
Initial State	11	11	11	—
Excavate for Riverside Reinforced Berm	11	11	11	—
Construct Reinforced Berm	11	11	11	—
Submergence of Reinforced Berm	60.5	60.5	60.5	—
Deposition of 10 ft of Riverside Silt on Reinforced Berm	60.5	60.5	60.5	55
Lowering River Elevation and Pool in Lock	4	4	40	55
Lowering Pool in Lock	4	4	4	55

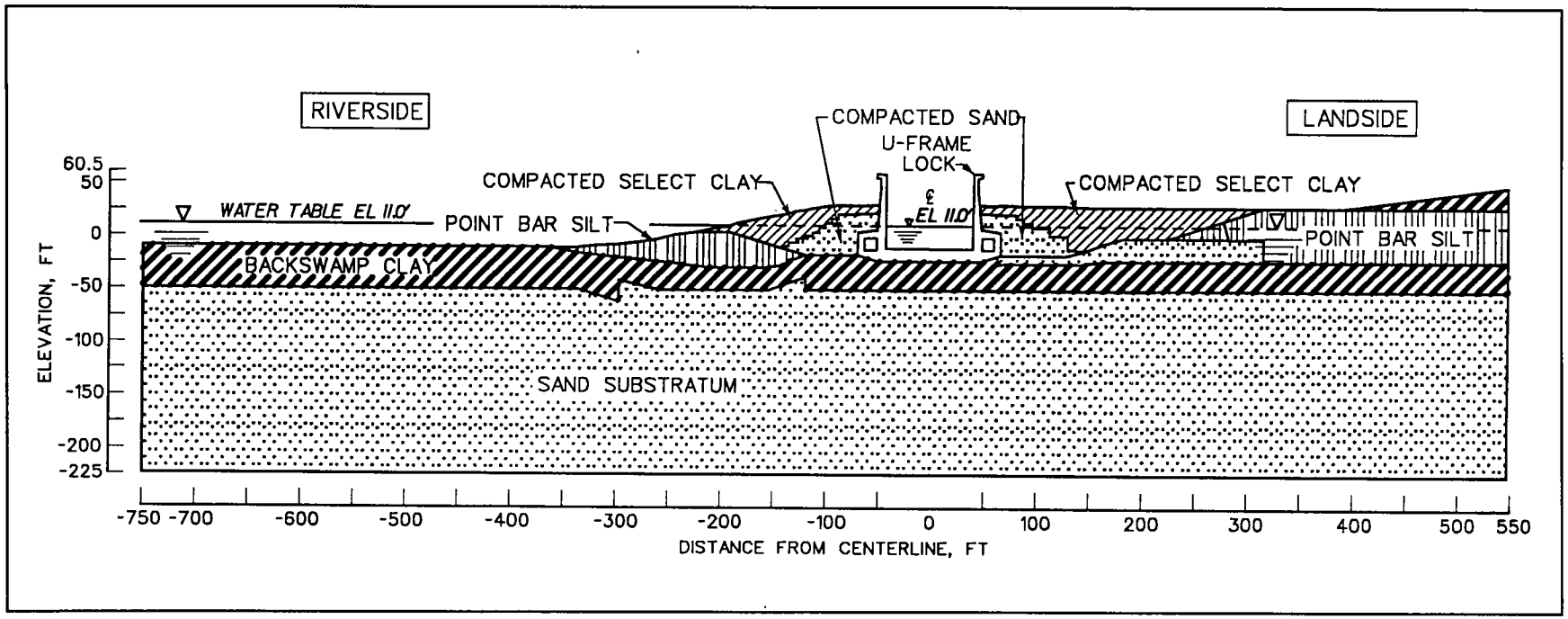

Figure 92. Lock monolith no. 10 and material regions with lower pool and pool in lock at el 11

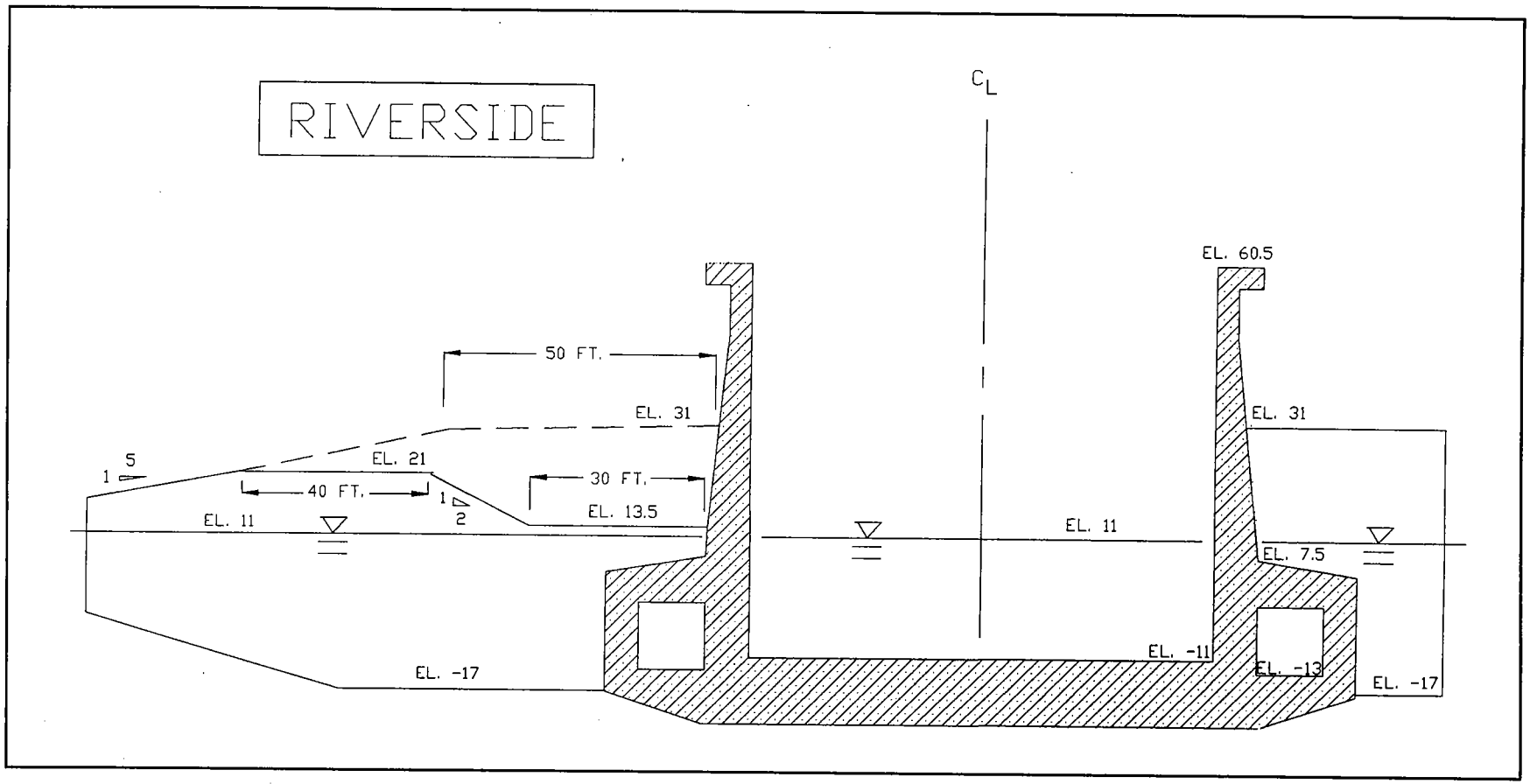

Figure 93. Riverside excavation for reinforced berm with lower pool and pool in lock at el 11

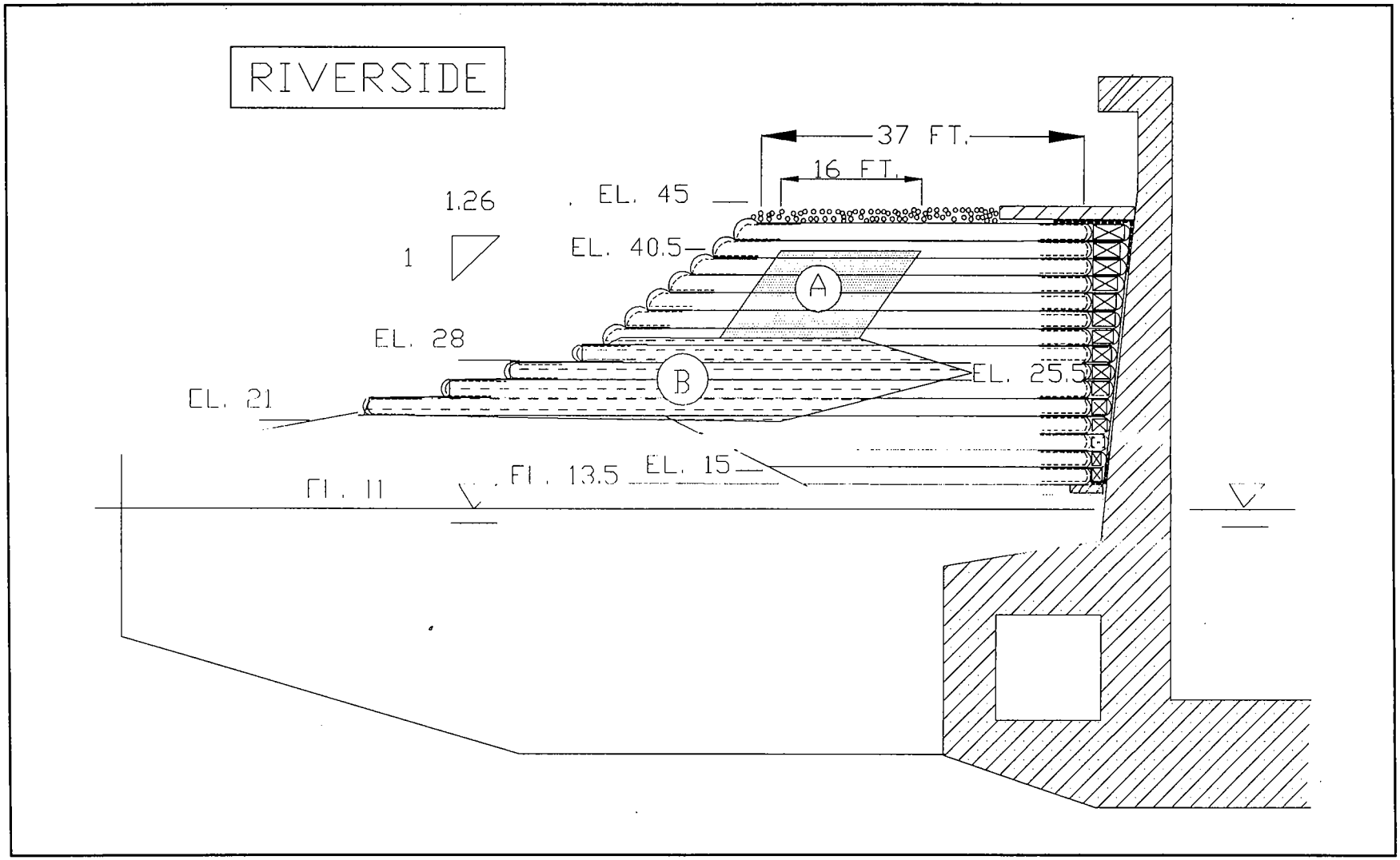

Figure 94. Riverside reinforced berm with lower pool and pool in lock at el 11

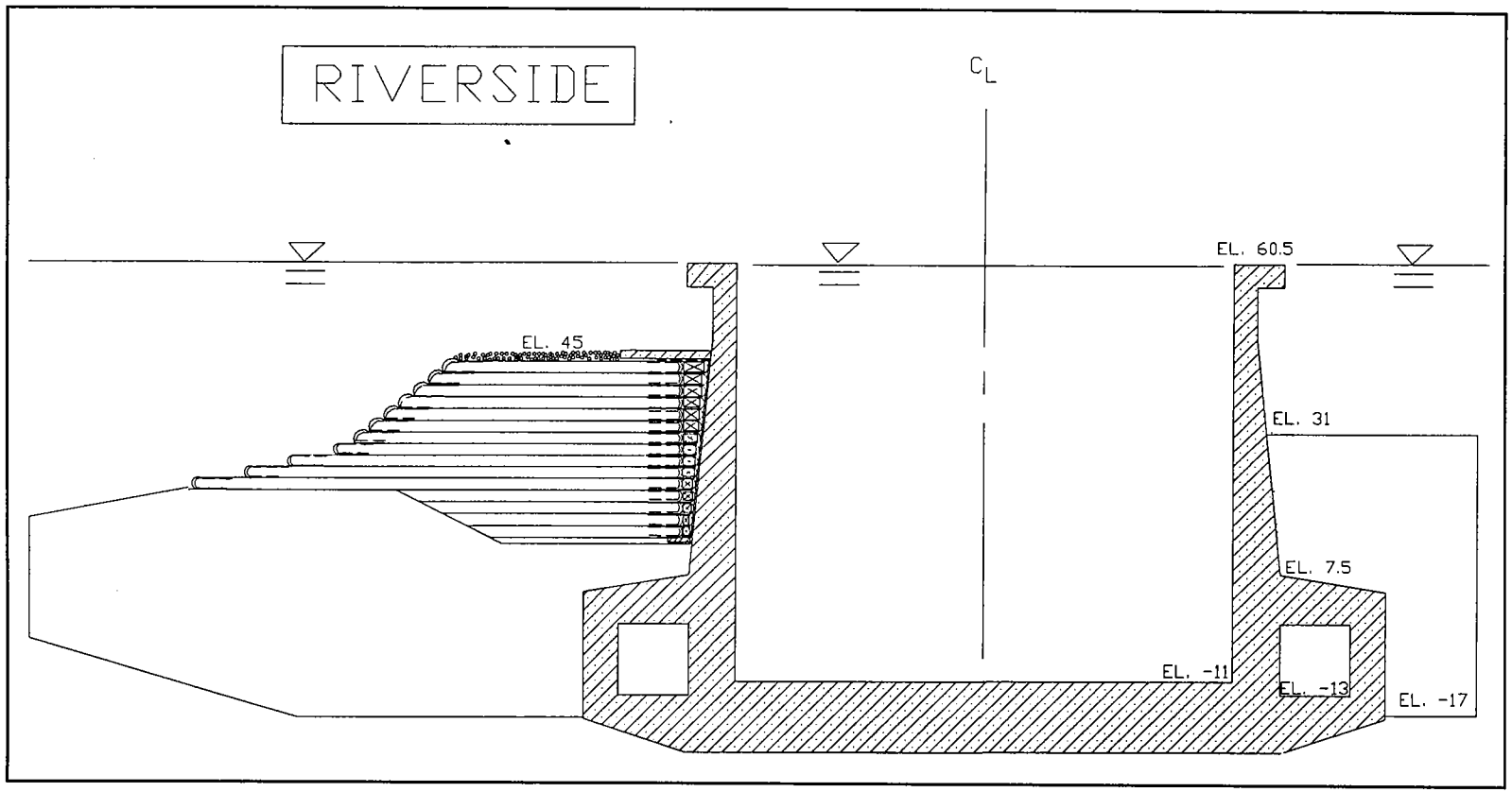

Figure 95. Riverside reinforced berm with lower pool and pool in lock at el 60

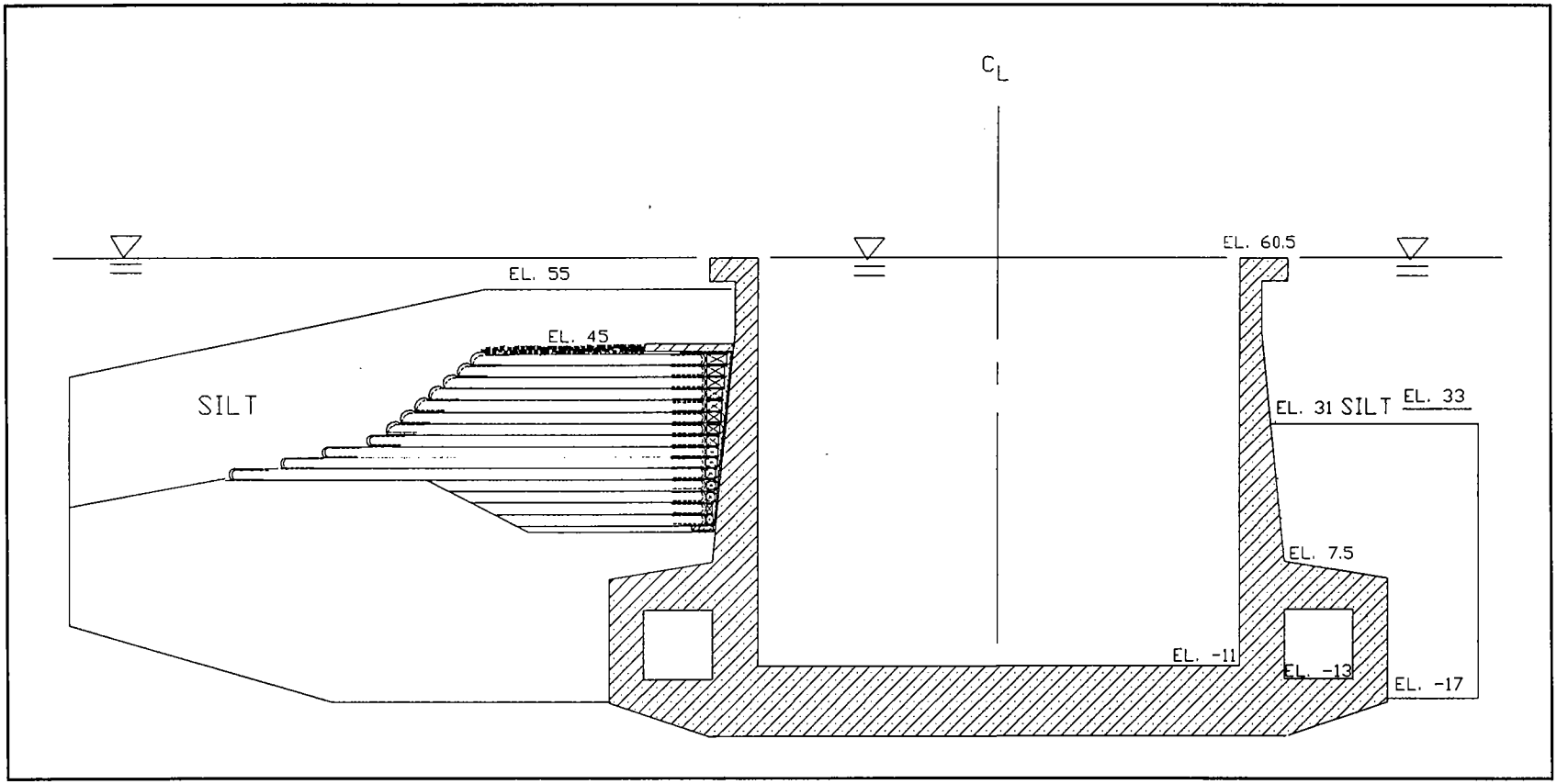

Figure 96. Reinforced berm with lower pool and pool in lock at el 60, deposition of riverside silt to el 55

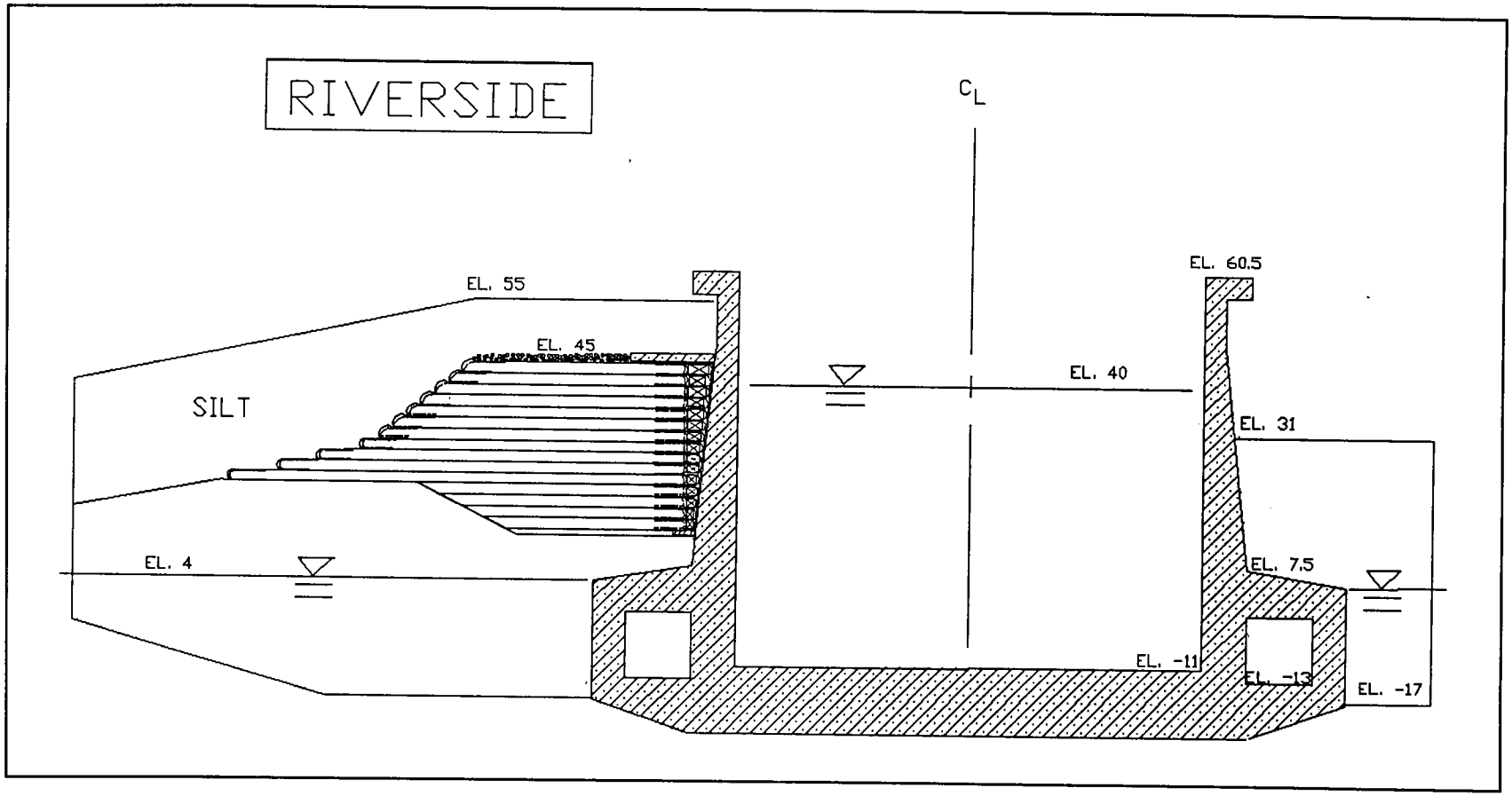

Figure 97. Reinforced berm with lower pool at el 4, pool in lock at el 40, and riverside silt at el 55

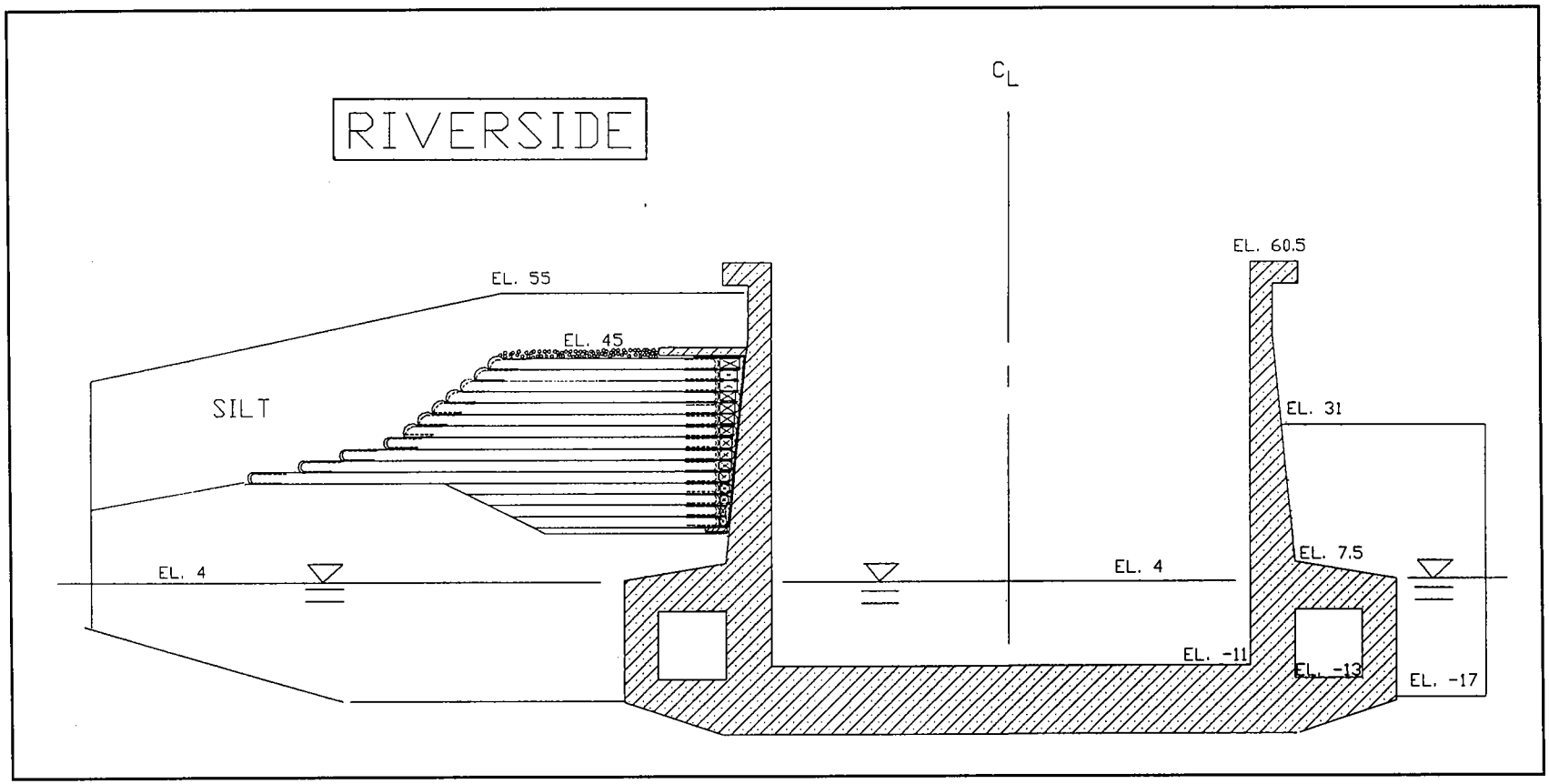

Figure 98. Reinforced berm with lower pool and pool in lock at el 4, riverside silt at el 55

the berm and against the stem walls of the lock during the high-water stage at the lock (Figure 96). This was followed by the lowering of both the river elevation and the elevation of the pool within the lock. The computed results for two sets of river elevations and pool in the lock elevations are discussed. The first group of results corresponded to the stage when the river elevation was at 4 ft and the pool elevation within the lock was at 40 ft (Figure 97). The second group of results corresponded to the final stage in the phase 2 analyses, in which the river elevation was at el 4 and the pool in the lock was lowered to el 4 (Figure 98).

The resulting stresses and displacements computed during the course of these analyses are reported for select points within the reinforced berm, soil foundation, soil backfill, and within the lock after the completion of each of these stages of loading. The format used to present the results is the same as that used to describe those results computed during the phase 1 analyses. The distribution of factored moments within the lock are reported for conditions that existed after the completion of each of the load stages.

Geometry of the Berm and Layout of the Reinforcement

The reinforced berm used in this series of analyses is to be constructed riverside of the lock and is shown in Figure 94. The geometry of the berm and reinforcement layout within the berm were from the preliminary design provided by the USAED, Vicksburg (1988). The top of the reinforced berm was at el 45, and the base was at el 13.5. The width of the berm increased with decreasing elevation, increasing from a width of 37 ft at the top of the berm to a maximum width of 93 ft at el 21. Below el 21, the berm was notched into the riverside backfill. The dimension of the berm followed the profile of the excavation. The riverside face of the berm had a slope equal to that for the existing backfill (5H:1V) between els 21 and 28. Above el 28, the slope steepened to 1.26H:1V. The lockside face of the reinforced berm was vertical. The soil comprising the reinforced berm was assumed to be a dense, well drained select sand. The material parameters for the sand comprising the reinforced berm and used in the finite element analyses are listed in Table 1. Proposed specifications for the sand to be used in construction of the reinforced berm are discussed in Chapter 4.

The reinforcement layout used in the analysis varied with location in the berm. The layout of the reinforcement scheme used in the finite element analyses consisted of what are referred to in this report as primary layers and secondary layers of reinforcement. Each primary layer of reinforcement extended across the entire width of the berm. The secondary reinforcement layers were located within the two shaded regions labeled A and B in Figure 94. Each of the primary and secondary reinforcement layers was at a constant elevation within the berm. The first primary layer

of reinforcement was placed 0.75 ft above the berm's base at el 14.25. From el 15 to el 41.5, the primary layers of reinforcement were spaced every 1.5 ft in elevation. Six, 16-ft-wide, secondary reinforcement layers were placed every 2 ft in elevation between 30.5 and 40.5 ft within the region labeled A. Five secondary reinforcement layers were placed within the region labeled B. Between els 21.75 and 24.75, the secondary layers were spaced at 1.5-ft elevations. The remaining two secondary reinforcement layers comprising region B were placed at els 26.5 and 28.5. Details regarding the reinforcement model used in the finite element analyses are discussed later in this chapter of the report. Design recommendations for the reinforced berm are presented in Chapter 4.

The gap between the stem wall and the vertical face of the reinforced berm will be closed by a filler material placed during the construction of the berm. The gap will minimize the effective earth pressures transferred from the reinforced berm to the riverside stem wall between els 13.5 and 45, resulting from the lateral deformation of the berm during its construction and from the lateral deformation of the berm in response to water loads and silt loads. The purpose of the filler material in the gap is to fill the gap to prevent the deposition of silt within the gap during periods of high water and eliminate the potential for soil raveling by the reinforced berm. A structral cap is required to distribute silt loads between the stem wall and the top of the reinforced berm, since the filler material is not likely to support the weight of the silt accrued above the gap. Chapter 4 of this report lists the desirable material characteristics that the filler material should possess and describes two possible materials that may fulfill these requirements.

Initial Conditions Prior to Excavation

Excavation and construction of the reinforced berm is expected to take place during the dry season at the lock. A lower pool at el 11 is consistent with the construction requirements and is often encountered during the dry season at the lock. Figure 92 shows the initial site conditions that were used in the finite element model. These initial stresses and displacements for the phase 2 analyses are computed at an intermediate stage of the phase 1 series of analyses in which the soil foundation and backfill were submerged below el 11 and in the lock was at el 11.

Excavation of Riverside Backfill to El 13.5 for Reinforced Berm

The first series of berm construction analyses models the partial excavation of the riverside backfill region outlined in Figure 93. The base of the completed excavation was at el 13.5 and was 30 ft wide adjacent to the

stem wall. Beyond 30 ft, the surface of the excavated backfill lay along an inclined slope (2H:1V) to el 21. At this elevation, the base of the excavation was horizontal and 40 ft wide. During the course of this series of analyses, the water table was maintained at el 11 below the base of the excavation.

The finite element mesh shown in Figure 51 was used in this series of analyses. The deepest excavation occurred adjacent to the riverside lock wall where the backfill was lowered by 17.5 ft, from el 31 to 13.5. The simulated excavation was done in the finite element analysis by use of the computer program SOILSTRUCT using four unload increments, removing 4.4 ft of backfill during each increment. Figure 99 shows a view of the mesh, including the lock, after completion of the excavation. The portion of the mesh that is shown in this figure corresponds to the same preexcavation mesh region shown in Figure 53. The material regions for the mesh shown in Figure 99 are shown in Figure 100. The drained soil parameters assigned during the phase 1 analyses were also assigned during these phase 2 analyses (Table 1).

The removal of as much as 17.5 ft of backfill relieved the lateral earth pressures acting along this region of the riverside stem wall and also unloaded the nonexcavated backfill and the soil foundation located below el 13.5. The variation in response of various soil elements to this unloading is described by the stress paths for select backfill and foundation elements. The stress paths for select backfill elements identified in Figure 62 are shown in Figures 63 through 69. Stress path point no. 5 corresponds to the initial effective stress state, while stress path point no. 6 represents the effective stress state after the partial excavation of the riverside backfill (Table 5).

The effective stress path for compacted sand backfill element 714 is shown in Figure 66. This element is adjacent to the riverside stem wall at el 13, and the top of this element defines the newly exposed ground surface after the completion of the 17.5-ft backfill excavation. The stress path from point no. 5 to point no. 6 for this element is to the left and extends downward below the p' horizontal axis. The stress path to the left reflects the reduction in effective stresses, while the location of stress point no. 6 below the p' axis shows the magnitude of the horizontal effective stress to be greater than the vertical effective stress after excavation. This later result is consistent with the overconsolidation of the soil element due to unloading.

Elements located farther from the excavated region, such as those backfill elements located on the other side of the lock, were much less affected by the riverside excavation (Figures 64 and 67) because of the nearly zero lateral movements and rotations of the landside stem wall in response to the riverside excavation.

The stress paths for compacted sand backfill element 649 and element 591 are shown in Figures 63 and 65, respectively. The centers of

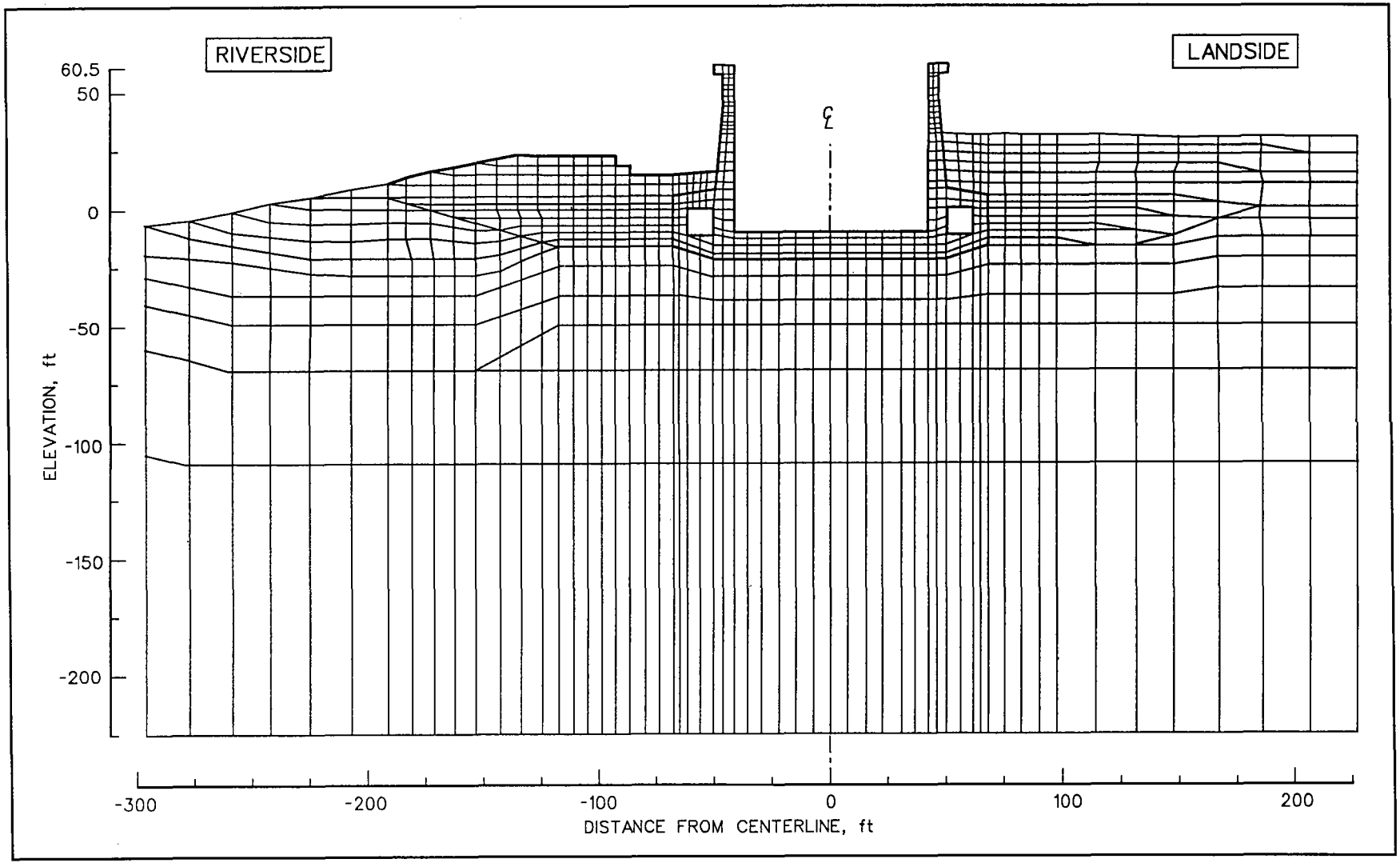

Figure 99. Enlargement of finite element mesh region encompassing lock structure after riverside excavation for reinforced berm

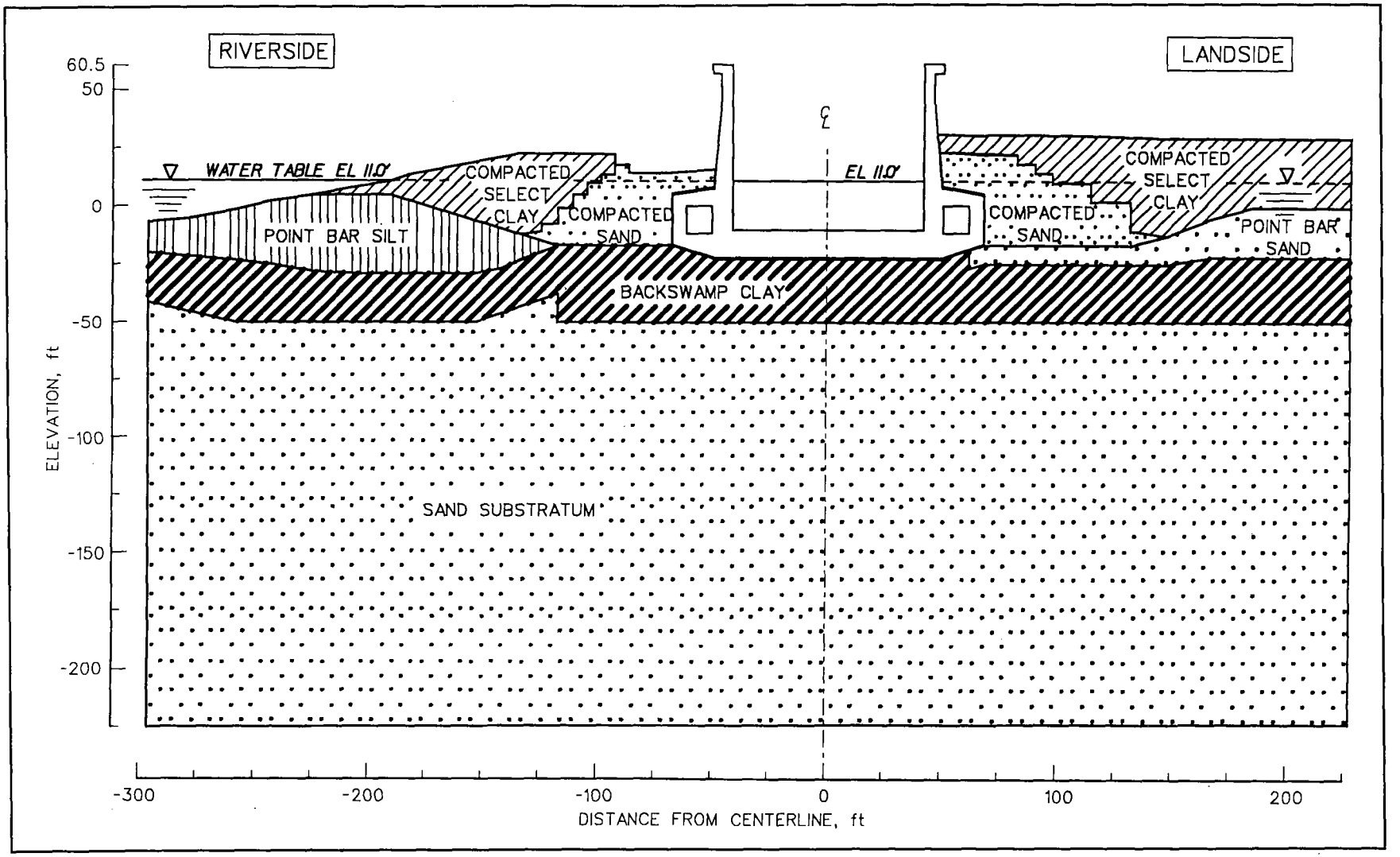

Figure 100. Material regions of finite element mesh region encompassing lock structure after riverside excavation for reinforced berm

these elements are both at el -6. Comparisons of the two stress paths during excavation showed the influence that the lock wall exerted on the soil. The wall provided not only a constraint on lateral displacements of the soil adjacent to the wall but also exerted both a shear force and normal force along the interface region between the wall and the adjacent soil elements. The magnitudes of these forces depended on the movement of the soil relative to the wall. Due to the interaction between the soil and the wall, the computed change in stress was greater for element 591 than for element 649 even though the amount of overburden removed above element 649 was greater than that removed above element 591, i.e., 16.5 versus 12 ft.

The stress paths for the select foundation elements identified in Figures 36 and 62, are shown in Figures 37 through 48. The greatest changes in stress occurred for those foundation elements closest to the excavation. The stress paths for the riverside foundation elements 725, 653, and 595, shown in Figures 39, 41, and 43, all exhibit a stress path that was downward and to the left. The stress path for element 653, located adjacent to the corner of the riverside culvert shows the magnitude of the horizontal effective stress to be greater than the vertical effective stress after excavation. This type of response is attributed to the interaction between this element and the lock culvert. As the distance from the backfill excavation region to the foundation elements increased, the magnitudes of the changes in stresses diminished.

During unloading, the stress-strain response for the soil elements followed the unload part of the stress-strain curve (Figure 13). This resulted in the computation of smaller displacements values than those displacements that would have been computed if the stress-strain response of the soil elements had followed the primary loading curve.

The results of the excavation phase of the analyses showed a decrease in effective stresses and shear stresses resulting from the excavation. The soil elements closer to the excavated region showed a greater change in the computed stress values. The resulting mobilized shear strength for all elements shown in these figures were computed to be less than the corresponding drained shear strength.

Construction of Reinforced Berm to El 45

The next series of finite element analyses models the construction of the reinforced berm shown in Figure 94. The finite element mesh of the lock, backfill, foundation, and reinforced berm is shown in Figure 101. The mesh consists of 1,152 two-dimensional elements and 1,257 nodes. The 31.5-ft-tall reinforced berm was modeled using 113 two-dimensional elements. The reinforcement was modeled using bar elements which were incorporated within each two-dimensional element comprising the berm. Each layer of reinforcement was modeled using bar elements which

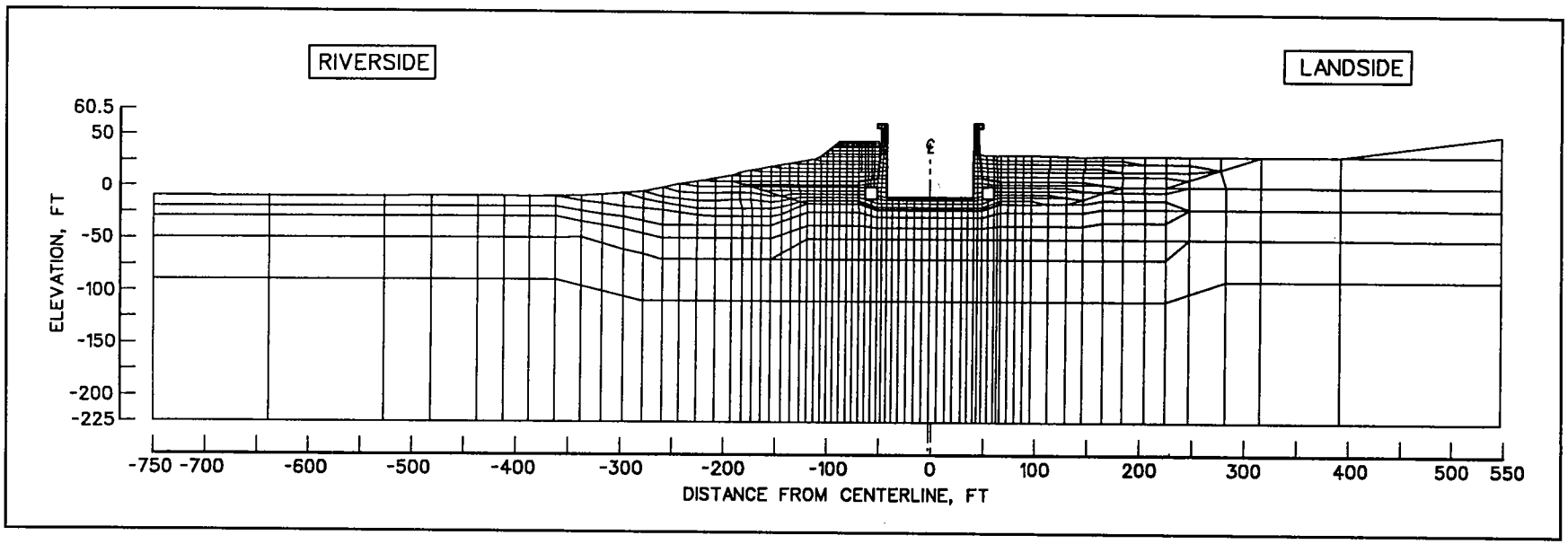

Figure 101. Finite element mesh after construction of reinforced berm

lay in series through the soil elements. A closeup view of the mesh that models the reinforced berm and lock structure is shown in Figure 102, with the material regions shown in Figure 103. A gap is included in mesh between the lockside face of the reinforced berm and the stem wall to eliminate the transfer of earth pressures to the lock between els 13.5 and 45. The elements modeling the lock, backfill, and soil foundation are the same elements that were used in previous analyses (Figure 51). The stresses and displacements computed after the partial excavation of the riverside backfill to el 13.5 were used as the initial values for this series of analyses. The water level was maintained at el 11 during the course of the construction of the reinforced berm.

Soil Reinforcement within the Berm

The layers of reinforcement will restrain the lateral spread of the reinforced soil berm during its construction and during subsequent water and silt loadings. The reinforcement within the berm was modeled using one-dimensional bar elements. Reinforcement will increase the stiffness of each of the two-dimensional QM5 soil elements in which reinforcement is used.

Reinforcement can be modeled by either of two methods. The first method consists of using bar elements, as tension-only elements, sandwiched between solid elements. With this method, the location of reinforcement must be accounted for in laying out the analysis mesh. This may become inconvenient if reinforcing layers are closely spaced.

The second method, developed for use on this project allows the reinforcement to be "embedded" into the interior of the two-dimensional element so that it is unnecessary to place reinforcement at element boundaries. The stiffness for the reinforcement "bar" element, $[K_b]$, which defines the relationship between the displacement $\{u_b\}$, is then related to the node displacements $\{u\}$ by the interpolation $\{u_b\} = [N]\{u\}$, where $[N]$ is the shape function. Thus, the effect of the bar on the element stiffness was obtained by adding to it the quantity $[N]^T[K_b]\,[N]$. The procedure can be repeated for any number of bars placed at any orientation within the element. Also, the procedure does not add to the total number of degrees of freedom. The only input required to add reinforcement by this method is the stiffness and location of the reinforcement layer. The individual soil elements of the berm that are affected by the layer are determined by the use of SOILSTRUCT.

During each analysis, the reinforcement model monitors the resulting total strains within each bar element and distinguishes between tensile and compressive strains. Typical soil reinforcement materials are very thin relative to their length and are not capable of resisting compressive strains. This restriction is incorporated within the reinforcement model by reducing the reinforcement bar stiffness to a value of nearly 0 when compressive

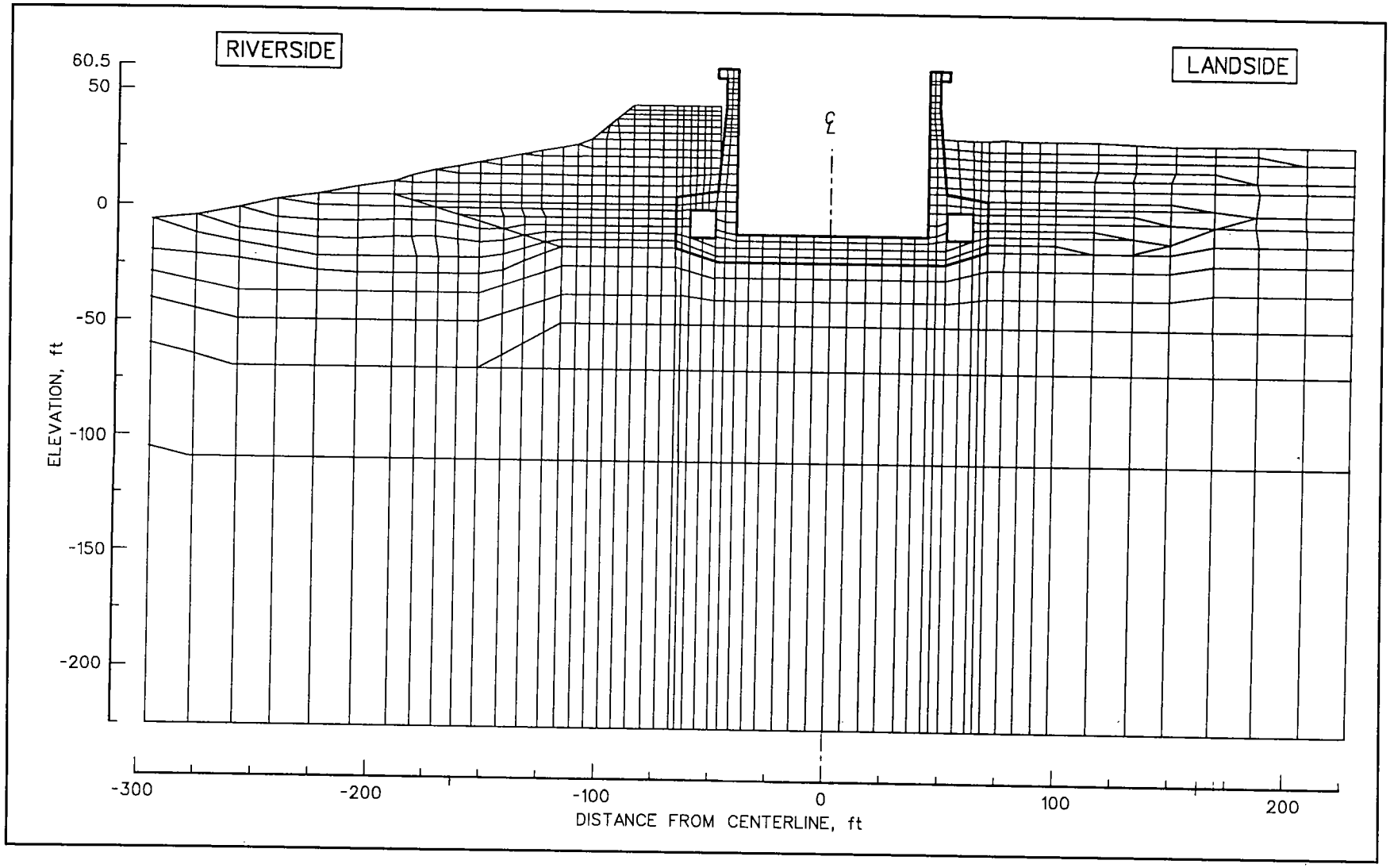

Figure 102. Enlargement of finite element mesh region encompassing lock structure after construction of reinforced berm

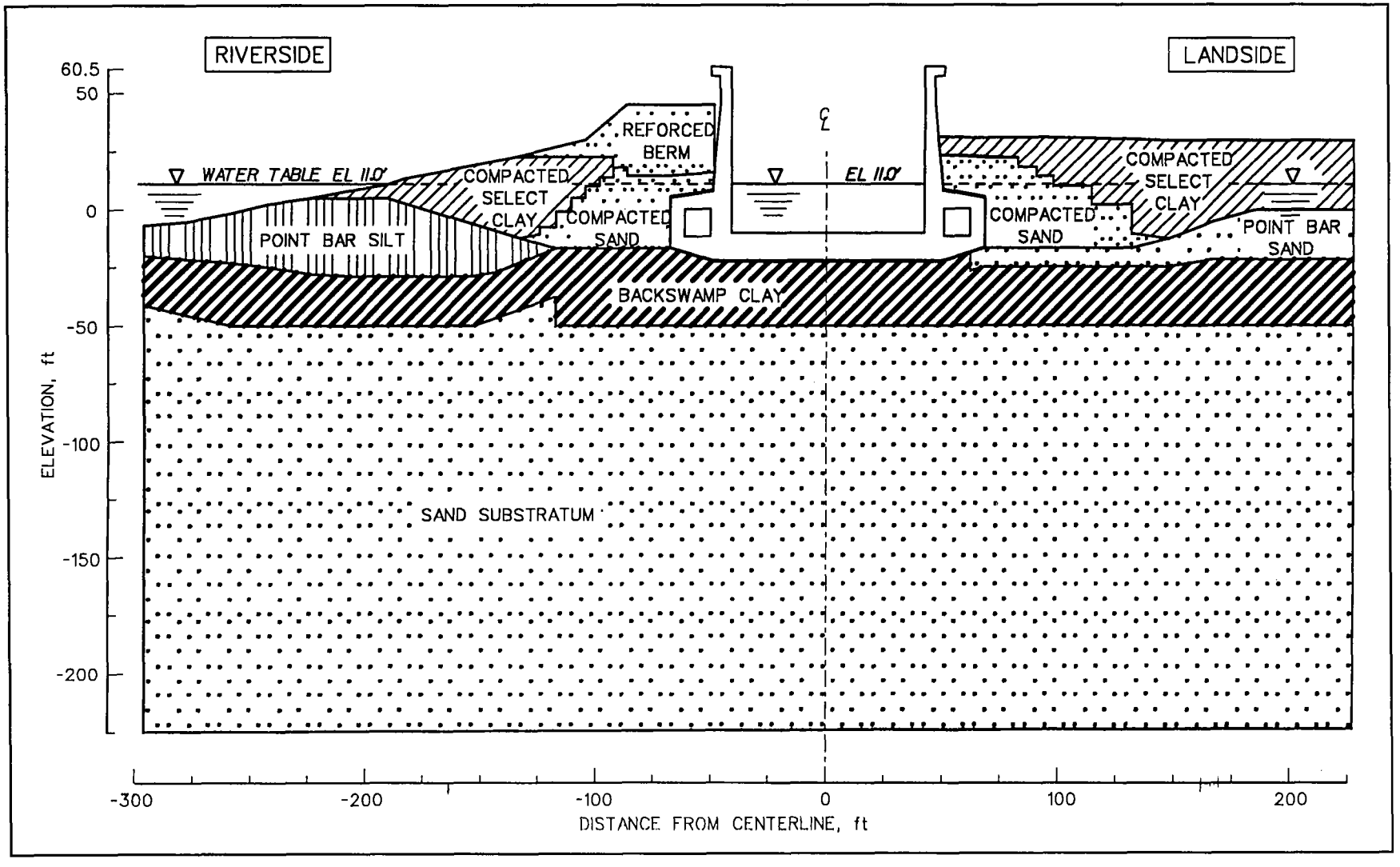

Figure 103. Material regions of finite element mesh region encompassing lock structure after construction of reinforced berm

strains are computed. The model can reestablish the tensile stiffness contribution of the reinforcement bar elements to the two-dimensional soil elements when and if tensile strains occur within the bars during subsequent loadings.

The layout of the reinforcement within the berm consists of primary and secondary reinforcement layers. Each primary layer of reinforcement extends across the width of the berm, in contrast to secondary layers, which are of finite length within the reinforced berm. The purpose of the secondary layers is to provide an additional reinforcement to assist the primary layers in select regions of the berm (Figure 94). The layout of the reinforcement is described in detail in the section entitled "Geometry of the Berm and Layout of the Reinforcement." In this series of finite element analyses, the construction of the 31.5-ft-high reinforced berm was simulated through the incremental placement of the elements comprising the berm. The construction of the berm was modeled by placing the soil elements comprising the berm in 10 lifts. Upon completion of the placement of each soil lift, the layer(s) of reinforcement contained within each of the newly placed soil elements were activated as described previously. The number of bar elements within each of the soil elements comprising the reinforced soil berm ranged from a minimum of one bar element per each reinforced soil element to as many as six bar elements. The material properties assigned to the bars modeling the reinforcement are given in Table 14. The long-term tensile modulus assigned to the bar elements was 50,000 lb per lin ft of berm, where the tensile modulus is the product of the long-term Young's modulus for the reinforcement and the cross-sectional area of the reinforcement per linear foot of berm. The allowable strength of the reinforcement was 3,800 lb per lin ft of berm.

Table 14
Material Parameters Assigned to Reinforcement Used Within Berm

Allowable Strength (lb per lin ft)	Long-Term Tensile Modulus at 2% Strain and 55 °F (lb per lin ft)
3,800	50,000

Results of Soil-Structure Interaction Analyses

Construction of the reinforced berm riverside of the lock resulted in the settlement of the lock, backfill, and the original soil foundation. Settlements also occurred within the reinforced berm during its construction due to the weight of the newly placed lift. In addition, because the width of the reinforced berm was finite, the resulting displacements of the lock and surrounding soils included lateral and vertical displacements.

Displacement results for lock

Figure 104 shows the computed displacements for the select points after completion of the construction of the berm. All the values for displacements of the points shown in this figure and all subsequent figures reporting displacements in Chapter 3 of this report are relative to their position **after** completion of the riverside backfill excavation. The displacements of the lock show a counterclockwise rotation of the lock about a point midway the landside stem wall. The settlement distribution along the base slab is curved, a response that is characteristic of a flexural member. The greatest value for settlement was computed along the base below the corner of the riverside culvert and was 1.1 in. The center line of the lock settled 0.3 in. below the corner of the landside culvert and the base rose 0.1 in. The horizontal movements at the tops of the stem walls were 0.9 in. in the direction of the river for the riverside stem and 0.2 in. in the same direction for the landside stem.

Below the riverside reinforced berm, the movements of the riverside backfill was downward and towards the river channel as a result of the construction of the reinforced berm. The greatest value of settlement within the riverside backfill was 2.4 in. and was located at a point 50 ft riverside of the stem wall at el 21. The magnitudes of the lateral movements within the backfill varied with location, but all were less than 1 in.

All regions of the reinforced berm settled as it was being constructed. The distribution of settlements within the reinforced berm showed the riverside half moving toward the river, whereas the landside half moved toward the lock. The computed displacements within the landside half of the reinforced berm was greater than those computed within the riverside half due to the vertical face and the greater mass associated with the landside geometry. The greatest displacements were computed midway of the vertical face of the reinforced berm at el 30, where the berm settled 4.4 in. and moved 3.2 in. toward the lock.

In summary, the computed deformations of the lock responded as a flexible structure, with a significant amount of soil-structure interaction occurring between the lock, reinforced berm, backfill, and foundation. Because of the finite geometry of the reinforced berm, the irregular geometry of the soil regions, and the nonlinear stress-strain response of the soils, the computed displacements varied throughout the soil mass.

The computed deformations within the soil elements comprising the mesh were dependent on the moduli values assigned to these elements. The hyperbolic stress-strain model distinguished between two types of stress-strain responses, primary loading, and unload-reload behavior, as described in Chapter 1 of this report. In general, the moduli corresponding to unload-reload stress-strain response were greater than those associated with the primary loading portion of the stress-strain curve and resulted in smaller values of computed displacements, given the same applied load(s). This stress-strain model is consistent with the fact that

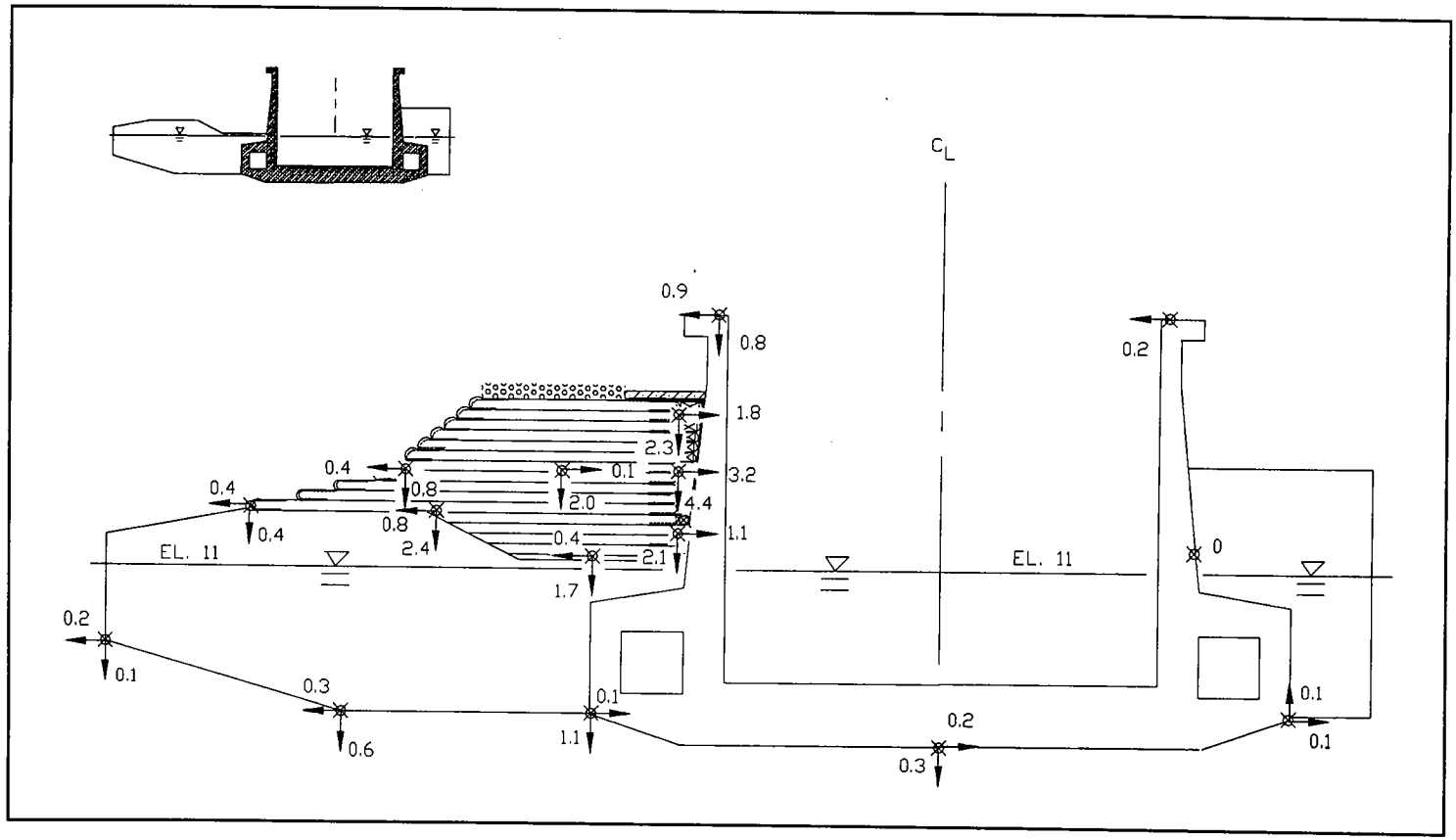

* Displacements of points are relative to their position after excavation for reinforced berm, in inches.

Figure 104. Relative displacements of lock, berm, and foundation after construction of reinforced berm

the response of soils to loadings depends upon the effective stress history of the soil. Overconsolidated soils will settle less than normally consolidated soils. SOILSTRUCT compares the value of the current deviator stress to the maximum value previously computed during prior stages of loading for each soil element to distinguish between unloading/reloading and primary loading. The initial excavation for the construction of the lock resulted in a significant reduction in values of effective stresses within the soil foundation, as described in Chapter 2. The construction of the lock resulted in the reestablishment of some but not all of the effective stress regime within the foundation, as did the construction of the reinforced berm. During excavation and construction, the foundation soils are first unloaded and then reloaded but not to the same level of effective stress that existed prior to site construction. To correctly model this situation, SOILSTRUCT assigns the unload-reload stress-strain soil moduli to all soil elements within the foundation during excavation and construction. One way of showing the level at which the foundation is loaded is by comparing the vertical effective stresses within the foundation to the effective preconsolidation pressures that were measured in the one-dimensional consolidation tests on samples of backswamp clays, conducted prior to excavation of the site. Figure 105 shows the locations of four sections within the foundation, labeled A-A, B-B, C-C and D-D, along which these comparisons are made.

Stress results

Section A-A is located 22 ft riverside of the culvert wall. Vertical effective stresses computed along section A-A are shown in Figure 106 along with the range in values of preconsolidation pressures for the backswamp clay samples. The vertical effective stresses within the soil elements of the foundation after completion of reinforced berm construction are labeled as Case 7 in this and subsequent figures (Table 5). The computed values of vertical effective pressures at all elevations along section A-A were less than the range in preconsolidation pressures for the backswamp clays.

The computed values of vertical effective stresses within the foundation below the riverside stem wall, below the center line of the lock, and below the landside stem wall are labeled sections B-B, C-C and D-D, and are shown in Figures 107 through 109, respectively. The computed values of vertical effective stress were less than the range in preconsolidation pressures for the backswamp clay samples, as can be observed along section A-A.

The results in Figures 106 through 109 show that the vertical effective stresses within backswamp deposit remained below the past preconsolidation pressures after the construction of the reinforced berm. SOILSTRUCT models the stress-strain response to loading on a soil element below the past preconsolidation pressures by assigning an unload-reload moduli to it. However, it is important to remember that the range in values of

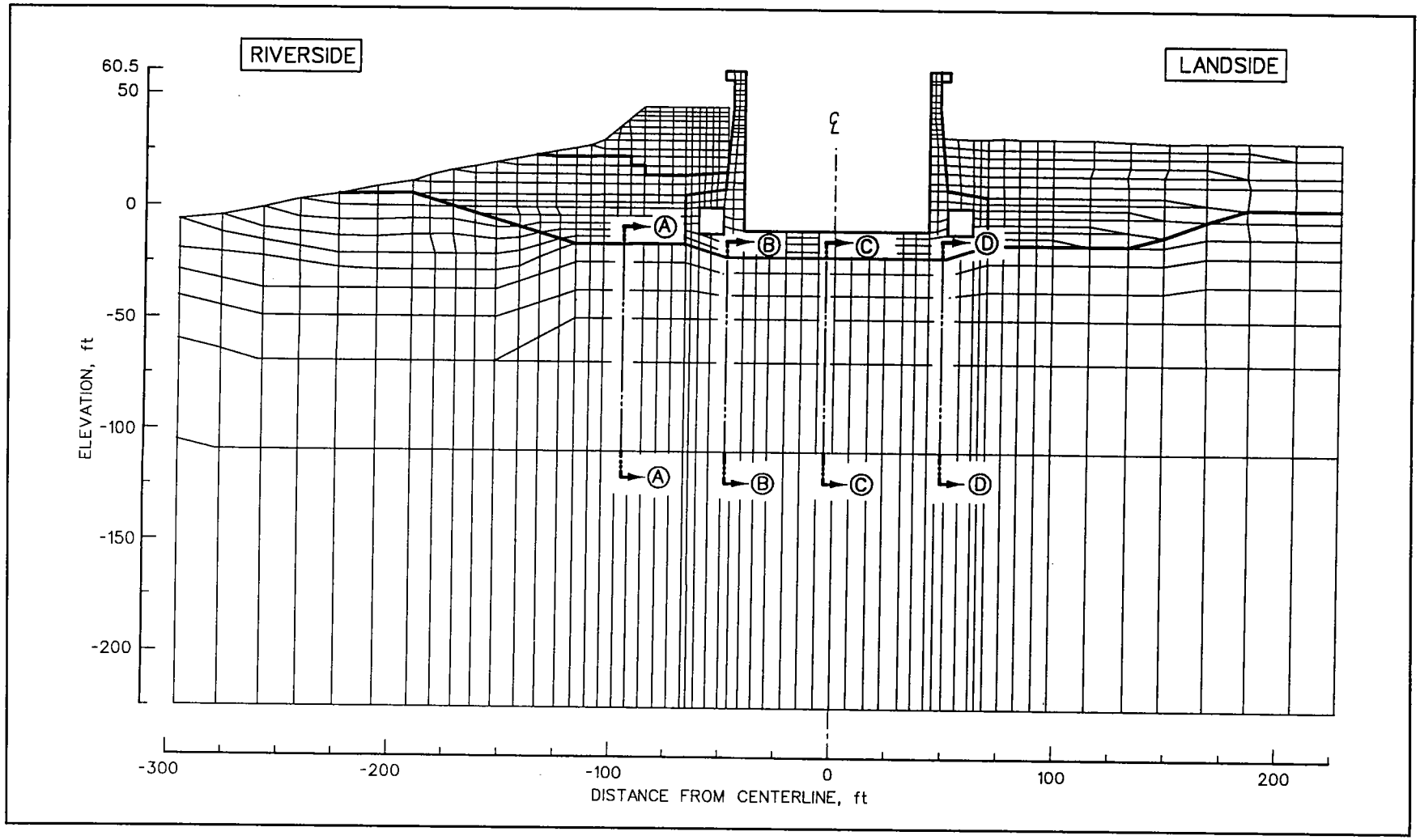

Figure 105. Four sections along which values of vertical effective stress are compared to range in preconsolidation pressure values within foundation

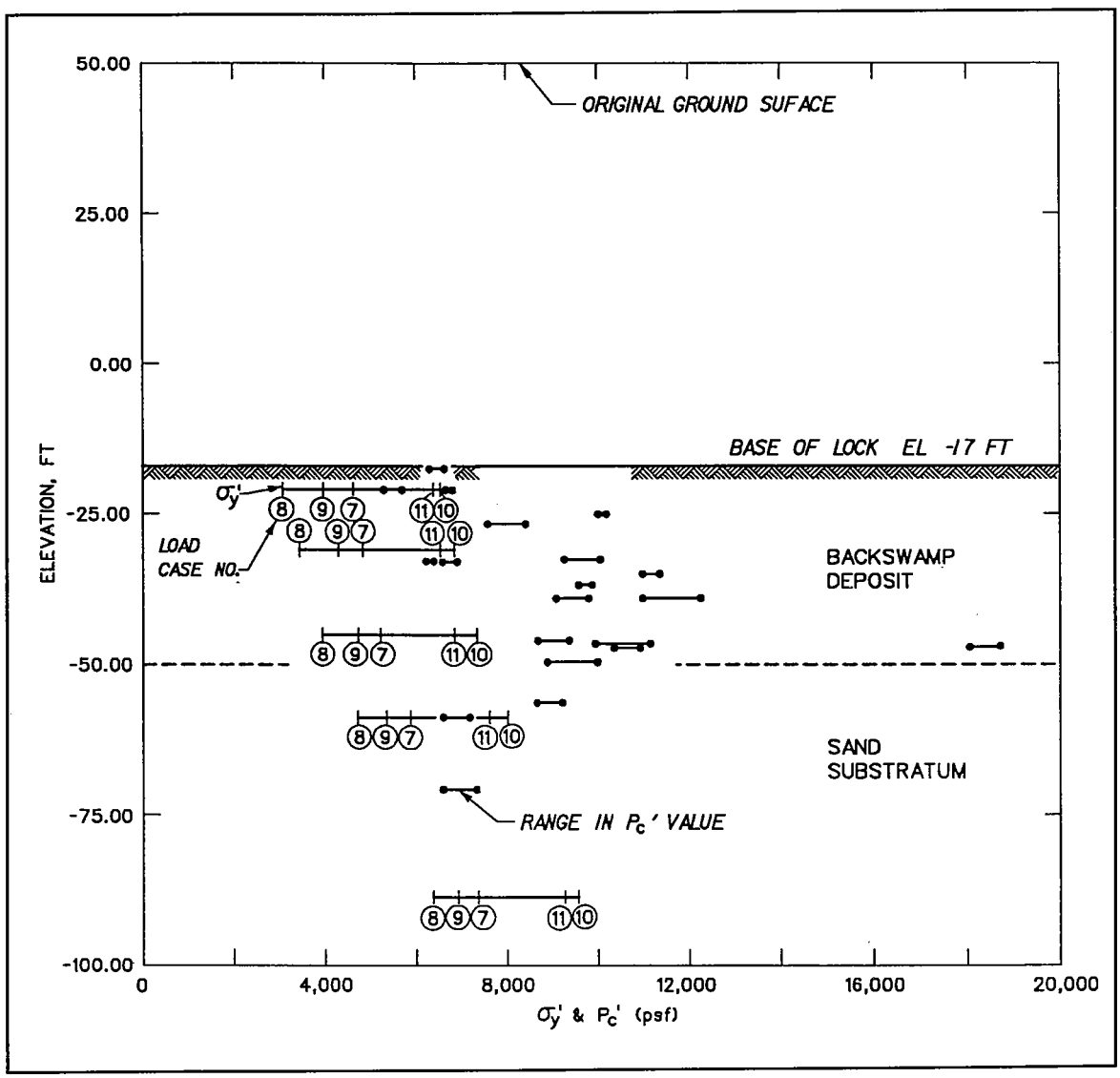

Figure 106. Values of effective vertical stress along section A-A'

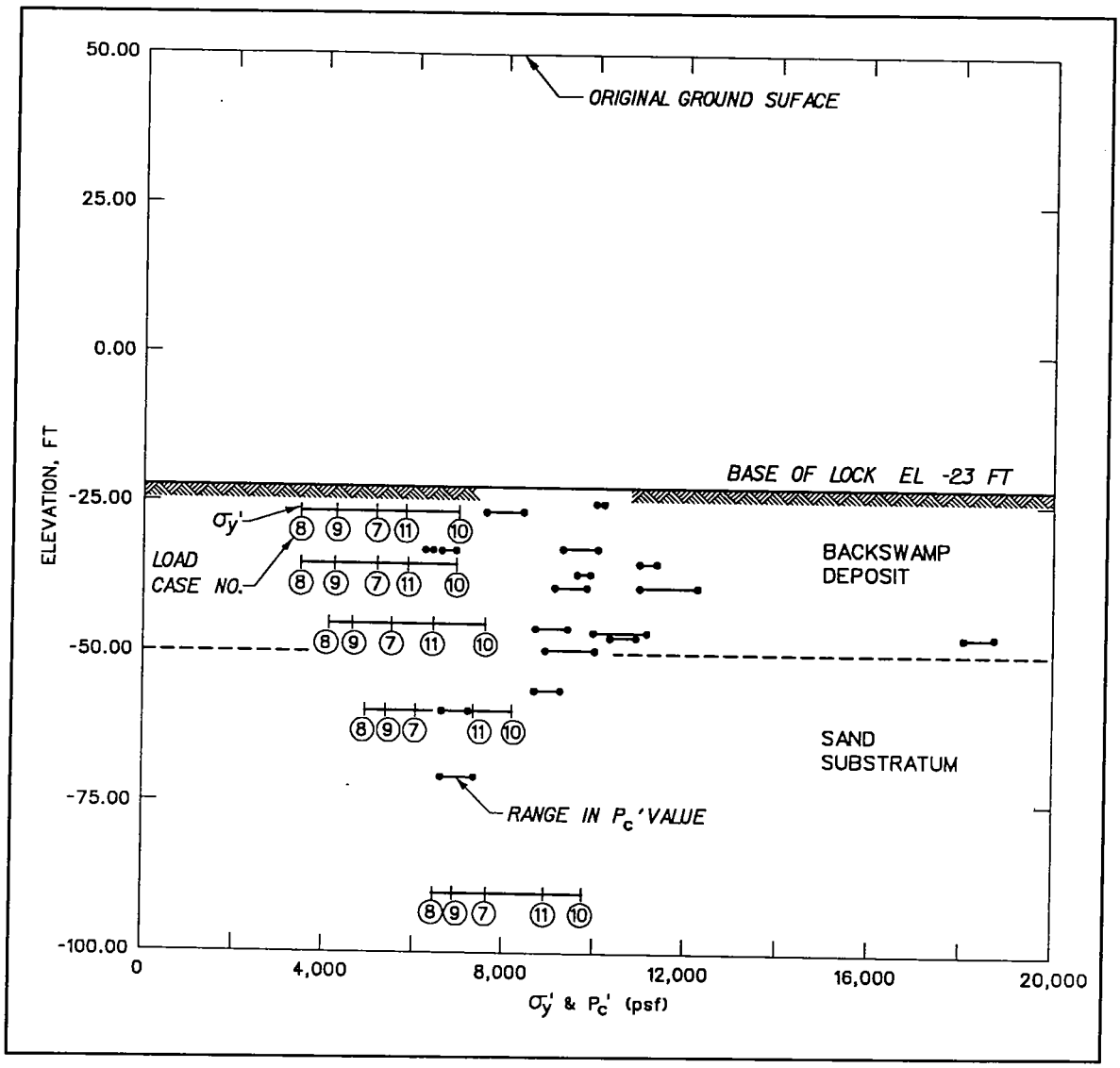

Figure 107. Values of effective vertical stress along section B-B'

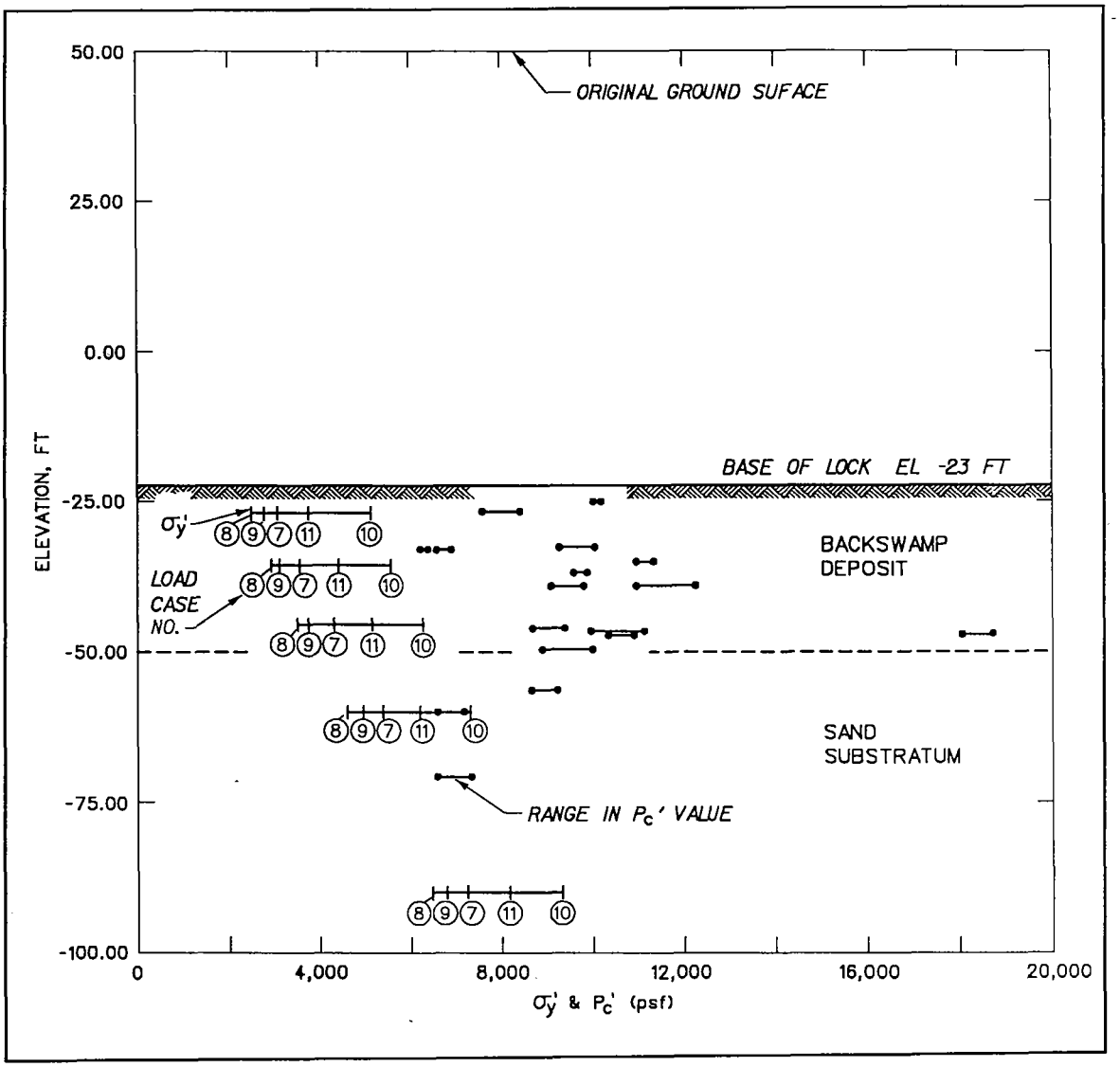

Figure 108. Values of effective vertical stress along section C-C′

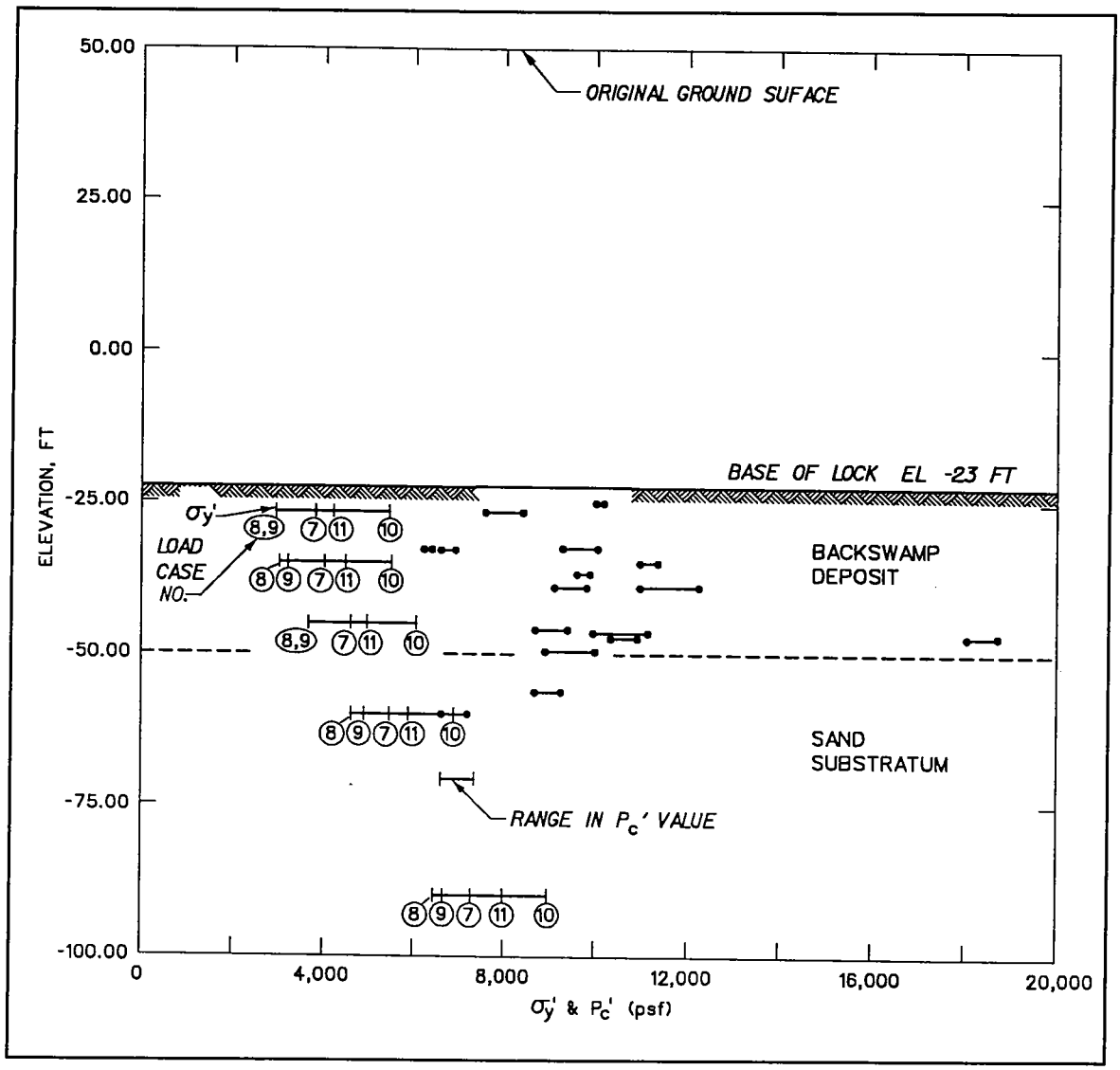

Figure 109. Values of effective vertical stress along section D-D'

preconsolidation pressures are from the one-dimensional consolidation test results on backswamp clay samples over the entire site of the lock and not just that from samples obtained near lock monolith no. 10. This aspect of the analysis will be further discussed in Chapter 4 of this report.

Figure 110 shows the computed total normal pressures and the hydrostatic water pressures (river at el 11) along the base of the lock and along the lock walls after construction of the reinforced berm. The computed base pressure is in the shape of an inverted saddle but due to the unsymmetrical loading from the berm, the results are no longer symmetric about the center line of the lock. Two of the three operational load case analyses discussed in Chapter 2 showed symmetrical results. The greatest total normal pressures were computed to be 7,084 and 5,870 psf below the riverside and landside stem walls, respectively. Below the center line of the lock, the total base pressure was 5,050 psf. The lowest value for the total pressure normal to the base of the lock was computed below the corner of the landside culvert and was 3,970 psf. The base pressure below the riverside corner of the culvert was 1,030 psf greater than the value computed below the landside corner, i.e. 5,400 psf.

The computed values of total pressures normal to each of the stem walls were not equivalent due to the construction of a reinforced berm riverside of the lock. The total normal pressures along the riverside stem wall were greater than the pressures computed along the landside stem wall by a factor of 2.6 at el 12.9 and by a factor of 1.7 at el 9. Above the base of the reinforced berm (el 13.5), the total normal pressures along the riverside stem wall were 0 because the reinforced berm was separated from the riverside stem wall. The difference in the magnitudes of the total normal pressures along the riverside and landside culvert walls decreased with increasing elevation. Below el 10, the values for total normal pressures along the culvert walls differed by as much as 20 percent. Between els -10 and 4.5, the values for total normal pressures along the culvert walls differed by less than 10 percent.

Figure 111 shows the computed effective normal pressures after construction of the reinforced berm. The values of effective normal pressures shown in this figure are equal to the difference between the values of total normal pressures and the values of hydrostatic pore water pressures shown in Figure 110. The greatest effective normal base pressures were computed to be 4,960 and 3,746 psf below the riverside and landside stem walls, respectively. Below the center line of the lock, the effective base pressure was 2,930 psf. The lowest computed value for the effective normal pressure was 2,150 psf and was located below the outside corner of the landside culvert. At the riverside corner of the culvert, the effective base normal pressure was 3,600 psf which is 1,450 psf greater than the value computed below the landside corner.

The effective normal pressures along the riverside stem wall are greater than those computed along the landside stem wall by the same factors as the total pressures, a factor of 2.6 at el 12.9 and a factor of 1.8 at

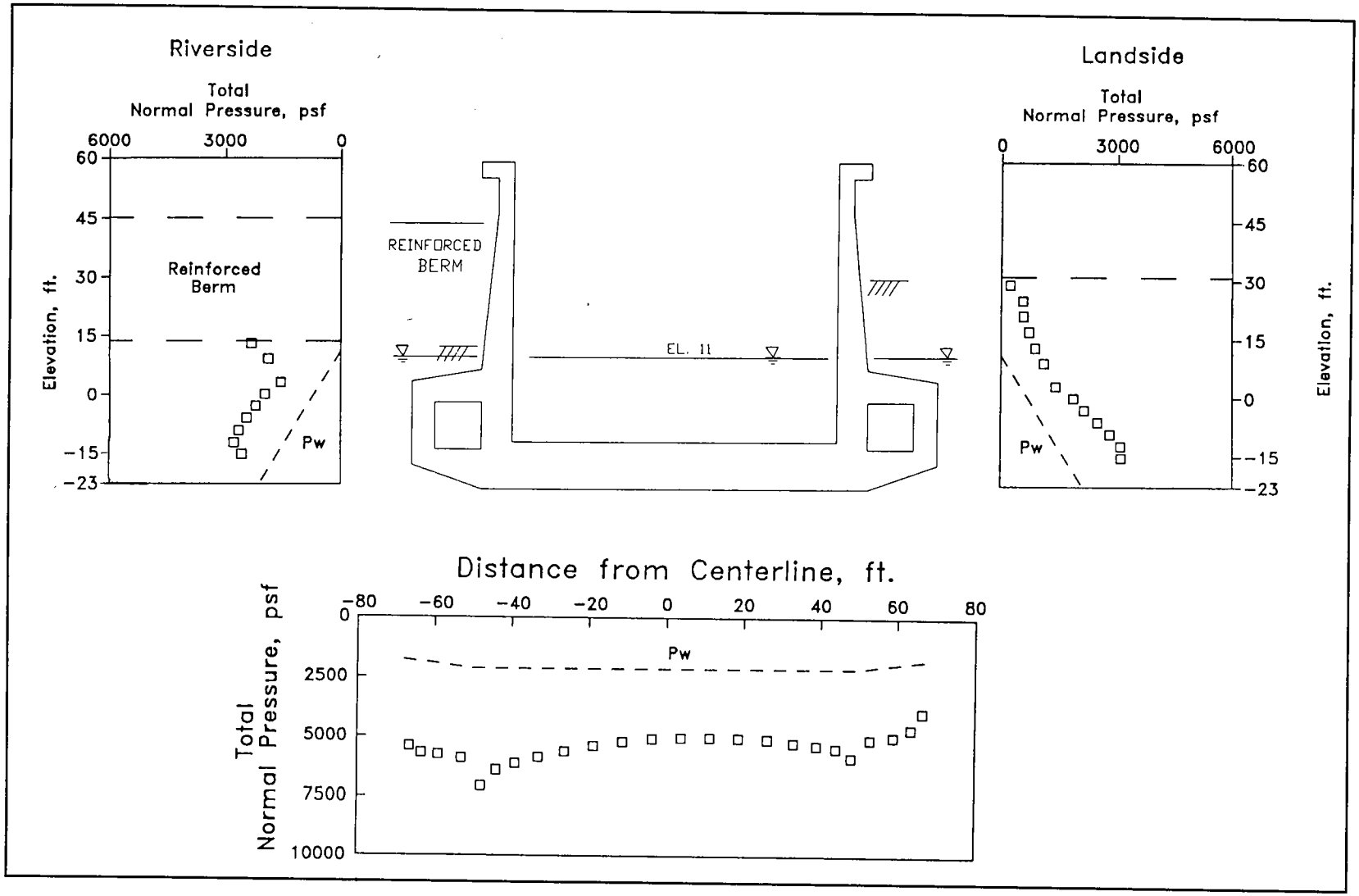

Figure 110. Total normal pressures after construction of reinforced berm, river and pool in lock at el 11

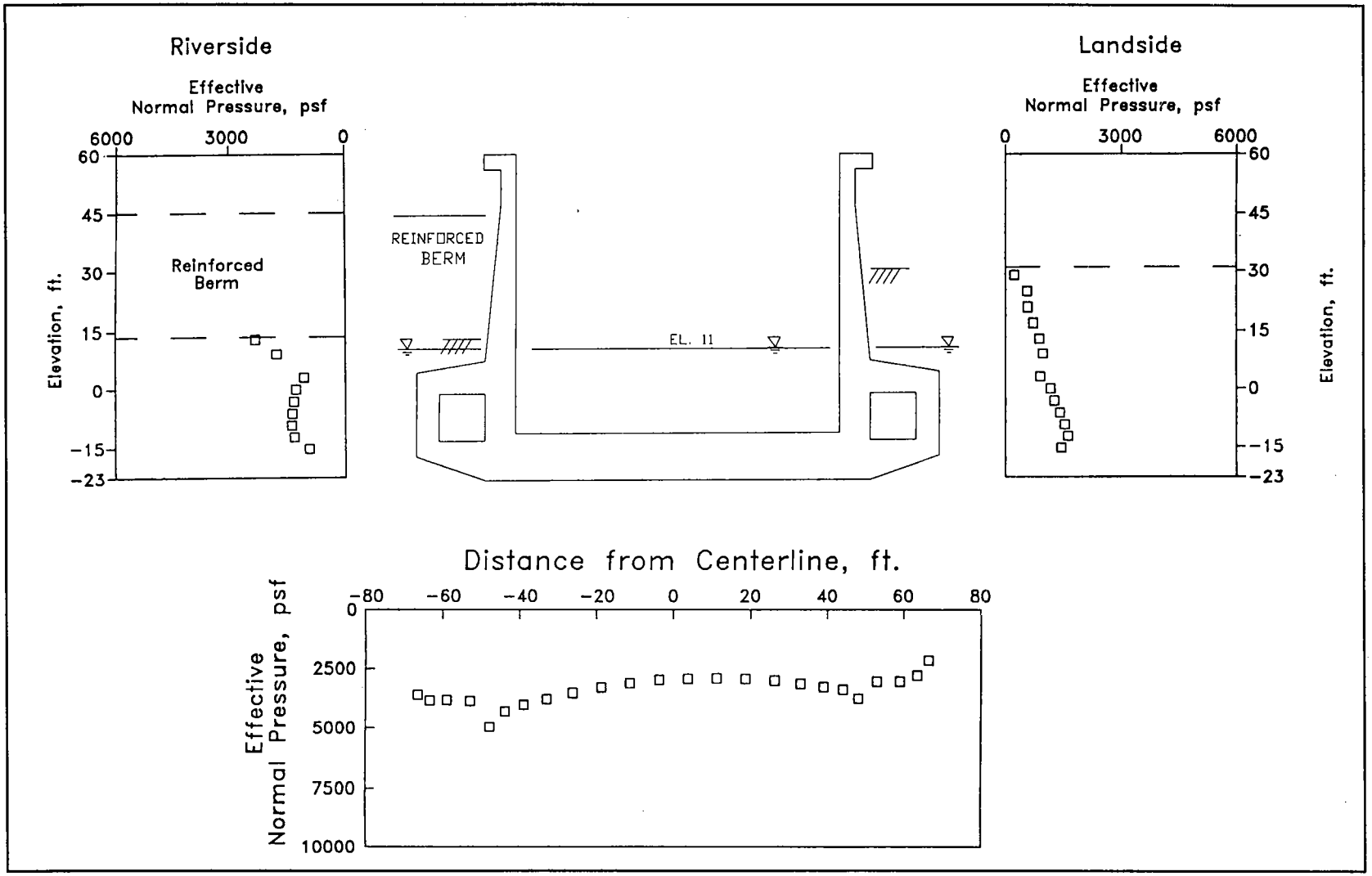

Figure 111. Effective normal pressures after construction of reinforced berm, river and pool in lock at el 11

el 9. Along the riverside culvert wall above el 0, the values of effective normal pressures were slightly greater than those values computed along the landside culvert walls, and vice versa below el 0.

The values of mobilized friction angles are shown in Figure 112. The greatest values of δ_{mob} along the base of the lock were computed below the stem walls. Along the base, δ_{mob} was 12 and 5 deg below the riverside and landside stem walls, respectively, and decreased to nearly 0 below the center line of the lock.

The greater values for δ_{mob} were computed along the riverside culvert wall, below the reinforced berm. Between els -17 and 4.5, δ_{mob} increased from 13 to 28 deg. Along the landside of the lock, the variation with elevation was much less, ranging from a low of 17 deg to a high of 22 deg. The values for δ_{mob} were smaller along the stem walls than were those along the culvert walls. Along the riverside stem wall, δ_{mob} was a constant 15 deg, whereas along the riverside stem wall, δ_{mob} ranged from 10 to 14 deg within the compacted backfill sand.

In Figure 112, δ_{mob} reflects the downdrag of the backfill along the lock wall due to the settlement of the backfill relative to the wall. This same shear force that acts downward along the face of the lock walls also acts upward on the soil backfill, opposite to the downward gravity forces acting within the soil backfill. This shear force reduces the vertical effective stresses within the soil backfill elements adjacent to the lock. Figure 113 shows the variation with elevation of the ratio of the vertical effective stress divided by the effective overburden pressure within the soil elements adjacent to the lock walls. This ratio is referred to as the overburden ratio. If the shear force were equal to 0, the vertical effective stress would be equal to the effective overburden pressure, and their overburden ratio would be equal to unity. The elevations in which the greatest values for δ_{mob} were computed corresponded to the elevations with the smallest values of overburden ratios. Along the landside stem wall, the overburden ratio decreased from 1.0 at el 31 to 0.77 at el 9. Below the riverside berm and between els 13.5 and 7.5, the overburden ratio ranged from 0.84 to 1.07. Along the culvert walls, the ratios were nearly constant. The average values for the overburden ratios along the culvert walls were 0.59 and 0.44 for the landside and riverside culverts, respectively.

The variation in horizontal earth pressure coefficients with elevation is shown in Figure 114. This figure shows that the value of K_h decreases with decreasing elevation along the stem walls and is nearly constant along the culvert walls. Along the landside stem wall, the maximum K_h value was 0.99 at el 29 and decreased with decreasing elevation to 0.40 at el 9. K_h ranged in values from 0.59 at el 13 to 0.41 at el 9 below the riverside berm. The distribution of K_h values were more uniform along the culvert walls, as compared to those values computed along the stem walls. Along the landside and riverside culvert walls, the average K_h values were 0.42 and 0.26, respectively (Table 15).

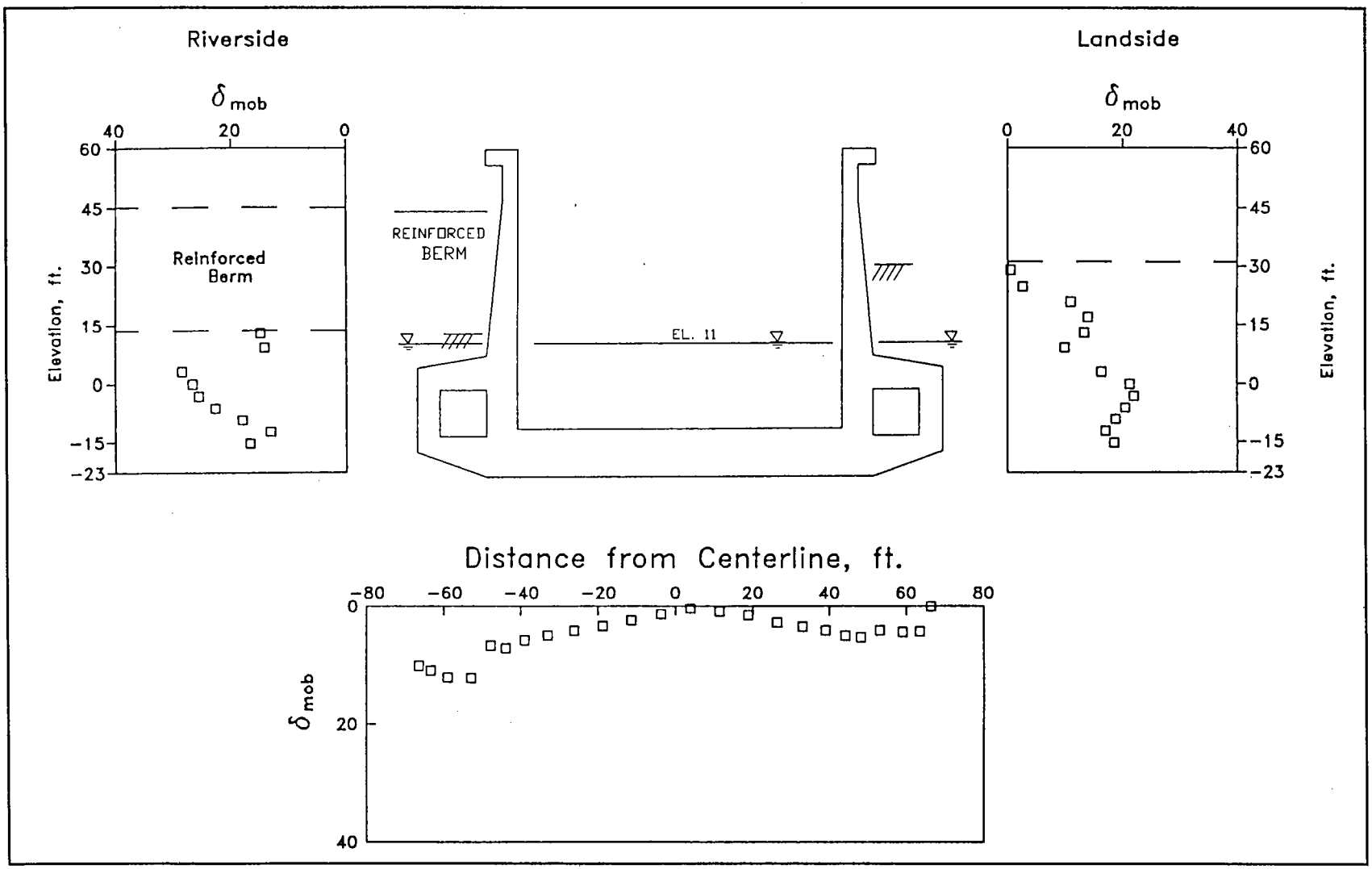

Figure 112. Mobilized friction angle along exterior of lock after construction of reinforced berm, river and pool in lock at el 11

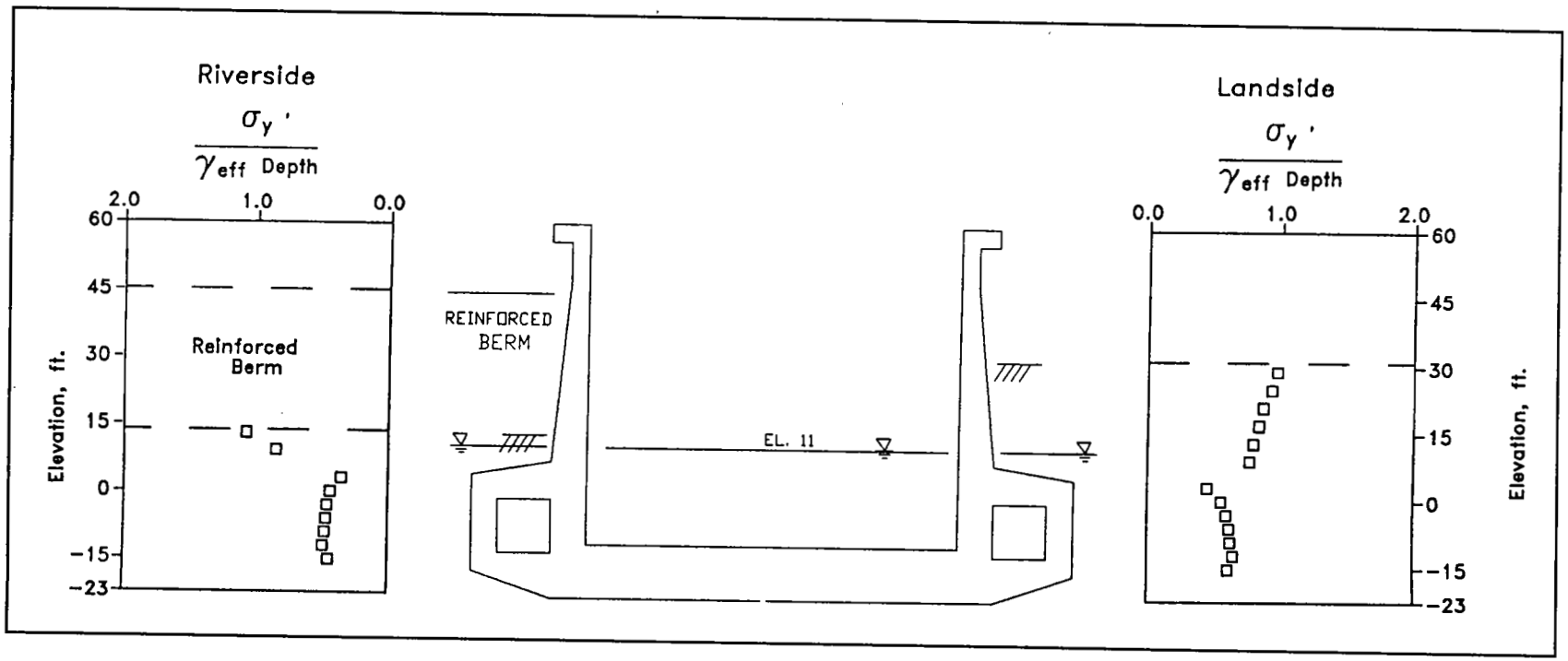

Figure 113. Ratio of effective vertical stress to effective overburden pressure after construction of reinforced berm, river and pool in lock at el 11

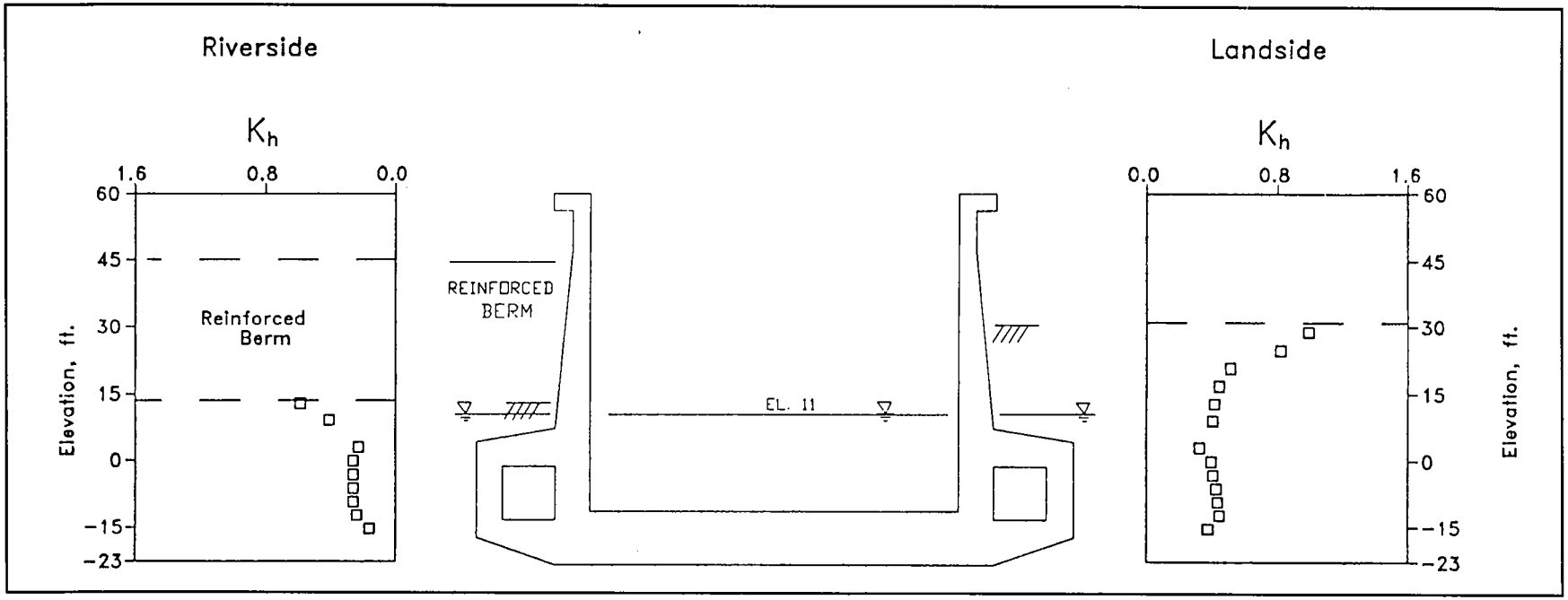

Figure 114. Horizontal earth pressure coefficient after construction of reinforced berm, river and pool in lock at el 11

Table 15
Average Values of Horizontal and Vertical Earth Pressure Coefficients after Construction of Reinforced Berm

Backfill Region	Backfill Material	Riverside K_h	Riverside K_v	Landside K_h	Landside K_v
Stem	Compacted select clay	—	—	0.9	0.02
Stem	Compacted sand	0.5	0.13	0.44	0.09
Culvert	Compacted sand	0.26	0.11	0.42	0.14

Elevation of river: 11 ft
Elevation of pool in lock: 11 ft
Elevation of river silt: —

The variation in the ratio of the horizontal effective stress divided by the vertical effective stress with elevation is shown Figure 115. The distribution of this ratio with elevation is similar to the distribution of K_h values in Figure 114. Since the values of vertical effective stress were smaller than the values of effective overburden pressure, the magnitudes of the ratio of the horizontal effective stress divided by the vertical effective stress were greater than the K_h values. The greatest differences were computed along the riverside culvert wall where K_h values were smaller by factors ranging in values from 2.0 to 2.8.

Figure 116 shows that the distribution in values of the vertical earth pressure coefficients varies with elevation along the landside stem wall and along both culvert walls. The greatest values for K_v computed along the landside and riverside stem walls were 0.11 at el 17 and 0.16 at el 12, respectively. The values of K_v along the culvert walls averaged 0.14, landside, and 0.11, riverside (Table 15).

The variation in the ratio of the shear stress computed along the wall divided by the vertical effective stress with elevation is shown Figure 117. The distribution of this ratio with elevation is similar to the distribution of K_v values in Figure 116. The greatest differences were computed along the riverside culvert wall where K_v values were smaller by factors ranging from 1.8 to 2.9. This difference was caused by smaller vertical effective stress values as compared to effective overburden pressure values.

Figure 118 shows the distributions of factored moments computed within the lock and the design moment capacity distributions. Results of the finite element analyses indicated that along the base slab, the entire top of the floor was in tension. The largest factored moment was computed at the center line of the lock and was -4,015 kip-ft. Because of earth pressures acting along the stem walls, the chamber sides of the stem walls were in compression. The maximum values for the factored

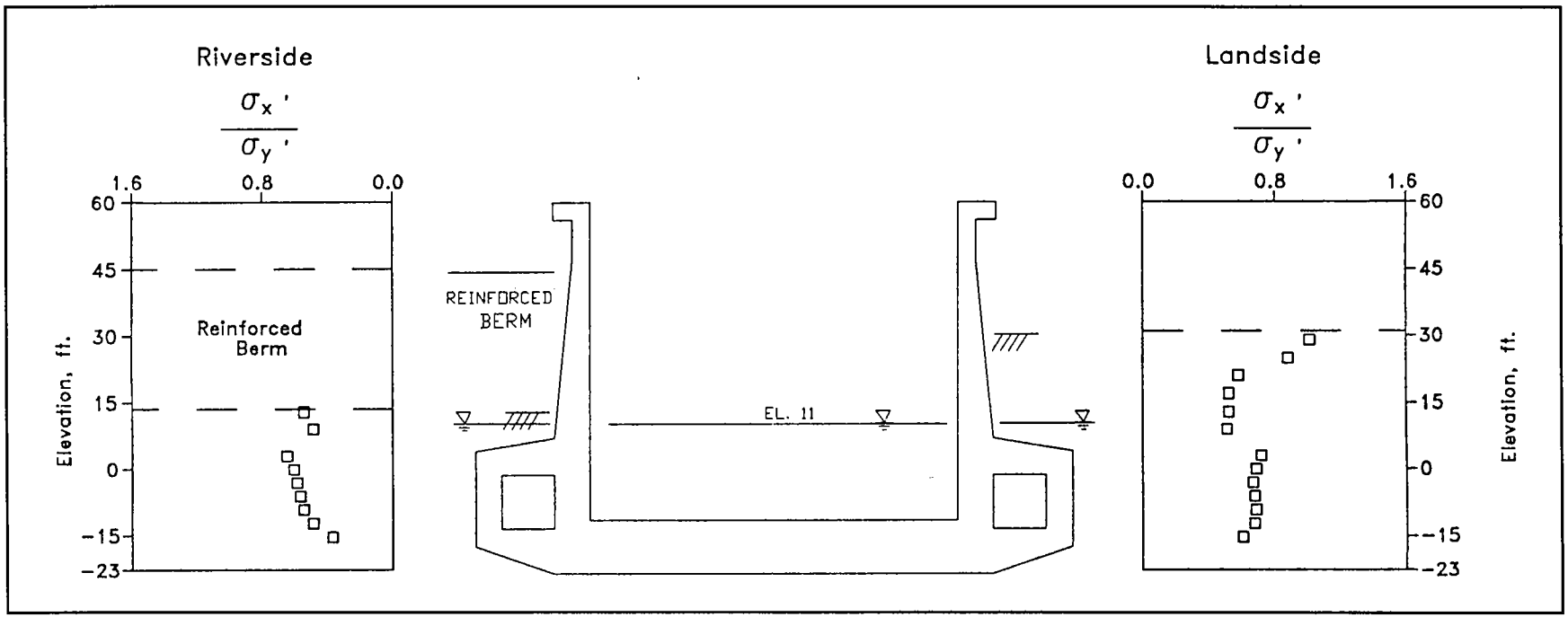

Figure 115. Ratio of effective horizontal stress to effective vertical stress after construction of reinforced berm, river and pool in lock at el 11

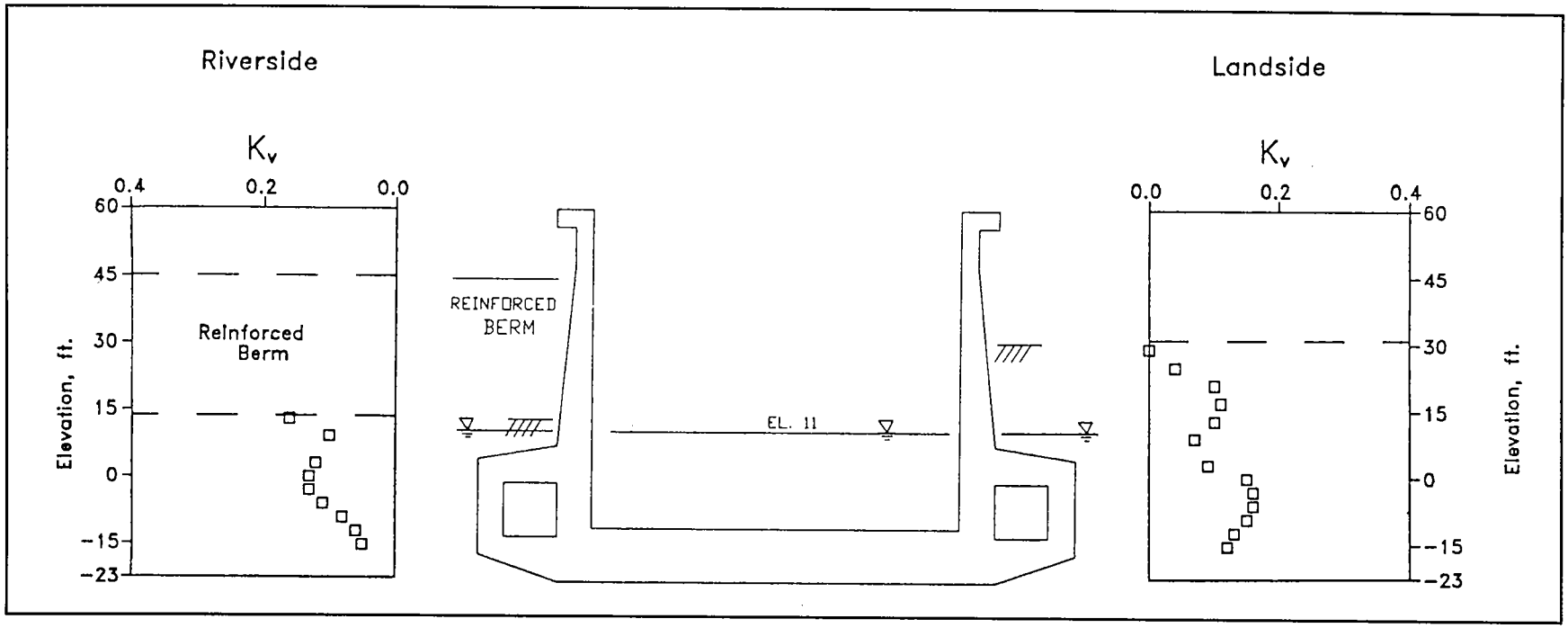

Figure 116. Vertical earth pressure coefficient after construction of reinforced berm, river and pool in lock at el 11

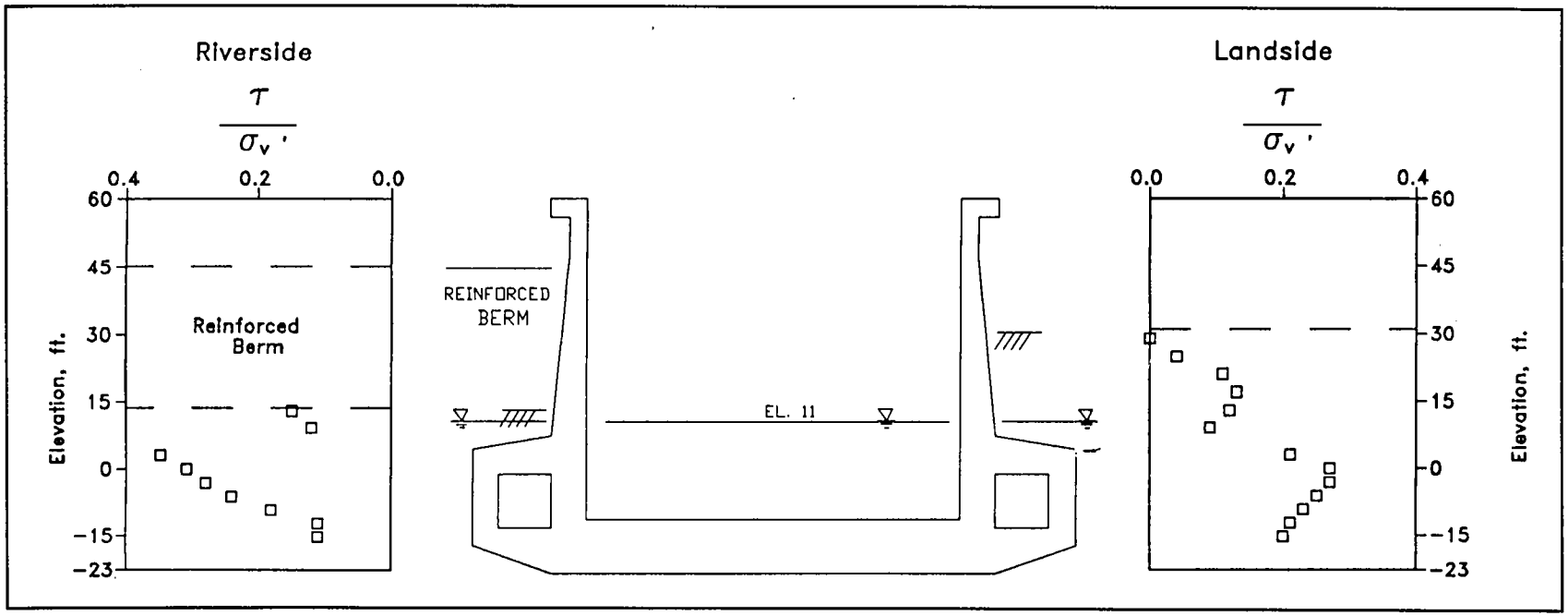

Figure 117. Ratio of shear stress to effective vertical stress after construction of reinforced berm, river and pool in lock at el 11

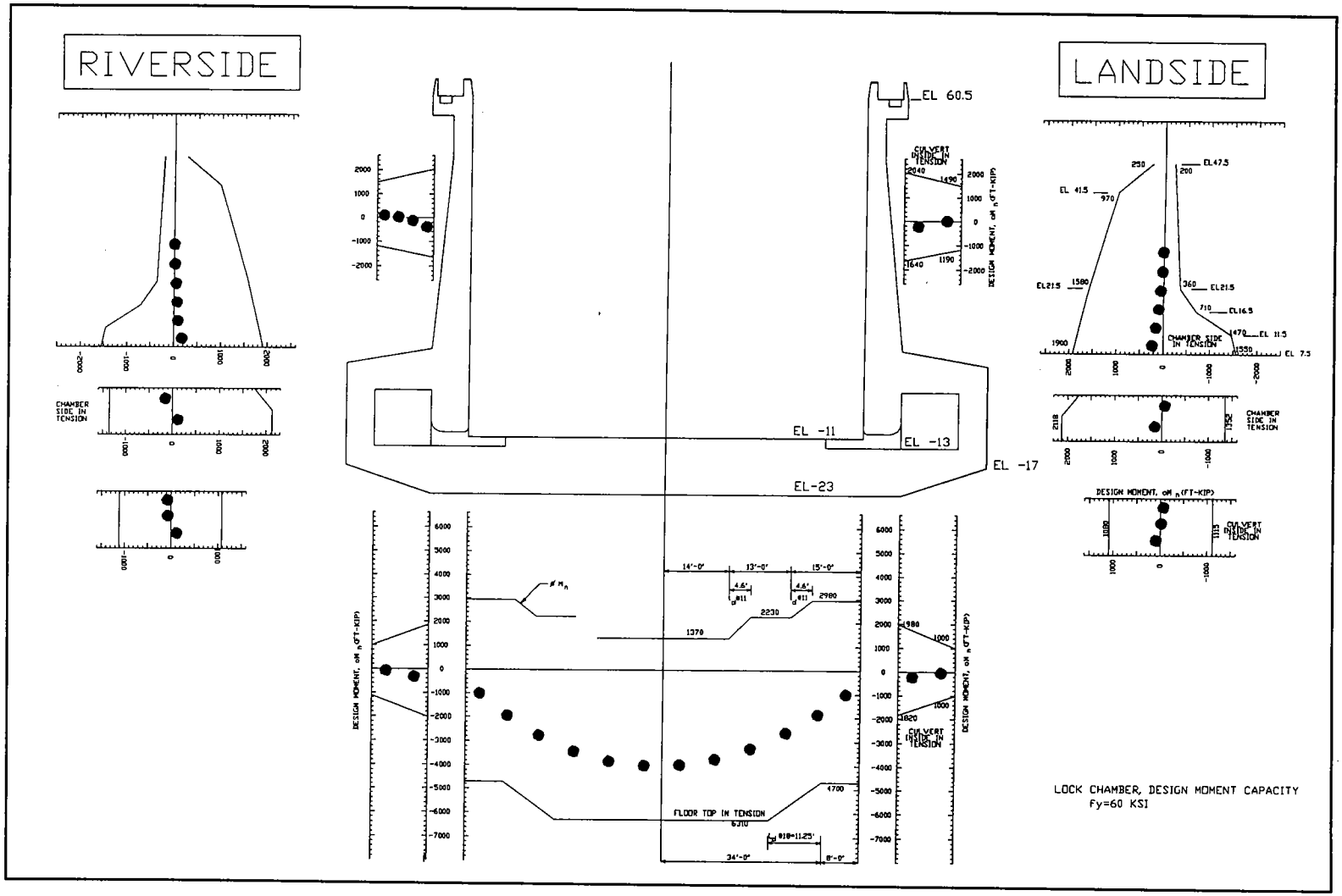

Figure 118. Distribution of factored moments after construction of reinforced berm and design moment capacity – river and pool in lock at el 11

moments computed within the stem walls at el 9.25 were 228 kip-ft at the landside stem wall and 178 kip-ft at the riverside stem wall. The value for the riverside factored moment was 22 percent less than the landside value at this elevation. The values for the factored moments within the lock were all well below the values for the design moment capacity.

Figure 119 shows the results from a pair of CUFRAM analyses compared to the distributions of factored moments within the lock from the results of finite element analyses. The earth and water pressures specified in the CUFRAM analyses equaled those computed in the finite element analysis. The lock was analyzed twice using the two extreme values for the RLF allowed within CUFRAM: RLF equals 0 and RLF equals 1.0. The greatest values for the moments were computed along the base at the center line of the lock in the two CUFRAM analyses and differed in value by less than 10 percent. The nearly perfect agreement among the results of the CUFRAM analyses indicates that the RLF factor does not have a significant influence on the computed moments **for this load case**. The factored moments computed using CUFRAM confirmed the values for the factored moments computed from the finite element results.

Stress paths for the four reinforced berm soil element numbers 715, 1152, 623 and 563, whose positions within the reinforced berm are shown in Figure 120, are depicted in Figures 121 through 124, respectively. In these figures, stress path point no. 1 corresponds to the initial effective stress state after placement of each of the reinforced berm elements, while stress path point no. 7 corresponds to the final effective stress state within the elements after completion of construction of the reinforced berm (Table 5). The stress paths for all four reinforced elements during berm construction were upward and to the right, indicating not only an increase in shear but also an increase in effective confining pressures within the elements. The presence of the reinforcement limited the deformations of the berm to finite values, as shown in Figure 104. Without reinforcement, the deformations would be excessive, and steep face slopes along the berm could not be constructed.

The movement of soil element 715, which defines the lower outside corner of the reinforced berm, were downward and to the right, away from the center of the reinforced soil mass, as shown in Figure 104. The directions of these movements were not unlike those of a wedge of unreinforced soil, whose movements are of sufficient magnitude to result in the transition from an at-rest state of stress within the soil wedge to a Rankine active state of effective stress, as shown in the idealized figures labeled A and B, respectively, in Figure 125. These types of movements within the soil mass resulted in a **decrease** in the magnitude of the horizontal confining pressure from an at-rest value to an **active** value, whereas the vertical pressure was maintained at a constant value equal to the overburden pressure. The stress paths for an element of soil located at the lower corner of the soil wedge is shown in Figure 125 and was upward and to the **left**. Although this stress path and the stress path for the reinforced soil element 715 (Figure 121) **both** caused full mobilization of shear resistance

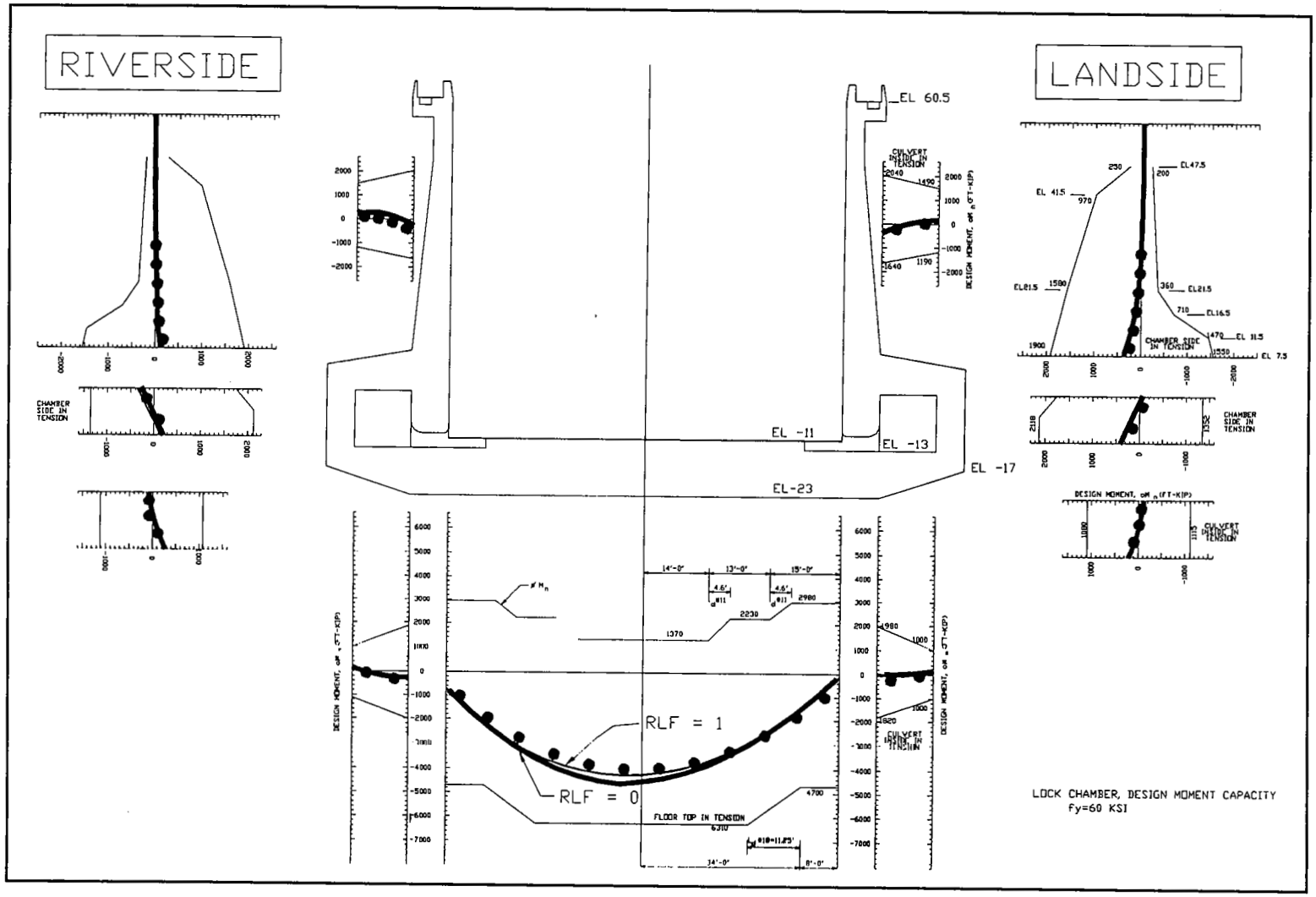

Figure 119. Distribution of factored moments, including CUFRAM results, after construction of reinforced berm – river and pool in lock at el 11

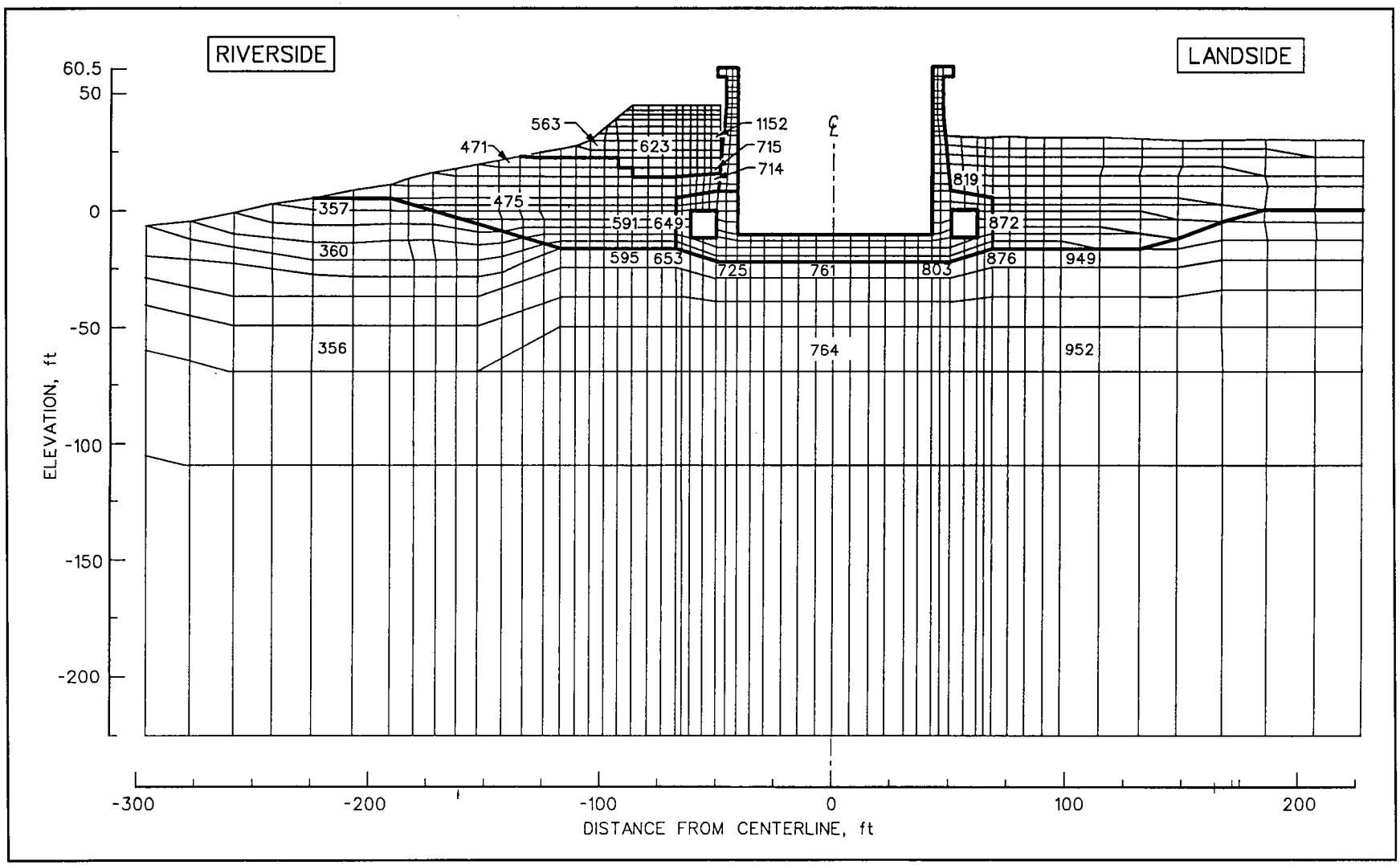

Figure 120. Locations of finite elements within the reinforced berm for which stress paths were computed

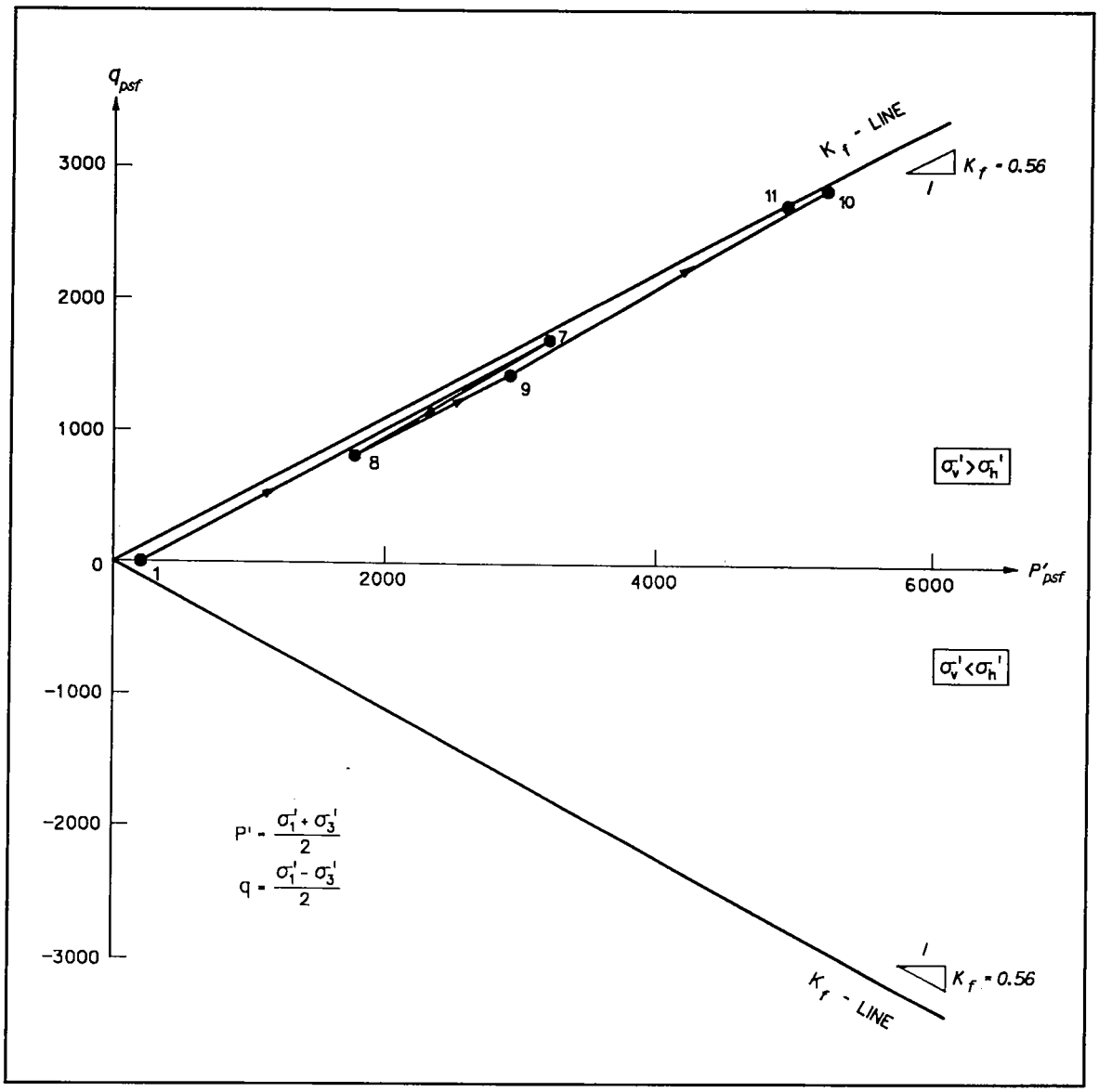

Figure 121. Stress paths for reinforced berm sand element 715, adjacent to riverside stem at el 16.5

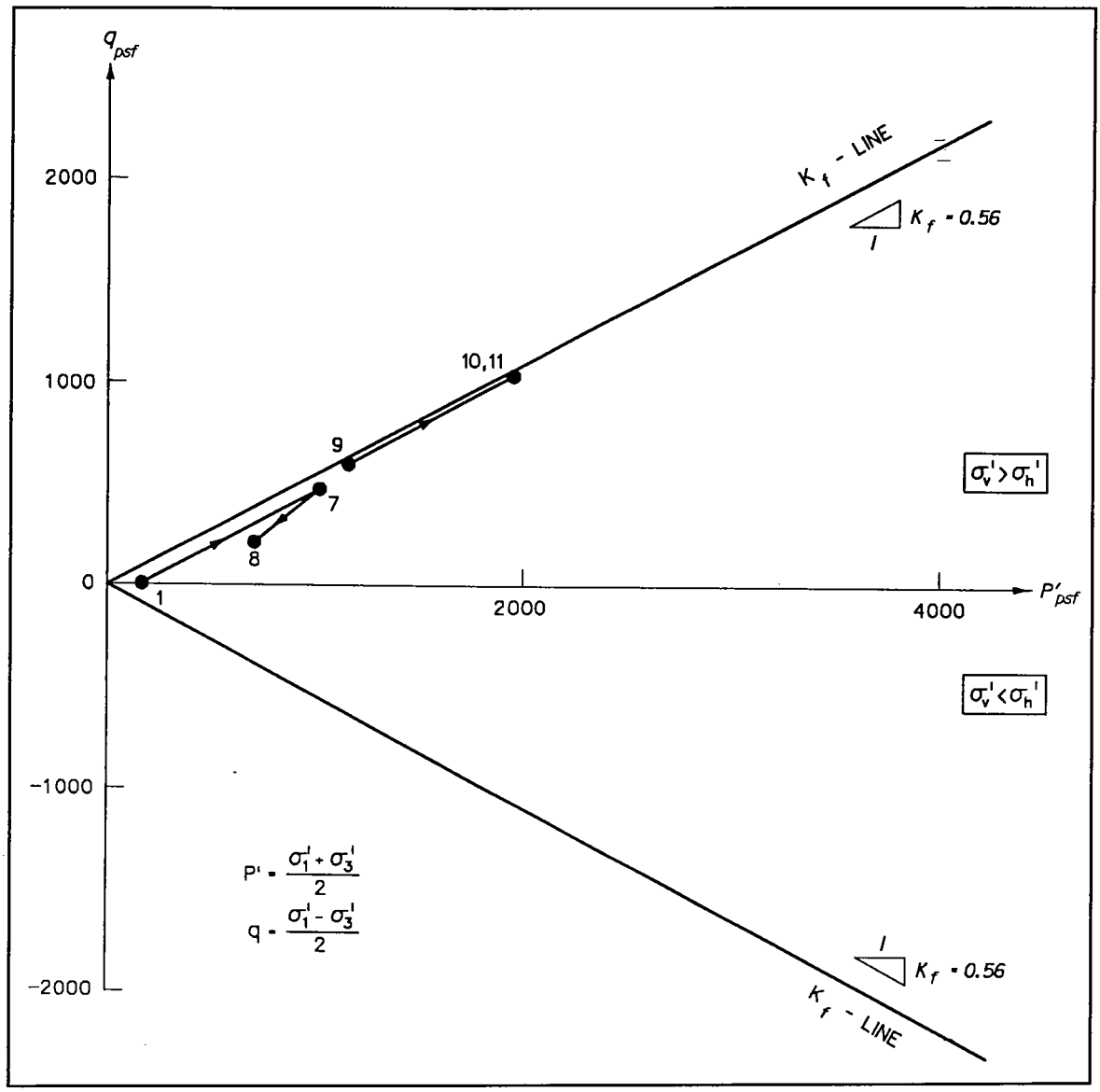

Figure 122. Stress paths for reinforced berm sand element 1152, adjacent to riverside stem at el 31

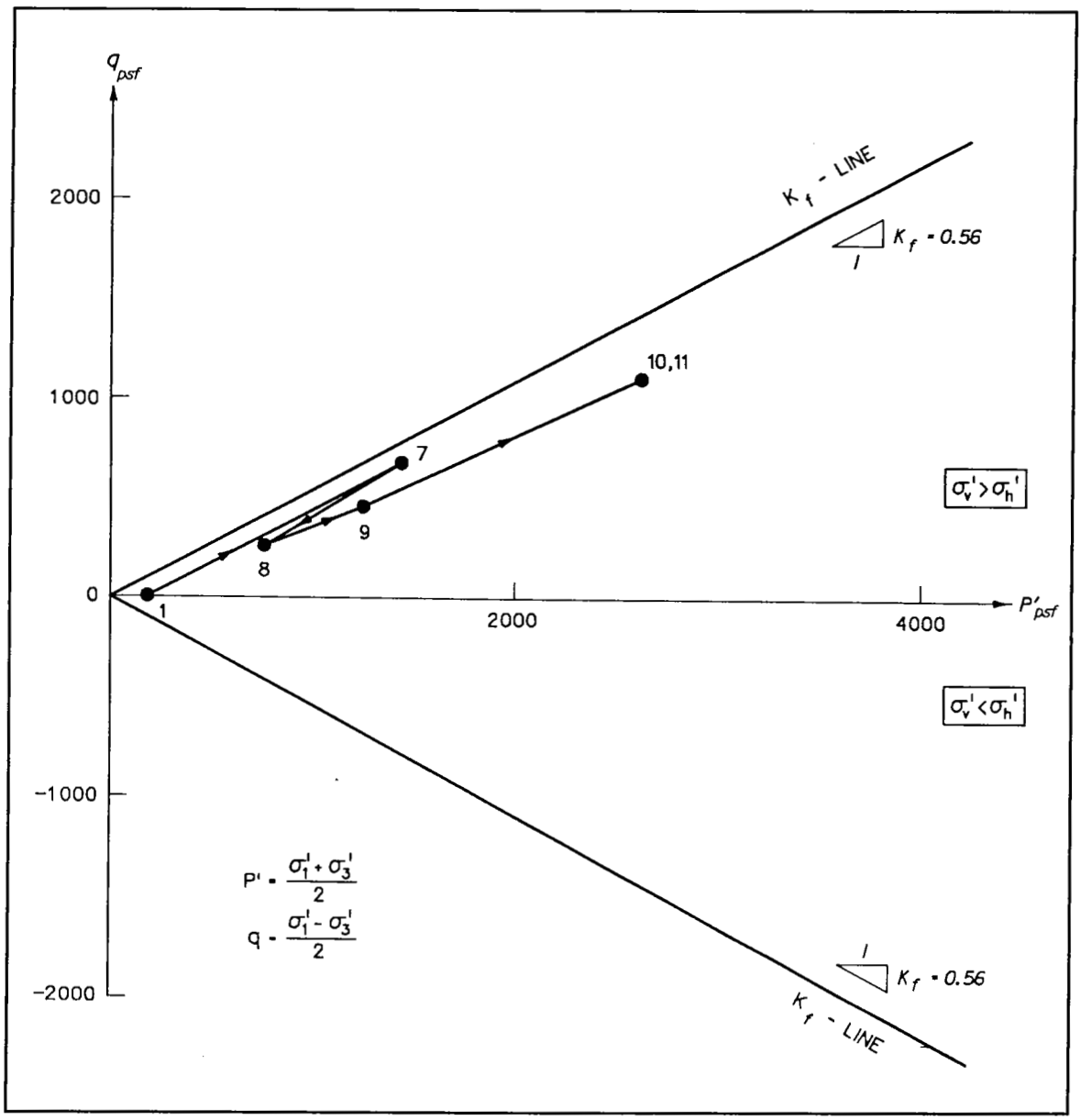

Figure 123. Stress paths for reinforced berm sand element 623, 77 ft riverside of lock center line at el 28

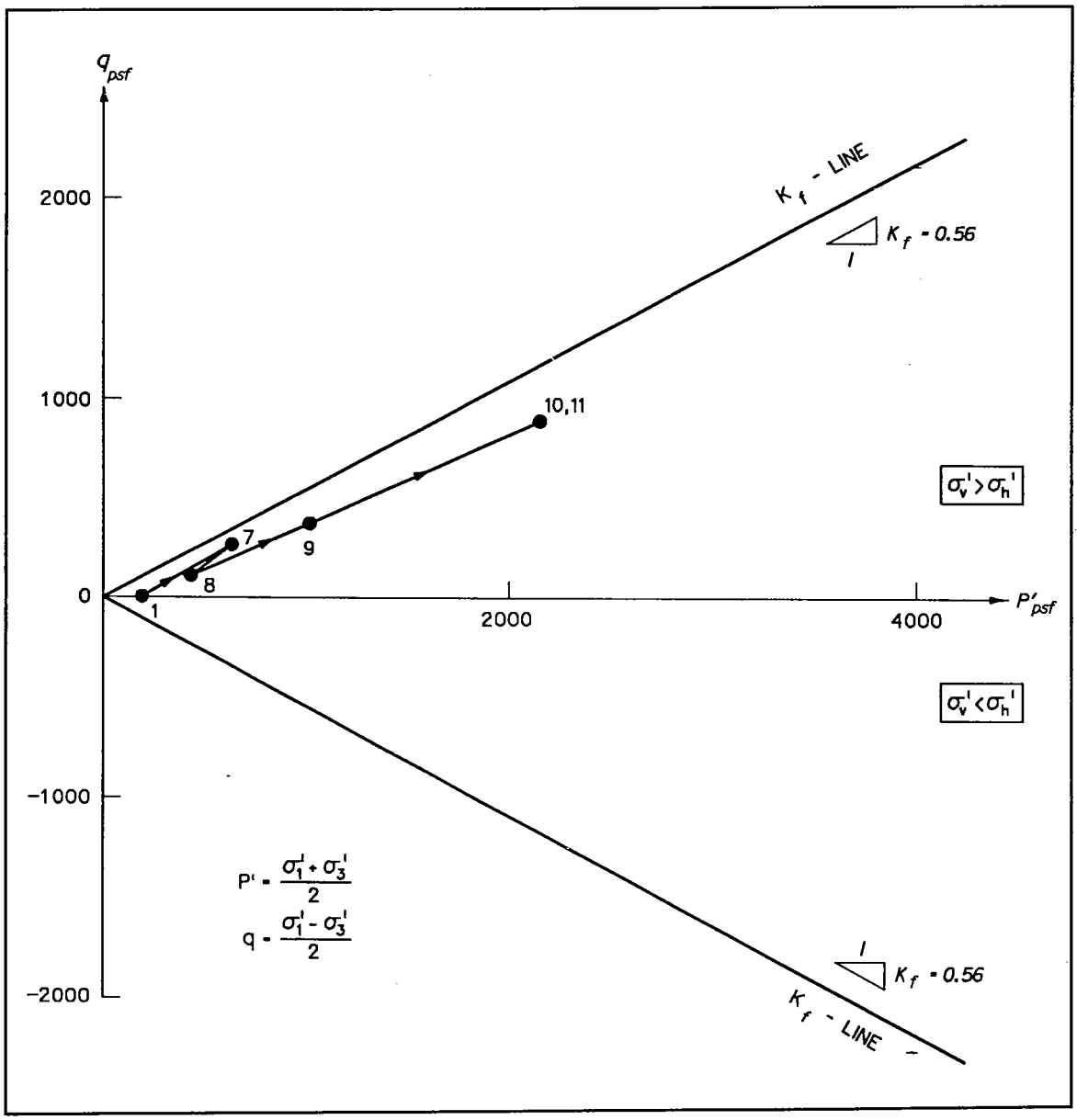

Figure 124. Stress paths for reinforced berm sand element 563, 101 ft riverside of lock center line at el 28

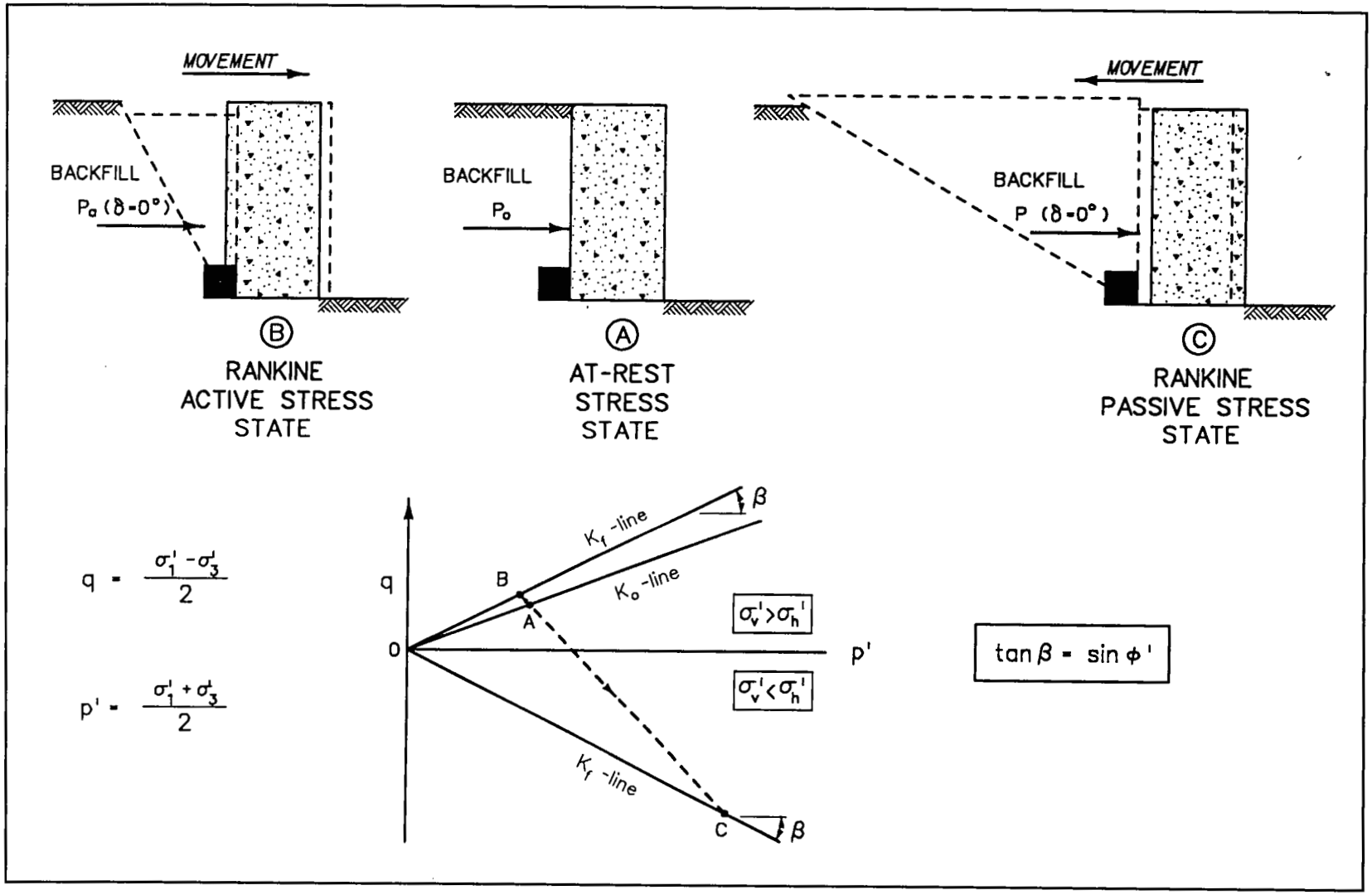

Figure 125. Stress paths for active and passive Rankine states of stress within backfill

within the soil element, the presence of the reinforcement **within** the soil berm restricted the soil deformations. For the condition shown in Figure 125, the soil had to rely on the wall to restrict the movements.

Figure 126 shows the variation in the mobilized shear resistance within the soil after construction of the reinforced berm. The soil comprising the side of the berm with the vertical face exhibited a higher level of mobilized shear when compared with the center and riverside regions of the reinforced soil berm. In fact, the region had fully mobilized shear resistance and resembled the wedge of soil that was formed in limiting equilibrium procedures for the layout of the reinforcement within the berms.

The variations in the maximum value for the reinforcement force within each of the elements modeling the 28 layers of reinforcement are shown in Figure 127. The tensile forces were developed within the layers of reinforcement by means of a shear transfer mechanism along the soil to reinforcement interface. This figure shows that the greatest forces were developed adjacent to the vertical face of the berm. These maximum tensile forces were computed to be less than 900 lb per lin ft of reinforcement, which is well below the limiting value of 3,800 lb per lin ft, indicating that the 28 layers of reinforcement are more than adequate for this level of loading.

Subergence of Berm - River and Pool in Lock at El 60.5

The first loading stage after construction of the berm corresponds to a high-water condition at the lock (Figure 95). In this analysis, the elevations of the river and the pool in the lock were raised in a series of 36 increments from el 11, 1.5 ft below the first layer of reinforcement in the reinforced berm to the top of the lock at el 60.5. The stresses and displacements computed after construction of the reinforced berm were used as the initial values for the mesh shown in Figure 101. The results showed that the interactions among the lock, berm, backfill, and foundation regions continued to be significant during the submergence of the berm and the flooding of the lock.

The submergence of the site resulted in both an increase in pore water pressures within the soil elements comprising the reinforced berm, backfill, and foundation regions and an increase in the water pressures along the chamber and exterior surfaces of the lock. During each of the incremental rises in the phreatic surface from els 11 to 31, the previously dry soil elements comprising all of the landside and riverside backfill and half of the soil elements comprising the reinforced berm were submerged. Incrementally raising the phreatic surface from el 31 to el 45 resulted in the submergence of the remaining one-half of the soil elements comprising the reinforced berm. When a soil element was submerged, the

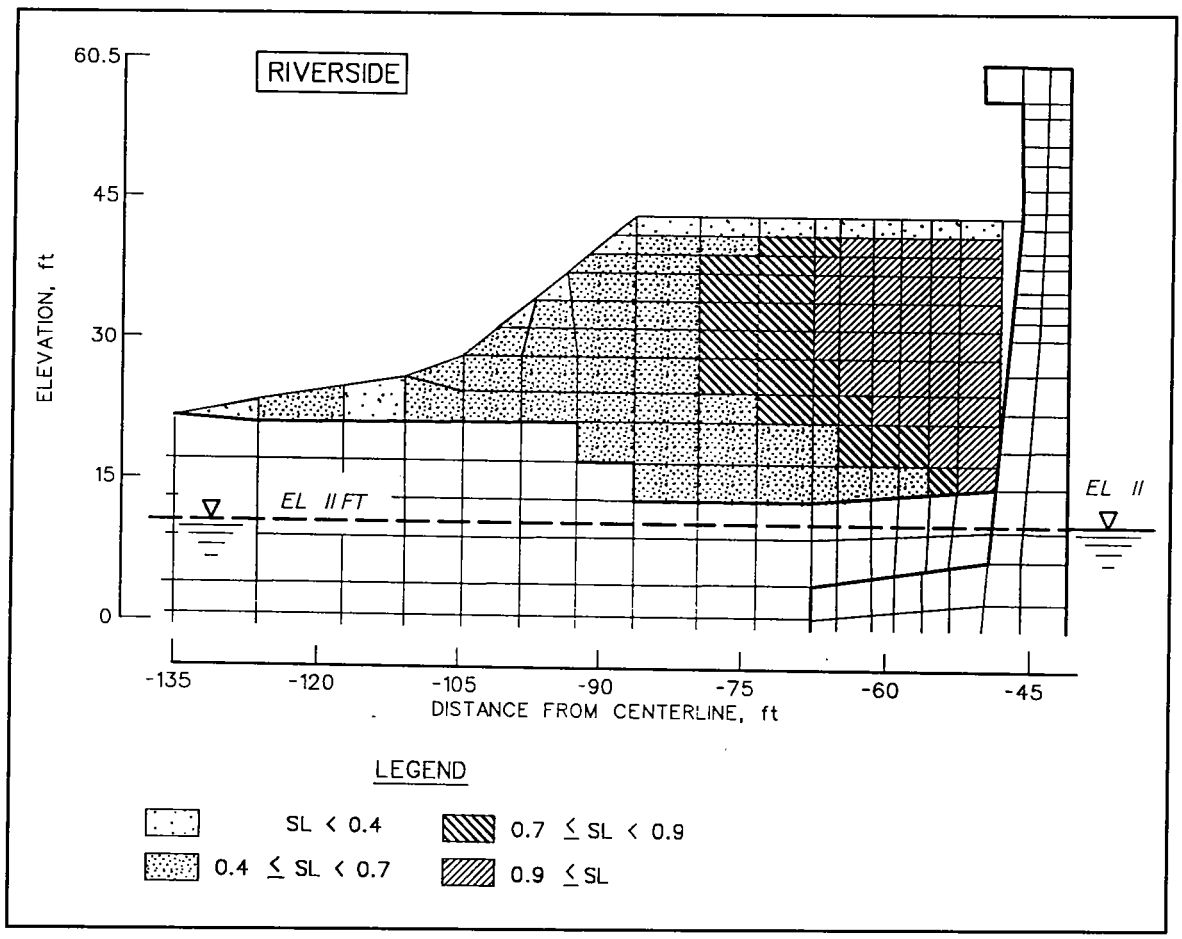

Figure 126. Variations in mobilized shear strength within reinforced berm after construction of berm

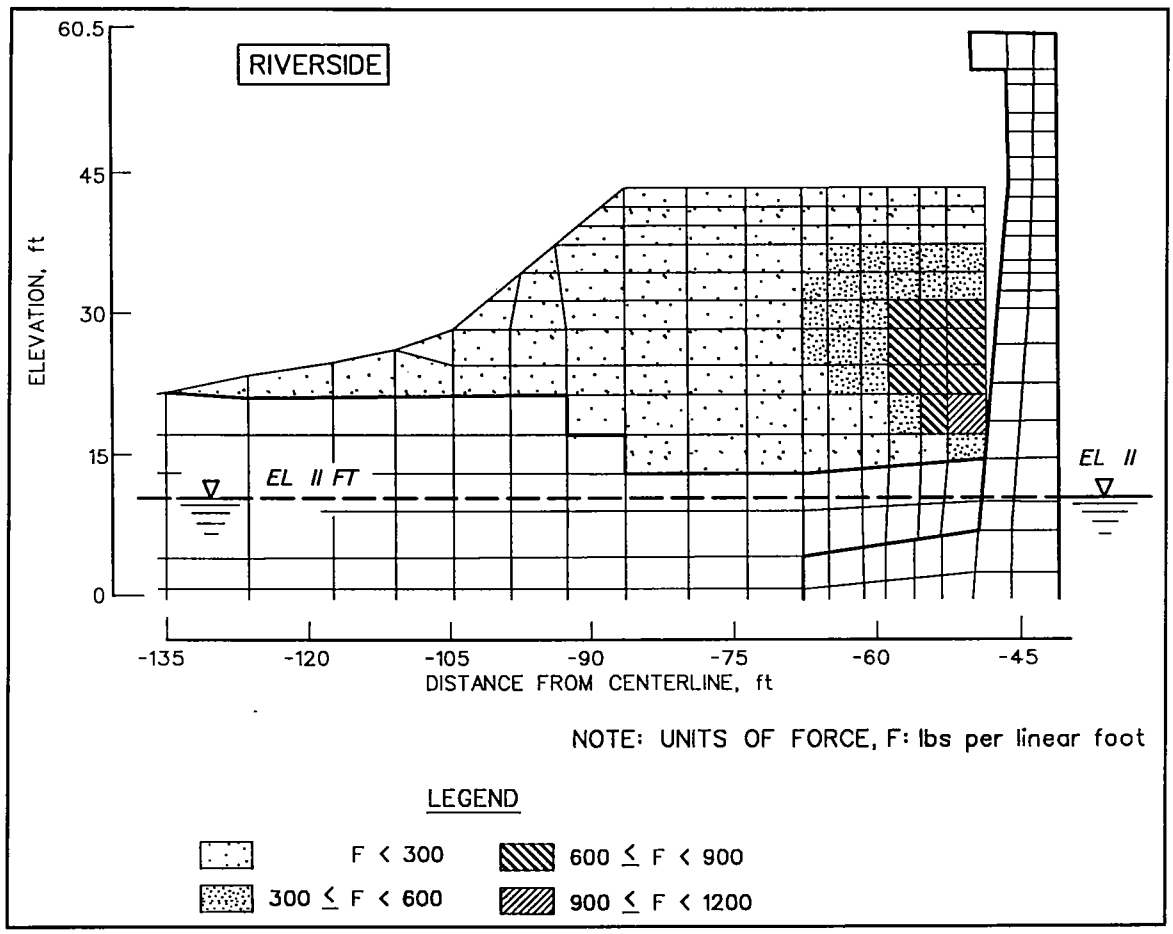

Figure 127. Variations in reinforcement force within reinforced berm after construction of berm

increase in water pressures produced an equivalent incremental **uplift** body force. SOILSTRUCT applies the uplift body forces to the soil elements by means of equivalent vertical nodal point forces. These uplift forces counter the body force due to gravity and result in the unloading of these soil elements. Submergence of the backfill and reinforced berm results in soil rebound and a reduction in both the effective stresses and shear stresses within the newly submerged soil elements.

Figure 128 shows the computed values of displacements, in inches, after submergence of the berm. These values of displacements are relative to those values computed after completion of the riverside backfill excavation and include both the settlements due to construction of the berm and those due to submergence of the soil. In general, the submergence of the site reduced the lock settlements, as compared to the results computed after the construction of the reinforced berm (Figure 104). The settlement of the riverside corner of the base slab was reduced from 1.1 in. after construction of the berm to 0.3 in. after submergence, a rebound of 0.8 in. The landside of the U-frame lock rebounded 0.4 in. The magnitude of rebound on the riverside of the lock was greater because of the greater soil mass that was submerged during flooding of the site, compared with the soil mass that was submerged on landside of the lock. Along the base slab, the final vertical displacements computed at the center line and at the corner of the landside culvert were 0.1 and 0.5 in., respectively. The horizontal movement at the top of the riverside stem wall during submergence was 0.7 in. in the landside direction, with a final horizontal displacement of 0.2 in. riverside.

Submergence of the berm resulted in computed rebound within the berm and the backfill below the berm, including the submerged portion of the backfill. For the points shown in Figure 128 that are within the backfill, the magnitude of rebound due to submergence ranged in value from 0.3 to 1.6 in. There was also a lateral movement of the riverside backfill toward the lock that ranged from 0.3 to 0.6 in. The magnitudes of the movements within the berm were greater than those computed within the backfill, with the greatest values computed along the top of the reinforced berm. At the riverside corner of the reinforced berm (el 45), the total rebound was 1.6 in. and the total lateral displacement was 0.8 in. The horizontal displacements along the vertical face of the reinforced berm during submergence ranged in value from 0.3 to 0.5 in. and were directed toward the gap. The total horizontal displacements at els 18, 30, and 41 were 1.4, 3.6, and 2.3 in., respectively. The magnitudes of the rebound during submergence increased in value with increasing elevation along the vertical face, reducing the magnitudes of the total settlement values. Rebound due to submergence at els 18, 30, and 41 and along the vertical face of the berm were 0.8, 1.0, and 1.2 in., with total settlements of 1.3, 3.4, and 1.1 in., respectively.

Figures 106 through 109 show a reduction in the vertical effective stresses within the foundation at the four sections, labeled A-A, B-B, C-C and D-D in Figure 105, after submergence of the backfill and the reinforced

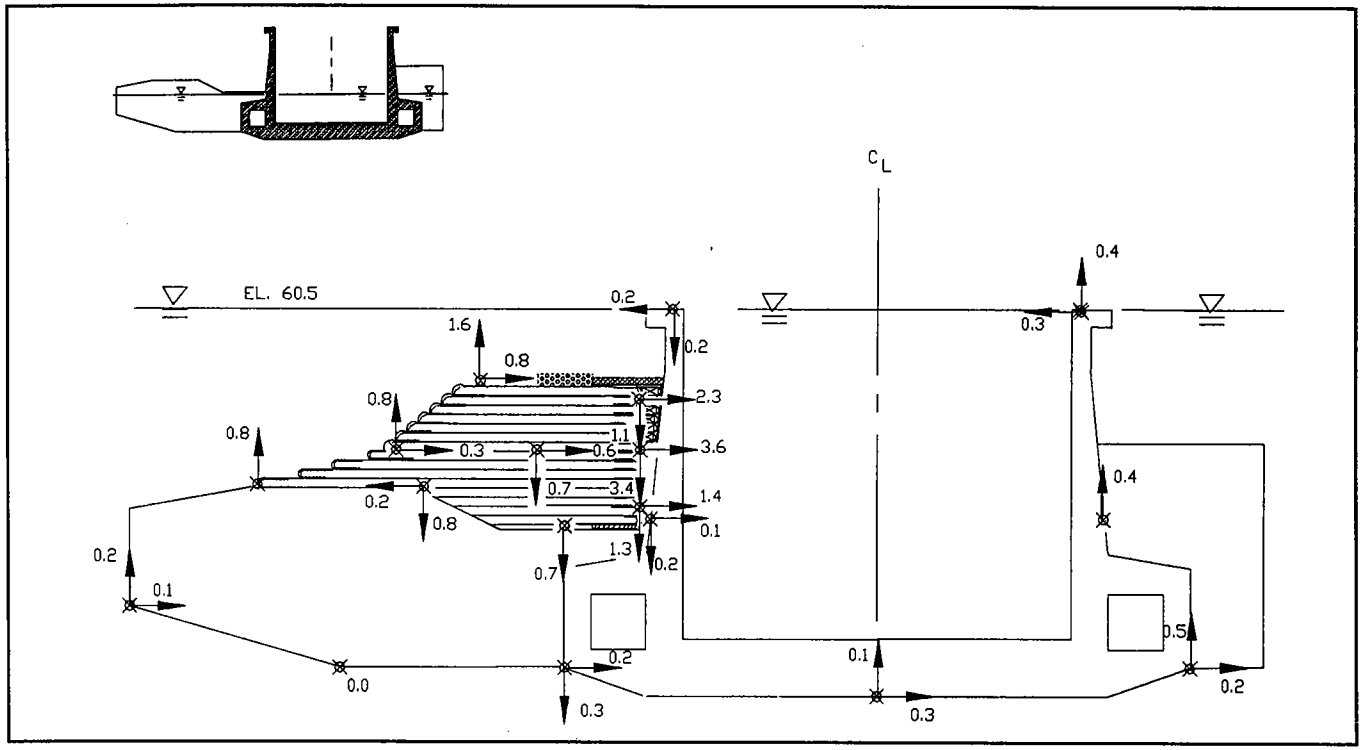

* Displacements of points are relative to their position after excavation for reinforced berm, in inches.

Figure 128. Relative displacements of lock, berm, and foundation after submergence of reinforced berm

soil berm, labeled Case 8 (Table 5). The reduction in the effective vertical stress values reflects unloading of the foundation soils during submergence and a corresponding increase in the values for the overconsolidation ratios of the backswamp clays. The stress-strain response to this unloading is modeled in SOILSTRUCT by assigning unload-reload moduli to the finite elements used to model the foundation soils.

Figure 129 shows the computed total normal pressures and the hydrostatic water pressures along the base of the lock and along the lock walls after the phreatic surface had been raised to el 60.5. The greatest total normal computed pressures were 8,650 and 8,020 psf below the riverside and landside stem walls, respectively. Below the center line of the lock, the total base pressure was 7,480 psf, and below the corners of the landside and riverside culverts, the base pressures were 6,260 and 7,030 psf, respectively.

The computed values of total pressures normal to the riverside wall between el -17 and the base of the reinforced berm at 13.5 ft were greater than those computed at the corresponding elevations along the landside wall. The greatest difference, 870 psf, was computed at el 12.9, corresponding to the element located immediately below the base of the reinforced berm. The total normal pressures at this elevation were 4,450 psf riverside and 3,580 psf landside. The greatest difference in the magnitudes of the total normal pressures along the riverside and landside culvert walls was 280 psf at both the top el 3 and bottom el -15.5 of the walls.

Figure 130 shows the computed effective normal pressures after submergence of the reinforced berm. The greatest computed effective normal base pressures were 3,440 and 2,810 psf below the riverside and landside stem walls, respectively. The effective base pressure decreased to 2,270 psf below the center line of the lock. The effective normal pressure below the outside corners of the riverside and landside culverts were 2,140 and 1,360 psf, respectively.

The ranges in values of the effective normal pressures along the riverside and landside lock walls were nearly the same. For example, along the riverside culvert the effective normal pressures ranged from 600 to 1,210 psf, and along the landside culvert the effective normal pressures ranged from 700 to 1,210 psf. With a hydrostatic water table, differences between the values of effective pressures normal to the riverside and landside lock walls were equivalent to the differences between the total pressures normal to the riverside and landside lock walls.

Mobilized friction angles are shown in Figure 131 and were nearly constant below the base of the riverside culvert, ranging from 10 to 12 deg. Along the portion of the base below the chamber, δ_{mob} was 7 deg or less. At the corner of the landside base, δ_{mob} was 12 deg. The values for δ_{mob} varied with elevation along the walls of the lock and were less than or equal to 21 deg at this stage of loading. The values of δ_{mob} in Figure 131 are less than the values of δ_{mob} in Figure 112 due to the application of

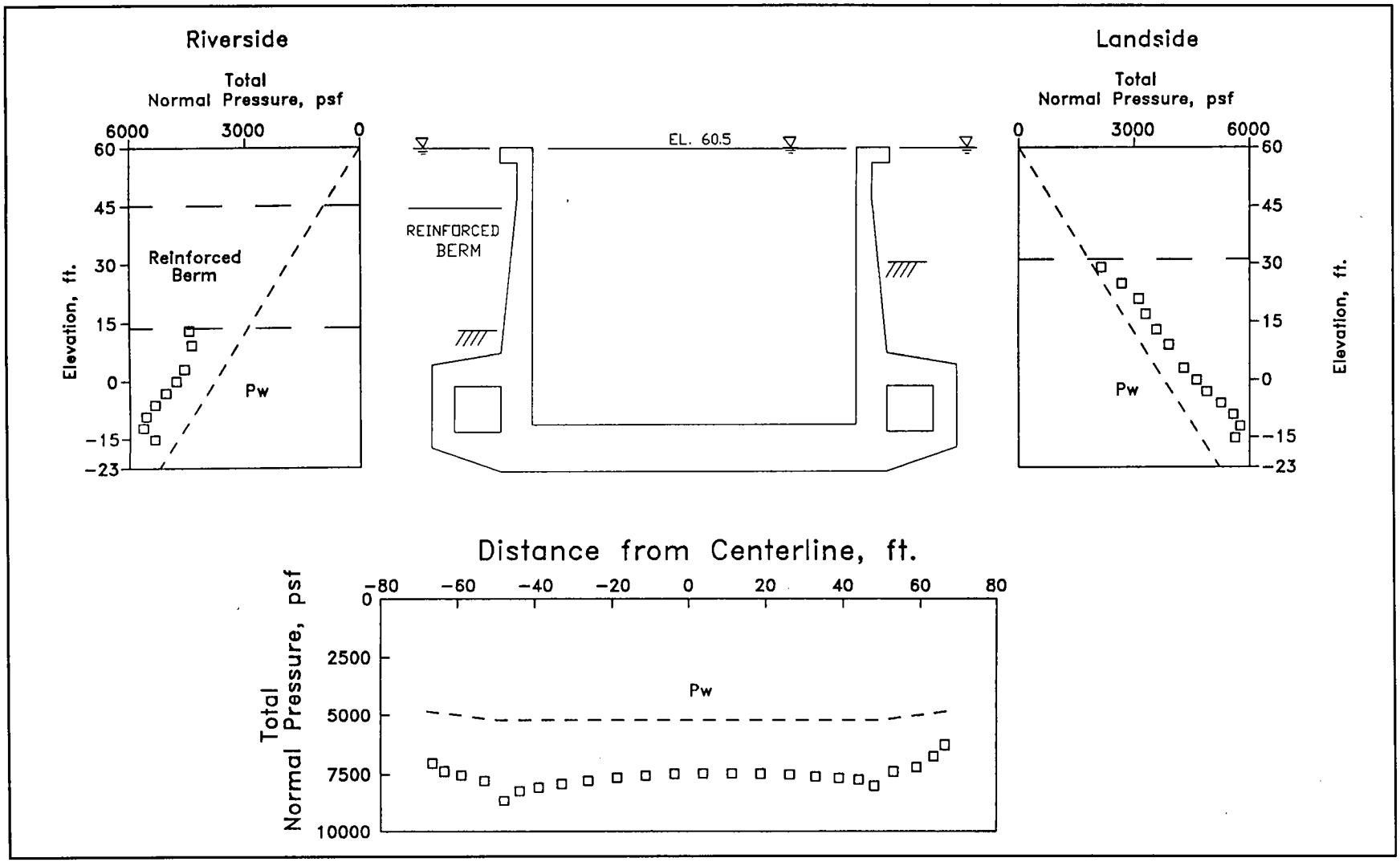

Figure 129. Total normal pressures after submergence of reinforced berm, river and pool in lock at el 60.5

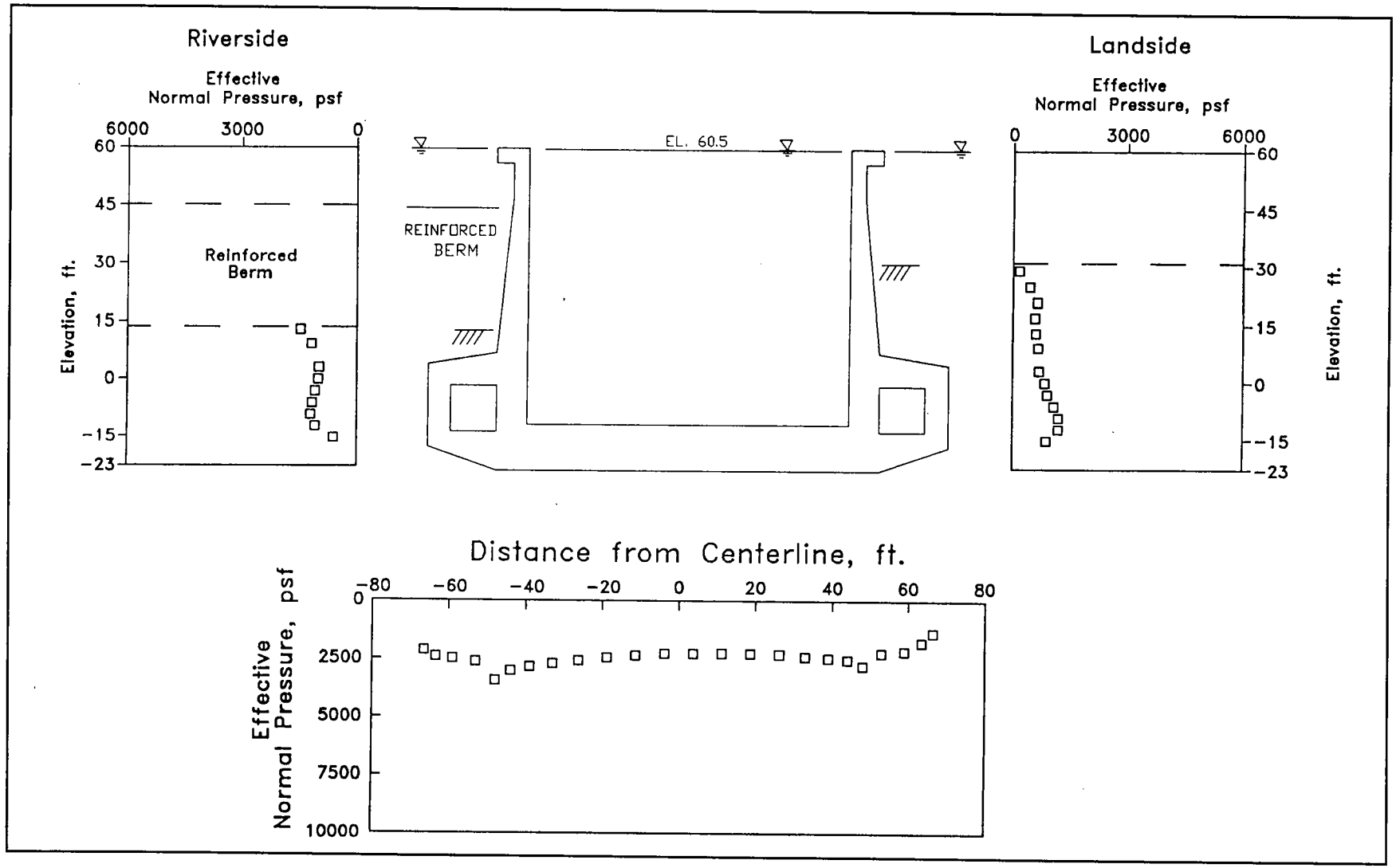

Figure 130. Effective normal pressures after submergence of reinforced berm, river and pool in lock at el 60.5

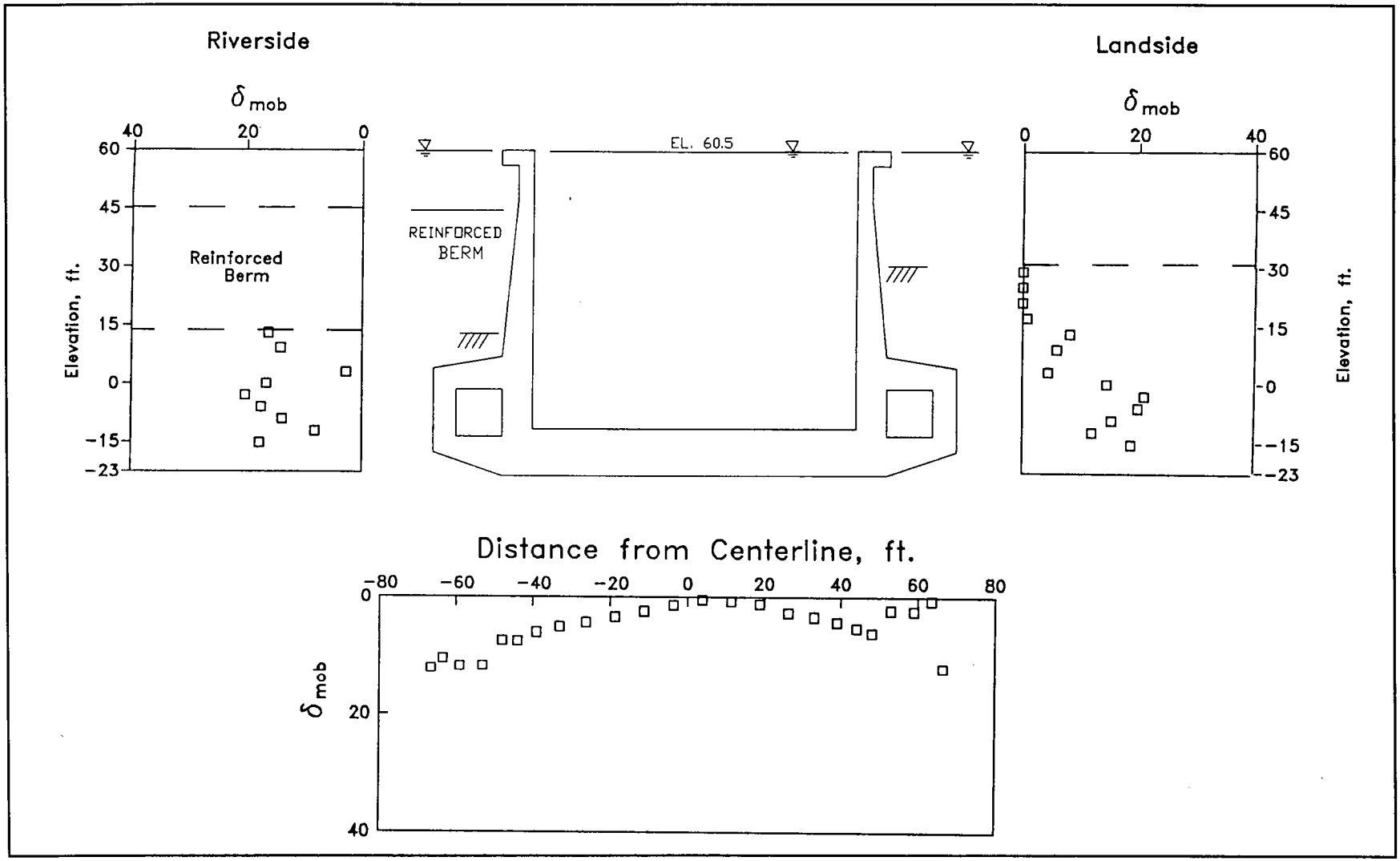

Figure 131. Mobilized friction angles along exterior of lock after submergence of reinforced berm, river and pool in lock at el 60.5

uplift forces during submergence of the soil backfill adjacent to the lock walls.

Variations in horizontal earth pressure coefficients with elevation are shown in Figure 132. This figure shows that K_h decreased with decreasing elevation along the stem walls and were nearly constant along the culvert walls. Along the landside stem wall, the maximum K_h was 1.6 at el 29 and 0.55 at el 9. K_h ranged from 0.77 at el 13 to 0.55 at el 9 below the riverside berm. Along the landside and riverside culvert walls, average K_h values were 0.49 and 0.36, respectively (Table 16). The values of K_h in Figure 132 are greater than the values of K_h in Figure 114 due to the reduction in the effective overburden pressures during the submergence of the soil backfill adjacent to the lock walls. An increase in values for K_h is consistent with increasing values for the overconsolidation of the soils.

Figure 133 shows the distribution in values of the vertical earth pressure coefficients to vary with elevation along the landside stem wall and along both culvert walls. The greatest values for K_v computed along the landside and riverside stem walls were 0.09 and 0.22, respectively, at el 12.9. The values of K_v along the culvert walls averaged 0.12 landside and 0.08 riverside (Table 16). Submergence of the backfill reduced the average K_v values for the three backfill regions listed in Table 15 by values ranging from 0.02 to 0.05.

Figure 134 shows the distributions of factored moments computed within the lock and the design moment capacity distributions. The results indicate that after the elevation of the river and the pool in the lock was raised to el 60.5, the factored moment at the center line of the lock decreased from -4,015 kip-ft (Figure 118) to -2,360 kip-ft, a 41-percent reduction. The entire top of the floor base slab remained in tension, and the **chamber sides** of the stem walls remained in compression during this phase of loading. The maximum values for the factored moments computed within the landside stem wall at el 9.25 decreased in value from 228 to 186 kip-ft, an 18-percent reduction in value upon submergence. The factored moment within the riverside stem wall at el 9.25 decreased by 37 percent upon submergence, from 178 to 112 kip-ft. The riverside factored moment at el 9.25 was 40 percent less than the landside factored moment at el 9.25. The values for the factored moments within the lock were well below the values for the design moment capacity.

The stress paths for reinforced berm soil elements 715, 1152, 623 and 563, showed both the shear stress and effective confining stresses to decrease upon submergence of the soil berm (Figures 121 through 124). During submergence, the stress paths were downward and to the left, due to the unloading of the soil elements comprising the reinforced berm. Stress path point no. 8 corresponds to the final effective stress state within the reinforced soil elements with a phreatic surface at el 60.5 (Table 5). Submergence of the reinforced berm also resulted in a decrease in the values of mobilized shear strength for the soil elements, as shown in Figure 135. The tensile forces within the layers of reinforcement remained

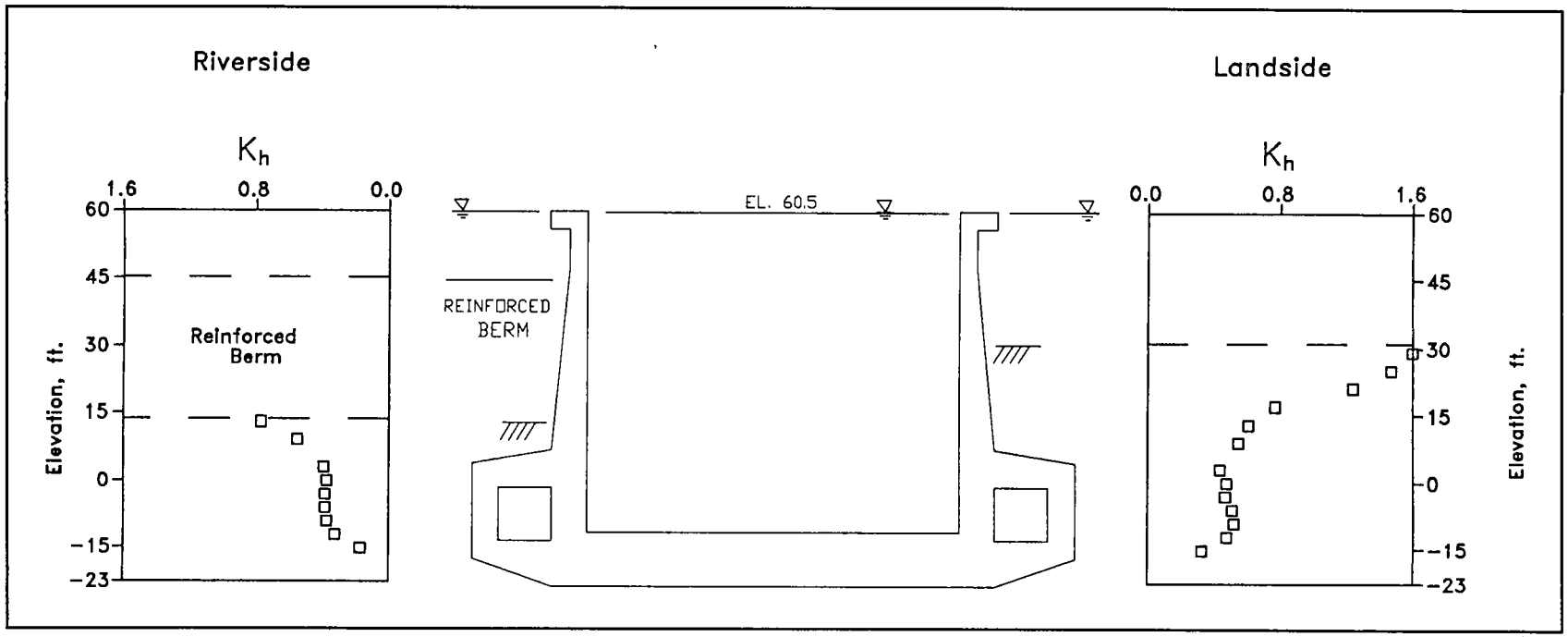

Figure 132. Horizontal earth pressure coefficient after submergence of reinforced berm, river and pool in lock at el 60.5

Table 16
Average Values of Horizontal and Vertical Earth Pressure Coefficients after Submergence of Reinforced Berm

Backfill Region	Backfill Material	Riverside K_h	Riverside K_v	Landside K_h	Landside K_v
Stem	Compacted select clay	—	—	1.5	0
Stem	Compacted sand	0.66	0.18	0.8	0.04
Culvert	Compacted sand	0.36	0.08	0.49	0.12

Elevation of river: 60.5 ft
Elevation of pool in lock: 60.5 ft
Elevation of riverside silt: —

essentially unchanged with the submergence of the soil berm. The maximum tensile forces were less than 900 lb per lin ft of reinforcement throughout the berm, which was below the limiting value of 3,800 lb per lin ft (Figure 136).

Siltation to El 55, Riverside - River and Pool In Lock at El 60.5

This series of analyses accounts for the response of the mesh (Figure 101) to siltation along the riverside of the lock to el 55 and siltation along the landside of the lock to el 33 during a high-water period (Figure 96). This corresponds to a 10-ft-thick deposit of silt resting on top of the reinforced berm and against the riverside stem wall with the elevation of the crest of the reinforced berm at 45 ft. With a silt surface slope of 5H:1V along the bank of the riverside channel, the average depth of the silt deposit was 20 ft. This analysis presumes that the design of reinforced berm and the material(s) placed within the gap between the berm and the wall: (a) prohibit the deposition of silt within the gap, and (b) do not transfer earth pressures from the reinforced berm to the riverside stem wall. Between els 13.5 and 45, no effective earth pressures are applied to the riverside stem wall in these analyses. Design details required to achieve this objective are discussed in Chapter 4 of this report. Landside of the lock, the silt deposit was 2 ft. The river and the pool in the lock were maintained at el 60.5 during this series of analyses. The stresses and displacements computed after submergence of the reinforced berm were used as the initial values for the soils and lock at the start of the series of silt loadings.

The silt loads were applied as incremental boundary pressures normal to the surface of the channel and normal to the surface of the reinforced berm and lock walls, as described in operational load Case analysis 4 in

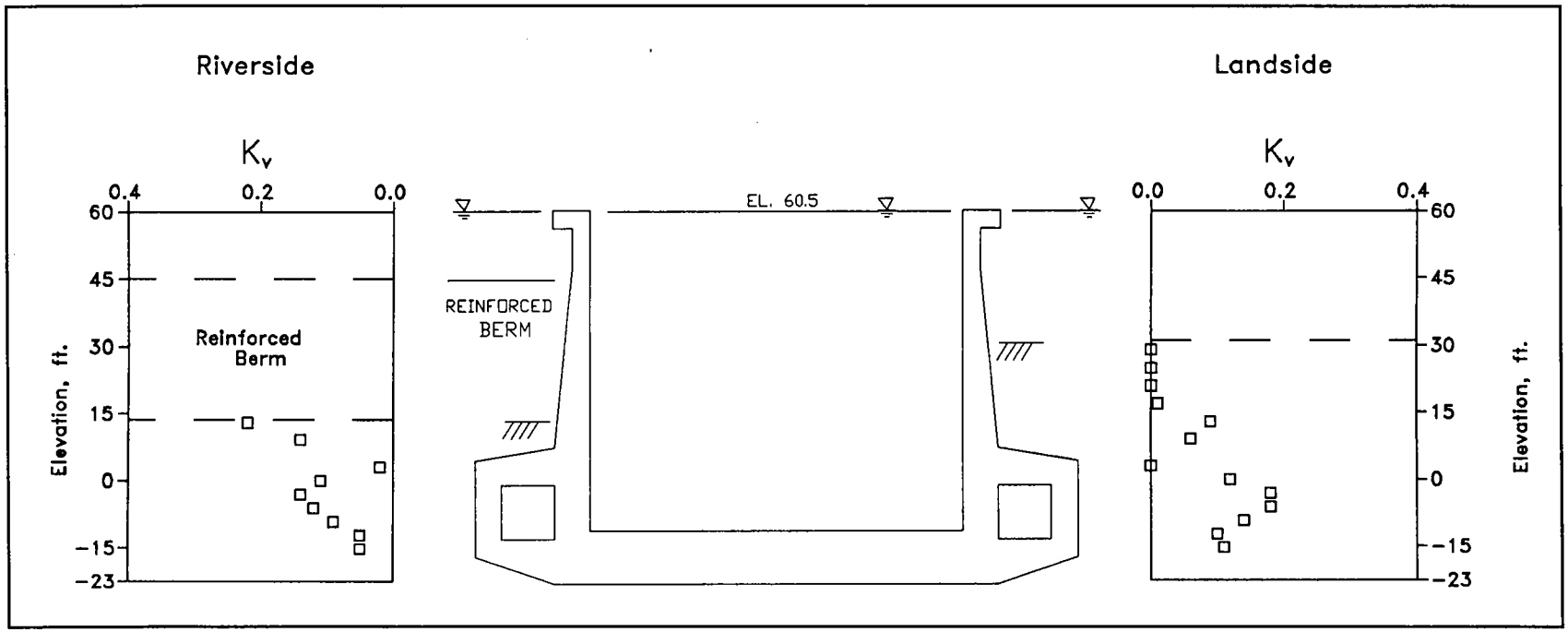

Figure 133. Vertical earth pressure coefficient after submergence of reinforced berm, river and pool in lock at el 60.5

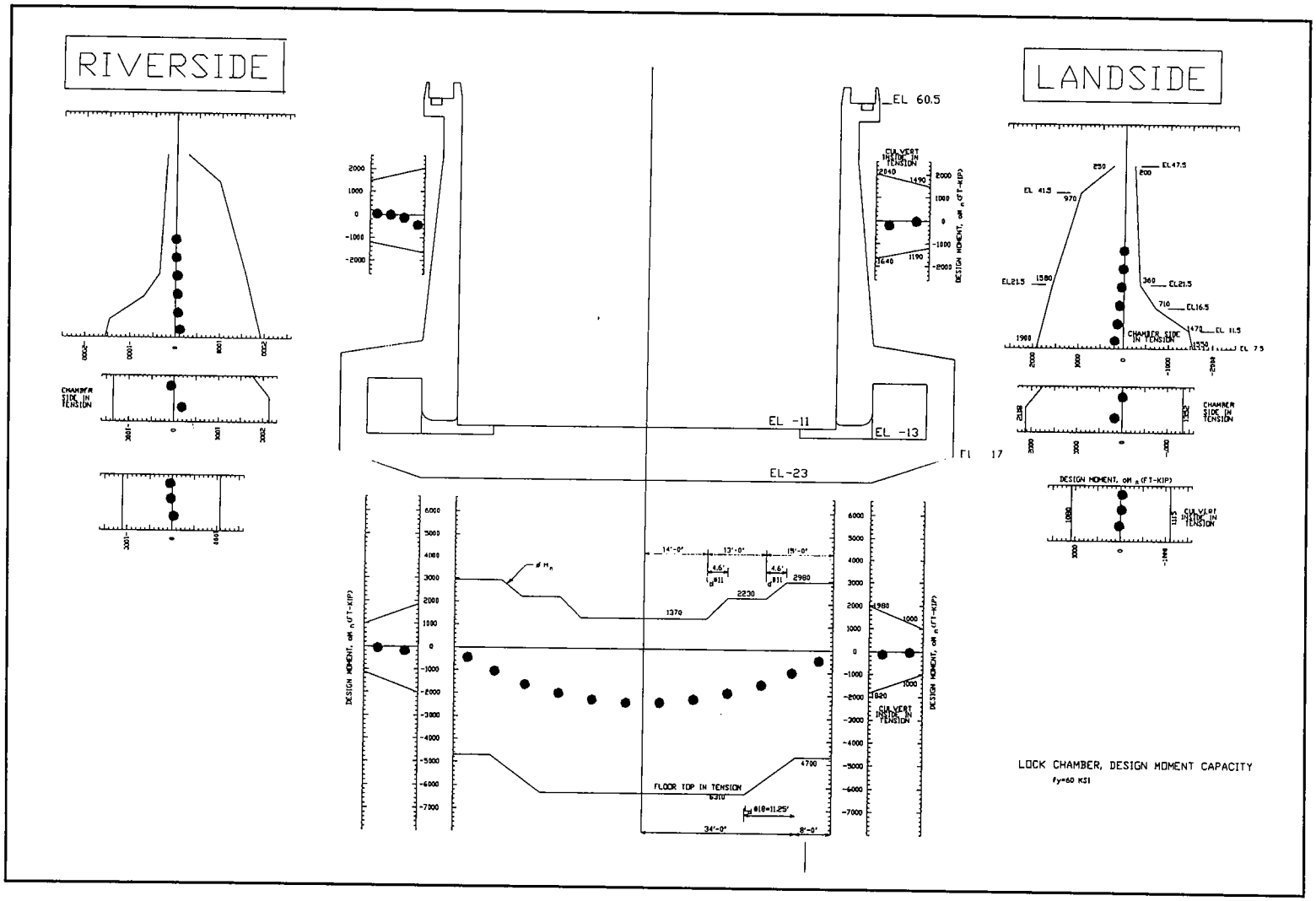

Figure 134. Distribution of factored moments after submergence of reinforced berm and design moment capacity – river and pool in lock at el 60.5

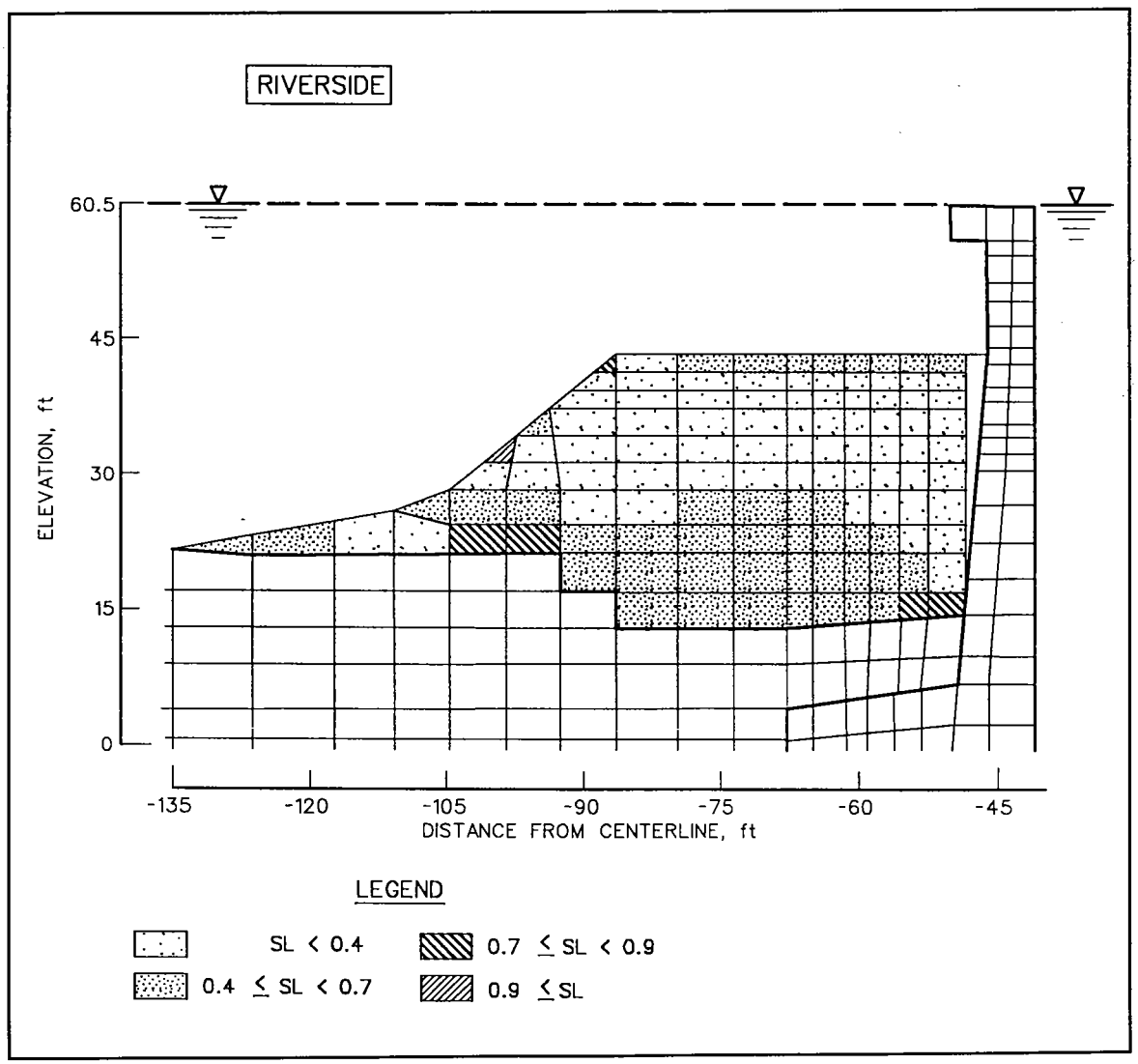

Figure 135. Variation in mobilized shear strength within reinforced berm after submergence of berm

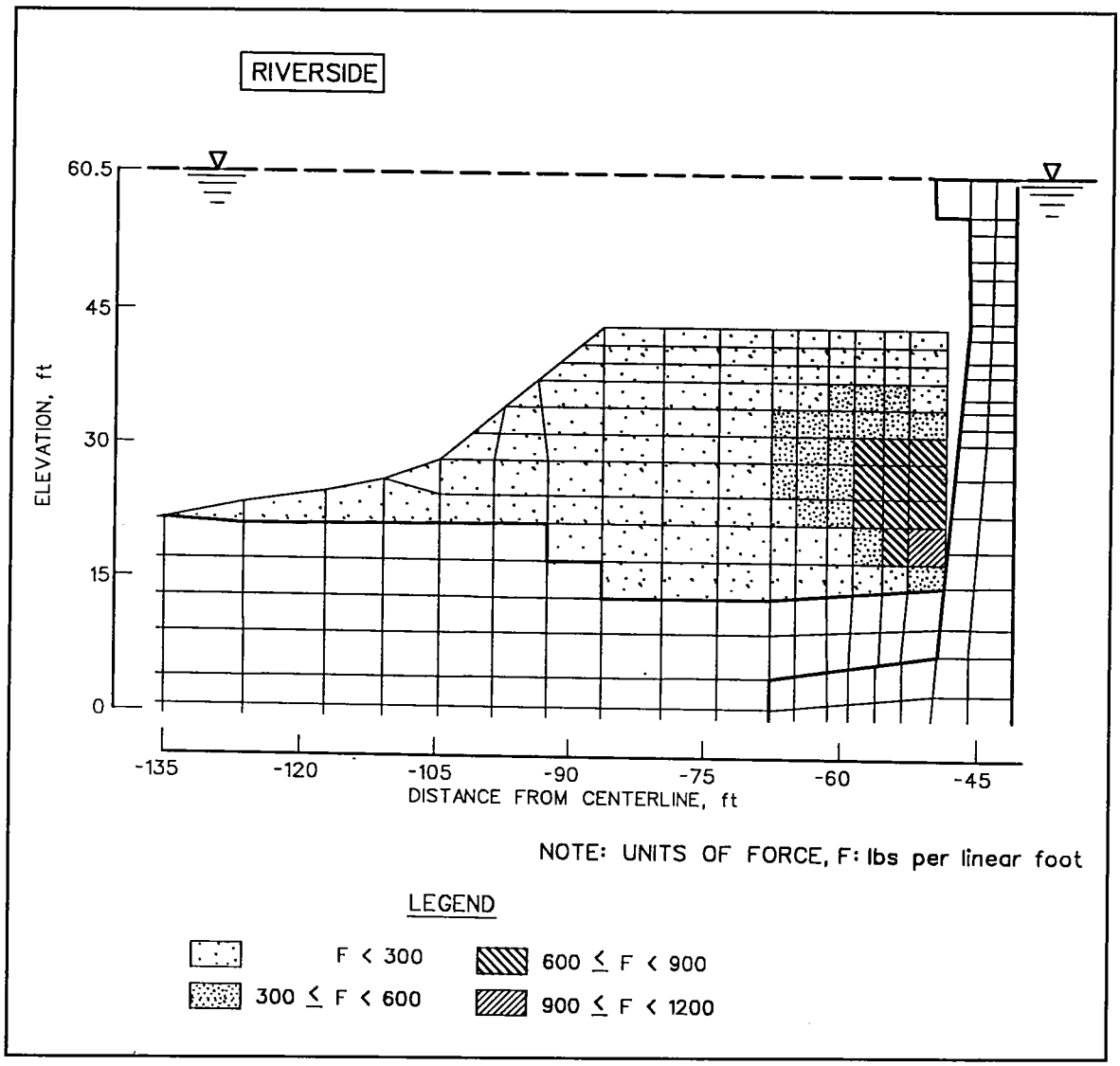

Figure 136. Variation in reinforcement force within reinforced berm after submergence of berm

Chapter 2 of this report. The total unit weight of the silt was 115 pcf, and the effective horizontal earth pressure coefficient was 1.0. The boundary silt pressures specified in the analyses were equal to the product of the buoyant unit weight times the depth of silt. Figure 137 shows the computed displacements, relative to those values computed after completion of the riverside backfill excavation. The riverside siltation resulted in the settlement of the riverside half of the lock and the surrounding soil regions and caused the reinforced berm and lock to be displaced toward landside. The settlement of the riverside corner of the base slab increased by 0.3 in., from a thickness of 0.3 in. after submergence to 0.6 in. after siltation. The center line of the lock settled 0.1 in. and the landside corner of the base slab heaved 0.1 in. The horizontal displacement of the base slab and most of the walls comprising the U-frame lock was 0.3 in. in the direction of the landside of the lock.

The riverside silt loadings resulted in the settlement of both the reinforced soil berm and the backfill below the berm. For the points within the backfill that are shown in Figure 137, the magnitudes of settlements due to silt loads ranged from 0.3 to 1.5 in. and were computed as the difference between the values of settlements reported in Figures 137 and 128. The magnitudes of the settlements within the reinforced berm due to siltation ranged in value from 0.4 to 1.7 in. At the riverside corner along the crest of the reinforced berm, the settlement due to siltation was 0.7 in., resulting in a total vertical movement of 0.8 in. The magnitudes of the settlement during siltation increased in value with increasing elevation along the vertical face. The incremental settlements at els 18, 30, and 41 were 0.4, 0.5, and 1.7 in., with total settlements of 1.7, 3.9, and 2.9 in., respectively. The horizontal component of the river channel silt loads caused the displacement of the berm toward the lock. These incremental horizontal displacements within the berm ranged from 0.3 to 1.7 in. At the riverside corner along the crest of the reinforced berm, the horizontal displacement increased by 0.4 in., from 0.8 in. prior to siltation to 1.2 in. afterwards. The weight of the silt above the berm resulted in movements along the vertical face of the berm which were directed downward and into the gap. The horizontal displacements at els 18, 30, and 41 increased by 0.3, 0.5, and 1.3 in., respectively, and totaled 1.7, 4.1, and 3.6 in.

Figures 106 through 109 show an increase in the vertical effective stresses within the foundation at sections A-A, B-B, C-C, and D-D (see Figure 105) with siltation. The computed effective vertical stress values, labeled Case 9 (Table 5), were greater than those values computed after submergence (Case 8), but less than those computed after construction of the reinforced berm (Case 7). The stress-strain response was modeled in SOILSTRUCT by assigning unload-reload moduli to the finite elements which modeled the foundation soils.

Figure 138 shows the computed total normal pressures and the hydrostatic water pressures along the base of the lock and along the lock walls after siltation at the lock. The greatest computed total normal pressures were 9,185 and 8,030 psf below the riverside and landside stem walls,

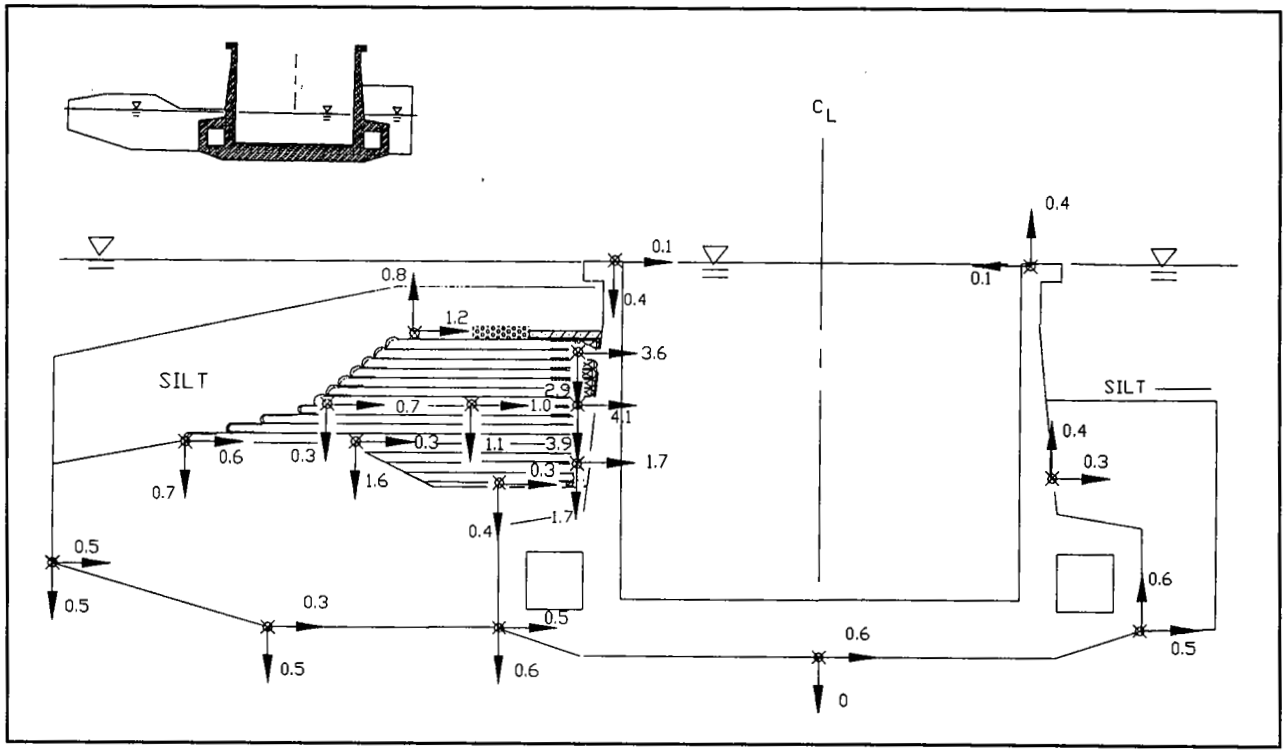

* Displacements of points are relative to their position after excavation for reinforced berm, in inches.

Figure 137. Relative displacements of lock, berm, and foundation after riverside siltation to el 55

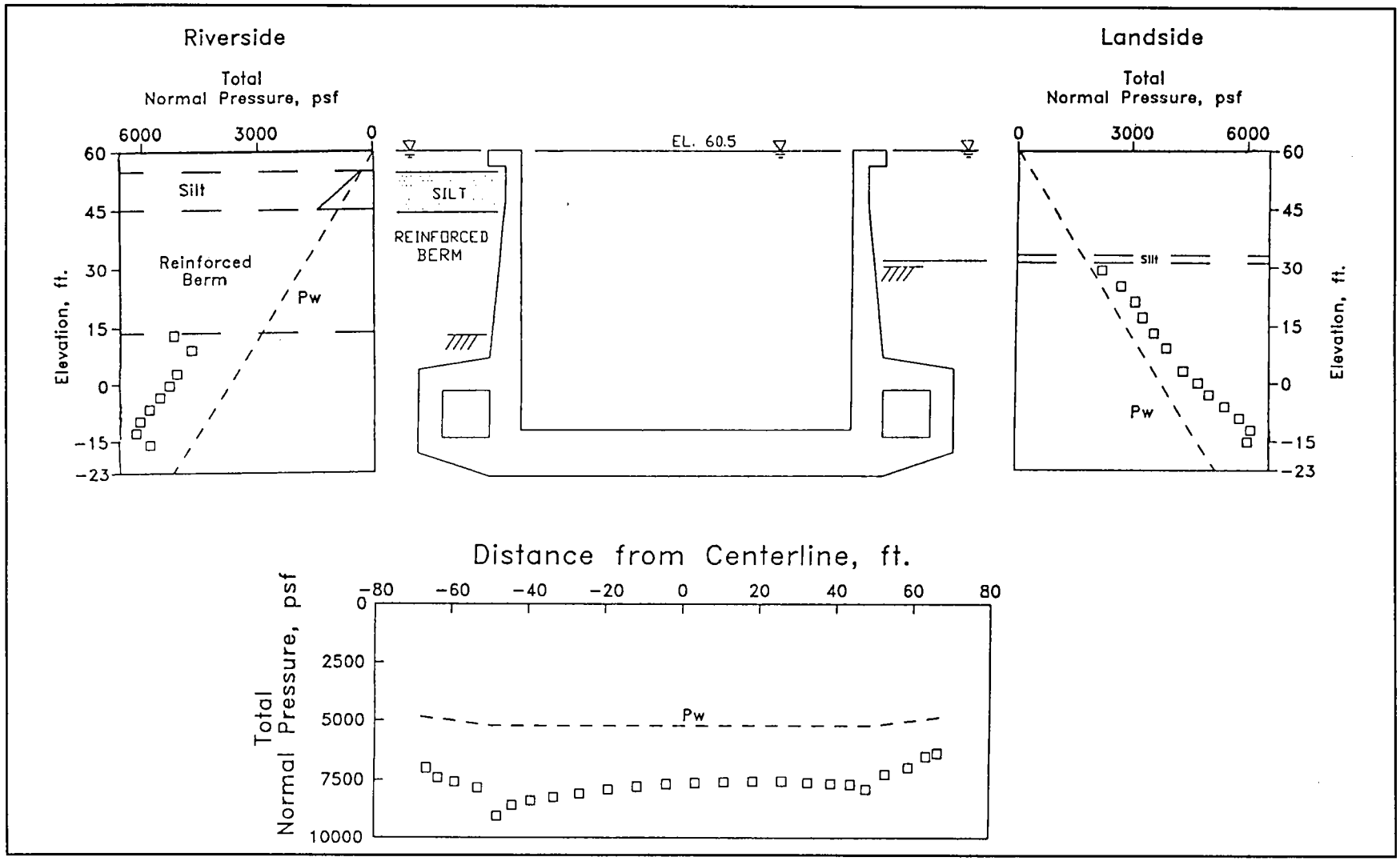

Figure 138. Total normal pressures after riverside siltation to el 55, river and pool in lock at el 60.5

respectively. Below the center line of the lock, the total base pressure was 7,720 psf, and below the corners of the landside and riverside culverts, the base pressures were 6,310 and 7,320 psf.

The unsymmetrical silt loads resulted in greater differences between the values of total pressures computed normal to the riverside wall and normal to the landside wall than those computed during submergence of the reinforced berm. The greatest difference was 1,670 psf and occurred immediately below the base of the reinforced berm at el 12.9. The total normal pressures at this elevation were 5,270 psf riverside and 3,600 psf landside. The greatest difference in the magnitudes of the total normal pressures along the riverside and landside culvert walls was 775 psf at el 3, the tops of the walls.

Figure 139 shows the computed effective normal pressures after submergence of the reinforced berm. The greatest computed effective normal base pressures were 3,970 and 2,820 psf below the riverside and landside stem walls, respectively. These values were greater than those computed in the previous analyses of the submergence of the reinforced berm by 530 psf riverside and 10 psf landside. The effective base pressure below the center line of the lock was 2,510 psf, which is 240 psf greater than the value computed in the previous analysis. The effective normal pressures below the outside corners of the riverside and landside culverts were 2,420 and 1,410 psf, respectively.

The effective normal pressures along the riverside stem wall ranged from 1,550 psf at el 9 to 2,300 psf at el 12.9. These values were greater than those computed after the submergence of the reinforced berm by 820 and 375 psf, respectively. Along the riverside culvert wall, the average effective normal pressure increased by 530 psf when compared with those values computed after submergence of the reinforced berm. The values for the effective normal pressures along the riverside wall were greater than those computed along the landside wall.

Figure 140 shows the variations in δ_{mob} along the base of the lock and along the walls of the lock. Along the base, δ_{mob} ranged in value from 0 to 13 deg, with the maximum values computed below the stem walls. The greatest computed values for δ_{mob} were 23 deg riverside and 21 deg landside at el -3 along the culvert walls. The values for δ_{mob} were less than 15 deg along the riverside stem wall and less than 8 deg along the landside stem wall.

Figure 141 shows that K_h decreased with decreasing elevation along the stem walls and was nearly constant along the culvert walls. In the compacted select clay along the landside stem wall, K_h ranged from 1.17 at el 29 to 1.23 at el 25, and averaged 1.20 (Table 17). Between els 23 and 7.5, the landside K_h values ranged from 0.53 to 1.04. Along the riverside stem and below the reinforced berm, K_h was 0.94 at el 13 and 0.58 at el 9. Along the landside and riverside culvert walls, the average K_h values

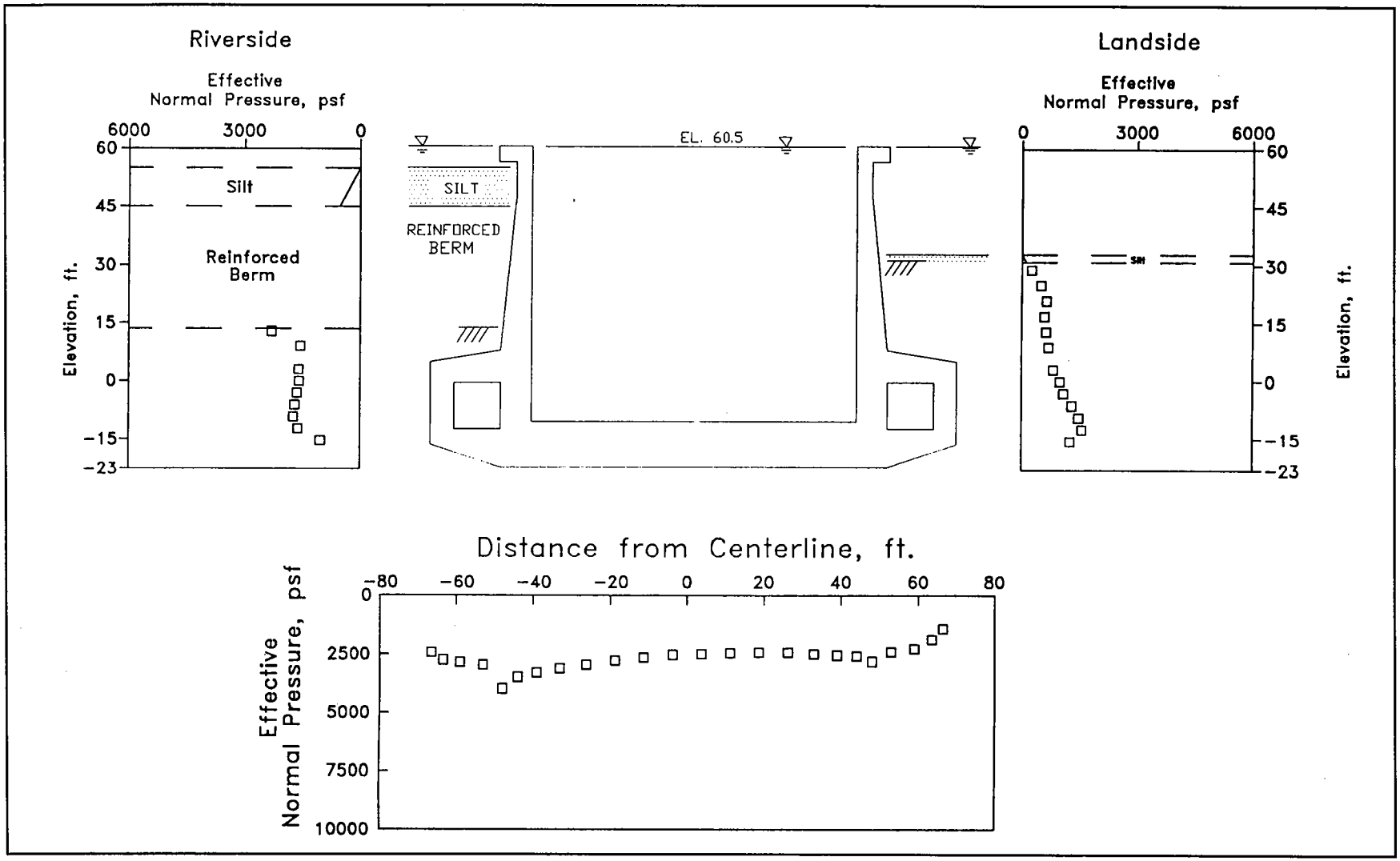

Figure 139. Effective normal pressures after riverside siltation to el 55, river and pool in lock at el 60.5

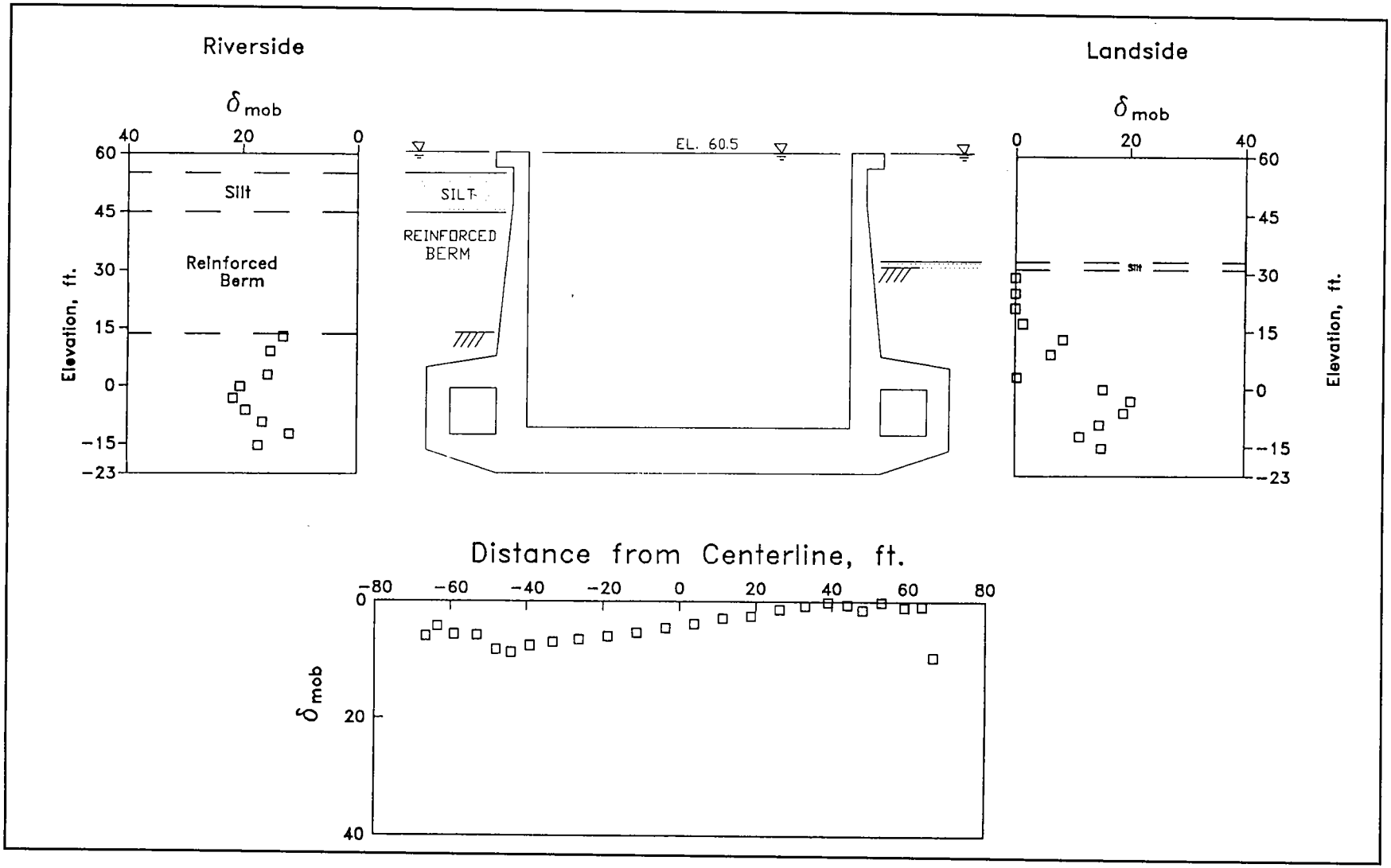

Figure 140. Mobilized friction angles along exterior of lock after siltation to el 55, river and pool in lock at el 60.5

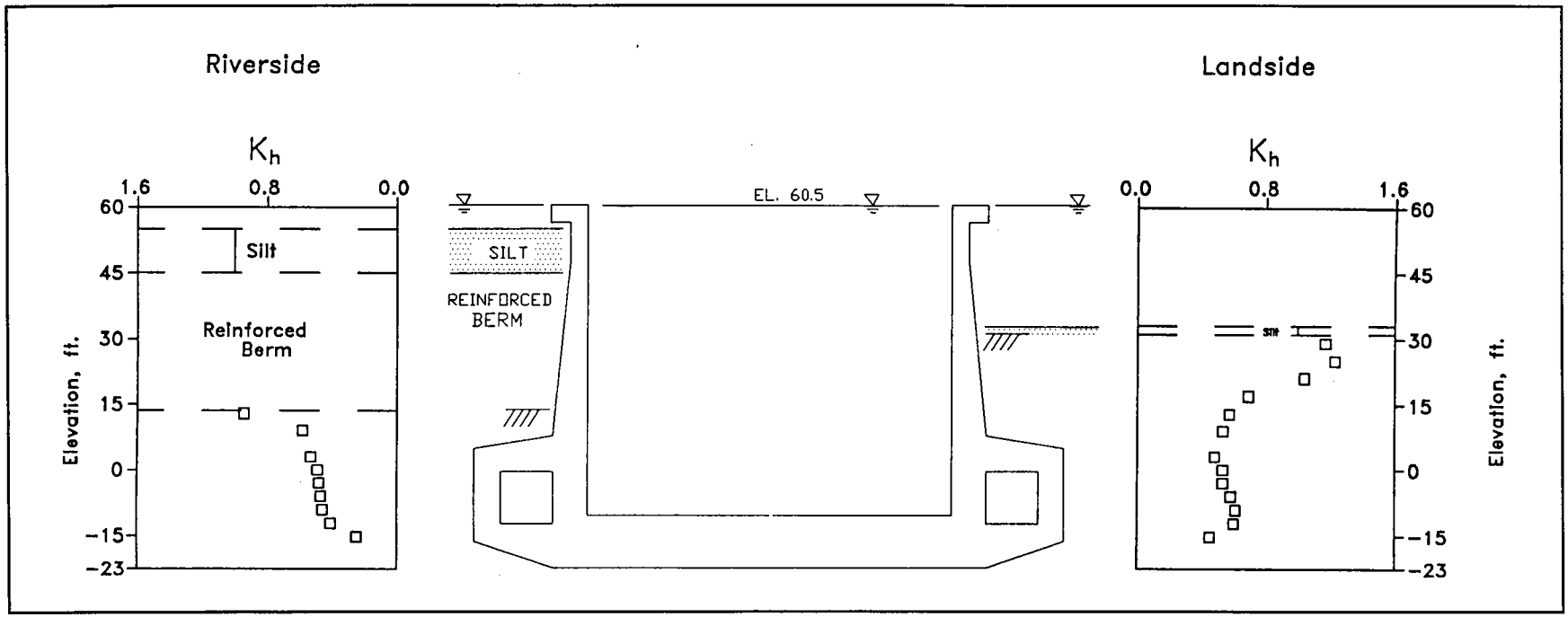

Figure 141. Horizontal earth pressure coefficients after riverside siltation to el 55, river and pool in lock at el 60.5

Table 17
Average Values of Horizontal and Vertical Earth Pressure Coefficients after Riverside Siltation to El 55

Backfill Region	Backfill Material	Riverside K_h	Riverside K_v	Landside K_h	Landside K_v
Stem	Compacted select clay	-	-	1.2	0
Stem	Compacted sand	0.76	0.18	0.71	0.04
Culvert	Compacted sand	0.46	0.14	0.57	0.13

Elevation of river: 60.5 ft
Elevation of pool in lock 60.5 ft
Elevation of riverside silt: 55 ft

were 0.57 and 0.46, respectively (Table 17). These average K_h values are greater than those listed in Table 16 by 0.08 landside and 0.1 riverside.

The maximum value of K_v was 0.21 at el 13 immediately below the reinforced berm (Figure 142). The greatest values for K_v computed at el -3 along the landside and riverside culvert walls were 0.20 and 0.19, respectively. The values of K_v along the culvert walls averaged 0.13 landside and 0.14 riverside (Table 17). The average K_v value along the riverside culvert wall after siltation of the lock was greater than the average K_v value after submergence of the backfill by a constant equal to 0.06.

The distributions of computed factored moments within the lock and the design moment capacity distributions are shown in Figure 143. After siltation, the factored moment at the center line of the lock increased by 140 kip-ft, from -2,360 kip-ft (Figure 134) to -2,500 kip-ft. The entire top of the base slab remained in tension, and the chamber sides of the stem walls remained in compression during siltation. The maximum computed values for the factored moments along the stem walls occurred at el 9.25. The factored moment within the riverside stem wall increased by a factor of 3 1/3, from 112 to 377 kip-ft. Within the landside stem wall, the value for the factored moment increased from 186 to 212 kip-ft. The values for the factored moments within the lock were well below the values for the design moment capacity.

Figure 144 shows the results from a pair of CUFRAM analyses, compared to the distributions of factored moments within the lock from the results of finite element analyses. The earth and water pressures specified in the CUFRAM analyses equaled those computed in the finite element analysis. The lock was analyzed twice, once using a rigid link factor (RLF) of 0 and once using an RLF of 1.0. The computed values for the CUFRAM moments at the lock center line of the lock differ in value by 3 percent, indicating that the RLF factor does not have a significant influence on the computed moments, as was observed for the CUFRAM

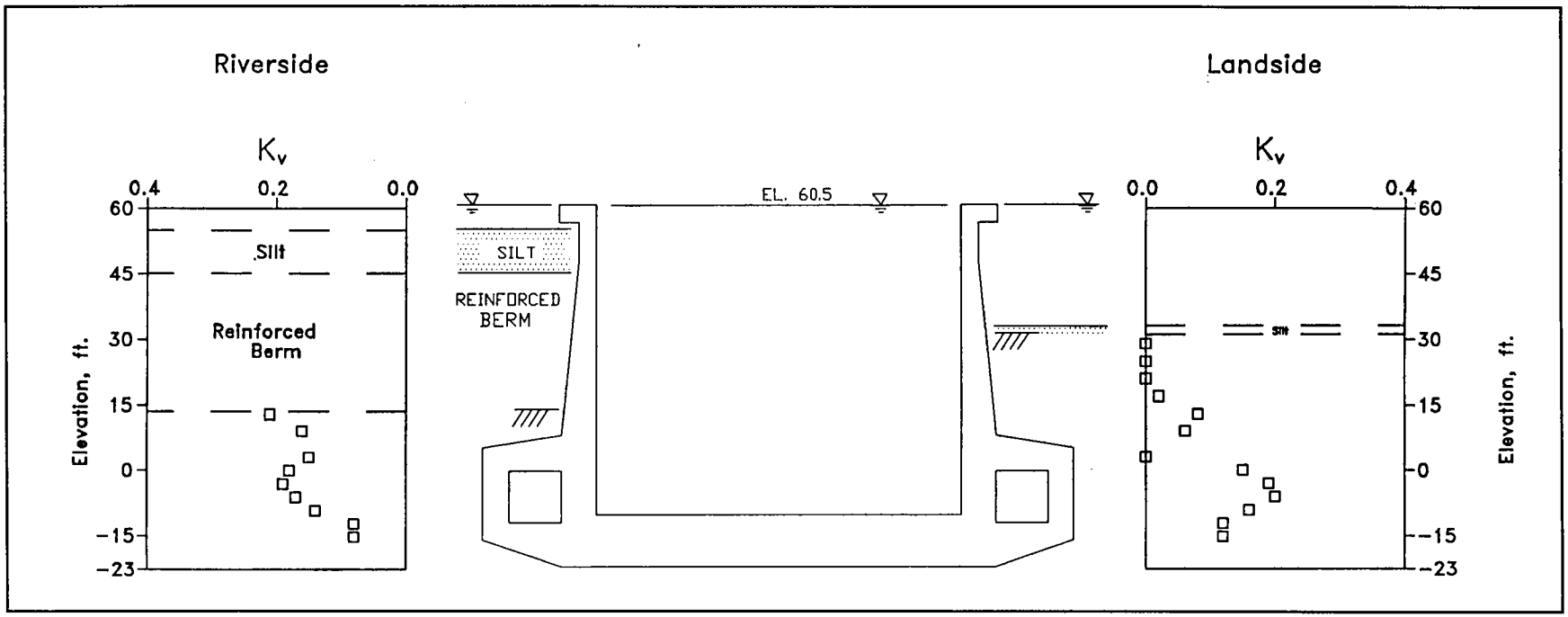

Figure 142. Vertical earth pressure coefficients after riverside siltation to el 55, river and pool in lock at el 60.5

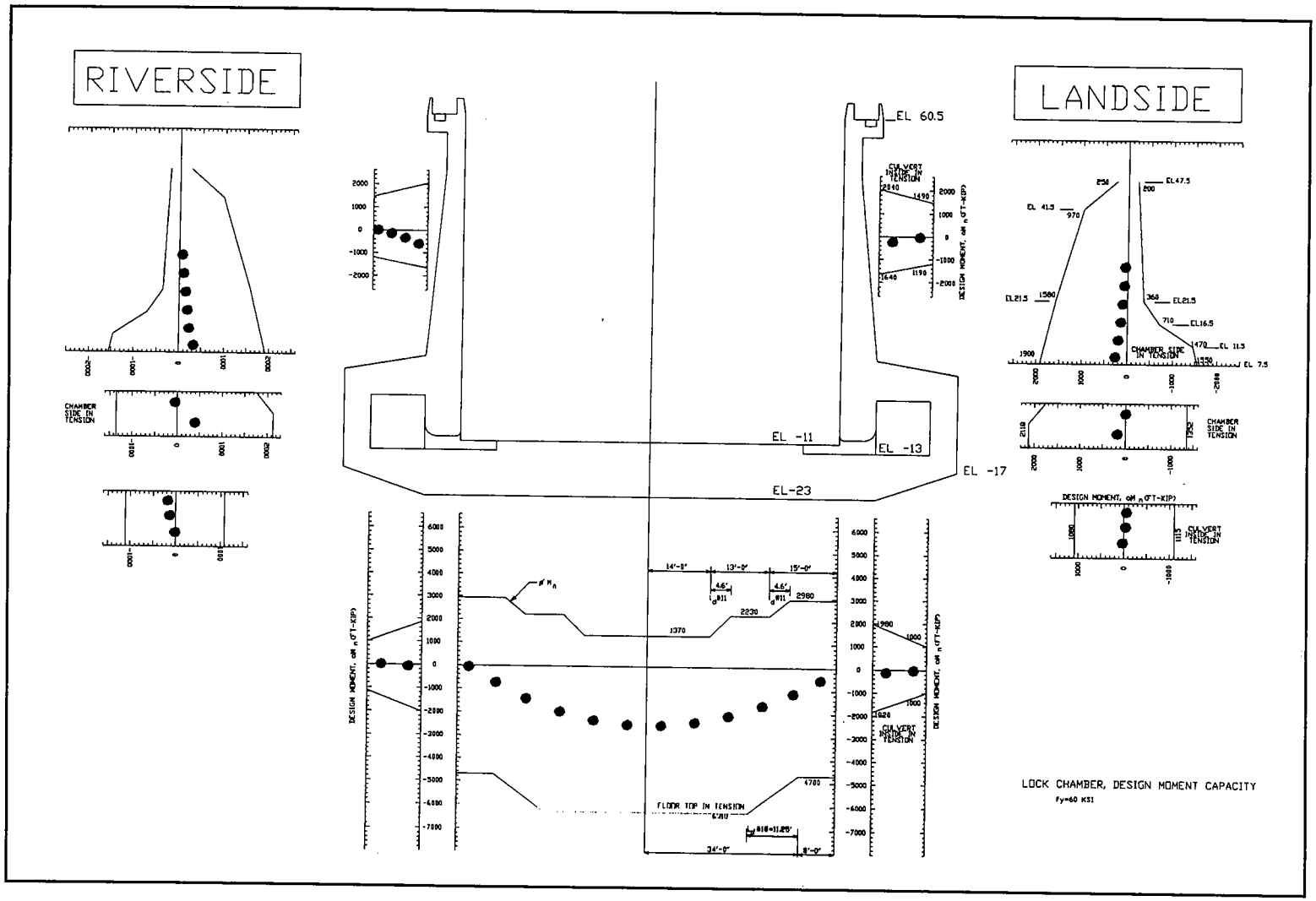

Figure 143. Distribution of factored moments after riverside siltation to el 55 and design moment capacity – river and pool in lock at el 60.5

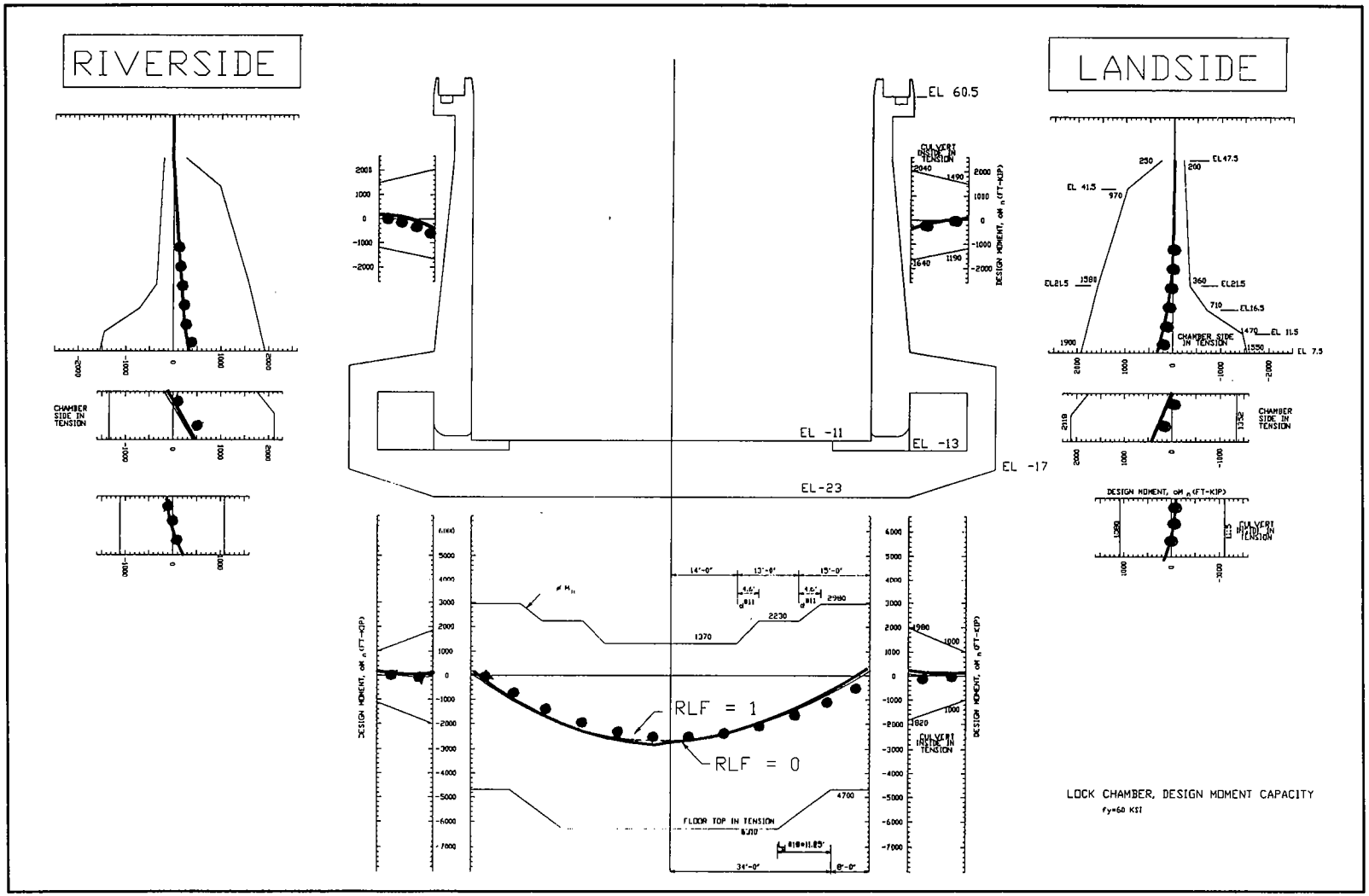

Figure 144. Distribution of factored moments, including CUFRAM results, after riverside siltation to el 55 – river and pool in lock at el 60.5

analyses of the lock upon completion of the construction of the reinforced berm. The factored moments computed using CUFRAM were in agreement with those computed from the finite element results.

The stress paths for the reinforced berm soil element numbers 715, 1152, 623, and 563 were upward and to the right, as shown in Figures 121 through 124, reflecting increases in both the shear stress and effective confining stresses upon siltation. Stress path point no. 9 corresponded to the final effective stress state within the reinforced soil elements after riverside siltation to el 55 (Table 5). The increase in weight of the silt on top of the reinforced berm continued to result in the complete, or nearly complete, mobilization of shear strength within the reinforced soil elements comprising the vertical face of the berm, as depicted in the stress paths for elements 715 and 1152 (Figures 121 and 122) and the values of mobilized shear strength, shown in Figure 145. These results were in contrast with stress paths for the reinforced soil elements along the riverside face of the reinforced soil berm, such as for element 563 shown in Figure 124. The confinment provided by the silt within the adjacent riverside channel had a more pronounced effect on the stress path for this element than did the shear induced by the weight of the silt acting on the reinforced berm. A similar type of response was observed for those soil elements comprising the central portion of the berm, such as element 623 (Figure 123). The maximum tensile forces were computed within the layers of reinforcement adjacent to the vertical face of the reinforced berm. These maximum values increased from 900 lb per lin ft of reinforcement to 1,500 lb per lin ft of reinforcement after riverside siltation occurred (Figure 146). The magnitude of the maximum tensile forces within these layers of reinforcement were below the limiting value of 3,800 lb per lin ft.

Lowering the Pool in Lock to El 40 and the River to El 4

Siltation of the river channel during high water was followed by analysis of the response of the lock (Figure 101) to the lowering of both the upper and lower pools. This section describes the results after lowering of the pool in the lock from el 60.5 to el 40 and the lowering of the river from el 60.5 to el 4. The riverside and landside silt deposits were retained during this series of analyses (Figure 97). Within the gap (el 13.5 to 45), no effective earth pressures were applied to the riverside stem wall. The stresses and displacements computed after siltation during the high water period were used as the initial values for the soils and lock at the start of the drawdown of the pools.

In the analysis, the drawdown of the river level was modeled by reducing the pore water pressures within the silts and the soils comprising the reinforced berm and backfill and between els 60.5 and 4, to values equal to zero. Within a soil element, this loss in water pressure produces

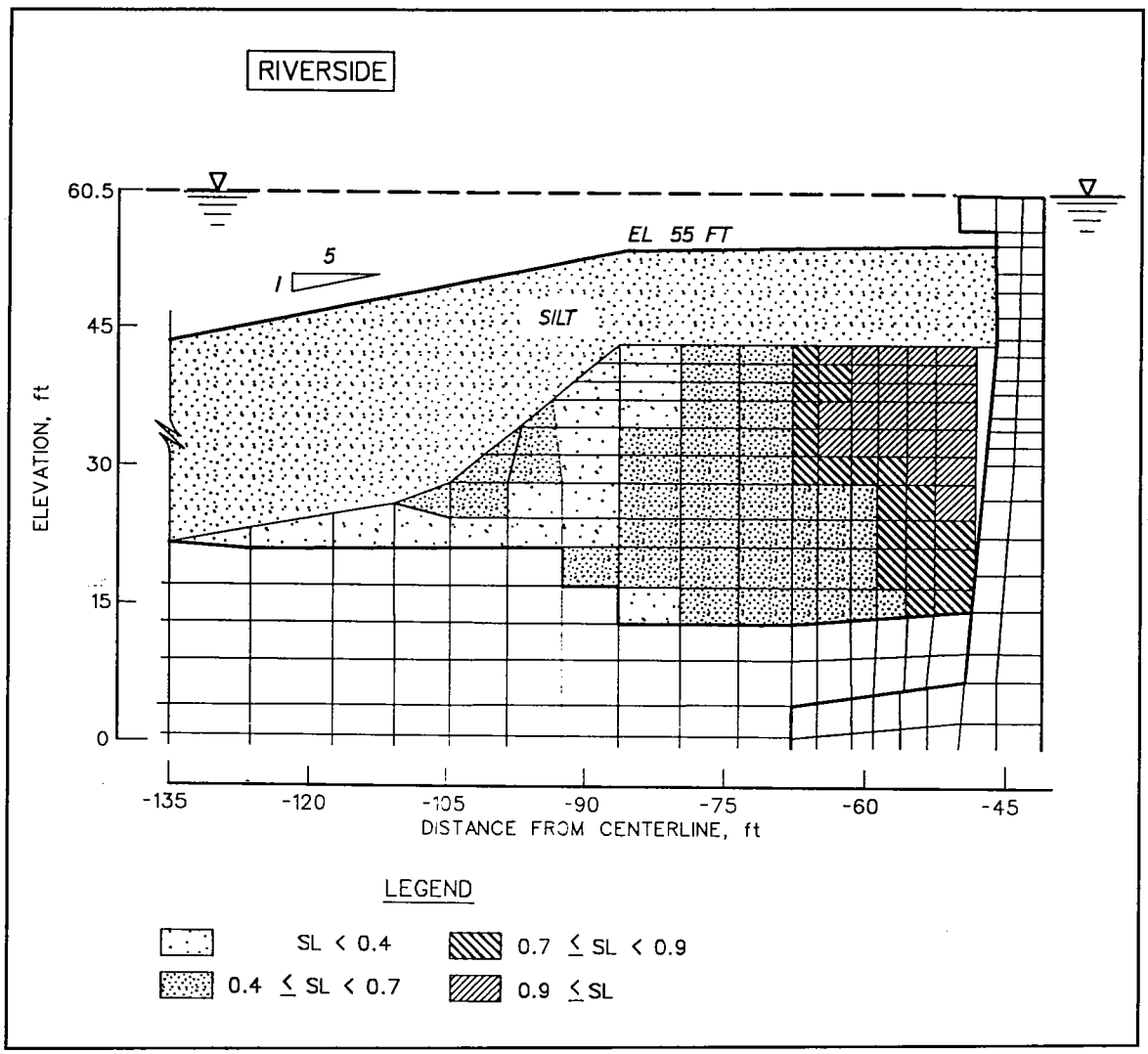

Figure 145. Variation in mobilized shear strength within reinforced berm after riverside siltation to el 55

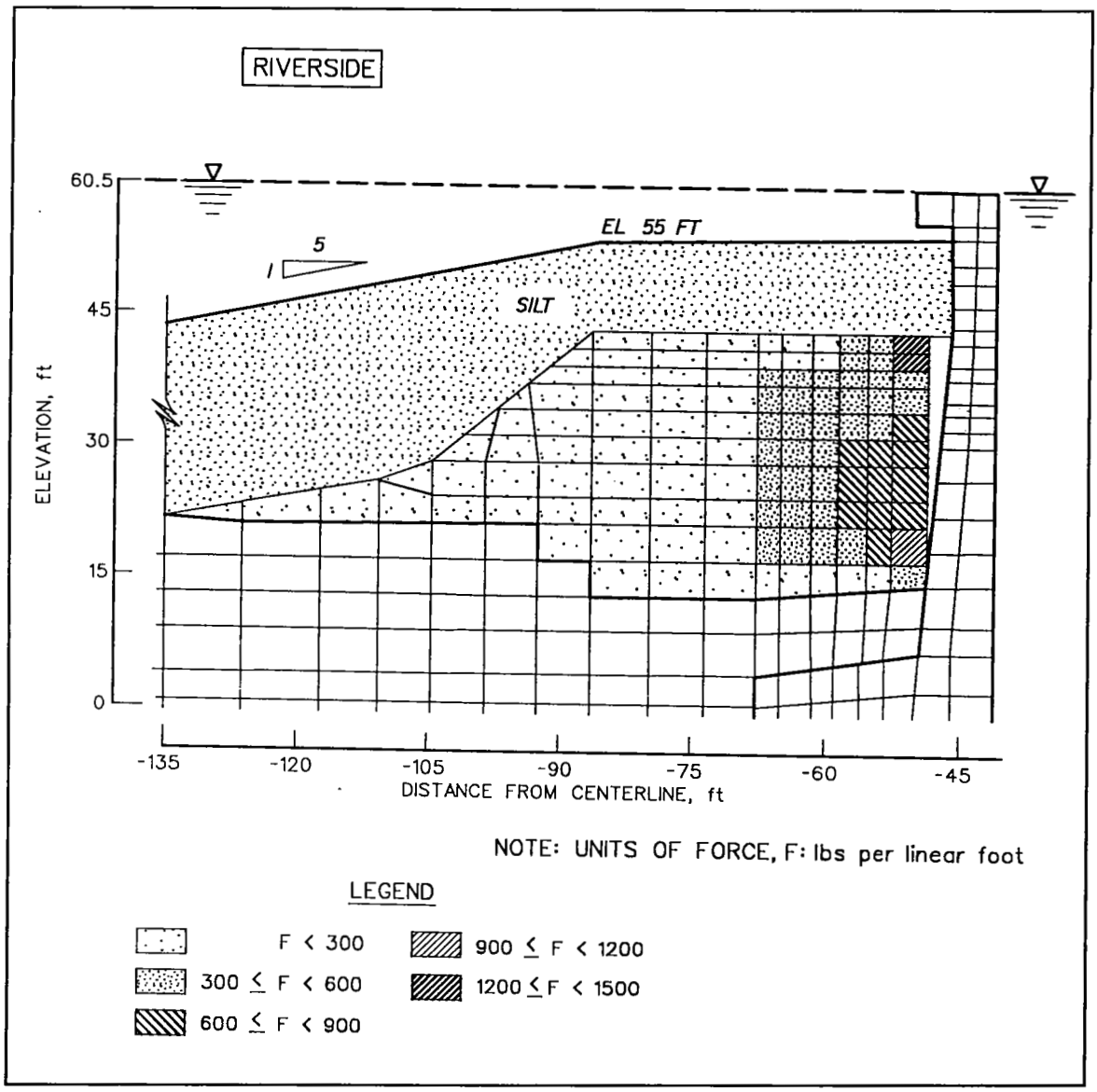

Figure 146. Variation in reinforcement force within reinforced berm after riverside siltation to el 55

an equivalent incremental body force acting downward. SOILSTRUCT applies the body forces to the soil elements using equivalent nodal point forces. The loss of soil buoyancy resulted in the settlement of the lock, the reinforced berm, the backfill and the soil foundation and increased the effective stresses within the soils.

Figure 147 shows that the values of displacements increased upon drawdown of the pools. The settlement of the riverside corner of the base slab increased by 1.7 in., from a value of 0.6 in. after siltation to 2.3 in. The settlement at the center line of the lock increased from 0 in. to 1.1 in. The landside corner of the base slab settled 1.0 in. to a total settlement of 0.4 in. The horizontal displacement of the base slab upon drawdown increased by 0.2 in. toward landside, with the displacements along the base totaling 0.8 in. in the same direction. The resulting horizontal displacments at the top of the landside and riverside stem walls were 0.5 and 0.7 in. respectively, as shown in Figure 137. The increases in the values of the horizontal displacements at the crests of the stem walls due to drawdown of the pools were 0.6 in. landside and 0.8 in. riverside and were directed away from the center line of the lock. The displacements of the walls were consistent with the net differential water pressures along the inside chamber walls and were directed away from the center line of the lock, a result of the higher pool elevation within the chamber compared to the river elevation.

The loss of buoyancy within the silt, reinforced soil berm, and the backfill produced settlements within all soil regions. The computed settlements within the backfill ranged from 1.8 to 4.7 in. after drawdown of the pools, as shown in Figure 147. The greatest settlements were computed along the top of the backfill. The point located below the riverside corner of the reinforced berm and at the top of the backfill settled 4.0 in., increasing from 0.7 in. prior to drawdown of the pools to 4.7 in. after drawdown. The total horizontal movements of all points within the backfill after drawdown were directed toward landside, as shown in Figure 147. The changes in the horizontal movements due to drawdown within the portion of the backfill located below the reinforced berm was less than 0.4 in. and was directed towards landside. The changes in the horizontal movements within the portion of the backfill located beyond the riverside toe of the reinforced berm were directed toward the river channel during drawdown and were 0.4 in. or less.

The settlement of the reinforced soil berm after drawdown ranged from 2.6 to 11.8 in. (Figure 147). At the riverside corner along the crest of the reinforced berm, the settlement due to drawdown of the pools was 3.4 in., with a total settlement of 2.6 in. The greatest computed settlement values occurred along the vertical face of the reinforced berm where the movements were directed downward and into the gap. Near the top of the vertical face at el 41, the settlement increased by 8.9 in., from 2.9 in. after siltation to 11.8 in. after drawdown. Midway the vertical face of the reinforced berm at el 30, the settlement due to drawdown increased by 4.7 in. to 8.6 in. Near the base along the vertical face at el 18, the settlement

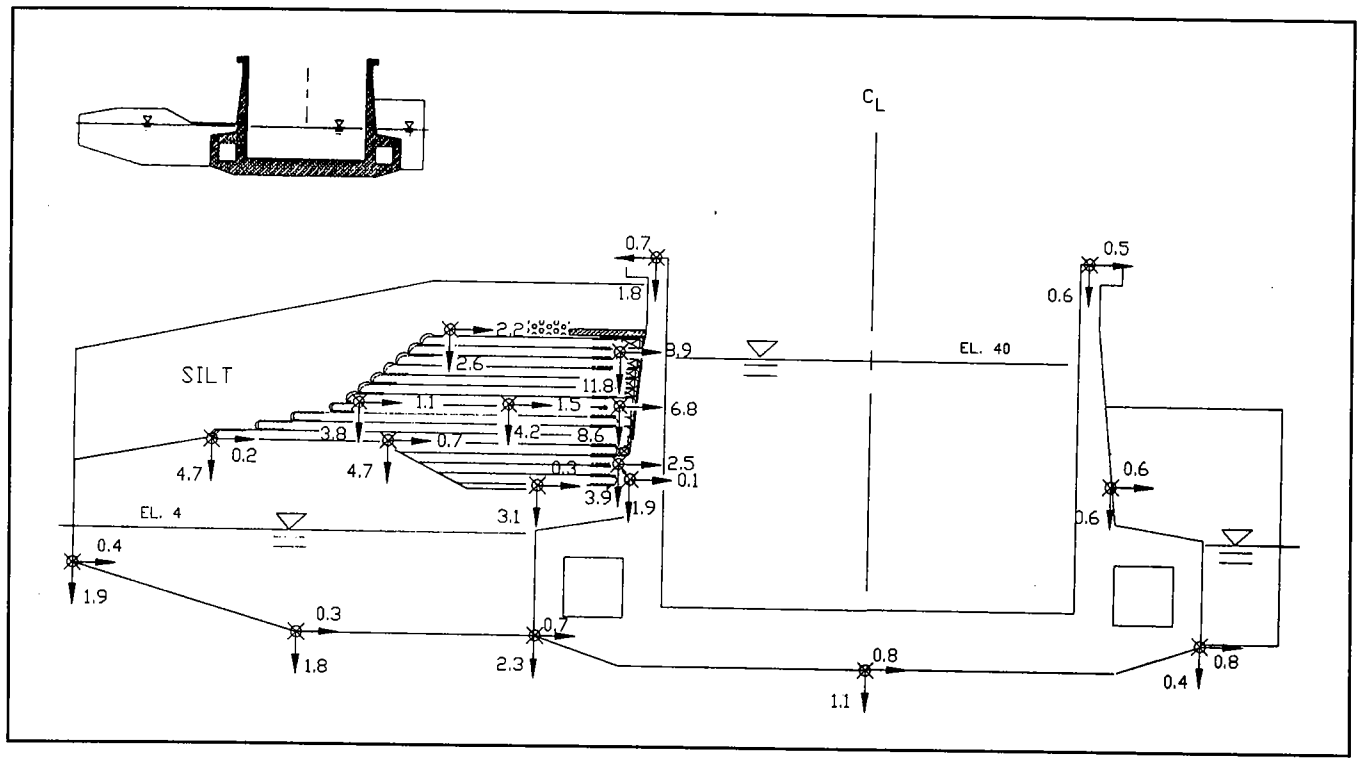

* Displacements of points are relative to their position after excavation for reinforced berm, in inches.

Figure 147. Relative displacements of lock, berm, and foundation after lowering pool in lock to el 40 and river to el 4

increased by 2.2 in. to 3.9 in. The horizontal displacements at els 41, 30, and 18 increased by 5.3, 2.7, and 0.8 in., respectively, and totaled 8.9, 6.8, and 2.5 in.

Increases in the effective stresses were computed within the foundation due to the loss of submergence of the upper soil regions during drawdown of the river elevation. Figures 106 through 109 show an increase in the values (Case 10) for the vertical effective stresses within the foundation. These values exceed those values for the effective vertical stresses computed after construction of the reinforced berm (Case 7). Along sections A-A and B-B within the foundation and below the riverside berm and riverside stem wall (Figure 105), Case 10 values within the backswamp clay deposit were lower than all but a few of the preconsolidation pressure values within the deposit. Along sections C-C and D-D (Figures 108 and 109) within the foundation and below the center line of the lock and landside stem wall, Case 10 values within the backswamp clay deposit were lower than all of the preconsolidation pressure values within the deposit. The unload-reload moduli were assigned to the finite elements modeling the foundation soils during this series of drawdown analyses.

The differences in the magnitudes of the riverside and landside loads are apparent from the differences between total pressure values at corresponding points about the center line of the lock in Figure 148. The greatest value of total pressures normal to the base was 8,550 psf below the riverside stem wall and was 1,850 psf greater than the 6,700 psf value computed below the landside stem wall. Below the center line of the lock the total base pressure was 6,420 psf. The total normal base pressures below the riverside culvert averaged 7,020 psf, while the values for the normal pressures below the landside culvert ranged from 4,800 to 6,290 psf. At el 12.9, the total pressure normal to the riverside stem wall was 4,750 psf, while the corresponding value normal to the landside stem wall was 1,080 psf, a 3,670-psf difference. The differences between the values computed along either side of the lock decreased with decreasing elevation. At el -12.5, the total pressures normal to both culvert walls were 3,550 psf.

Figure 149 shows the effective normal pressures after drawdown of the river and pool in the lock. The greatest computed effective normal base pressures were 6,860 and 5,200 psf below the riverside and landside stem walls, respectively. With the high pool of water in the chamber (el 40) and the low river level (el 4), these effective base pressure values were greater than those computed in the previous analyses after siltation by 2,890 psf riverside and by 2,380 psf landside. The effective base pressure below the center line of the lock was 4,740 psf, 2,230 psf greater than the value computed in the siltation analysis. The effective normal pressures below the outside corners of the riverside and landside culverts were 5,490 and 3,610 psf, respectively.

The effective normal pressures along the riverside stem wall decreased in value with decreasing elevation from 4,750 psf at el 12.9 to 3,060 psf at

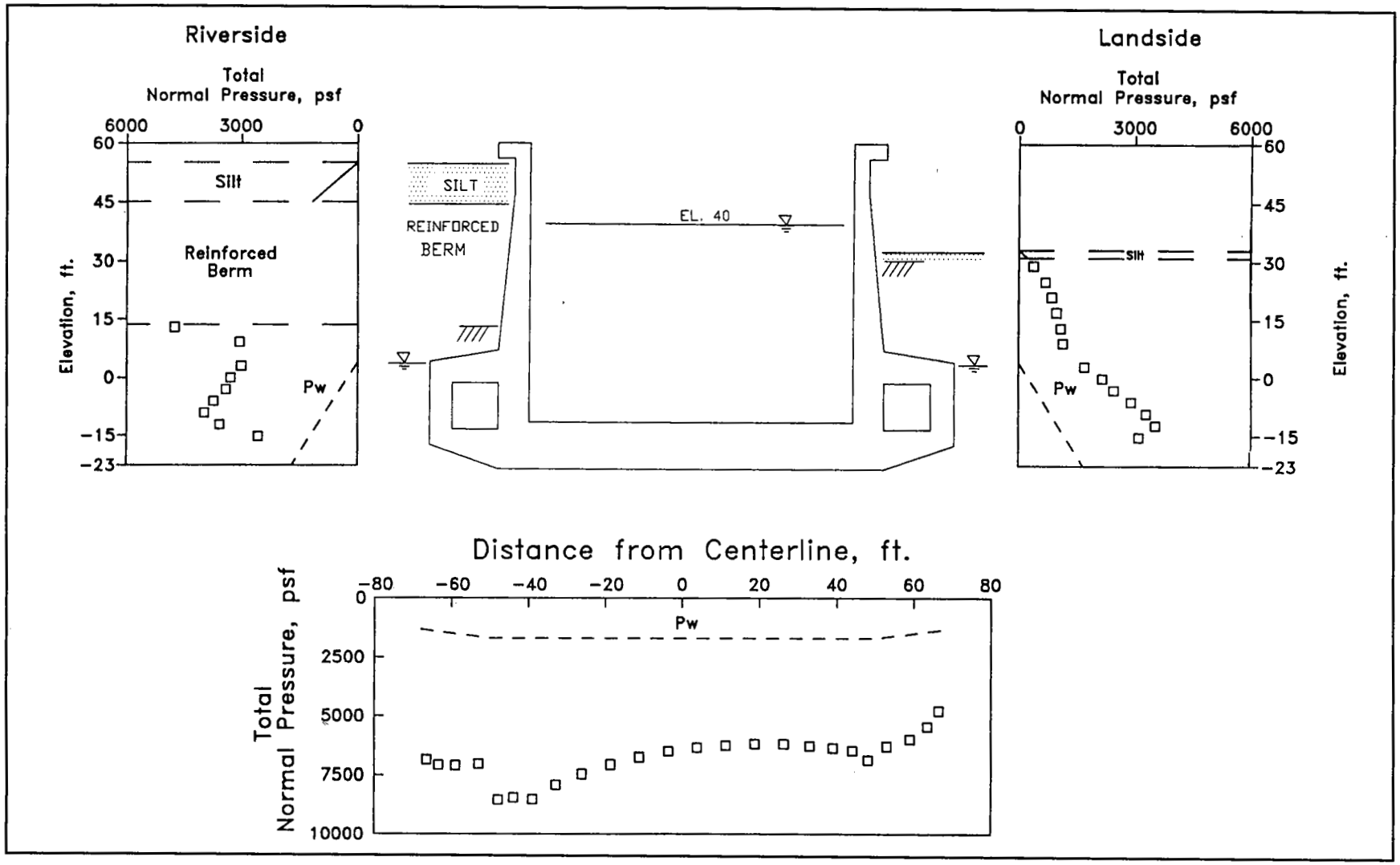

Figure 148. Total normal pressures after lowering pool in lock to el 40 and river to el 4

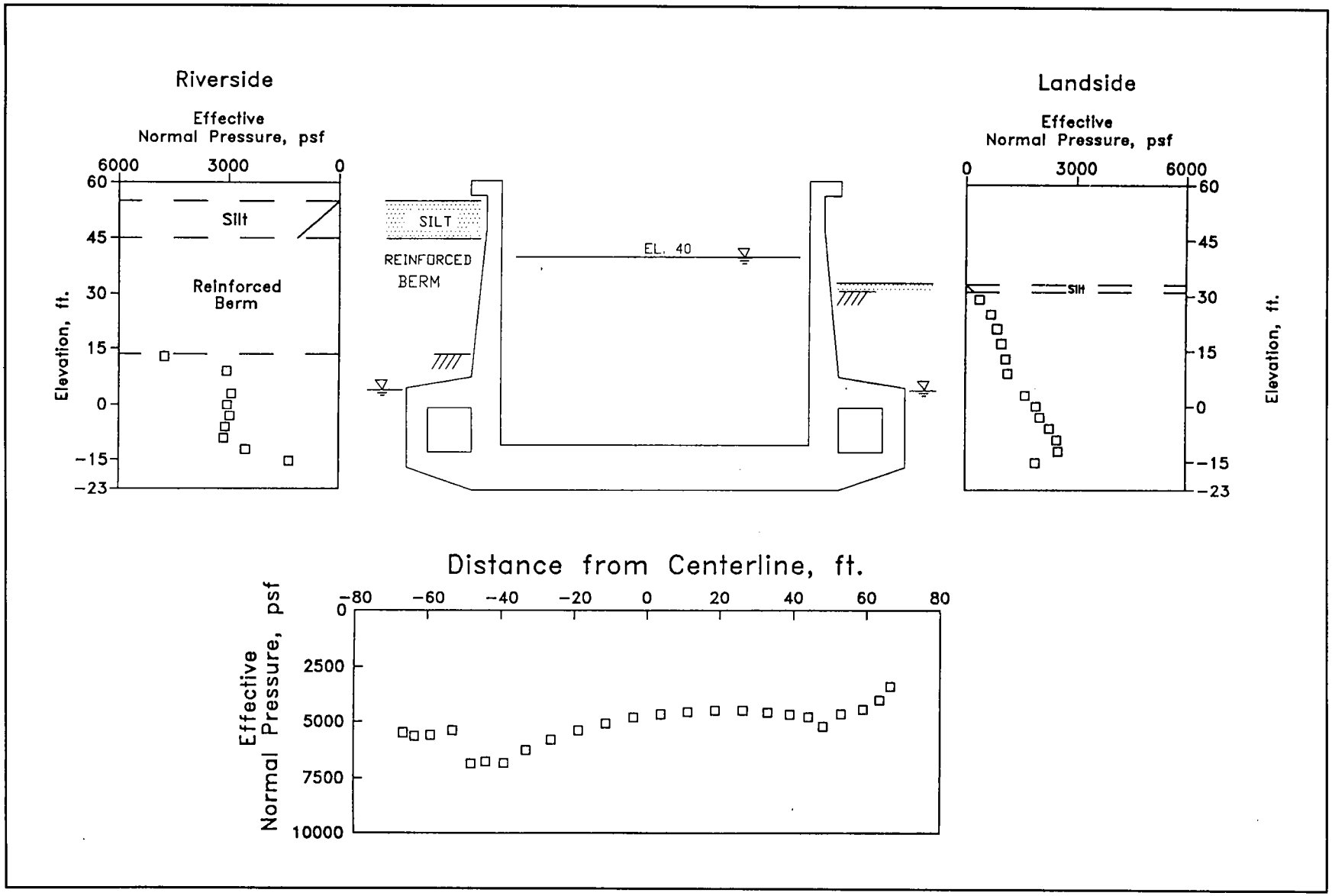

Figure 149. Effective normal pressures after lowering pool in lock to el 40 and river to el 4

el 9. These pressures were greater than those computed after the siltation by 2,460 and 1,510 psf, respectively. Along the riverside culvert wall, the increase in the effective normal pressure ranged from 330 to 1,450 psf when compared with those pressures computed after siltation. The differences between the effective pressures normal to the riverside and landside walls were equal to the differences between the total pressures normal to the riverside and landside walls.

Figure 150 shows the unsymmetrical variations in δ_{mob} along the base of the lock. Below the landside stem wall, δ_{mob} ranged from 0 deg to 14 deg below the riverside culvert. The greatest value for δ_{mob} was 22 deg at el 3 along the riverside culvert wall; δ_{mob} decreased to 0 deg at el -12.5. Along the landside culvert wall, δ_{mob} ranged from 3 to 12 deg. The greatest δ_{mob} value computed along the landside stem wall was 17 deg at el 17.

Figure 151 shows that K_h decreased with decreasing elevation along the stem walls and was nearly constant along the culvert walls. In the compacted select clay along the landside stem wall, K_h ranged from 0.81 at el 29 to 0.75 at el 25, and averaged 0.78 (Table 18). Between els 23 and 7.5, the landside K_h values ranged from 0.40 to 0.62, with an average value of 0.5. The average K_h values along the landside stem wall after drawdown of the river were less than those that occurred after siltation (Table 17) by 0.42 for the compacted select clay and 0.21 for the compacted sand. These landside average K_h values were comparable with those values listed in Table 15, which were computed after construction of the reinforced berm. Because the river elevations for both analyses were below the top of the culvert, the pore pressures within the backfill adjacent to the stem walls were equal to 0. Along the riverside stem and below the reinforced berm, K_h was 0.94 at el 13 and 0.55 at el 9, with an average value of 0.75. The average K_h value listed in Table 18 is nearly the same as the average K_h value listed in Table 17, differing by only 0.01. Along the landside and riverside culvert walls, the average K_h values were 0.55 and 0.44, respectively (Table 18), and differed from those values listed in Table 17 by 0.02.

The maximum value for the vertical earth pressure coefficient was 0.25 at el 12.9 immediately below the reinforced berm (Figure 152). The average K_v value was 0.20 (Table 18), which was greater than the average K_v value after siltation by 0.02. Drawdown of the water table to below the tops of the culverts increased the average K_v values along the landside stem wall from 0 to 0.08 adjacent to the compacted select clay and from 0.04 to 0.13 adjacent to the compacted sand. The increase in the K_v values along the stem wall was due to the greater magnitude settlements within the backfill adjacent to the wall during the drawdown of the river, as compared with the magnitudes of the settlement of the stem walls. Along the culvert walls, the soil-to-structure interaction was more complex. The greatest computed K_v value occurred at the top of the culvert walls and was 0.19 (Figure 152). K_v decreased in value with decreasing elevation. Negative K_v values, which correspond to an upward shear

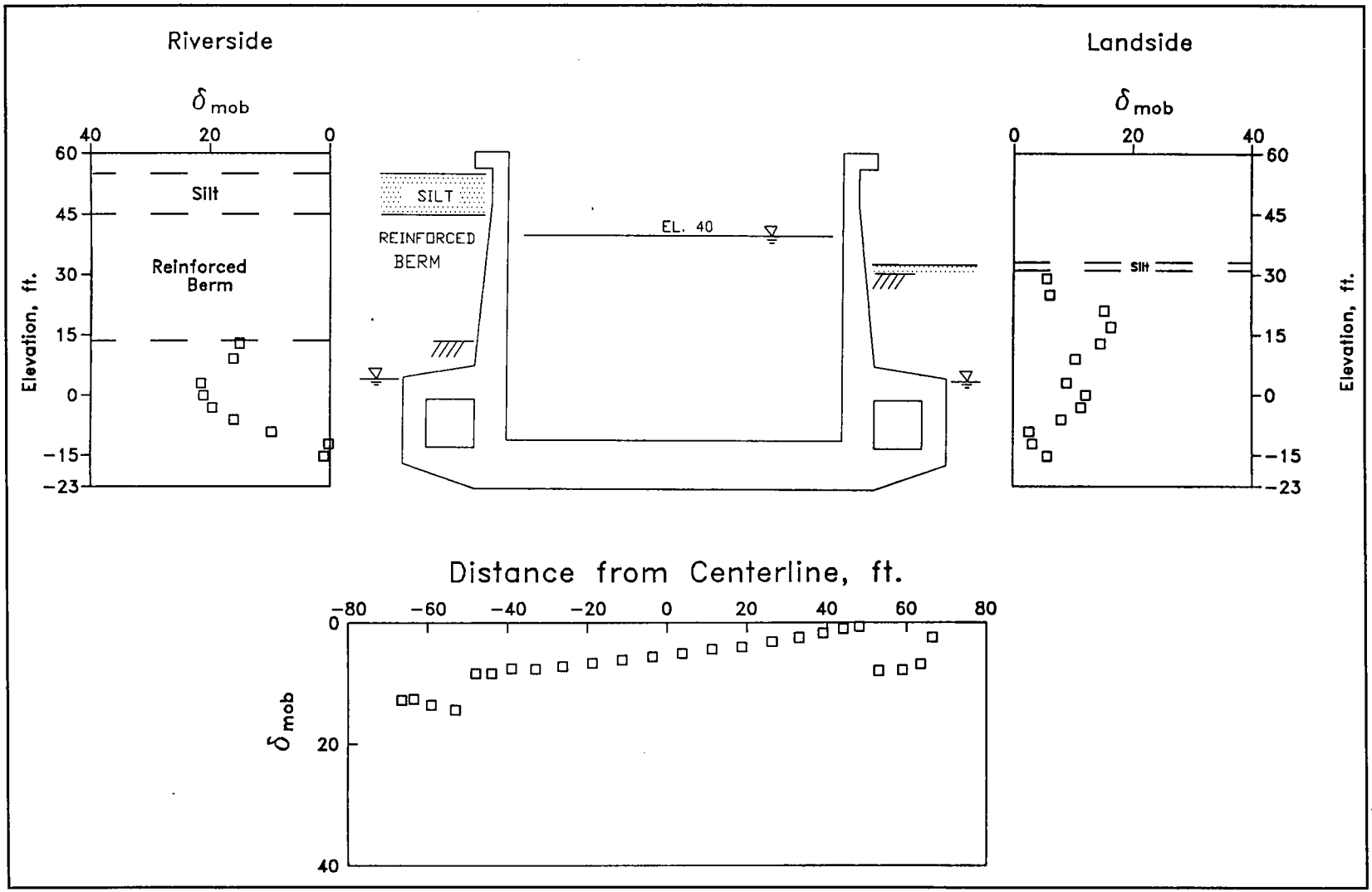

Figure 150. Mobilized friction angles along exterior of lock after lowering pool in lock to el 40 and river to el 4

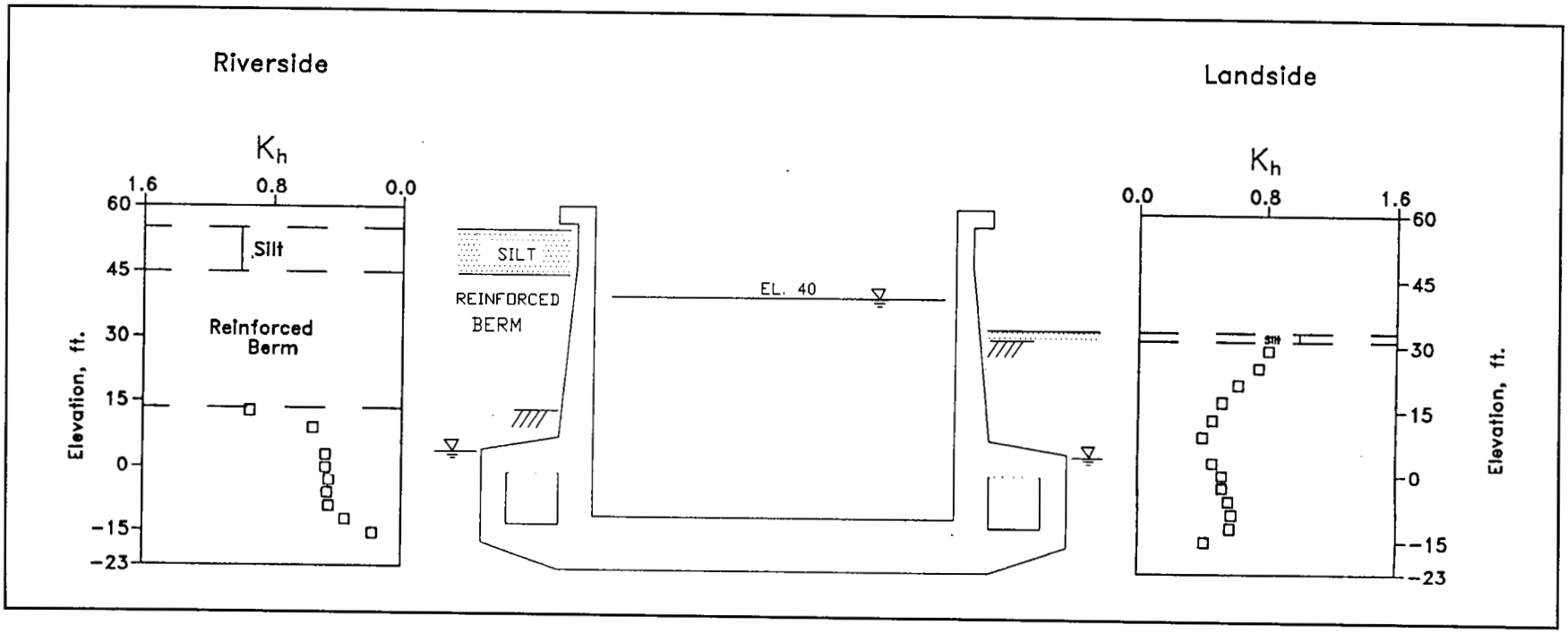

Figure 151. Horizontal earth pressure coefficients after lowering pool in lock to el 40 and river to el 4

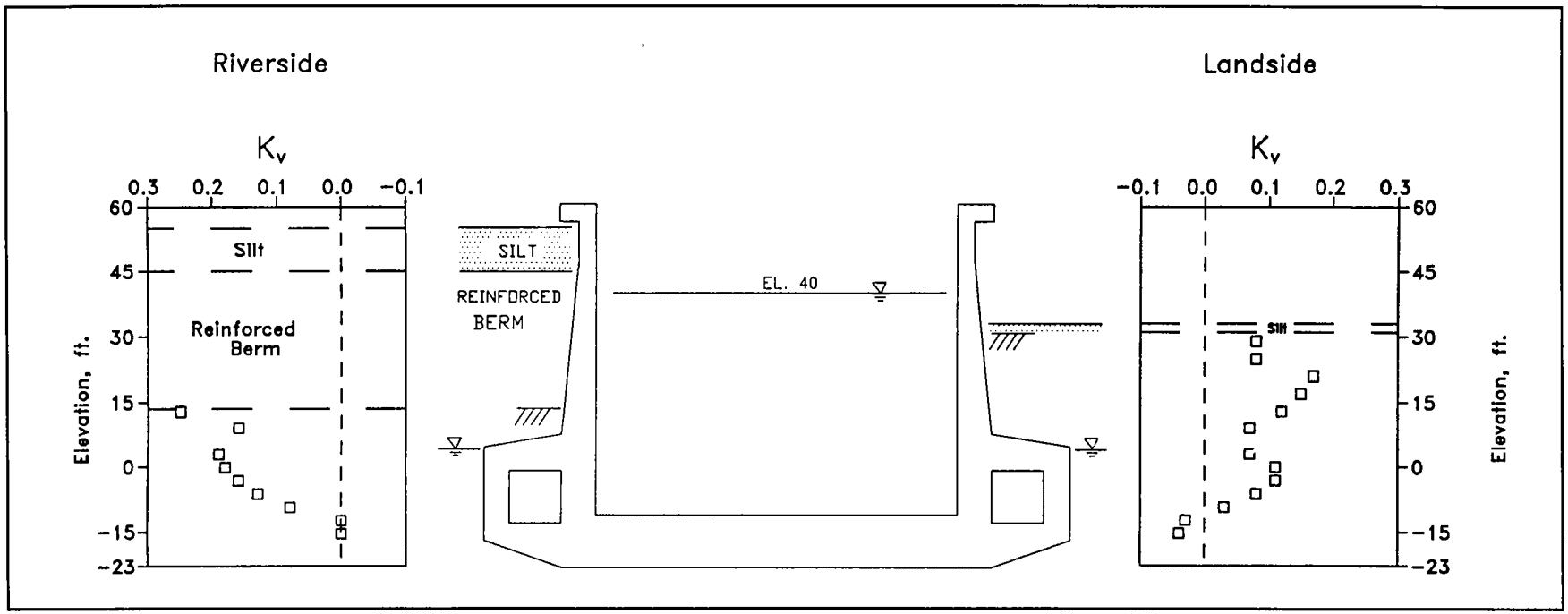

Figure 152. Vertical earth pressure coefficients after lowering pool in lock to el 40 and river to el 4

Table 18
Average Values of Horizontal and Vertical Earth Pressure Coefficients after Lowering Pool in Lock to El 40 and River to El 4

Backfill Region	Backfill Material	Riverside K_h	Riverside K_v	Landside K_h	Landside K_v
Stem	Compacted select clay	-	-	0.78	0.08
Stem	Compacted sand	0.75	0.20	0.5	0.13
Culvert	Compacted sand	0.44	0.1	0.55	0.05

Elevation of river: 4 ft
Elevation of pool in lock: 40 ft
Elevation of riverside silt: 55 ft

force, were computed along the lower elevations of the landside lock. This type of response can be attributed to two factors: (a) a high pool elevation maintained within the lock, and (b) the loss of uplift pressures along the base of the lock with the lowering of the river elevation in the analysis. Both factors resulted in greater computed settlements along the lower portions of the culvert walls compared with the settlements within the adjacent backfill.

The distributions of computed factored moments within the lock and the design moment capacity distributions are shown in Figure 153. The factored moment at the center line of the lock increased by 1,650 kip-ft, from -2,500 kip-ft after siltation (Figure 143) to -4,150 kip-ft upon drawdown of the upper and lower pools. The entire top of the base slab remained in tension and the **chamber side** of the riverside stem wall remained in compression. With drawdown of the pools, the **chamber side** of the landside stem wall changed from compression to tension. The factored moment within the riverside stem wall at el 9.25 decreased from 377 to 64 kip-ft, while at el 25 the factored moment increased in value from 148 to 237 kip-ft. At el 9.25 within the landside stem wall, the factored moment decreased by 582 kip-ft, from 212 to -370 kip-ft. The factored moments within the lock were greater than those computed in previous analyses but less than the values for the design moment capacity.

Figure 154 shows a comparison of the results from a CUFRAM analysis with a rigid link factor of 1.0 with the results of finite element analyses. The earth and water pressures specified in the CUFRAM analyses equaled those computed in the finite element analysis. The greatest difference between the results from the two analyses occurred along the base of the lock, riverside of center line. The values for the computed factored moments within the base using CUFRAM were 17 percent greater than the computed factored moment from the finite element results at the center line of the lock. This difference increased to 85 percent at the section

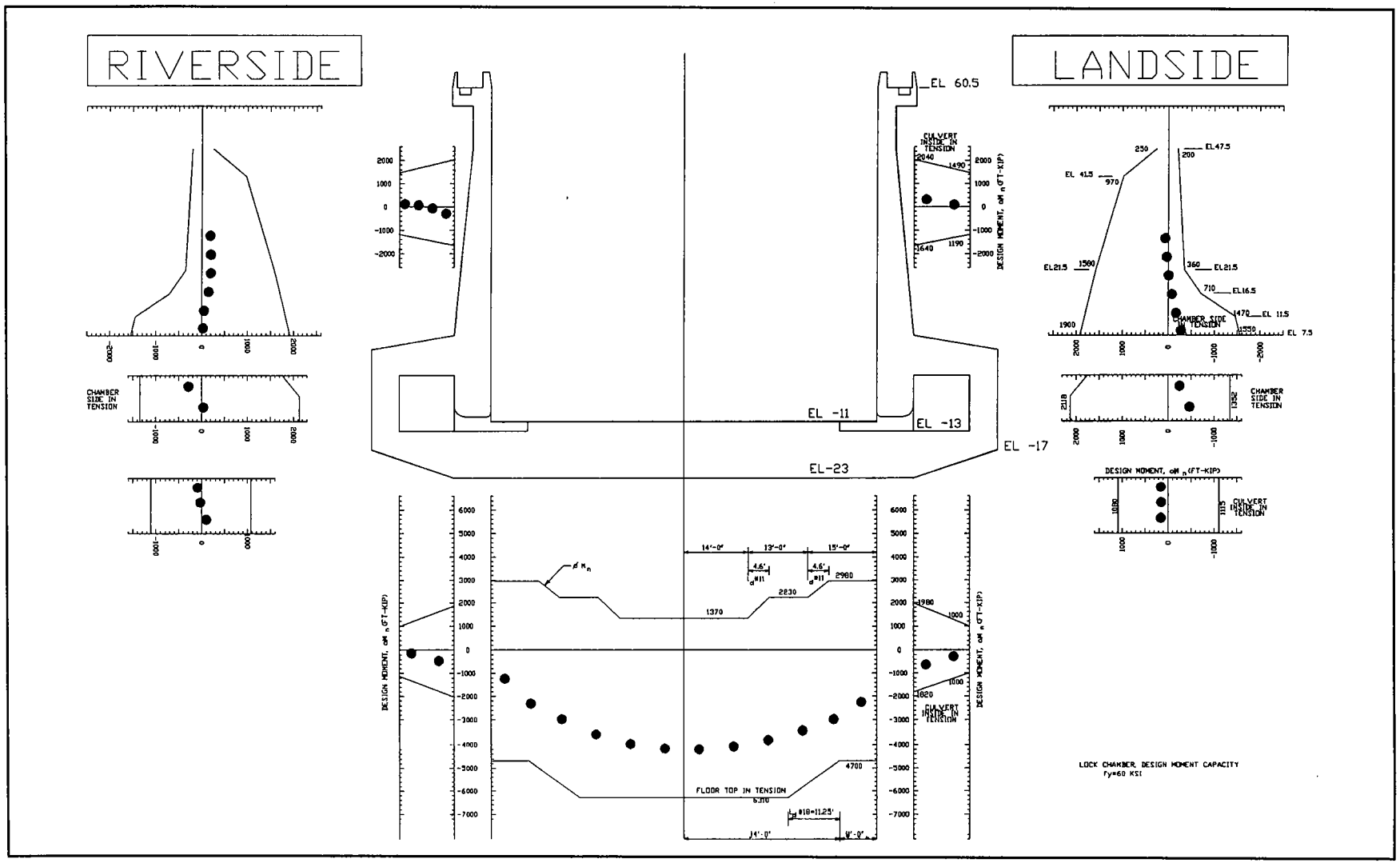

Figure 153. Distribution of factored moments and design moment capacity – pool in lock at el 40 and river at el 4

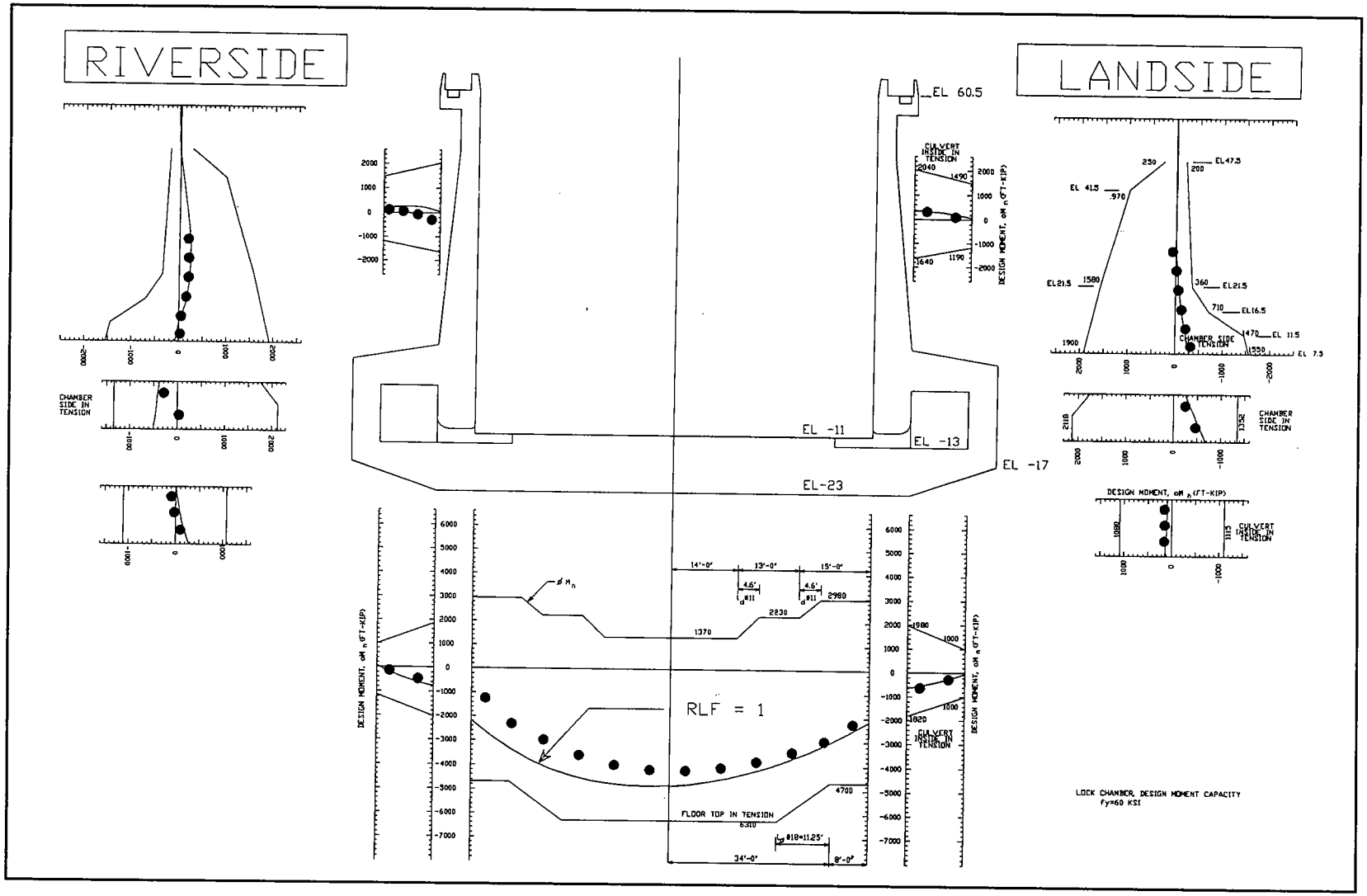

Figure 154. Distribution of factored moments, including CUFRAM results – pool in lock at el 40 and river at el 4

adjacent to the riverside chamber wall. The reason for these differences is not clear but is believed to be associated with the procedure used by CUFRAM to redistribute the vertical forces to attain moment equilibrium at the center line of the lock. The factored moments from the CUFRAM analysis were less than the values for the design moment capacity.

The loss of submergence for the silt and the soil comprising the reinforced berm resulted in an increase in both the effective confining pressures and the shear stresses within the berm, as shown in the stress paths for reinforced berm elements 715, 1152, 623, and 563 in Figures 121 through 124. Stress path point no. 10 corresponds to the final effective stress state within the reinforced soil elements after drawdown of the pool in the lock to el 40 and the river to el 4 (Table 5). The results shown in Figure 155 and the stress paths for elements 715 and 1152 (Figures 121 and 122), show the complete, or nearly complete, mobilization of shear strength within the reinforced soil elements comprising the vertical face of the berm. The silt within the riverside channel continues to have the effect of providing more confinement than shear, as evidenced by the stress path for elements 563 (Figure 124) and 623 (Figure 123). The maximum computed tensile forces occurred within the layers of reinforcement adjacent to the vertical face of the reinforced berm. With the exception of the layers of reinforcement within the top landside corner of the berm, the maximum tensile forces increased from 1,500 to 1,800 lb per lin ft of reinforcement after drawdown of the river elevation (Figure 156). Within the top landside corner of the berm, the maximum tensile force was 2,600 lb per lin ft of reinforcement. The tensile forces and deformations computed within this region indicated that additional reinforcement may be required to limit the deformations. The magnitudes of the maximum tensile forces within these layers of reinforcement were below the limiting value of 3,800 lb per lin ft.

Lowering the Pool in Lock to El 4 - River at El 4

The lowering of the pool in the lock from el 40 to 4, as shown in Figure 98, is described in this chapter. The elevation of the river and water table was maintained at el 4, and the silt remained along the banks of the river channel and on top of the berm. This analysis is the seventh and final in a series of soil-to-structure interaction studies of the response of the lock and the reinforced soil berm to combinations of water and silt loads that are listed in Table 13. The stresses and displacements computed after the previous series of drawdown analyses were used as the initial values for the soils and lock at the start of these analyses of the mesh shown in Figure 101.

The drawdown of the pool within the lock to el 4 was accomplished in 10 stages. During each stage the pool was lowered 4 ft. Each stage of unloading was modeled by applying the incremental change in boundary water pressures normal to the chamber walls and base. These incremental

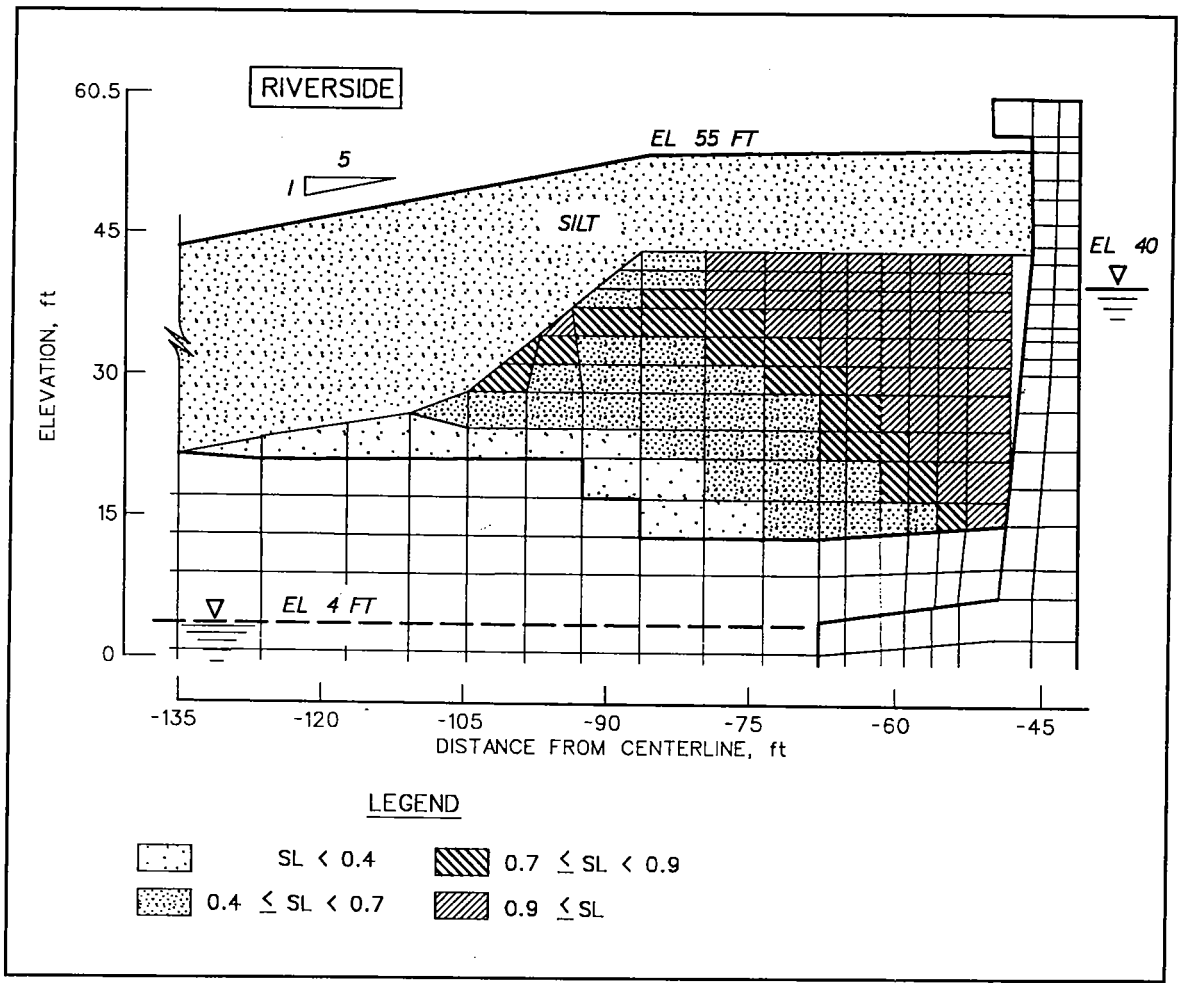

Figure 155. Variation in mobilized shear strength within reinforced berm after lowering pool in lock to el 40 and river to el 4

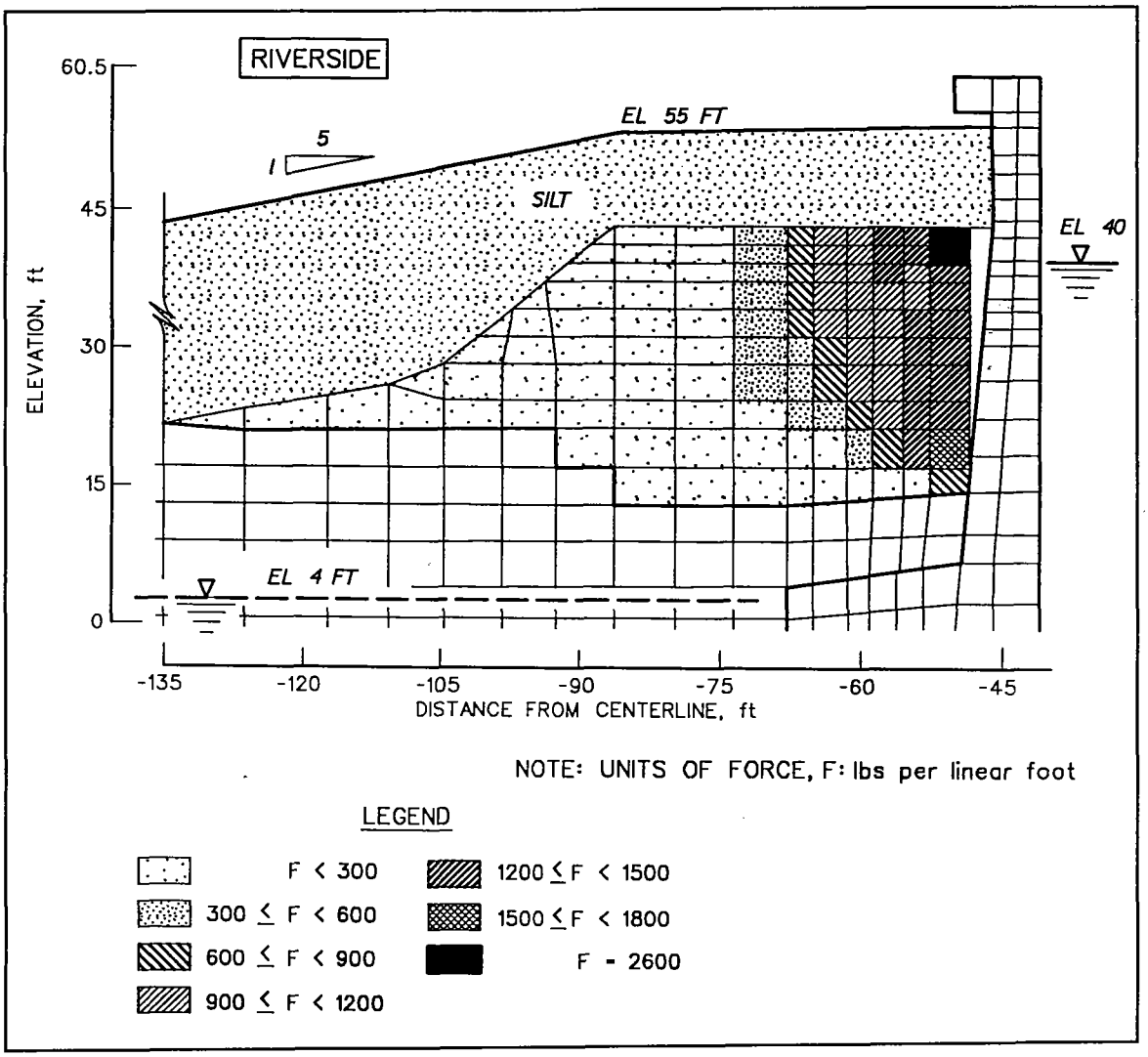

Figure 156. Variation in reinforcement forces within reinforced berm after lowering pool in lock to el 40 and river to el 4

changes in pressures were directed away from the faces of the chamber. The lowering of the pool in the chamber by 36 ft reduced the total weight applied to the soil foundation and resulted in the rebound of both the foundation and adjacent backfill. With no change in the elevation of the river, the values of the long-term pore water pressures within the soils remained unchanged from previous analyses. The decrease in the level of water within the lock, in conjunction with constant pore water pressures within the foundation, resulted in a reduction in the values of the effective stresses within the soil foundation and the adjacent backfill. Within the gap (el 13.5 to 45), no effective earth pressures were applied along the outside face of the riverside stem wall.

Figure 157 shows that the values of displacements relative to the values computed after excavation for the berm decreased with the lowering of the pool in the lock. The rebound of the riverside corner of the base slab was 0.5 in., from a displacement of 2.3 to 1.8 in. The center line of the lock rebounded 0.5 in. and the landside corner of the base slab rebounded 0.4 in. The horizontal displacement of the base slab upon drawdown of the pool in the lock was very small (less than or equal to 0.1 in.) toward landside, with the displacements along the base totaling 0.8 in. toward landside. The incremental horizontal displacements at the crest of the stem walls due to drawdown of the pool were directed toward the center line of the lock and were 0.3 in. for the landside wall and 0.4 in. for the riverside wall. The directions of these movements were consistent with loss of water pressures within the chamber during drawdown.

The computed rebound within the backfill and reinforced soil berm were consistent with the reduction in the gross weight of the lock and the expected mass movements within the adjacent soil regions. For the points within the backfill that are shown in Figure 157, the magnitudes of rebound due to drawdown of the pool in the lock ranged from 0.1 to 0.4 in. and was computed as the differences between the values shown in Figures 157 and 147. The magnitudes of the rebound within the reinforced berm ranged from 0.1 to 0.5 in. At the riverside corner along the crest of the reinforced berm, the rebound due to drawdown of the pool in the lock was 0.2 in., resulting in a total settlement of 2.4 in. The rebound along the vertical face of the reinforced berm was a constant 0.5 in., with total settlements at els 18, 30, and 41 equal to 3.4, 8.1, and 11.3 in., respectively. The incremental horizontal displacements within the berm due to drawdown of the pool was less than or equal to 0.2 in., toward riverside. At the riverside corner along the crest of the reinforced berm, the horizontal displacement decreased from 2.2 in. prior to the drawdown of the pool in the lock to 2.0 in. The total movements along the vertical face of the berm were directed downward and into the gap. The horizontal displacements at els 18, 30, and 41 decreased by a constant 0.1 in. and totaled 2.6, 6.7, and 8.8 in., respectively.

The computed effective stresses within the foundation decreased due to the loss of the weight within the lock, as shown in Figures 106 through 109 (Case 11). Changes in the computed vertical effective stresses below

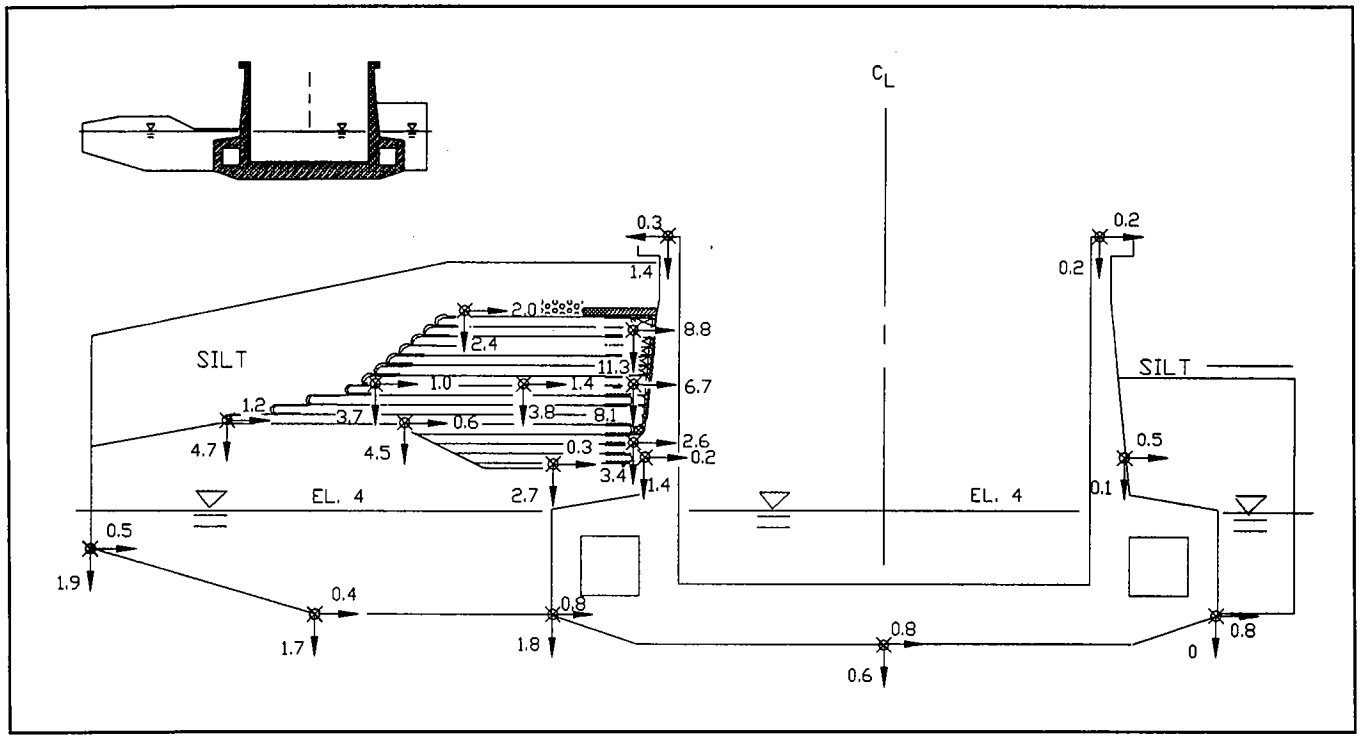

* Displacements of points are relative to their position after excavation for reinforced berm, in inches.

Figure 157. Relative displacements of lock, berm, and foundation after lowering pool in lock to el 4 – river at el 4

the lock (along sections B-B, C-C, and D-D) were greater than those below the backfill (along section A-A). The unload-reload moduli were assigned to the finite elements modeling the foundation soils, consistent with the unloading of the foundation soils during this series of analyses.

Figure 158 shows total pressures normal to the walls and along the base of the lock. The upper and lower pool elevations were 4 ft. The greatest value of total pressure normal to the base was 7,300 psf below the riverside stem wall, 1,620 psf greater than the 5,680-psf computed pressure below the landside stem wall. Below the center line of the lock, the total base pressure was 5,300 psf. The total normal base pressures below the riverside culvert averaged 5,900 psf, while the values for the normal pressures below the landside culvert ranged from 3,690 to 5,290 psf. The total pressures normal to the base of the lock after drawdown of the pool in the lock to el 4 were from 1,000 to 1,370 psf less than the values corresponding to pool el 40 (Figure 148).

The total pressures normal to the riverside stem and culvert walls were greater than the pressures normal to the landside walls. At el 12.9, the total pressure normal to the riverside stem wall was 4,350 psf, while the corresponding value normal to the landside stem wall was 910 psf, a 3,440 psf difference. The differences between the riverside pressures and the landside pressures decreased with decreasing elevation. The smallest differences in total normal computed pressures occurred near the lower corner of the culvert walls, at el -15.5, where the difference in normal pressures was 640 psf.

Lowering of the pool inside the lock by 36 ft reduced the total pressures normal to the riverside and landside walls, with the exception of the lower 5 ft along the riverside culvert wall, where the total normal pressures increased. The greatest decrease in total computed normal pressures occurred along the landside culvert wall at el -12.5 and was 910 psf, the difference between the value in Figure 158 and the value in Figure 148. Along the landside stem wall, the greatest decrease in total normal pressure occurred at el 21 and was 280 psf. Along the riverside stem wall, the greatest decrease in total normal pressure occurred at el 12.9 and was 400 psf. The total pressures normal to the riverside culvert wall decreased above el -12 and increased below this elevation. Near the top of the riverside culvert wall, el 3, the decrease in total normal pressure was 200 psf, and near the bottom of the riverside culvert wall, el -15.5, the increase in total normal pressure was 370 psf. At el -12 along the riverside culvert wall, there was no change in the total normal pressure (3,600 psf) upon drawdown of the pool in the lock.

Figure 159 shows the effective normal pressures after the pool in the lock was lowered by 36 ft to el 4. The greatest computed effective normal base pressures were 5,680 and 4,000 psf below the riverside and landside stem walls, respectively. The effective base pressure below the center line of the lock was 3,620 psf, and the effective normal pressures below the outside corners of the riverside and landside culverts were 4,120 and

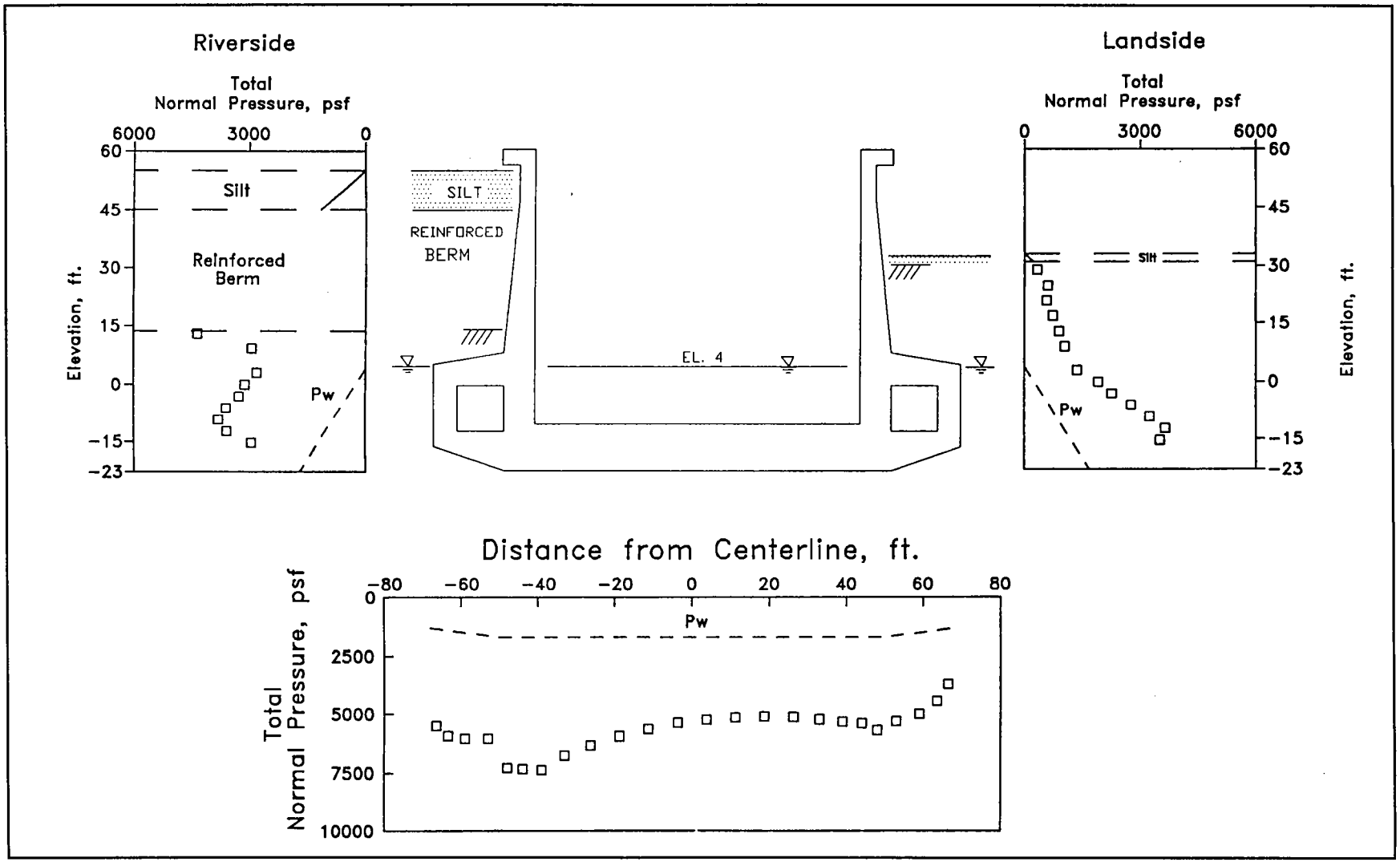

Figure 158. Total normal pressures after lowering pool in lock to el 4 – river at el 4

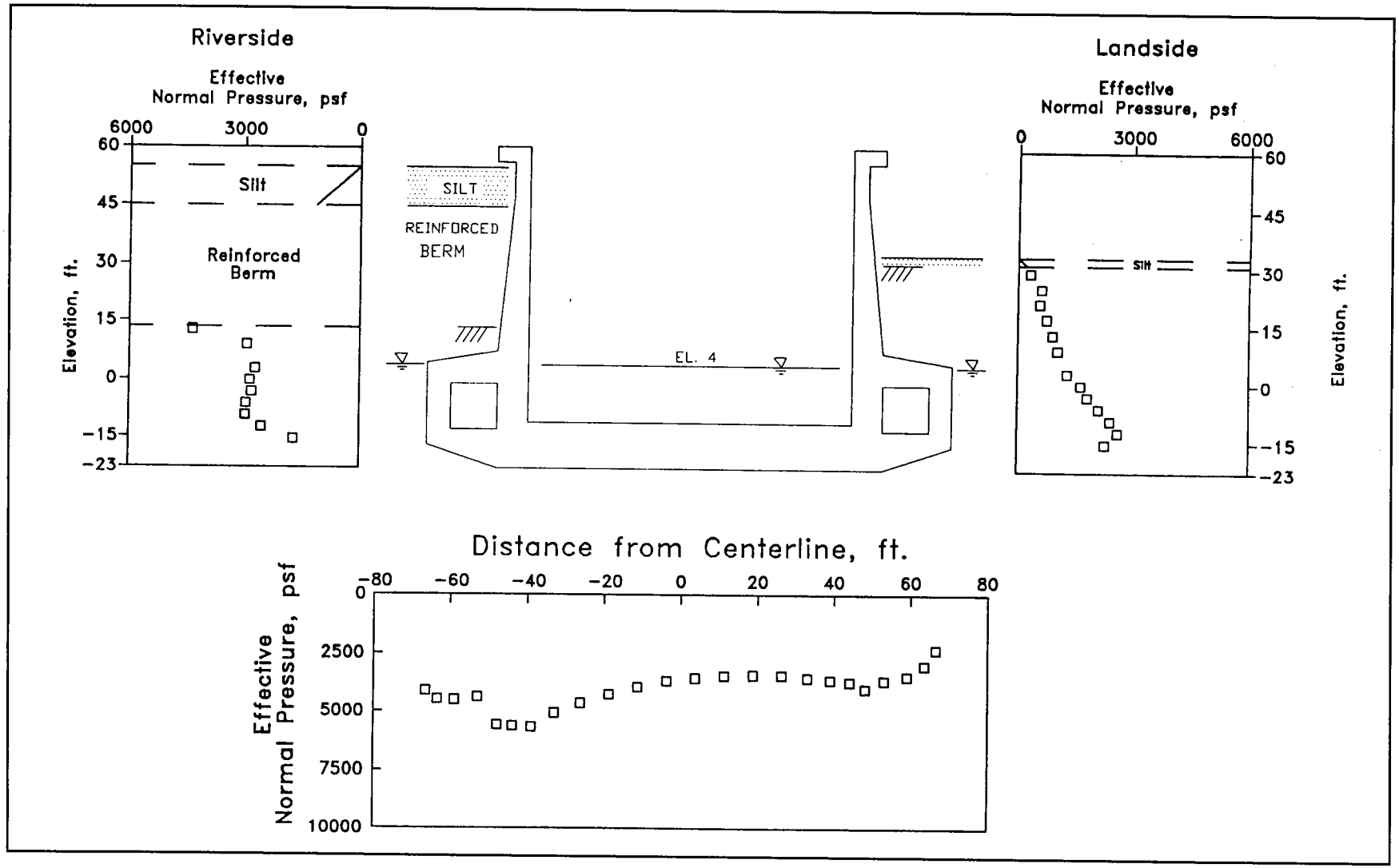

Figure 159. Effective normal pressures after lowering pool in lock to el 4 – river at el 4

2,320 psf, respectively. Since the river elevation remained unchanged from el 4, the differences between the effective stresses upon drawdown of the pool in the lock equaled the differences in the values of the total normal pressures. The effective pressures normal to the base of the lock after drawdown (Figure 159) are less than those computed prior to drawdown (Figure 149) by values ranging from 1,000 to 1,370 psf.

Effective normal pressures along the riverside stem wall were 4,350 psf at el 12.9 and 2,940 psf at el 9. Along the riverside culvert wall at els -15.5 and -12.5, the effective normal pressures increased from 1,720 to 2,550 psf. Between els -9.5 and 4.5, the effective normal pressures were nearly constant, averaging 2,860 psf. These effective pressures were greater than those computed values that occurred at the corresponding elevations along the landside walls. The differences between the effective pressures normal to the riverside and landside walls were equal to the differences between the total pressures. The magnitudes of the changes in the effective normal pressures after drawdown equaled the changes in the total normal pressures.

Comparison of the δ_{mob} values in Figure 150 with those values in Figure 160 shows that lowering the pool in the lock from el 40 to 4 increased the δ_{mob} values along the lock walls by as much as 14 deg, while the increase in the δ_{mob} values along the base of the lock was 2 deg or less. Upon lowering of the pool in the lock, δ_{mob} ranged from 2 deg below the landside stem wall to 15 deg below the riverside culvert (Figure 160). The maximum computed δ_{mob} values along the riverside and landside culvert walls were 26 and 24 deg, respectively. The values for δ_{mob} along the culvert walls showed the greatest changes after drawdown. For example, the minimum δ_{mob} values along the riverside and landside culvert walls in Figure 160 are 14 and 10 deg, respectively. These values are much greater than the values of 0 deg riverside and 3 deg landside shown in Figure 140. The greatest computed δ_{mob} values along the stem walls were 23 deg at el 21 landside and 17 deg below the riverside reinforced berm.

Figure 161 shows a decrease in K_h values after the drawdown of the pool by 36 ft as compared with the K_h values when the pool was at el 40 (Figure 151). In the compacted select clay along the landside stem wall, K_h ranged in value from 0.69 at el 29 to 0.66 at el 25. Between els 23 and 7.5, the landside K_h values ranged from 0.37 to 0.42, with an average value of 0.39. The average K_h values along the landside stem wall (Table 19) are less than the average K_h values shown in Table 18 by 0.1. Along the riverside stem and below the reinforced berm, K_h was 0.86 at el 13 and 0.53 at el 9, with an average K_h value of 0.70. This average K_h value was less than the Table 18 average K_h value by 0.05. Along the landside and riverside culvert walls, the Table 19 average K_h values were 0.52 and 0.42, respectively, which were greater than the Table 18 values by 0.03 and 0.02.

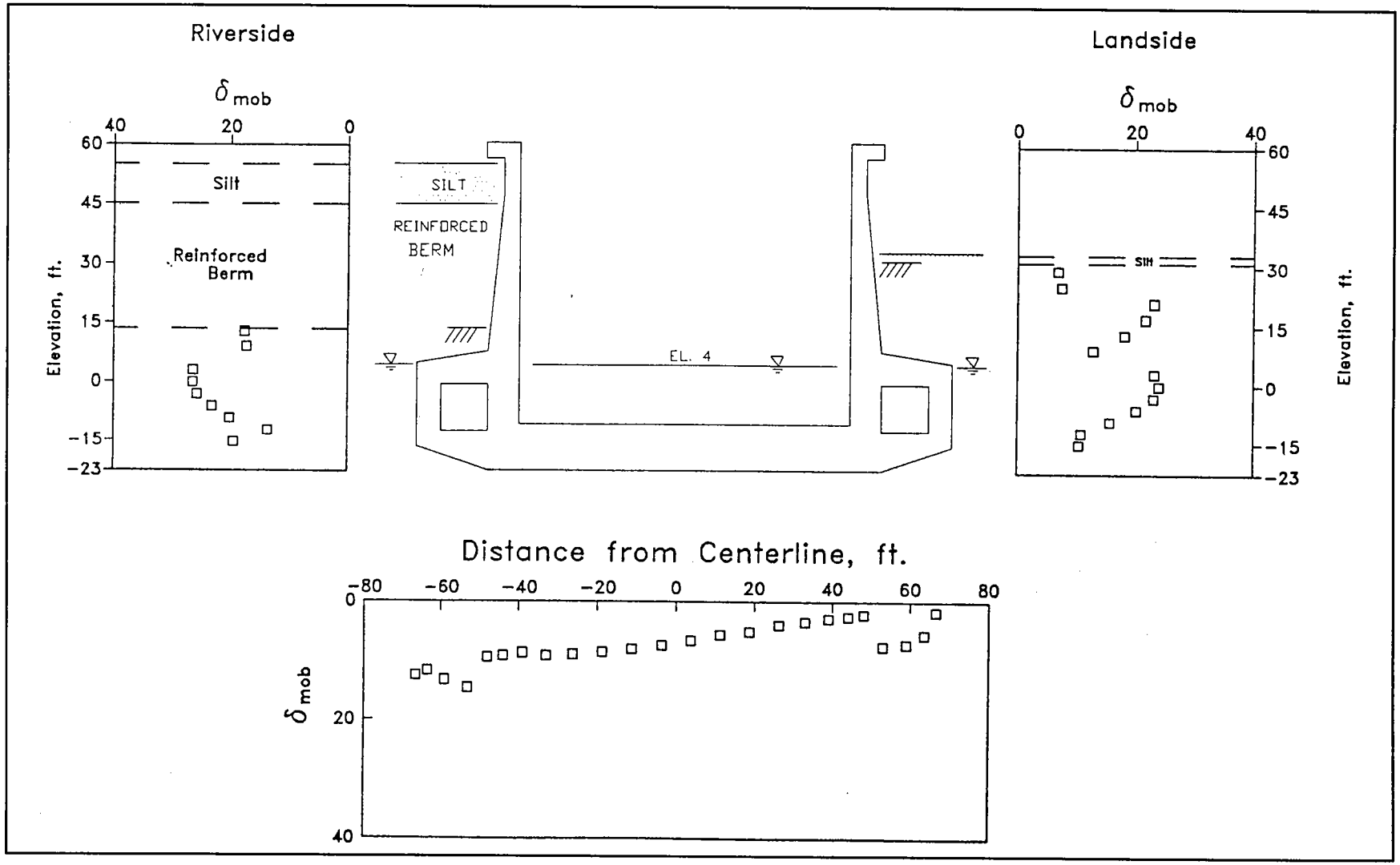

Figure 160. Mobilized friction angles along exterior of lock after lowering pool in lock to el 4 – river at el 4

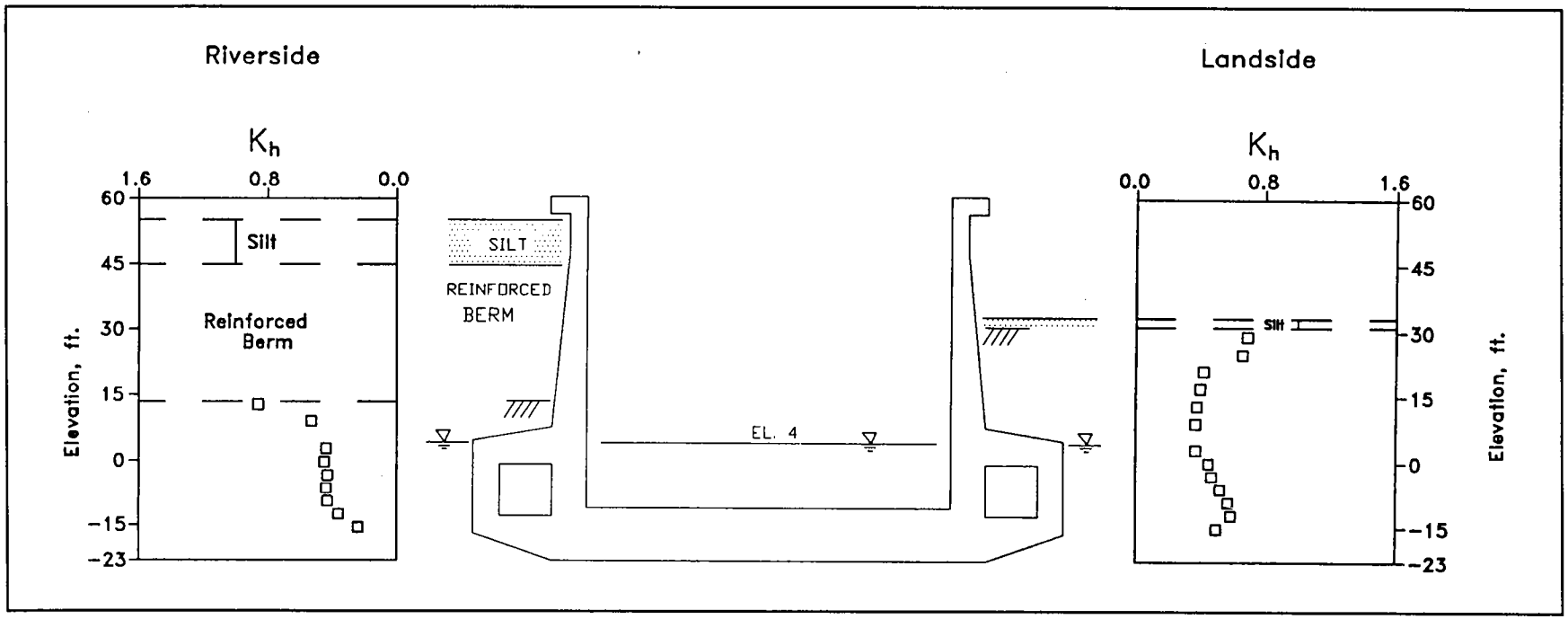

Figure 161. Horizontal earth pressure coefficients after lowering pool in lock to el 4 – river at el 4

Table 19
Average Values of Horizontal and Vertical Earth Pressure Coefficients after Lowering Pool in Lock to El 4 – River at El 4

Backfill Region	Backfill Material	Riverside K_h	Riverside K_v	Landside K_h	Landside K_v
Stem	Compacted select clay	-	-	0.68	0.08
Stem	Compacted sand	0.07	0.21	0.39	0.14
Culvert	Compacted sand	0.42	0.17	0.52	0.16

Elevation of river: 4 ft
Elevation of pool in lock: 4 ft
Elevation of riverside silt: 55 ft

The magnitude of downdrag along the lock walls increased with decreasing pool elevations within the lock. This increase in shear force was due to larger vertical displacements of the lock relative to the computed values within the adjacent backfill. Due to the increase in the downdrag forces, the K_v values in Figure 162 are greater than those shown in Figure 152. Below the reinforced berm and at el 12.9, the maximum computed K_v value was 0.27, or 0.02 greater than the predrawdown value. The average K_v value along the riverside stem wall was 0.21 (Table 19). The average K_v values along the landside stem wall, adjacent to the compacted select clay backfill and adjacent to the compacted sand backfill were 0.08 and 0.14, respectively. The largest increase in the computed K_v values occurred at the top of the riverside culvert wall and was 0.22 (Figure 162), 0.03 greater than the predrawdown value. K_v averaged 0.17 along the riverside culvert wall and 0.16 along the landside culvert wall.

The distributions of computed factored moments within the lock and the design moment capacity distributions are shown in Figure 163. The factored moment at the center line of the lock increased by 540 kip-ft from -4,150 kip-ft (Figure 153) to -4,690 kip-ft upon drawdown of the pool within the lock. Thirty-nine feet riverside of base center line, the drawdown of the pool within the chamber reduced the factored moment from -1,240 to 35 kip-ft. The magnitude of the moment 39 ft landside of base center line was reduced by a factor of approximately 2.0, i.e. from -2,429 to -1,270 kip-ft. All of the 84-ft-wide base slab **floor top** remained in tension except the 3 ft of base slab adjacent to the riverside stem wall. All of the **chamber side** of the stem walls were in compression after drawdown. The **chamber side** of the landside stem wall changed from tension (Figure 153) to compression (Figure 163) with the drawdown of the pool to el 4, due to the loss of the hydrostatic water pressures along 36 ft of the chamber wall. The factored moment within the riverside stem wall at el 9.25 increased from 64 to 714 kip-ft. At el 9.25 within the landside stem wall, the value for the factored moment increased by 600 kip-ft, from -370 to 230 kip-ft. The inside face of the top of the riverside culvert

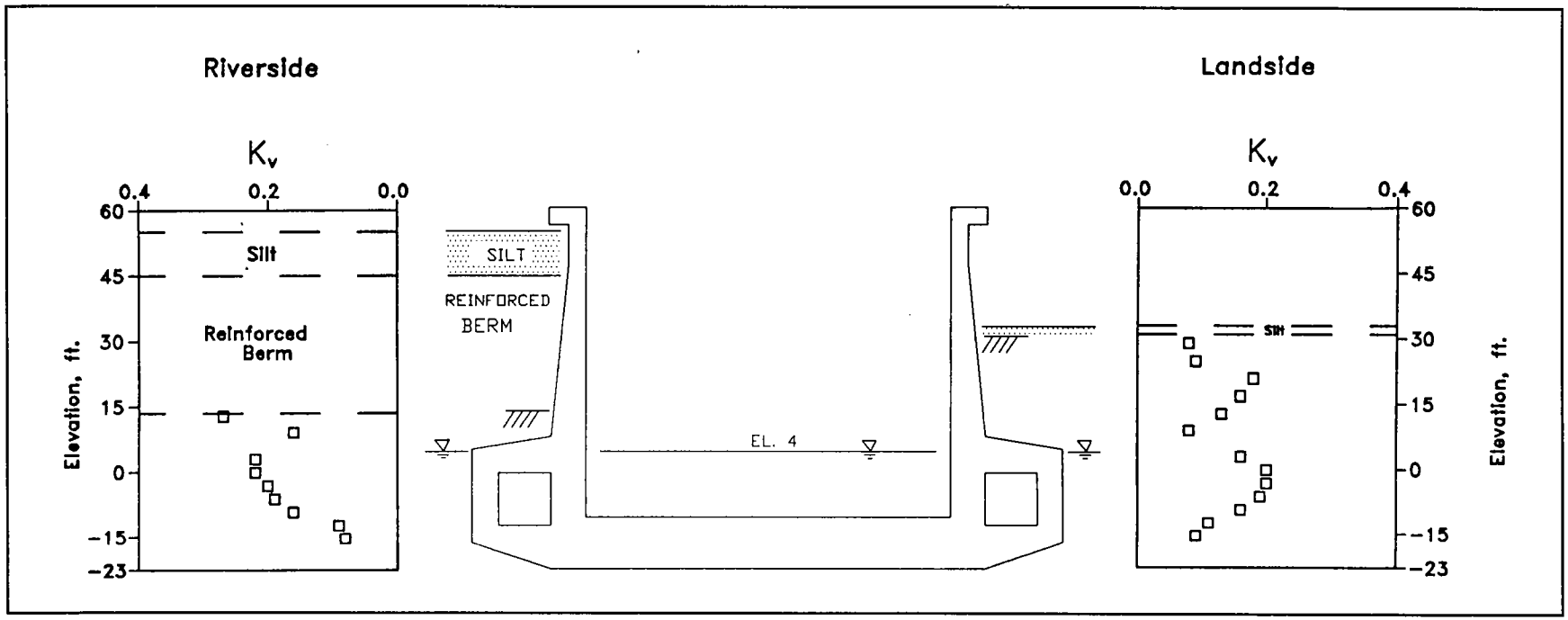

Figure 162. Vertical earth pressure coefficients after lowering pool in lock to el 4 – river at el 4

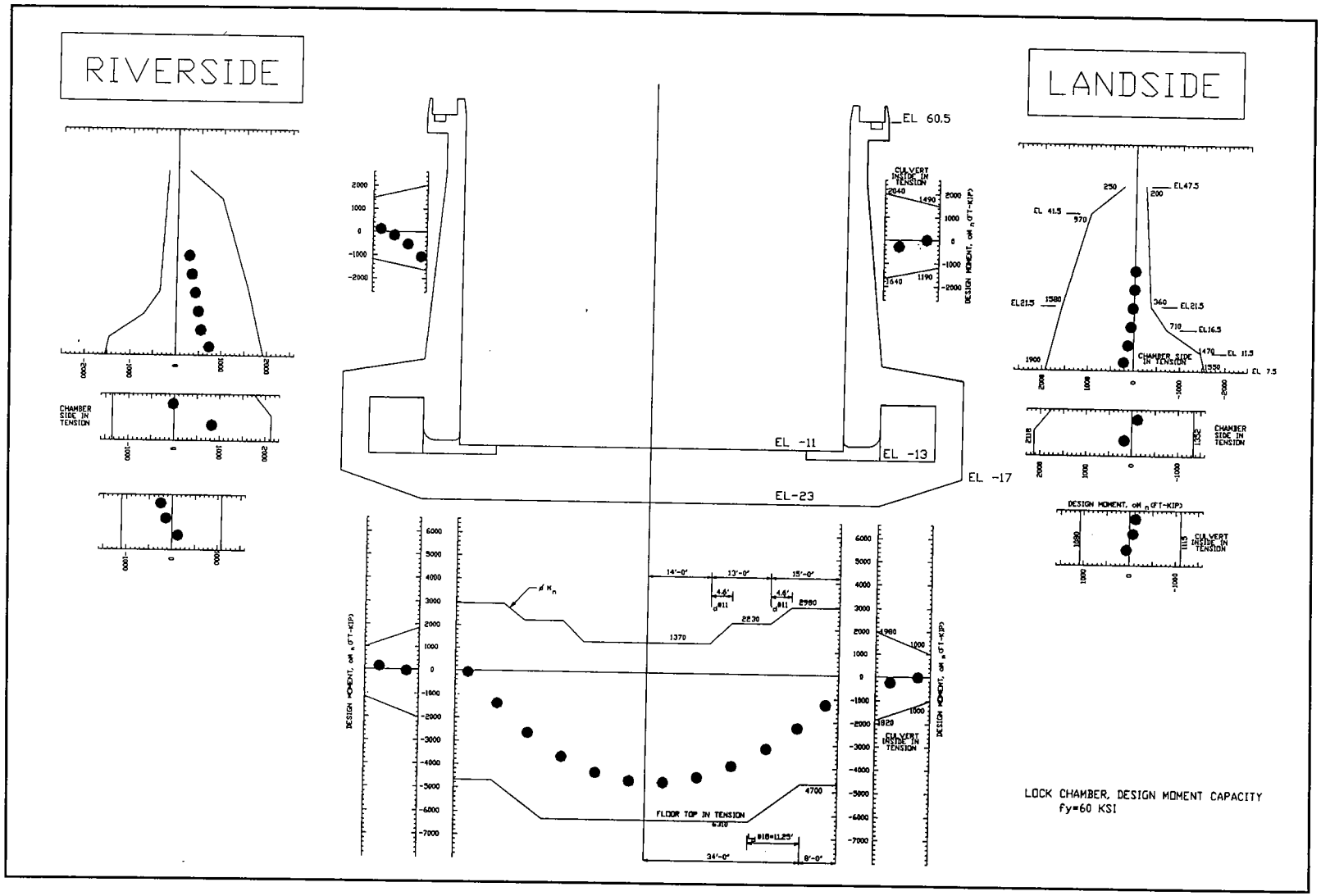

Figure 163. Distribution of factored moments and design moment capacity – pool in lock at el 4 and river at el 4

remained in compression during drawdown, but there was a significant increase in the bending moment for the member. The factored moment at the top of the riverside culvert and adjacent to the inside culvert wall increased to -1,090 kip-ft, which was 500 kip-ft less than the design moment capacity at this location. The values for the factored moments throughout the lock were less than those for the design moment capacity.

The lowering of the pool in the lock had little effect on the magnitude of the stresses within the soil comprising the reinforced berm, as shown in the stress paths for the reinforced berm soil elements 715, 1152, 623, and 563 in Figures 121 through 124, respectively. Stress path point no. 11 corresponded to the final effective stress state within the reinforced soil elements after drawdown of the pool in the lock to el 4 (Table 5). The mobilized shear strength within the soil comprising the reinforced berm and the computed tensile forces within the layers of reinforcement, shown in Figures 164 and 165, remained unchanged from the predrawdown values. The maximum tensile force was 2,600 lb per lin ft of reinforcement at the top, landside corner of the reinforced berm. The tensile forces and deformations computed within this region indicated that additional reinforcement was needed to limit the deformations, as noted in the Case 10 analysis. The magnitudes of the maximum tensile forces within these layers of reinforcement were below the limiting value of 3,800 lb per lin ft.

Summary

This part of the report summarizes the results from a series of soil-to-structure interaction analyses assessing potential lock performance with the construction of a reinforced berm adjacent to the riverside lock wall and the response of the berm and wall to water and silt loads. These phase 2 analyses consist of seven stages of construction and loadings. The first two series of analyses model the excavation of the riverside backfill and the construction of the reinforced soil berm. Water and silt loads were applied to the lock in two series of analyses, i.e., the raising of the elevations of the river and the pool in the lock to 60.5 ft, and the siltation riverside of the lock to el 55. These series were followed by the lowering of the river elevation and the pool in the lock in two stages. In the first stage, the river elevation was lowered to 4 ft and the pool in the lock to el 40. In the final stage, the pool in the lock was lowered to 4 ft.

The analyses presented in this chapter showed significant soil-to-structure interactions among the lock, the reinforced soil berm, the backfill, and the foundation regions of the mesh. The responses of these regions to the various loads were dependent upon both their locations and the applied loads. Careful evaluation showed that there are trends in the computed results for specific regions. These trends are summarized as follows:

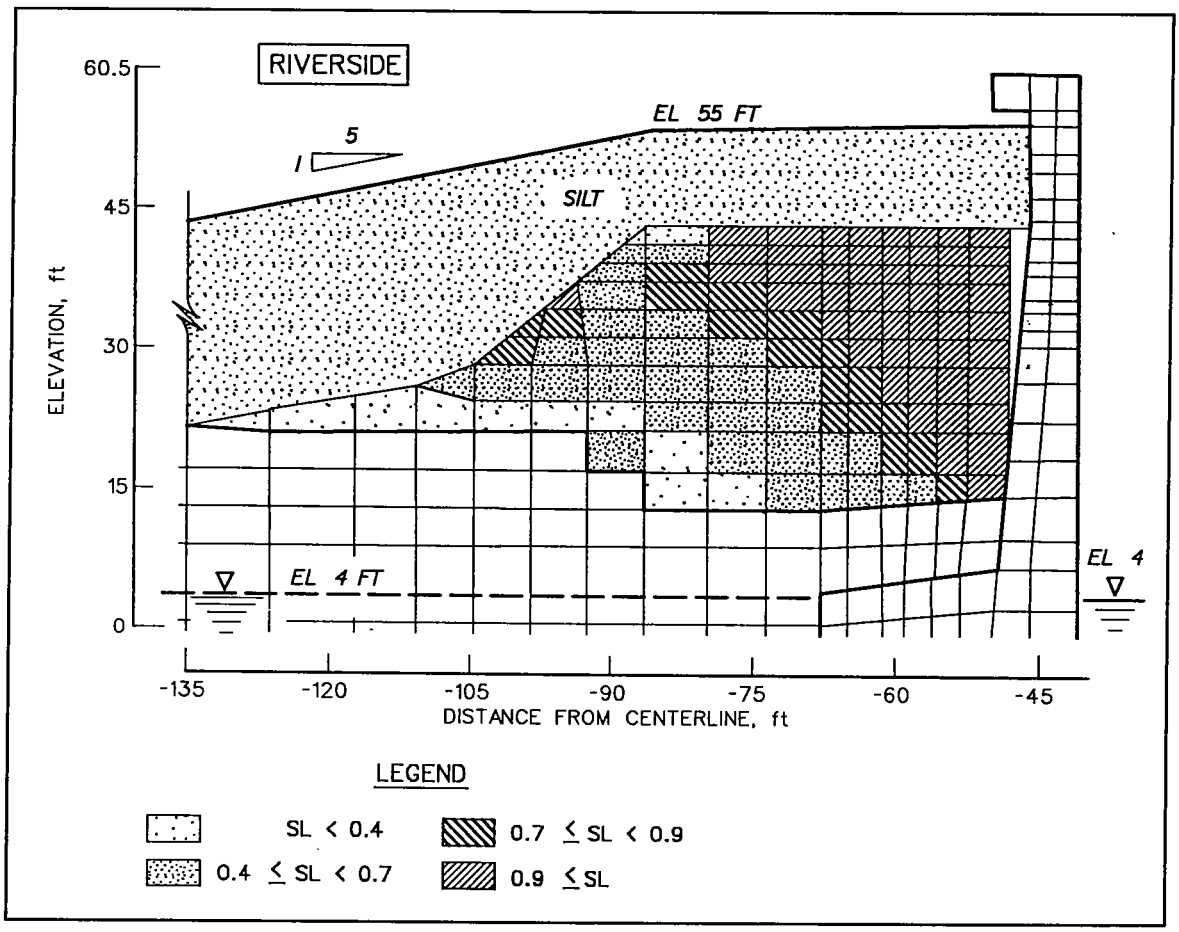

Figure 164. Variation in mobilized shear strength within reinforced berm after lowering pool in lock to el 4 – river at el 4

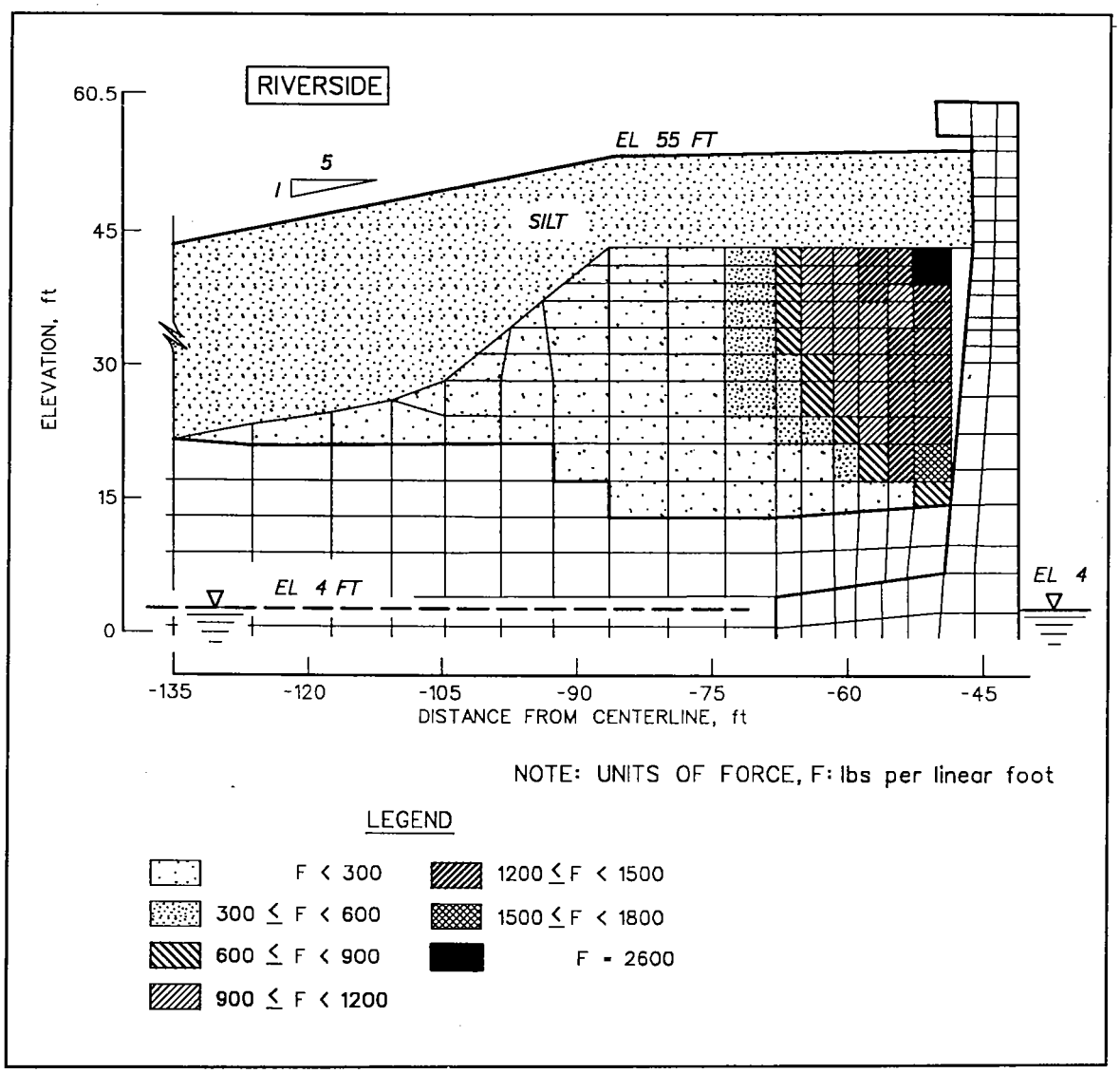

Figure 165. Variation in reinforcement force within reinforced berm after lowering pool in lock to el 4 – river at el 4

a. The soil-to-lock interactions at the base of the lock and at the walls of the lock were distinguishable, as shown by changes in the normal pressures, shear stresses, and displacements in the different load cases analyzed.

b. The responses of the culvert walls to water loads and silt loads differed from the responses of the upper and lower portions of the stem walls, as observed in the changes in the K_h and K_v values resulting from the load cases analyzed. The responses of these three soil-to-lock wall interface regions to water loadings depended upon: (1) the elevations of the river and the phreatic surface within the backfill; (2) the elevation of the pool in the lock; and (3) the difference between these two elevations. For example, raising the water table within the backfill from within the backfill to above the surface of the backfill resulted in an increase in K_h values, especially within the upper portions that were closer to the surface of the backfill. Another example is the case in which the pool elevation within the lock was lowered, with the river at a constant elevation. Along the culvert walls, the values for K_v increased in magnitude in proportion to the decrease in pool elevation.

c. The construction of the riverside reinforced soil berm alters the soil-to-structure interaction along the riverside of the lock, compared with the soil-to-structure interaction landside of the lock. The responses of the lock and soil regions are no longer symmetrical about the center line of the lock, even in the case of symmetrical water loads applied to the lock, such as during raising or lowering of the river and the pool in the lock.

d. With siltation to el 45 riverside of the lock, greater computed changes in displacements and stresses occurred riverside of the lock center line than landside of lock center line.

The following paragraphs summarize the variation in the computed displacements, stresses, values of δ_{mob}, K_h, K_v and factored moments with the construction of the reinforced soil berm and the application of water loads and silt loads at the lock site.

Construction of the reinforced soil berm to el 45 resulted in the placement of 15 ft of soil above the original top of riverside backfill. This additional soil load resulted in the settlement of the backfill and lock below the newly constructed reinforced soil berm and the counterclockwise rotation of the lock. Larger computed lock displacements occurred below riverside of lock center line, compared with those landside of center line. The greatest computed settlement occurred at the riverside corner along the base of the lock and was 1.1 in. Submergence of the site and the filling of the pool in the lock to el 60.5 resulted in rebound of the lock and the soil. The computed rebound at the riverside corner along the base was 0.8 in., resulting in a cumulative settlement of 0.3 in. Riverside siltation to el 55 resulted in additional settlements within the riverside berm, backfill, and foundation.

There was an additional counterclockwise rotation of the lock. The cumulative computed settlement at the riverside corner along the base increased to 0.6 in. Lowering of the river to el 4 and the pool in the lock to 40 ft increased the computed settlements of the lock, reinforced berm, backfill, and foundation. The total settlement increased by 1.7 to 2.3 in. at the riverside corner of the lock base. Lowering the pool in the lock to el 4, with the river elevation and the phreatic surface within the soil maintained at el 4, resulted in heave within the soil foundation of the lock. This reduced the settlement at the riverside corner of the lock base by 0.5 in., to a cumulative settlement of 1.8 in.

The computed total and effective base pressure distributions were in the shape of an inverted saddle for all seven analyses. Maximum computed base pressures were computed below the riverside stem wall and minimum values occurred below the outside corner of the landside culvert. The greatest effective computed base pressures occurred when the river was at el 4, and the pool in the lock was at el 40 (load Case 10 in Table 5).

The mobilized wall friction angles reflect the magnitude of the shear force acting along the soil-to-lock interface relative to the magnitude of the effective pressure normal to the surface of the lock. The magnitudes of these shear forces were dependent on the movement of the soil relative to the movement of the lock. Settlements of the backfill adjacent to the lock walls during backfilling were typically greater than those of the lock. This type of net movement downward along the interface resulted in the development of a shear force acting downward along the surface of the lock wall and is referred to as a downdrag force. In general, the greater the magnitudes of the vertical movements of the backfill **relative** to those of the lock wall, the greater the downdrag force. These analyses show that the values of δ_{mob} along the riverside lock walls differed from the computed values that occurred along the landside lock walls after construction of the reinforced soil berm because of increased settlement within the soil stratum below the berm relative to the settlement of the riverside lock wall. In addition, the values for δ_{mob} varied, depending on the elevation of the river, the elevation of the pool in the lock, and the difference between the two water elevations.

Submergence of the soil adjacent to the lock and the raising of the pool in the lock resulted in greater vertical movements of the backfill compared with the vertical movements of the lock. The vertical relative displacement resulted in a vertical shear force along the interface. This vertical shear force reduced the downdrag force and thereby reduced the δ_{mob} values. The results showed a greater change in δ_{mob} values along the stem wall than the change in δ_{mob} values along the culvert wall. The δ_{mob} values decreased with the raising of the water levels. Conversely, lowering the river elevation produced the opposite effect, increasing the computed δ_{mob} values along the walls.

Lowering the pool elevation in the lock chamber resulted in greater vertical movements of the lock compared with the vertical movements of the

adjacent backfill. The net **relative** displacements along the interface between the backfill and the wall resulted in additional downdrag forces, thus increasing the magnitudes of the total downdrag forces. This, in turn resulted in greater δ_{mob} values upon drawdown of the pool in the lock. Greater changes in computed δ_{mob} values occurred along the culvert walls compared with computed δ_{mob} values along the stem walls.

Computed δ_{mob} values along the base were less than or equal to 14 deg, with the maximum computed values in each of the analyses occurring below the riverside stem wall and/or riverside culvert. The greatest computed δ_{mob} values occurred along the culvert walls. Along the riverside culvert wall δ_{mob} was equal to 28 deg or less for all seven analyses, and along the landside culvert wall, δ_{mob} was 24 deg or less.

The horizontal earth pressure coefficients, K_h, along the riverside walls did not equal the K_h values along the landside walls with the construction of a reinforced soil berm. The maximum computed values of K_h occurred at the surface of the landside backfill for all analyses. Greater computed K_h values occurred along the stem walls, compared with the computed values along the culvert walls. The values of K_h along the riverside culvert wall were less than the values of K_h along the landside culvert wall. The ranges in average K_h values for the three geometrical and material regions riverside and landside of the lock walls are given in Table 20. The greater average K_h values were associated with the cases in which the backfill and the reinforced soil berm were submerged (Cases 8 and 9).

Table 20
Range of Average Values of Horizontal Earth Pressure Coefficients – Phase 2 Finite Element Analyses

Backfill Region	Backfill Material	Riverside Min	Riverside Max	Landside Min	Landside Max
Stem	Compacted select clay	—	—	0.68	1.5
Stem	Compacted sand	0.5	0.76	0.39	0.80
Culvert	Compacted sand	0.26	0.46	0.42	0.57

The factors affecting the values of δ_{mob} also affected the values of the vertical earth pressure coefficients since both of these parameters reflected the magnitude of the shear forces acting along the lock walls. One difference between the two indices was that the sign associated with the K_v value reflected the direction of the downdrag force. A positive K_v value implied a downdrag force along the lock wall. Conversely, a negative K_v value implied a shear force acting upward along the lock wall. For example, in load Case 10 negative computed K_v values occurred along the lower portion of the riverside culvert wall (Figure 152). The phase 1 analyses showed that raising the elevation of the pool with a constant river elevation decreased the computed K_v values along the walls. The

phase 2 analyses showed that lowering the elevation of the pool with a constant river elevation increased the K_v values. The greater values for the computed vertical earth pressure coefficients occurred along the culvert walls as compared with the computed values along the stem walls. The K_v values along the riverside walls were greater than the values of K_v along the landside culvert wall in the seven analyses. The ranges in average K_v values for the three geometrical and material regions riverside and landside of the lock walls are given in Table 21. The greater average K_v values were associated with Case 11 in which the reinforced soil berm and most of the backfill were above the water table (river elevation equal to 4 ft) and the pool within the lock was low at el 4.

Table 21
Range of Average Values of Vertical Earth Pressure Coefficients – Phase 2 Finite Element Analyses

Backfill Region	Backfill Material	Riverside Min	Riverside Max	Landside Min	Landside Max
Stem	Compacted select clay	—	—	0	0.08
Stem	Compacted sand	0.13	0.21	0.04	0.14
Culvert	Compacted sand	0.08	0.17	0.05	0.16

The results of all of the phase 2 finite element analyses, with the exception of one load case, indicated that the **floor top** of the base slab was in tension. The exception was load Case 11 in which the elevations of the river and the pool in the lock were at el 4. Three feet of the base slab floor top, adjacent to the riverside stem wall, were computed to be in compression in this load case. For all of the cases analyzed, the greatest computed factored moment occurred along the base and at the center line of the lock, as was the case for the four phase 1 analyses. Load Case 11 resulted in a maximum moment value of -4,690 kip-ft at the center line of the lock. The distribution of factored moments were unsymmetrical about the center line of the lock. The magnitudes of the computed factored moments along the base, adjacent to the stem walls, were greatest for load Case 10, in which the river elevation was 4 ft and the elevation of the pool in the lock was 40 ft. The values for the factored moments along the base were less than the design moment capacity values in all of the load cases.

The **chamber side** of the riverside stem wall was computed to be in compression for all analyses. This was also true for the landside stem wall, with the exception of load Case 10. The factored moments at a given elevation within the riverside stem wall were not equivalent in value when compared with the computed factored moments within the landside stem wall for these phase 2 analyses. The factored moments along the stem walls of the lock were less than the design moment capacity values in all of the load cases.

The values for the factored moments around the culverts were also less than the design moment capacity values in all of the load cases. The magnitudes of the computed factored moments throughout the culverts were greatest at the top of the riverside culvert, adjacent to the riverside stem wall, when the elevations of the river and pool in the lock were at 4 ft (load Case 11).

The CUFRAM analyses of the lock monolith no. 10 to the earth pressures and water pressures computed in load Cases 7 and 9 indicated that the computed distribution of moments within the lock were independent of the value assigned to the RLF. In addition, the computed factored moments using CUFRAM in load Cases 7 and 9 confirmed the values for the computed factored moments from the finite element results. The reason for the difference between the values for the factored moments along the base, computed from the finite element results and computed using CUFRAM, in load Case 10 is unclear at this time. These differences are believed to be associated with the procedure used within the CUFRAM program for the redistribution of forces to satisfy moment equilibrium at the center line of the lock. Additional evaluations of the force redistribution procedure used by CUFRAM for the special case of nonsymmetrical base pressures about the center line of the lock are required to resolve this issue.

4 Summary, Limitations, Conclusions, and Recommendations

Summary

This chapter summarizes the results of a series of soil-to-structure interaction analyses of the U-frame lock at Red River Lock and Dam No. 1 to water and silt loadings and its response with the construction of a reinforced soil berm riverside of the lock. This study was conducted in two phases, each phase involving a series of incremental, equivalent linear finite element analyses of lock monolith no. 10 and the corresponding geologic section D-D at this monolith (Figure 11). During the first phase of analyses, the finite element model of the lock, backfill, and foundation were subjected to water and/or silt loads consistent with after construction and three operational load cases for which instrumentation measurements at lock monolith no. 10 were available. The computed total and effective normal pressure distributions along the base and walls of the lock were in agreement with the instrumentation measurements recorded at the lock, as described in Chapter 2 of this report.

In the second series of analyses, described as the phase 2 studies in Chapter 3, the construction of a reinforced soil berm riverside of the lock was modeled first, followed by the application of a series of water and silt loads that were applied to both the lock and the reinforced berm. These series of analyses showed significant soil-to-structure interactions among the lock, the reinforced soil berm, the backfill, and the soil foundation. Construction of the reinforced soil berm and subsequent water loadings, siltation, and water unloading resulted in the displacement of the lock, riverside backfill, and soil foundation. The greatest computed values of lock displacements occurred below the riverside corner along the base. The greatest computed changes in both the total and effective stresses for the soils occurred within the backfill and foundation regions that were below the riverside berm, which corresponds to the side of the lock with the greatest earth and silt loadings. Since a portion of the reinforced soil berm was to be constructed over the riverside culvert of the lock, significant

changes in the total and effective stresses were also computed within the soil foundation below this portion of the lock. The factored moments throughout the lock were less than the design moment capacities in all load cases.

Limitations

Assumptions were made during the course of this study regarding both the characterization of the engineering properties for the soils and for some details of the analysis procedure. Specifically, the long-term changes in the computed deformations and effective stresses that occurred within the reinforced soil berm, backfill, and foundation to various water and silt loads applied to the lock during these analyses. Short-term loading using undrained soil properties were not considered. Drained material stiffnesses were assigned to all soils in these long-term analyses. Secondly, no results of drained triaxial tests were available for any of the soil stratum. The parameters for drained material were assigned to the soil stratum and were based on empirical relationships with other types of available test data and/or previous experience with properties of drained material properties for similar types of materials.

The unload-reload moduli were assigned to the soils comprising the foundation throughout the analyses as a result of both the large seasonal fluctuations in the phreatic surface measured at the site and the high preconsolidation pressures measured within the backswamp clay deposits. The computed settlements within the soils comprising the foundation were less than those that would have been computed if stiffness associated with primary loading had been assigned. The assignment of unload-reload moduli was appropriate for a given soil element if the magnitudes of the computed stresses within the soil element were greater than the maximum values computed during a previous stage of loading. One approach used during the course of this study to evaluate the appropriateness of assigning unload-reload moduli to the foundation soils was to compare the values for the computed vertical effective stresses that occurred along four vertical sections within the backswamp deposit at the end of each stage of loading with the preconsolidation pressure values for the entire backswamp deposit (Figures 106 through 109). At two of the four sections within the soil foundation, located below the reinforced berm (Figure 106) and below the riverside stem wall (Figure 107), the greatest computed vertical effective stresses occurred during phase 2 load Cases 10 and 11 (Table 5) and were within the lower range of preconsolidation pressure values that were measured within the backswamp clays. These backswamp clay samples, whose consolidation test results are shown in Figures 106 through 109, were recovered throughout the site but not specifically within the portion of the backswamp strata that was immediately below the riverside culvert and riverside backfill. This factor introduced some uncertainty regarding the magnitudes of the computed settlements that occurred within the foundation region adjacent to and below the riverside culvert.

These analyses were only for the response of lock monolith no. 10 to water and silt loads. When the computed results for lock monolith no. 10 were extrapolated to other monoliths, there were two primary factors to be considered. Both factors were associated with the stiffness, or equivalently, the compressibility, of the soils comprising the foundation and the variations in their values throughout the foundation. These variations in the stiffness within the foundation affected both the computed displacements and stresses but had a greater influence on the computed displacements.

The first factor to be considered during the extrapolation of the computed results to other monoliths was associated with the variations in the thickness of the soil stratum below the riverside backfill, in particular, the variation in the thickness of the backswamp deposit. The geologic cross section D-D at monolith no. 10 shows that the lock foundation comprised two deposits, the backswamp deposit and the sand substratum. The backswamp deposit was more compressible than the substratum sand deposit. Figure 7 shows that the thickness of the backswamp deposit varied along the length of the lock. Greater settlements may be anticipated at the monoliths with the thicker backswamp deposits. With the backswamp deposit being overconsolidated, these potential increases in settlements for the thicker backswamp deposits will be significantly smaller than they would be if the backswamp deposit were normally consolidated. In addition, the presence of shear keys between monoliths tended to help the lock bridge over any localized variations in settlements, resulting in no differential settlements at monolith joints and a more uniform settlement pattern along the chamber of the lock.

A second factor to be considered during the extrapolation of the computed results to other monoliths was associated with the variation in the compression characteristics of the soils comprising the backswamp deposit. At geologic cross section D-D (monolith no. 10), the backswamp deposit is heterogeneous, consisting of interbedded clays of medium to high plasticity, silts, sands, and silty sands (Figure 12). Due to the size of the elements within the finite element model of the foundation, one set of stiffness parameters was assigned to each element modeling the backswamp deposit. At the site of lock monolith no. 10, the stiffness value assigned to the backswamp region of the mesh was a composite stiffness, representing the interbedded layers of the different soils comprising the backswamp deposit. This composite stiffness was greater than the stiffness value that represents a highly plastic backswamp clay. Settlements at other locations along the lock may be greater than those values computed in these analyses if the composite stiffness for the backswamp stratum decreases. The extreme case is if the backswamp deposit consists of a homogeneous fat clay. A fat clay is defined as a clay with a liquid limit greater than 50 percent. Both consolidation test results and empirical relationships showed that the compressibility of clays increased with increasing liquid limit values.

Conclusions

The results of the finite element analyses of lock monolith no. 10 showed that the construction of a reinforced soil berm riverside of the lock was effective in reducing the negative impact that riverside siltation has on the behavior of the lock. These analyses also helped to identify additional features to be considered during the design of the reinforced soil berm and some of the types of analyses to be done during the design of the berm itself. These recommendations are summarized in the following section.

Recommendations

The finite element analyses of the lock model provided insight into the performance of the lock and its interaction with the reinforced soil berm, the backfill, and the foundation during various water and silt loadings. These soil-to-structure interaction analyses showed the need for additional factors to be considered during the design of the reinforced soil berm. Each of these factors is grouped into one of four categories in the following paragraphs.

Field investigation and laboratory testing

These analyses showed that the greatest computed vertical effective stresses occurred within the soil foundation below the riverside culvert and below the riverside backfill. In some load cases, the computed vertical effective stresses approached the lower limits of the range in preconsolidation pressure values measured within the backswamp clay deposit.

Recommendation No. 1: Conduct a field investigation and sample recovery program within the riverside backfill and the riverside foundation. The purpose is twofold: (a) determine the stratification of the soils comprising the foundation, especially the backswamp deposit, and (b) recover samples for laboratory testing.

Recommendation No. 2: Conduct one-dimensional consolidation tests on samples from the backswamp deposit to determine the variation in the preconsolidation pressure values with elevation and along the length of riverside backfill.

Design details for reinforced soil berm

This study has demonstrated the importance of the long-term material properties of the reinforcement material and number of layers of reinforcement placed within the reinforced soil berm on limiting its deformations

into the gap between it and the riverside stem wall. The phase 2 analyses showed a need for the following design features:

Recommendation No. 1: Construct the reinforced soil berm so that a gap exists between the reinforced berm and the riverside stem wall to allow for the horizontal movements which will naturally occur within the reinforced berm. These deformations within the reinforced soil berm will occur both during its construction and during subsequent loadings. These analyses showed that the magnitudes of these movements depend upon: (1) the long-term stiffness and strength of the reinforcement placed within the berm, (2) the density of the layering of the reinforcement, and (3) the magnitude and orientation of the applied loads. It is recommended that the face of the reinforced berm be constructed against the lock wall at the base of the reinforced soil berm, el 13.5. Between els 13.5 and 18, the face slope of the reinforced soil berm should be 9V:1H, at a minimum. With the face slope of the lock wall equal to 10V:1H, the minimum width of the gap, without consideration of berm and lock movements, would increase from 0 (no gap) at el 13.5 to 11.4 in. at el 18. Above el 18, the reinforced berm may be constructed with a vertical face. At els 30, 41, and 45, the minimum width of the gap, without consideration of berm and lock movements, equaled 25.8, 39, and 43.8 in., respectively. In actuality, the movements of the reinforced berm and lock will reduce the width of the gap. For the load cases considered in these analyses, the greatest computed lateral movements of the reinforced soil berm occurred when the river and lock pool were at els 4 and 40, respectively, and with riverside siltation to el 55. The lateral displacements along the vertical face of the reinforced berm at els 15, 30, and 41 were 2.5, 6.8, and 8.9 in., respectively, and were directed into the gap (Figure 147). These lateral movements of the reinforced soil berm would decrease the width of the gap at els 18, 30, and 41 to widths of 8.9, 19, and 30.1 in., respectively.

Recommendation No. 2: Prevent heave into the gap at the base of the reinforced berm. One approach is the construction of a concrete footing below the gap, extending from the riverside lock wall to below the reinforced berm.

Recommendation No. 3: With the possibility of siltation above the top of the berm, a permanent structural cap is needed to support any permanent silt loads which may accrue over the gap. The analyses showed that additional reinforcement and other structural details associated with the cap and its support will be required to limit the deflections within this region of the berm.

Recommendation No. 4: Steps must be taken to prevent the migration of soil out of the reinforced berm, due to the fluctuation of the river at the lock. The flow of water into and out of the berm could result in the removal of the soil comprising the reinforced soil berm through the faces of the reinforced berm. Two common approaches used in forming the face of the reinforced berm are the use of prefabricated face panels or the use of a layer of reinforcement up the face of the berm that would be connected to

the next layer of reinforcement prior to placement of the next soil lift. If an open grid reinforcement is used and the face(s) of the reinforced soil berm is(are) formed by continuing the grid up along the face of the berm and into the next layer of reinforcement, filter fabric should be placed between the exposed face(s) of the reinforcement and the soil comprising the reinforced soil berm. In addition, after the face of the berm is formed, the grid reinforcement should be pretensioned and securely fashioned to the next layer of reinforcement to minimize displacements.

Recommendation No. 5: Place a filler material within the gap to reduce the volume of soil particles that migrate into the gap. Recommendations for filler materials are discussed in the following section.

Recommendation No. 6: The material properties of the reinforcement will affect the performance of the reinforced berm. In these analyses, performance is defined in terms of displacements and forces. Both polymer and metal reinforcements each have characteristics which alter their performance with time and/or the environment. These characteristics must be given careful consideration during the design of the berm. For example, polymers creep under sustained loads. Properties determined from long-term creep testing, such as load-deformation as well as strength, should be used during the design of the berm. Consideration should also be given to the potential degradation of the reinforcement if it is exposed to sunlight, a potential problem if the riverside face of the berm is formed by continuing a polymer grid up along the face of the berm and into the next layer of reinforcement. Thermal effects on material properties are not expected to be a factor on this project, but this should be verified by the designers. If a metal reinforcement is used, the possibility of degradation of the reinforcement through corrosion should be considered during the design.

Filler material placed within the gap

The objective of the filler material within the gap is to reduce the available space for any soil particles that are able to migrate into the gap. The ideal filler would behave as an elastic material that would continually occupy the space within the gap during the movements of the reinforced berm relative to the movements of the stem wall. A low stiffness for the filler material would ensure that when the reinforced berm and the riverside lock wall move toward one another, large compressive strains could occur within the filler material without the filler material transferring earth loads to the lock wall. However, the stiffness cannot be so low that it would allow the filler material to collapse when submerged during high river levels. During the high water levels, water pressures will act normal to the riverside stem wall that forms the gap, as well as along the surface of the filler material placed within the gap. This will result in significant uplift forces acting on the filler material, which must be accounted for through some sort of anchoring procedure. The options available for anchoring the filler material will depend upon both the type of filler material selected and the design selected for the face of the reinforced berm. Two

options that may be considered are: (a) glue the filler to the face of the lock and/or the face of the reinforced soil berm, or (b) wrap sections of the filler in reinforcement layers that are anchored to the layers of reinforcement within the reinforced soil berm.

Geoinclusion between Reinforced Soil Berm and Lock Wall

The basic concept behind the planned construction of the reinforced berm is to relieve or reduce the lateral earth pressures that might develop against the lock walls from the silt buildup during high water. It is well established that a soil mass with horizontal layers of tensile reinforcement will essentially be self supporting if a facing material is provided to prevent localized loss of the material at the face. However, lateral deformation of the soil mass is necessary for the horizontal layers of reinforcement to develop sufficient tension to make the soil mass self supporting. The magnitude of the lateral deformation to develop sufficient tension in the reinforcement is dependent upon the stiffness of the reinforcement and the deformation characteristics of the soil. The analyses presented in this report have shown that if the reinforced berm is constructed directly adjacent to the lock, the lock walls would not move sufficiently to develop any appreciable tension in the reinforcement and, therefore, would not provide any significant contribution to the stability of the soil mass or to the reduction of lateral earth pressures against the lock. The analysis presented in this report shows that with adequate reinforcement, the vertical face of the proposed reinforced berm must be free to move approximately 6 in. for the berm to be self supporting.

For the horizontal layers of reinforcement in the berm to activate their tensile capacity, a mechanism must be developed to allow the vertical face of the reinforced berm to deform laterally without applying a significant lateral stress to the lock. It is impractical to have a void between the vertical face of the berm and the lock walls. A void would be a nuisance during construction and would result in maintenance problems after construction. Therefore, the space between the vertical face of the berm and the lock walls must be filled with a material to form an inclusion that would allow the soil mass to deform sufficiently to activate tensile resistance of the reinforcement to a point at which the soil mass is self supporting. Obviously, the compressibility of the material used for the inclusion must be sufficiently soft that it will offer nearly zero restraints to the deforming soil mass and, simultaneously, transfer essentially **no lateral stress** to the lock walls as it compresses.

As with many engineering innovations, a review of the literature reveals that this design concept of placing a compressible material between a soil mass and a rigid wall is not a radically new idea. Yet, the basic ideas have evolved only within the past few years. In recent articles on

the subject, this concept has been referred to as a geoinclusion (Horvath 1990, 1991a, 1991b). In a literature review by Horvath (1990), he found that Partos and Kazaniwsky (1987) had presented a case history in which a compressible geoinclusion, without any horizontal reinforcement, was used to reduce the lateral earth pressures on a basement wall. The data indicate that lateral earth pressures were reduced from a design level of at-rest to a level significantly below the active state. In the McGown, Andrawes, and Murray (1988) publication, the combined effects of horizontal reinforcement and a compressible geoinclusion were discussed along with the results of a model test. The model test data support the concept of achieving nearly zero lateral earth pressure by employing horizontal reinforcement and a compressible geoinclusion. One of many useful findings from their work is that the horizontal reinforcement should be closely spaced in the vertical direction to ensure a relatively uniform reduction in earth pressures. Edgar, Puckett, and D'Spain (1988) presented data from a case history in which a compressible geoinclusion and reinforcement were used together against highway bridge abutments. In this case, the compressible material was a thin layer of cardboard which upon saturation with water allowed the embankment to move horizontally to activate the reinforcement. Reductions in earth pressures were assessed based on the geotechnical instrumentation measurements installed at the site.

Selection of appropriate material

A key component for a successful design for the proposed reinforced berm is to find the appropriate material to be used for the geoinclusion. One such available material for the geoinclusion is a product called GeoTech Drainage Panel or Board (GDP) manufactured by Geotech Systems Corporation. GDP is the same material used in the case history reported by Partos and Kazaniwsky (1987), in which it reduced lateral earth pressures against basement walls of an underground parking garage. Other similar materials may be available. In this application, no lateral reinforcement was used in the backfill. In numerical studies reported by Horvath (1990, 1991a, 1991b), earth pressures against a rigid wall dropped to nearly zero, Figure 166, when 24 in. of GDP were used in conjunction with lateral reinforcement in the backfill. GDP is a prefabricated composite of a panel of expanded polystyrene (EPS) beads that are fused together in an open, popcorn-like structure and covered by a geotextile. It is used primarily to provide water pressure relief (drainage) for underground structures. EPS is an extremely versatile material and can be easily produced with a wide range of strengths and compressibilities. For use as a geoinclusion, it can be manufactured with a high compressibility (i.e., low modulus). It is available in thicknesses from 1 to 24 in. The product has predictable stress-strain relationships making it easier to assess its potential performance. EPS is also a desirable material for use as a geoinclusion from an environmental perspective, because it does not produce or use any gases that have been identified as environmentally detrimental.

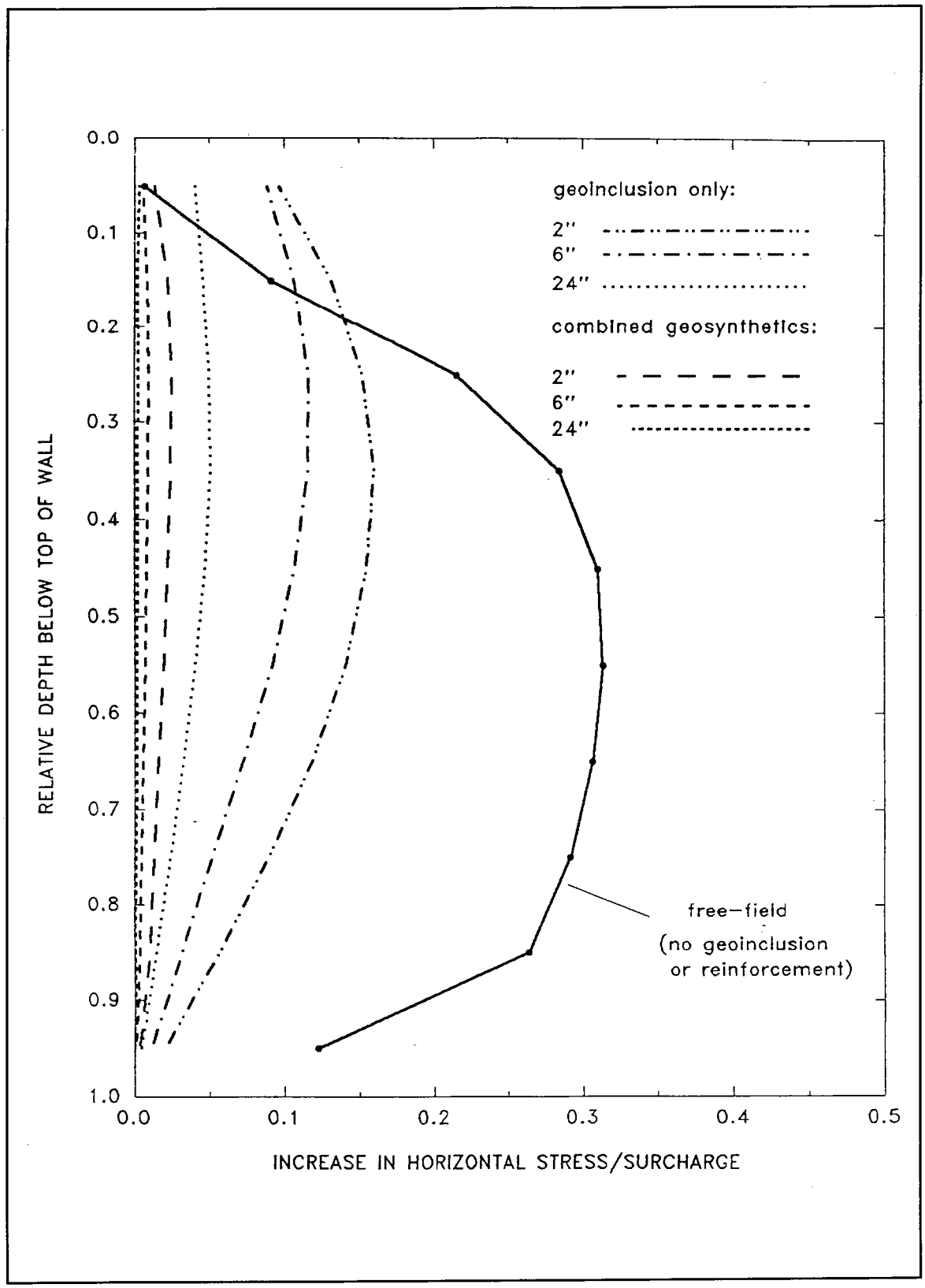

Figure 166. Lateral earth pressure reduction by use of geoinclusion and lateral reinforcement (Horvath 1991b)

An additional benefit of GDP is that it can also function as a drain between the berm and lock wall.

Stability

The analyses described in this report consider the long-term stability and response of the structure to select water and silt loadings. Because of the complexities involved in this type of analysis, all the combinations and types of load cases are not exhausted. For example, other load cases which should be evaluated during the design of the reinforced soil berm are the evaluation of the short-term stability of the reinforced soil berm and its foundation. The cases analyzed should include silt deposition on top of the reinforced berm but without silt in the channel. Silt along the riverside face of the backfill and reinforced berm may act to buttress the structure. This situation could arise if the channel silt would be first eroded by river currents some time after initial deposition on top of the berm.

Once the filler fabric is selected, additional CUFRAM analyses are recommended to evaluate the variations in moments throughout the lock if the material within the gap is not perfectly effective in eliminating the transfer of earth pressures. Again, because of the porosity of the adjacent soils comprising the reinforced berm, water pressures will continue to act normal to the entire riverside stem wall.

References

American Society of Testing Materials. (1990). "Standard test method for classification of soils for engineering purposes," Practice No. D2487-90, *1990 Book of ASTM Standards, Philadelphia, PA. (309-319).*

Anderson, John M., and Vanadit-Ellis, Wipawi. (1987). "Instrumentation data summary—Lock and Dam No. 1 Red River Waterway, LA," U.S. Army Engineer Waterways Experiment Station, Vicksburg, MS.

Chalaturnyk, R. J., Scott, J. D., and Chan, D. H. K. (1990). "Stresses and deformations in a reinforced soil slope." *Canadian Geotechnical Journal* 27(2), 224-232.

Clough, G.W., and Duncan, J. M. (1969). "Finite element analyses of Port Allen and Old River Locks," Report No. TE-69-3, U.S. Army Engineer Waterways Experiment Station, Vicksburg, MS.

Dawkins, W. P. (1987). "User's guide: Computer program for two-dimensional analysis of U-frame structures (CUFRAM)," Instruction Report ITL-87-1, U.S. Army Engineer Waterways Experiment Station, Vicksburg, MS.

Doherty, W. P., Wilson, E. L., and Taylor, R. L. (1969). "Stress analysis of axisymmetric solids utilizing higher-order quadrilateral finite elements," Report No. SESM 69-3, Structural Engineering Laboratory, University of California, Berkeley, CA.

Duncan, J. M., and Chang, C. Y., 1970. "Nonlinear analysis of stress and strain in soils," *Journal, Geotechnical Division, American Society of Civil Engineers* 96(SM5), 1629-1653.

Duncan, J. M., Byrne, P., Wong, K. S., and Mabry, P. (1978). "Strength, stress-strain and bulk modulus parameters for finite element analyses of stresses and movements in soil masses," Report No. UCB/GT/78-02, University of California, Berkeley, CA.

Ebeling, R. M., Mosher, R. L., and Abraham, K. (1991). "Numerical material characterization of Red River Lock and Dam No. 1 site," Technical Report ITL-91-X, U.S. Army Engineer Waterways Experiment Station, Vicksburg, MS.

Ebeling, R. M., Peters, J., and Clough, G. W. (1990). "Users guide for the incremental construction, soil-structure interaction program SOILSTRUCT," Technical Report ITL-90-6, U.S. Army Engineer Waterways Experiment Station, Vicksburg, MS.

Edgar, T.V., Puckett, J.A., and D'Spain, R. B. (1988). "Effects of geotextiles on lateral pressure and deformation in highway embankments," *Geotextiles and Geomembranes* 8(4), 275-292.

Goodman, R. E., Taylor, R. L., and Brekke, T. L. (1968). "A model for the mechanics of jointed rock," *Journal of the Soil Mechanics and Foundations Divisions*, American Society of Civil Engineers, 94(SM3), 637-659.

Hall, Robert L. (1987). "Structural evaluation of Lock and Dam No. 1," Unpublished report for U.S. Army Engineer District, Vicksburg, by U.S. Army Engineer Waterways Experiment Station, Vicksburg, MS.

Horvath, J.S. (1990). "The use of geosynthetics to reduce lateral earth pressures on rigid walls: concept evaluation," Research Report No. CE/GE-90-2, Manhattan College, Bronx, NY.

_____. (1991a). "Using geosynthetics to reduce earth loads on rigid retaining structures," *Geosynthetics '91 - The North American Regional Conference on Geosynthetics*, Atlanta, GA.

_____. (1991b). "Using geosynthetics to reduce surcharge-induced stresses on rigid retaining structures," *Transportation Research Board 1991 Annual Meeting*, Washington, D.C.

Kaufman, R. I., and Sherman, W. C. (1964). "Engineering measurements for Port Allen Lock," *Journal of the Soil Mechanics and Foundations Divisions, American Society of Civil Engineers* Proceedings Paper 4020, 90(SM5), 221-247.

McGowan, A., Andrawes, K.Z., and Murray, R.T. (1988). "Controlled yielding of the lateral boundaries of soil retaining structures," *Geosynthetics for Soil Improvement.* Geotechnical Special Publication No. 18, R.D. Holtz(ed.), American Society of Civil Engineers, 193-210.

Partos, A.M. and Kazaniwsky, P.M. (1987). "Geoboard reduces lateral earth pressures," *Proceedings of Geosynthetics '87*, IFAI, 628-639.

Peterson, M. S., Kulhawy, F. H., Nucci, L. R., and Wasil, B. A. (1976). "Stress-deformation behavior of soil-concrete interfaces," Contract Report B-49 to Niagara Mohawk Power Corporation, Syracuse, NY, Dept. of Civil Engineering, Syracuse University, Syracuse, NY.

Potyondy, J. G. (1961). "Skin friction between various soils and construction materials," *Geotechnique* 11(4), 339-353.

U.S. Army Engineer District, Mobile. (1988). "Lock and Dam No. 1, Red River Waterway, volume 1 - lock masonry and embedded metals (revised), supplement no. 7 - sediment study," Detail Design Memorandum No. 11, Mobile, AL.

U.S. Army Engineer District, New Orleans. (1977). "Lock and Dam No. 1, detail design phase 2, soils data and foundation design; Red River Waterway, LA, Tex., Ark., and Oka. Mississippi River to Shreveport, LA," Design Memorandum No. 9, New Orleans, LA.

_____. (1984). "Foundation report, Red River Waterway, LA, Lock and Dam No. 1," New Orleans, LA.

U.S. Army Engineer District, Vicksburg. (1988). "Preliminary design for the reinforced soil berm riverside of the lock at Red River Lock and Dam No. 1, LA," unpublished data.

_____. (1989). Unpublished data from an investigation of siltation at Red River Lock and Dam No. 1, Louisiana.

Vanadit-Ellis, Wipawi, Hall, Robert L., and Graham, Paul W. (1988). "Analysis of data from instrumentation program, Lock and Dam No. 1, Red River Waterway, LA," Unpublished report for U.S. Army Engineer District, Vicksburg, by U.S. Army Engineer Waterways Experiment Station, Vicksburg, MS.

Appendix A
Incremental Construction Procedure for Modeling Nonlinear Stress-Strain Behavior for Soils and Interface Elements

Nonlinear Soil Model

The procedure used to model nonlinear stress-strain behavior of soils in the finite element analysis of Red River Lock and Dam No. 1 was an incremental, equivalent linear approach. In this approach, the loads were divided into several increments. For each increment of loading, the values of the two elastic parameters assigned to each of the soil elements were adjusted to correspond to the current stress level developed within that element. In general, an isotropic elastic material was described in terms of two elastic constants. In this formulation, these constants were the Young's modulus and bulk modulus for the material. Each soil element was assigned a value of Young's modulus, E_t, where the subscript t refers to the tangent value, and bulk modulus, *BULK*. The values for the two elastic parameters were constant for each element during each load increment. The values of E_t and *BULK* were adjusted after each load increment according to the computed deviatoric stress level and/or value of confining stress developed within each element. Like E_t, the value assigned to the unload/reload Young's modulus, E_{ur}, was also dependent upon the confining stress.

The relationships defining the values of Young's modulus, E_t, E_i, and E_{ur}, and the bulk modulus, *BULK*, are listed in Table 1 in the main text of this report. E_t is defined in terms of three parameters, the initial Young's modulus, E_i, the failure ratio, *RF*, and the stress level (*SL*). These terms and the parameters used to define them are described in the following paragraphs.

The failure ratio, R_F, is a curve-fitting parameter used to relate the deviator stress at failure to the ultimate deviator stress, the asymptote to the

hyperbolic stress-strain curve. The deviator stress at failure is defined by the conventional Mohr-Coulomb criterion, with the soil strength parameters specified by the friction angle and the cohesion.

The *SL* is defined as the ratio of the current deviator stress to the deviator stress at failure. *SL* ranges in value from 0 to complete mobilization at a value equal to 1. Under primary loading, the greater the value of the stress level, the smaller the value of Young's modulus, E_t, assigned to the element. If the computed stresses in an element exceed those allowed by the Mohr-Coulomb limits, the Young's modulus is set to a very low value so that the element will not take on any additional shear stresses. However, the hydrostatic stresses can increase. The value assigned to the bulk modulus is set so that the corresponding value of Poisson's ratio is equal to 0.49.

K, K_{ur}, and K_B are material constants independent of units. The exponent n describes the change in values of E_i and E_{ur} with confining pressure. The exponent m describes the change in value of *BULK* with confining pressure. P_A is the value of atmospheric pressure and is used to introduce the appropriate units into the relationships for the material parameters.

Soil-to-Lock Interface Model

The hyperbolic shear stress-relative shear displacement relation for the soil-to-lock interface elements is shown in Figure 14. The incremental equivalent linear solution procedure that is used to model the nonlinear stress-strain behavior of the soil elements is also used to model this nonlinear relationship. The value of the tangent shear stiffness, k_t, is adjusted after each load increment according to the computed shear stress level and the value of confining stress developed within each interface element. The relationships defining the values of interface shear stiffnesses, k_{st} and k_{si}, are listed in Table 2 in the main text of this report. Like E_t, k_{st} is defined in terms of three parameters, the initial interface shear stiffness, k_{si}, the stress level, SL_i, and the failure ratio, R_{Fi}.

SL_i is defined as the ratio of the current shear stress to the shear at failure. The failure ratio, R_{Fi}, is a curve fitting parameter used to relate the shear stress at failure to the ultimate shear stress, the asymptote to the hyperbolic stress-strain curve. The shear stress at failure is defined by the conventional Mohr-Coulomb criterion, with the soil strength parameters specified by the friction angle and the cohesion.

K_j is a material constant independent of units. The exponent n_j describes the change in values of k_{si} with normal pressure. The unit weight of water, $_w$, and P_A are used to introduce the appropriate units into the interface shear stiffness relationship.

REPORT DOCUMENTATION PAGE

Form Approved
OMB No. 0704-0188

1. AGENCY USE ONLY *(Leave blank)*	2. REPORT DATE	3. REPORT TYPE AND DATES COVERED
	September 1993	Final report

4. TITLE AND SUBTITLE

Soil-Structure Interaction Study of Red River Lock and Dam No. 1 Subjected to Sediment Loading

5. FUNDING NUMBERS

6. AUTHOR(S)

Robert M. Ebeling, Reed L. Mosher, Kevin Abraham, John F. Peters

7. PERFORMING ORGANIZATION NAME(S) AND ADDRESS(ES)

US Army Engineer Waterways Experiment Station
Information Technology & Geotechnical Laboratories
3909 Halls Ferry Road, Vicksburg, MS 39180-6199

8. PERFORMING ORGANIZATION REPORT NUMBER

Technical Report ITL-93-3

9. SPONSORING/MONITORING AGENCY NAME(S) AND ADDRESS(ES)

US Army Engineer District, Vicksburg
Vicksburg, MS 39180

10. SPONSORING/MONITORING AGENCY REPORT NUMBER

11. SUPPLEMENTARY NOTES

Available from National Technical Information Service, 5285 Port Royal Road, Springfield, VA 22161.

12a. DISTRIBUTION/AVAILABILITY STATEMENT

Approved for public release; distribution is unlimited.

12b. DISTRIBUTION CODE

13. ABSTRACT *(Maximum 200 words)*

Lock and Dam No. 1 on the Red River Waterway has experienced a serious siltation problem since its completion in 1983. This technical report summarizes the results of a soil-structure interaction analysis of a potentially permanent, low-maintenance solution to this problem, i.e., construction of a reinforced soil retaining wall adjacent to the riverside lock wall.

The principal objective of this research was to assess potential lock performance after construction of a reinforced soil retaining wall adjacent to the riverside lock wall. Due to the nature of the problem, the conventional analysis techniques, which are based upon the equations of equilibrium and used in the design of reinforced soil retaining walls, did not provide sufficient information to satisfactorily evaluate performance of this structure with regard to its interaction with the lock and the surrounding foundation soil strate. The general-purpose, nonlinear, incremental construction, finite element computer program, SOILSTRUCT was used to analyze the complex soil-structure interaction by simulating the staged construction.

(Continued)

14. SUBJECT TERMS

Earth pressures
Finite elements
Soil reinforcement
Soil-structure interaction

15. NUMBER OF PAGES

283

16. PRICE CODE

17. SECURITY CLASSIFICATION OF REPORT	18. SECURITY CLASSIFICATION OF THIS PAGE	19. SECURITY CLASSIFICATION OF ABSTRACT	20. LIMITATION OF ABSTRACT
UNCLASSIFIED	UNCLASSIFIED		

13. (Concluded).

This analysis was conducted in two phases. In Phase 1, the finite element model of the lock was calibrated by using the instrumentation data recorded during the construction and operation of the lock. In Phase 2, the potential lock performance with the construction of a reinforced soil berm adjacent to the riverside lock wall and the soil-structure interaction due to subsequent silt loading was evaluated.

The results of the Phase 1 finite element analyses compared favorably with instrumentation readings for the four load cases analyzed. The response of the lock to staged construction of the reinforced soil berm and subsequent staged silt and water loadings of the Phase 2 analyses are summarized herein. Also, recommendations regarding additional design details for the proposed reinforced soil berm are included.